

**University of Bologna**

---

Faculty of Engineering  
Department of Electrical Engineering

Ph.D. Thesis in Electrical Engineering  
XXIII cycle  
Power electronics, Electrical machines and Drives (ING/IND-32)

**Hybrid  
e-CVT Power Split  
Drivelines**

**Ph.D. Thesis of:**

Piero Corbelli

**Tutor:**

Dott. Ing. Claudio Rossi

**Ph.D. Coordinator**

Prof. Ing. Domenico Casadei

---

**March 2011**



# Table of contents

Table of contents .....	1
Preface .....	7
References .....	9
Chapter 1 Hybrid drivelines .....	11
1.1 Planetary gearings .....	11
1.1.1 Operation's principle and functional characteristics .....	11
1.1.2 Relationships regarding the speeds .....	12
1.1.3 Transmitted torque and power distribution.....	13
1.1.4 Dynamic model of the planetary gear train.....	15
1.1.5 Complete drive train dynamic model .....	16
1.1.6 Model of losses in the planetary driveline .....	18
1.2 Automotive hybrid drivelines .....	22
1.2.1 Concept of hybrid vehicle drivetrain .....	22
1.2.2 Series hybrid drivetrain.....	23
1.2.3 Parallel Hybrid Drivetrains .....	24
1.2.4 Series/parallel Hybrid Drivetrains (power split driveline) .....	29
References .....	33
Chapter 2 Hybrid E-CVT power split driveline for tractors.....	35
2.1 Introduction.....	35
2.2 Concept of the e-CVT driveline.....	35
2.3 Case study.....	38
2.4 Operating modes overview .....	38
2.4.1 All electric traction mode.....	40
2.4.2 Hybrid CVT traction mode .....	40
2.4.3 Hybrid fixed ratio traction mode.....	44
2.5 The drivetrain control strategy.....	46
2.5.1 The ICE control system .....	47
2.5.2 The MG/1 machine control system .....	49
2.5.3 The MG/2 machine control system .....	49
2.6 Simulations .....	50
2.6.1 Simulation results .....	51

2.7	Conclusions.....	69
	References .....	70
Chapter 3 Hybrid e-CVT ship propulsion .....		71
3.1	Introduction.....	71
3.2	Concept of the HySP e-CVT driveline .....	72
3.3	Operating modes overview .....	74
3.3.1	Pure electric propulsion .....	74
3.3.2	Pure thermal propulsion.....	75
3.3.3	Hybrid mode.....	76
3.4	Case study: analysis of the operating limits .....	77
3.4.1	Propeller (CARRIER).....	77
3.4.2	Diesel Engine (RING) .....	78
3.4.3	Electrical machine (SUN).....	78
3.4.4	Choice of the planetary gear set .....	79
3.4.5	Operating limits of the driveline in Hybrid mode .....	81
3.5	The control algorithm.....	83
3.5.1	Layout of the control system.....	83
3.5.2	LEVEL 1: Sequence control .....	84
3.5.3	LEVEL 2: Determination of the speed references .....	86
3.5.4	LEVEL 3: Speed control loops .....	93
3.6	Simulations .....	94
3.6.1	Simulations (a) .....	95
3.6.2	Simulations (b) .....	103
3.6.3	Simulations (c) .....	111
3.7	Conclusions.....	116
	References .....	117
Chapter 4 Power split E-CVT driveline for WECS .....		119
4.1	Introduction.....	119
4.2	Description of the system .....	120
4.2.1	Wind turbine characteristic .....	120
4.2.2	E-CVT WECS mechanical configuration.....	123
4.2.3	E-CVT WECS electrical configuration .....	124
4.3	Design criteria .....	126
4.4	System modeling and control algorithm.....	129
4.4.1	Model of the system .....	129
4.4.2	Model of the control algorithm .....	131
4.5	Simulations .....	132
	Conclusions .....	142

References .....	143
Chapter 5 Experimental results .....	145
5.1 The experimental setup.....	145
5.1.1 The test bench .....	145
5.1.2 The lab scale E-CVT power split system.....	146
5.2 WT-CVT lab test: setting of the system.....	151
5.2.1 Scaling of the E-CVT system.....	151
5.2.2 Scaling of the turbine system .....	152
5.3 WT-CVT experimental results.....	154
5.3.2 Description of the tests .....	154
5.3.3 Test of (a) typology .....	156
5.3.4 Test of (b) typology .....	158
5.4 Conclusions.....	158
References .....	159



# Preface

The continuous increase of the global energy demand requires many questions to be faced by the human beings. Problems like the insecurity and exhausting of fossil fuels supply, the air pollution and the climate change trends introduce a lot of variables on the future of energy sources procurement. Furthermore the Western world is assisting to the high growth rate of the Far Eastern economies, like China and India, which are peopled by almost 1/3 of the world citizens, and are overcoming most of the western economies. The energy requirements of these new protagonists of the global economy are growing with a very high rate, and this trend is going to be stable or to increase further.

All of these considerations yields to a question: how to get a secure energy source provision, reducing environmental problems? The European answer after the Kyoto conference of the 1997 has been the 20-20-20 strategy, concerning in three goals to be respected within 2020:

- -20% of energy consumptions;
- -20% of greenhouse emissions;
- +20% of renewable energy production.

This policy is intended to limit the temperature growth within 2°C respect to the pre-industrial period.

Transportations, residential and commercial buildings, industrial production, are the three sector where focusing on energy saving.

One way to save energy is to avoid using it when it is unnecessary, adopting policies of sustainability, for example organizing towns for a bicycle or public transportation means based mobility.

Another way to save energy is to enhance the efficiency of the energy conversion devices, allowing fuel saving and a more environment-friendly energy production.

This thesis deals with the application of an electrical hybrid power line technology which has previously been widely applied in the automotive field: the series-parallel **power split e-CVT (electrical continuously variable transmission) device**.

Hybrid drivelines have been used since the birth of the automobile, where battery supplied electrical motors were used to enhance the performances of the early internal combustion engines, which had very low powers [1]. After the World War I the technical progress brought to powerful ICE (internal combustion engine) technologies, and the electrical assisted hybrid solutions were totally abandoned. Only in the last 35 years a new interest for hybrid electric vehicles has been discovered, thanks to the technological advances of electric machines driven by static power electronic converters, and to new and more performing energy storage devices (Lithium batteries, supercapacitors, fuel cells, etc.).

The continuously variable transmission is a technological solution applied on many vehicles, realized in various ways, by means of mechanical, hydro-static, hydro-dynamic, electric conversion systems. Its main feature is to change continuously the speed ratio between two shafts, avoiding the presence of shifting gears, clutches and torque converters, often very critical and inefficient drivelines components. In this Ph.D. work the e-CVT device has been conveniently applied on three particular fields:

- Terrestrial off-road vehicles;
- Marine ship propulsion;
- Wind energy conversion systems;

In Chapter 1 the hybrid drivelines technology applied to HEV is introduced, preceded by a mathematical introduction dedicated to the planetary gear transmission. The series, parallel and series-parallel hybrid solutions are presented, with advantages and drawbacks of each solution.

In Chapter 2 a novel power split transmission for agricultural tractors is presented. This solution can be conveniently applied to off-road vehicles, thanks to the improvement of the ICE torque rating, precise and smoothed control of the ground speed, pure electric propulsion and many further advantages. A case study of a 120 HP tractor propeller is presented, the possible operating modes are shown and the control system is described in detail. Finally numerical simulations show the dynamic and stationary behavior of the controlled system. A prototype of this tractor is now on construction with the support of LEMAD – DIE – Bologna laboratory.

In Chapter 3 a new concept of power line for Ship propellers is presented. The proposed power split e-CVT driveline can be introduced on an existing vessel replacing the ordinary gearbox. A detailed description of the control algorithm concept for this application is given, and dynamic numerical simulations show the all in one capability of the transmission to propel the vessel and to supply the on board electric system, or alternatively to exploit a pure electric propulsion for low speed operations.

In Chapter 4 the e-CVT power split transmission is applied to a wind energy conversion system. Wind power production is exploding worldwide, and its global electric production share is expected to grow up until 20% by 2030 [2], thus a secure grid connection of the wind turbines is necessary to keep a stable electrical system under grid faults or disturbances. The proposed concept allows to vary the turbine speed with a fixed generator speed, obtaining maximum efficiency and a flexible transmission which is capable to decouple the turbine shaft from the generator and avoid mechanical and electrical stresses in overload conditions (wind gusts and grid faults). The control system layout is presented, and the numerical simulations carried out to show these features on the examined 2 MW case study wind turbine.

Chapter 5 shows the LEMAD (Laboratory of electrical machines and drives) experimental test setup, and the experimental tests on a scale lab system of wind turbine equipped with power split driveline.

## References

- [1] G.Y. Ehsani M., Gao Y., e Ehmadi A., “Hybrid Electric Vehicles,” *Modern Electric, Hybrid Electric, and Fuel Cell Vehicles*, CRC Press, 2011, pagg. 123-150.
- [2] Global wind energy outlook 2010 (GWEC)



# Chapter 1

## Hybrid drivelines

### 1.1 Planetary gearings

#### 1.1.1 Operation's principle and functional characteristics

The planetary gearing represents the mechanical core of a CVT power-split device, allowing the redistribution of the power coming from an input shaft between two different paths. It is characterized by having three incoming shafts, carried by three different components of the gearbox.

Epicyclic gearing or planetary gearing consists of one or more outer gears, or *planet* gears, revolving about a central, or *sun* gear. Typically, the planet gears are mounted on a movable arm or *carrier* which itself may rotate relative to the sun gear. Epicyclic gearing systems also incorporate the use of an outer *ring* gear or *annulus*, which meshes with the planet gears. The axles of the intermediate gears can be parallel to the main shaft axle, in this case the gearing is called “flat”, otherwise it is called “spheric”. Generally both the configurations can be found in different applications; one of the most diffused applications of the spherical gear is the automotive differential.

Advantages of planetary gears over parallel axis gears include high power density, large reduction ratio in a small volume, multiple kinematic combinations, pure torsional reactions, and coaxial shafting. Disadvantages include high bearing loads, inaccessibility, and design complexity [1]. The planetary gearbox arrangement is an engineering design that offers many

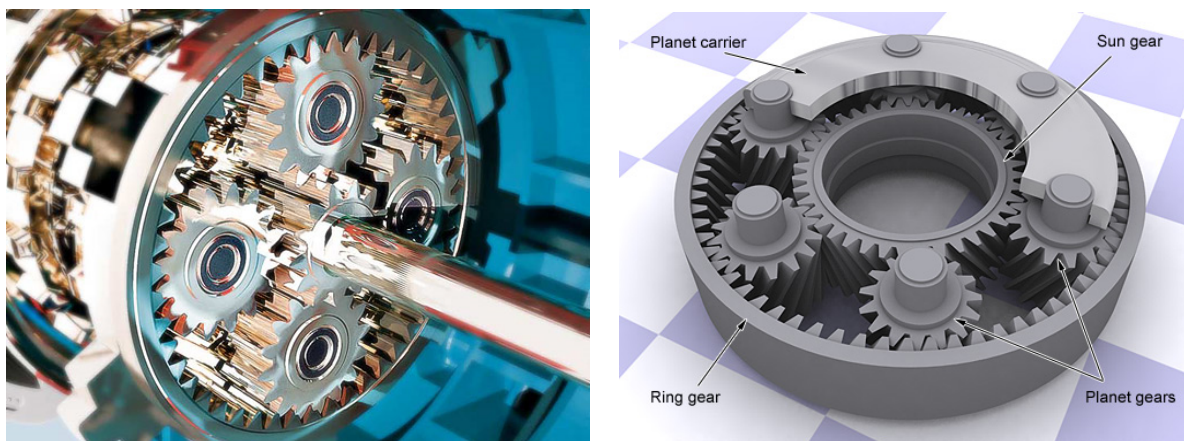


Fig. 1.1 – Planetary gear set layout

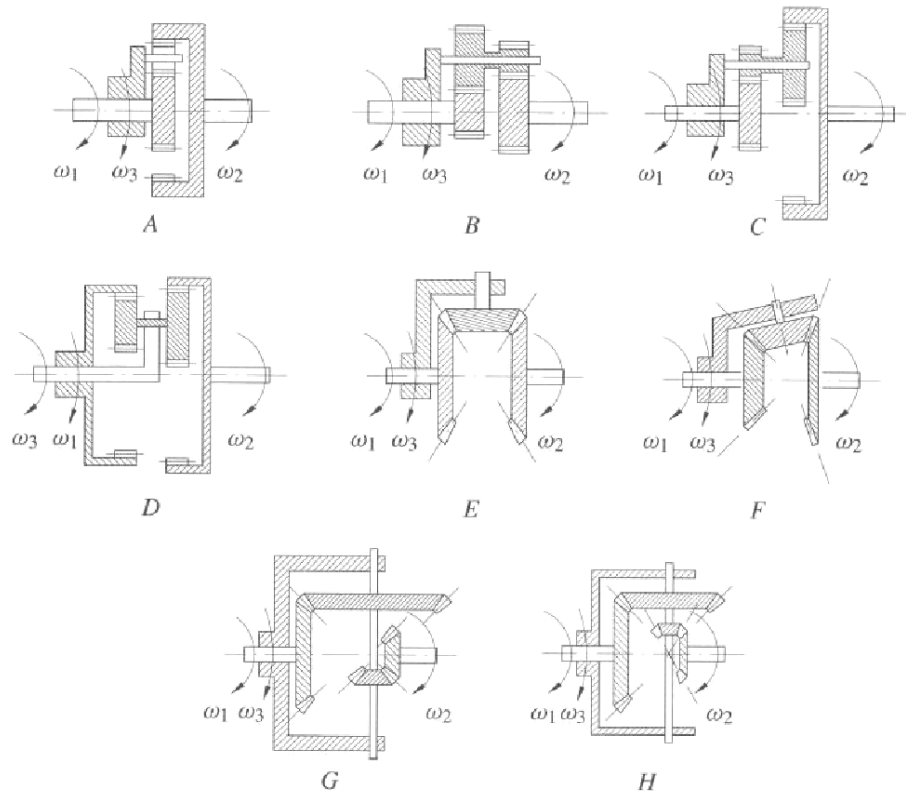


Fig. 1.2 – Planetary gearings in flat (A-D) and spheric (E-H) layouts

advantages over traditional gearbox arrangements. One advantage is its unique combination of both compactness and excellent power transmission efficiency. A typical efficiency loss in a planetary gearbox arrangement is only 3% per stage. This type of efficiency ensures that a very high share of the energy being input is transmitted through the gearbox. Another advantage of the planetary gearbox arrangement is load distribution. Since the load being transmitted is shared between multiple planets, torque capability is greatly increased. The more planets in the system, the greater load ability and the higher the torque density. The planetary gearbox arrangement also creates greater stability due to the even distribution of mass and increased rotational stiffness .

### 1.1.2 Relationships regarding the speeds

Generally, the relationships governing the speed ratios in a planetary geartrain are different from those valid for the ordinary gearbox. The fundamental parameter of the epicyclic gearbox is the geartrain fundamental ratio,  $\tau_0$ , defined as follows:

$$\tau_0 = -\frac{R}{S} \quad (1.1)$$

where:

$R$  is the number of teeth of the ring;

$S$  is the number of teeth of the sun;

Furthermore, since in general all the flat epicyclic gears have the same module, the condition of matching of the axes of the sun and ring implies the following relation between their teeth number and those of the satellites:

$$\mathbf{R} = \mathbf{S} + 2\mathbf{P} \quad (1.2)$$

where:

$\mathbf{P}$  is the number of teeth of the satellites.

The kinematic of a planetary gear, namely the determination of its transmission ratio, it's easy considering that its operation analysis is not affected by a change of reference frame, i.e. if the speeds are quantified with respect to a moving reference frame rather than a fixed one. Choosing the carrier speed as the speed of the new reference system, and referring the ring and sun speeds to this one, the following relationship can be written [2]:

$$\tau_0 = \frac{\omega_{SC}}{\omega_{RC}} = \frac{\omega_S - \omega_C}{\omega_R - \omega_C} = -\frac{\mathbf{R}}{\mathbf{S}} \quad (1.3)$$

where:

$\omega_R$  ring rotational speed;

$\omega_C$  carrier rotational speed;

$\omega_S$  sun rotational speed.

The fundamental speed ratio ( $\tau_0$ ) is a negative quantity and represents the sun/ring speed ratio when the carrier is stopped, and defines the relationship between the three wheels speeds. The *Willis formula* can be obtained by developing the (1.3)

$$\omega_C = \omega_S \left( \frac{1}{1 - \tau_0} \right) - \omega_R \left( \frac{\tau_0}{1 - \tau_0} \right) \quad (1.4)$$

### 1.1.3 Transmitted torque and power distribution

Assuming a unique positive sense for the torques acting on the three members of the gear set, e.g. the clockwise sense, the following relationships subsist (in steady state):

$$\mathbf{T}_R + \mathbf{T}_S + \mathbf{T}_C = 0 \quad (1.5)$$

$$\frac{\mathbf{T}_R}{\mathbf{T}_S} = \tau_0 \quad (1.6)$$

The eq. (1.5) means that, in steady state, the gear set is in equilibrium respect to its main axis, thus if no member is accelerating the resultant applied torque can only be zero. Eq (1.6) is rather justified by the theory of the ordinary gear trains: keeping the carrier stopped, the planetary gear train becomes an ordinary gear train, for which the speed ratio expressed by (1.3) is the reciprocal of the torque ratio, changed of sign.

By (1.5) and (1.6) it can be stated that, knowing one of the three torques and  $\tau_0$ , the remainders are determined, furthermore, if one of the three shafts has no torque applied, then no torque is transmittable, because the other two are null (at steady state). The over cited relationships are valid in ideal operation, then neglecting losses.

Combining conveniently (1.5) and (1.6), the relationships between carrier torque and sun and ring torques, for the specific  $\tau_0$ , are obtained:

$$\mathbf{T}_R = \mathbf{T}_C \frac{\tau_0}{1-\tau_0} \quad (1.7)$$

$$\mathbf{T}_S = -\mathbf{T}_C \frac{1}{1-\tau_0} \quad (1.8)$$

From (1.7) and (1.8) the equations of the power can be written, reminding that  $T=P/\omega$ :

$$\frac{\mathbf{P}_R}{\omega_R} = \frac{\mathbf{P}_C}{\omega_C} \frac{\tau_0}{1-\tau_0} \quad (1.9)$$

$$\frac{\mathbf{P}_S}{\omega_S} = \frac{\mathbf{P}_C}{\omega_C} \frac{1}{1-\tau_0} \quad (1.10)$$

Equations (1.7)-(1.10) have been written considering the same sign for the torque and the speed of the three wheels (Fig. 1.3).

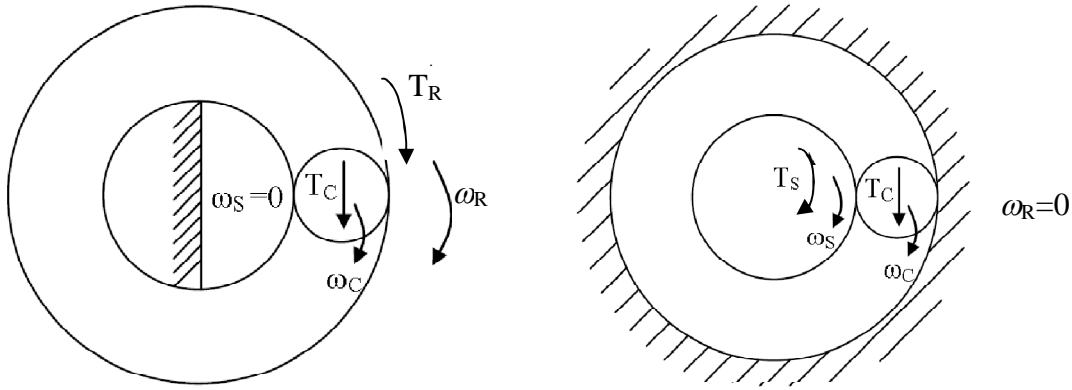


Fig. 1.3 – Torques and speeds of the planetary gear. a) SUN blocked. b) RING blocked.

Eq. (1.9) and (1.10) can be rewritten as:

$$\mathbf{P}_R = \mathbf{P}_C \frac{\omega_R}{\omega_C} \frac{\tau_0}{1-\tau_0} \quad (1.11)$$

$$\mathbf{P}_S = -\mathbf{P}_C \frac{\omega_S}{\omega_C} \frac{1}{1-\tau_0} \quad (1.12)$$

Applying the Willis formula (1.4) to (1.10) yields to the following:

$$\mathbf{P}_S = -\mathbf{P}_C \left[ 1 + \frac{\omega_R}{\omega_C} \frac{\tau_0}{1-\tau_0} \right] \quad (1.13)$$

which allows to introduce the *carrier base speed*, defined as the carrier speed at zero sun speed:

$$\omega_{C0} = -\frac{\tau_0}{1-\tau_0} \omega_R \quad (1.14)$$

Finally the power relationships become:

$$\mathbf{P}_R = -\frac{\omega_{C0}}{\omega_C} \mathbf{P}_C \quad (1.15)$$

$$\mathbf{P}_S = -\left(1 - \frac{\omega_{C0}}{\omega_C}\right) \mathbf{P}_C \quad (1.16)$$

The eq.(1.15) and (1.16) define the power flow depending on the carrier speed referred to the carrier base speed  $\omega_{C0}$ :

1. If  $\omega_C = \omega_{C0}$  the sun has zero speed ( $\omega_S = 0$ ), thus it develops no mechanical power, even if its reaction torque has a finite value, given by eq.(1.8). The power is entirely transferred from the carrier to the ring or vice-versa.
2. If  $\omega_C \leq \omega_{C0}$  the sun power is entering the gear train ( $P_S > 0$ ) if the carrier power is incoming ( $P_C > 0$ ), and it's outgoing the gear train ( $P_S < 0$ ) if the carrier power is leaving the gearbox ( $P_C < 0$ ). Generally the carrier power has the same sign of the sun power.
3. If  $\omega_C \geq \omega_{C0}$  sun and carrier powers have opposite signs.

#### 1.1.4 Dynamic model of the planetary gear train

Since now the equations of the planetary gear set have been referred to stationary conditions, in order to obtain the relationship between torques and speeds in steady state operation. In the current paragraph, the equations are developed to introduce non stationary operation of the gear set, thus accelerations and inertial effects.

Introducing the accelerations means that the torque equilibrium is no more respected, and the equations (1.7) and (1.8) become:

$$\mathbf{T}_R - \mathbf{T}_C \left( \frac{\tau_0}{1 - \tau_0} \right) = \mathbf{J}_R \dot{\omega}_R - \mathbf{J}_C \dot{\omega}_C \left( \frac{\tau_0}{1 - \tau_0} \right) \quad (1.17)$$

$$\mathbf{T}_R + \mathbf{T}_C \left( \frac{1}{1 - \tau_0} \right) = \mathbf{J}_S \dot{\omega}_S + \mathbf{J}_C \dot{\omega}_C \left( \frac{1}{1 - \tau_0} \right) \quad (1.18)$$

which can be written, underlying the ring and sun accelerations  $\dot{\omega}_R, \dot{\omega}_S$ , as:

$$\mathbf{T}_R - \mathbf{T}_C \left( \frac{\tau_0}{1 - \tau_0} \right) = \mathbf{J}_{RC} \dot{\omega}_R + \mathbf{J}'_C \dot{\omega}_S \quad (1.19)$$

$$\mathbf{T}_S + \mathbf{T}_C \left( \frac{1}{1 - \tau_0} \right) = \mathbf{J}'_C \dot{\omega}_R + \mathbf{J}_{SC} \dot{\omega}_S \quad (1.20)$$

where:

$$\mathbf{J}_{RC} = \mathbf{J}_R + \mathbf{J}_C \left( \frac{\tau_0}{1 - \tau_0} \right)^2 \quad (1.21)$$

$$\mathbf{J}_{SC} = \mathbf{J}_S + \mathbf{J}_C \left( \frac{1}{1 - \tau_0} \right)^2 \quad (1.22)$$

$$\mathbf{J}'_C = -\mathbf{J}_C \left( \frac{\tau_0}{1-\tau_0} \right)^2. \quad (1.23)$$

The equations set describing the dynamic operation of the planetary gear set is composed by eq. (1.4), (1.19) and (1.20).

The equations of the dynamic model have been rewritten in the state space form, as follows:

$$\begin{aligned} \mathbf{x}(t) &= \mathbf{A}\mathbf{x}(t) + \mathbf{B}\mathbf{u}(t) \\ \mathbf{y}(t) &= \mathbf{C}\mathbf{x}(t) + \mathbf{D}\mathbf{u}(t) \end{aligned} \quad (1.24)$$

where  $x(t), y(t)$  and  $u(t)$  are respectively the states array, the output array and the input array. For the planetary gear train system they have been defined as follows:

$$\begin{aligned} \mathbf{x}(t) &= [\omega_R(t), \omega_S(t)]^T \\ \mathbf{y}(t) &= [\omega_R(t), \omega_S(t), \omega_C(t)]^T \\ \mathbf{u}(t) &= [T_R(t), T_S(t), T_C(t)]^T \end{aligned} \quad (1.25)$$

Resolving the system of equations (1.4, 2.19, 2.20) yields to a particular expression of the matrices A, B, C, D:

$$\mathbf{A} = 0 \quad (1.26)$$

$$\mathbf{B} = \frac{1}{h} \begin{pmatrix} (1-\tau_0)^2 \mathbf{J}_{SC} & \tau_0 \mathbf{J}_C & -(1-\tau_0)\tau_0 \mathbf{J}_S \\ \tau_0 \mathbf{J}_C & (1-\tau_0)^2 \mathbf{J}_{RC} & (1-\tau_0) \mathbf{J}_S \end{pmatrix} \quad (1.27)$$

$$\mathbf{C} = \frac{1}{h} \begin{pmatrix} 1 & 0 \\ 0 & 1 \\ -\frac{\tau_0}{1-\tau_0} & \frac{1}{1-\tau_0} \end{pmatrix} \quad (1.28)$$

$$\mathbf{D} = 0 \quad (1.29)$$

where:

$$h = (1-\tau_0)^2 \mathbf{J}_A \mathbf{J}_S + \mathbf{J}_C (\mathbf{J}_A + \tau_0^2 \mathbf{J}_S) \quad (1.30)$$

So far an ideal model has been examined, and it doesn't deal with the torsional and dissipative effects of the main shaft and gearings. In the following paragraphs these aspects will be treated.

### 1.1.5 Complete drive train dynamic model

In fig. 2.2 a complete scheme of the planetary geared driveline is represented. To get a general model, usable in different applications, the following elements have been considered:

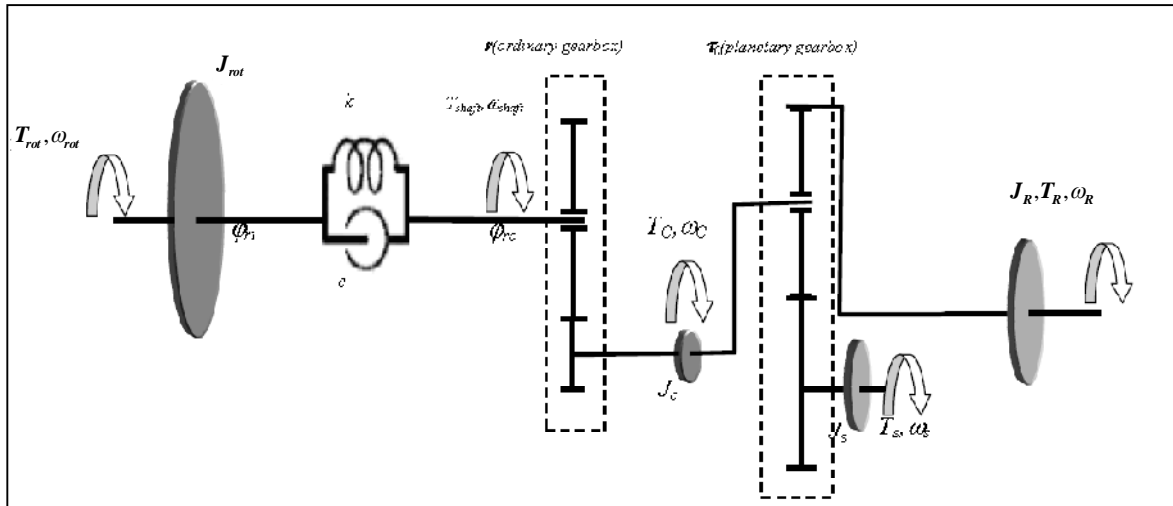


Fig. 1.4 – Scheme of the complete E-CVT transmission model

- An ordinary gearbox placed on the carrier side of the transmission.
- A flexible low speed shaft coupled to the ordinary gearbox primary wheel.
- A stiff high speed shaft coupled to the carrier of a planetary gear set.
- A stiff shaft coupled to the ring side.
- A stiff shaft coupled to the sun wheel.

In this formulation the torsional effect of the carrier shaft has been considered, while the shafts connected at the ring and at the sun are considered completely stiff.

The preceding assumptions allow to write the following expression for the torque transmitted at the high speed side of the ordinary gearbox:

$$T_{shaft} = k(\varphi_{ri} - \varphi_{ro}) + c\left(\omega_{rot} - \frac{\omega_c}{r}\right) \quad (1.31)$$

where:

$r$  = transmission ratio of the ordinary multiplier;

$\omega_{rot}$  = low speed shaft speed;

$\omega_c$  = carrier speed;

$k$  =rotational stiffness constant low speed shaft;

$c$  =rotational damping constant low speed shaft;

The dynamic equation at the low speed shaft is represented as

$$T_{rot} - T_{shaft} = J_{rot} \dot{\omega}_{rot} \quad (1.32)$$

where  $J_{rot}$  is the inertia at the low speed shaft and  $T_{rot}$  its applied torque. The equations (1.31) and (1.32) describe the dynamic of the low speed shaft. The new set of equations, related to the model of Fig. 1.4, are resumed below:

$$\omega_c = \omega_s \left( \frac{1}{1 - \tau_0} \right) - \omega_R \left( \frac{\tau_0}{1 - \tau_0} \right) \quad (1.33)$$

$$\mathbf{T}_R - \mathbf{T}_C \left( \frac{\tau_0}{1 - \tau_0} \right) = \mathbf{J}_{RC} \dot{\omega}_R + \mathbf{J}'_C \dot{\omega}_S \quad (1.34)$$

$$\mathbf{T}_S + \mathbf{T}_C \left( \frac{1}{1 - \tau_0} \right) = \mathbf{J}'_C \dot{\omega}_R + \mathbf{J}_{SC} \dot{\omega}_S \quad (1.35)$$

$$T_r - T_{shaft} = J_r \dot{\omega}_r \quad (1.36)$$

$$T_C = \frac{T_{shaft}}{r} = k(\varphi_{ri} - \varphi_{ro}) + c \left( \omega_p - \frac{\omega_C}{r} \right) \quad (1.37)$$

### 1.1.6 Model of losses in the planetary driveline

The stationary equations of the planetary gear train must be modified in order to keep in account the power losses for friction between the tooth of the gears.

The efficiency of the planetary gearbox at carrier zero speed is defined as:

$$\eta_0 = -\frac{T_R \omega_R}{T_S \omega_S} = -\frac{T_R}{\tau_0 T_S} \quad (1.38)$$

where symbols have already been defined.

Since the power direction is variable (from sun to ring or from ring to sun), it is necessary to correct the eq. (1.38) as shown below [3]:

$$\eta_0^K = -\frac{T_R}{\tau_0 T_S} \quad (1.39)$$

where:

$$K = \text{sign}[T_S(\omega_S - \omega_C)] \quad (1.40)$$

can assume only the values 1, -1 or 0. This coefficient represents the sign of the power transmitted from the sun wheel to the carrier wheel, and it's fundamental to determine the direction of the power flow.

The torque expressions (1.7) and (1.8) become:

$$\mathbf{T}_R = \mathbf{T}_C \frac{\tau_0 \eta_0^K}{1 - \tau_0 \eta_0^K} \quad (1.41)$$

$$\mathbf{T}_S = -\mathbf{T}_C \frac{1}{1 - \tau_0 \eta_0^K} \quad (1.42)$$

Similarly to the ideal case it's possible to obtain the power equations:

$$\mathbf{P}_R = \mathbf{P}_C \frac{\omega_R}{\omega_C} \frac{\tau_0 \eta_0^K}{1 - \tau_0 \eta_0^K} \quad (1.43)$$

$$\mathbf{P}_S = -\mathbf{P}_C \frac{\omega_S}{\omega_C} \frac{1}{1 - \tau_0 \eta_0^K} = \mathbf{P}_C \left( \frac{1 - \tau_0}{1 - \tau_0 \eta_0^K} + \frac{\tau_0}{1 - \tau_0 \eta_0^K} \frac{\omega_R}{\omega_C} \right) \quad (1.44)$$

By developing the eq. (1.43) and (1.44) the expression of the geartrain efficiency can be obtained in the different operation fields of the driveline.

The carrier base speed has been defined by the (1.14), and it can be used to define the operational regions of the epicyclic driveline, in terms of exchanged power and efficiency of the transmission. This quantity identify the operation of the gear set with blocked sun.

Another particular condition is verified when the three wheels are rotating at the same speed:

$$\omega_C = \omega_R = \omega_S \quad (1.45)$$

The carrier and sun speeds can be written as follows:

$$\omega_C = \alpha \omega_{C0} = \alpha \left( -\frac{\tau_0}{1-\tau_0} \right) \omega_R \quad (1.46)$$

$$\omega_S = \tau_0 (1-\alpha) \omega_R \quad (1.47)$$

The parameter  $\alpha$  defines the carrier speed in relation to the carrier base speed, and makes possible the determination of the gearbox efficiency varying the carrier speed at a fixed ring speed  $\omega_R > 0$  (rotating in the “positive” direction) :

1.  $\alpha \leq 0$  In this case the carrier speed is counter rotating respect to the positive rotating direction. The sun speed is negative ( $\omega_S < 0$ ), and two cases are possible, depending on the torque:
  - 1.a  $T_R > 0$   $T_C < 0$  The mechanical power flows from the carrier and the ring towards the sun.
  - 1.b  $T_R < 0$   $T_C > 0$  The mechanical power flows from the sun and the ring towards the carrier.
2.  $0 < \alpha \leq 1$  In this case the carrier speed is rotating in the positive rotating direction. The sun speed is negative ( $\omega_S < 0$ ) or zero when  $\alpha=1$ , and two cases are possible, depending on the torque:
  - 2.a  $T_R > 0$   $T_C < 0$  The mechanical power flows from the ring towards the sun and the carrier.
  - 2.b  $T_R < 0$   $T_C > 0$  The mechanical power flows from the carrier and the sun towards the ring.
3.  $1 < \alpha \leq \frac{\tau_0 - 1}{\tau_0}$  In this case the carrier speed is rotating in the positive rotating direction. The sun speed is positive ( $\omega_S > 0$ ), and two cases are possible, depending on the torque:
  - 3.a  $T_A > 0$   $T_C < 0$  The mechanical power flows from the ring and the sun towards the carrier.
  - 3.b  $T_A < 0$   $T_C > 0$  The mechanical power flows from the carrier towards the sun and the ring.

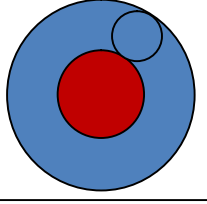
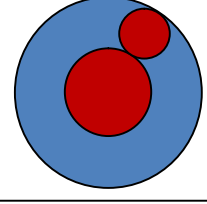
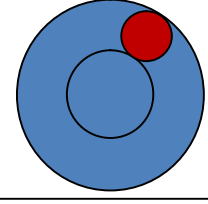
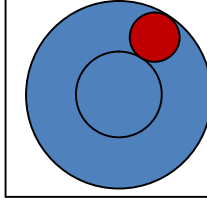
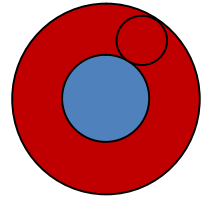
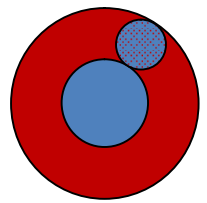
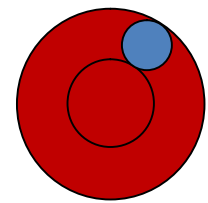
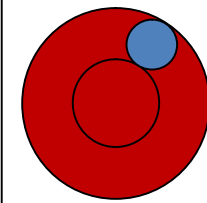
When  $\alpha = \frac{\tau_0 - 1}{\tau_0}$ , the carrier, ring and sun wheels have the same speed, and this is

the condition of 100% efficiency, due to no frictional effects between the teeth.

4.  $\alpha > \frac{\tau_0 - 1}{\tau_0}$  The power flow is the same as case 3, but the relative speed sun-carrier is now positive, and this determines a change in the K coefficient (cfr. eq. 1.40).

The table 1 reports all the possible operating way of the transmission described above, for a fixed ring speed, and for different conditions of torque and carrier speed. The various colors indicate the power flow, as indicated below:

- RED: power incoming in the wheel
- BLUE: power outgoing from the wheel

	$\omega_c < 0$	$0 < \omega_c < \omega_{c0}$	$\omega_{c0} < \omega_c < \alpha\omega_{c0}$	$\omega_c > \alpha\omega_{c0}$
$T_C > 0$ $T_R < 0$				
	$\omega_s < 0; T_s < 0$ $\omega_R > 0$ $K = 1$ $\eta = \frac{P_C + P_R}{P_S}$	$\omega_s < 0; T_s < 0$ $\omega_R > 0$ $K = 1$ $\eta = \frac{P_R}{P_S + P_C}$	$\omega_s > 0; T_s < 0$ $\omega_R > 0$ $K = 1$ $\eta = \frac{P_R + P_S}{P_C}$	$\omega_s > 0; T_s < 0$ $\omega_R > 0$ $K = -1$ $\eta = \frac{P_R + P_S}{P_C}$
$T_C < 0$ $T_R > 0$				
	$\omega_s < 0; T_s > 0$ $\omega_R > 0$ $K = -1$ $\eta = \frac{P_S}{P_C + P_R}$	$\omega_s < 0; T_s > 0$ $\omega_R > 0$ $K = -1$ $\eta = \frac{P_S + P_C}{P_R}$	$\omega_s > 0; T_s > 0$ $\omega_R > 0$ $K = -1$ $\eta = \frac{P_C}{P_R + P_S}$	$\omega_s > 0; T_s > 0$ $\omega_R > 0$ $K = 1$ $\eta = \frac{P_C}{P_R + P_S}$

Tab. 1.1 – Operating conditions and efficiencies of the planetary gear set for  $\omega_R > 0$

When the ring part rotates in the opposite direction ( $\omega_R < 0$ ), the same considerations can be done, and the operation of the gear train is dual.

Applying the (1.43) and (1.44) at the cases represented in Tab. 1.1 yields to a representation of the driveline efficiency in the carrier speed/ring speed system of coordinates (Fig. 1.5). In Fig. 1.5 the efficiency map is shown, where the four areas described before are delimited by dashed lines.

Observing the diagram of *Fig. 1.5* it's possible to identify the line where the efficiency is maximum (right dashed line), which corresponds to the operation at  $\omega_c = \alpha\omega_{c0}$ , thus each of the three wheels have the same speed.

The middle dashed line represents the  $\omega_s = 0$  operation, where the planetary gear set as an ordinary gear train between carrier and ring shafts.

The left dashed line represent the case  $\omega_c = 0$ , and this is the case where the efficiency match with the characteristic efficiency ( $\eta_0=0,95$  in this case), the lowest possible, because corresponds to the maximum frictional effects on the gear set.

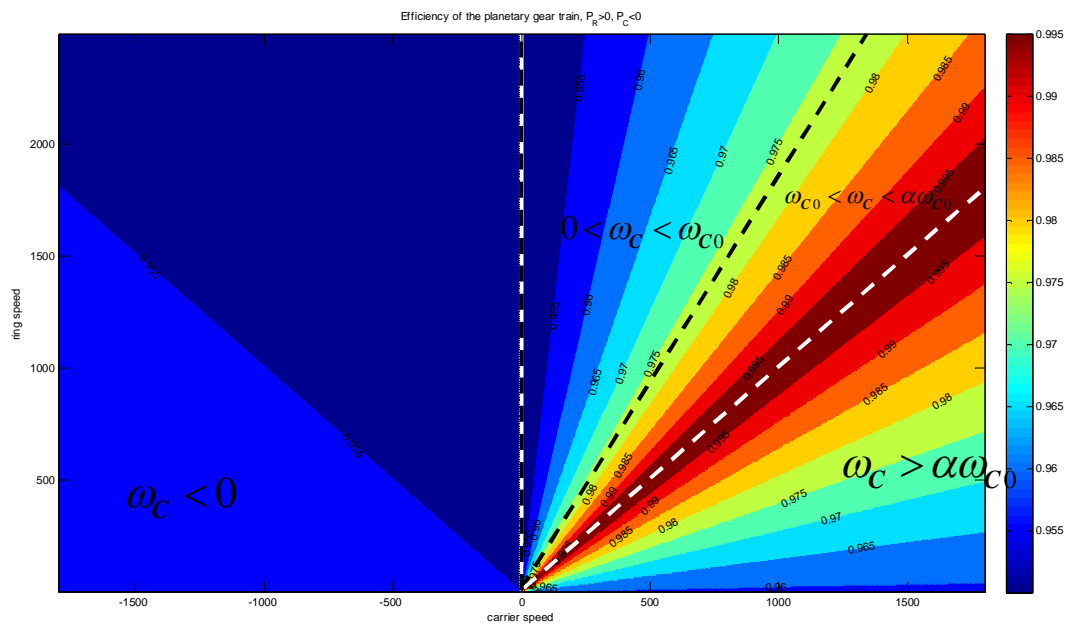


*Fig. 1.5 – Efficiency map of the planetary gearing ( $\eta_0=0,95$ ,  $\tau_0=-4,49$ )*

## 1.2 Automotive hybrid drivelines

### 1.2.1 Concept of hybrid vehicle drivetrain

Any vehicle powertrain is essentially required to:

- develop sufficient power to meet the demands of vehicle performance;
- hold a sufficient energy storage on-board to supply the vehicle along the given range;
- have a high efficiency;
- emit few environmental pollutants.

Generally, a vehicle may have more than one energy source and energy converter (power source), such as gasoline/diesel-IC engine system, hydrogen-fuel cell-electric motor system, and chemical battery-electric motor system.

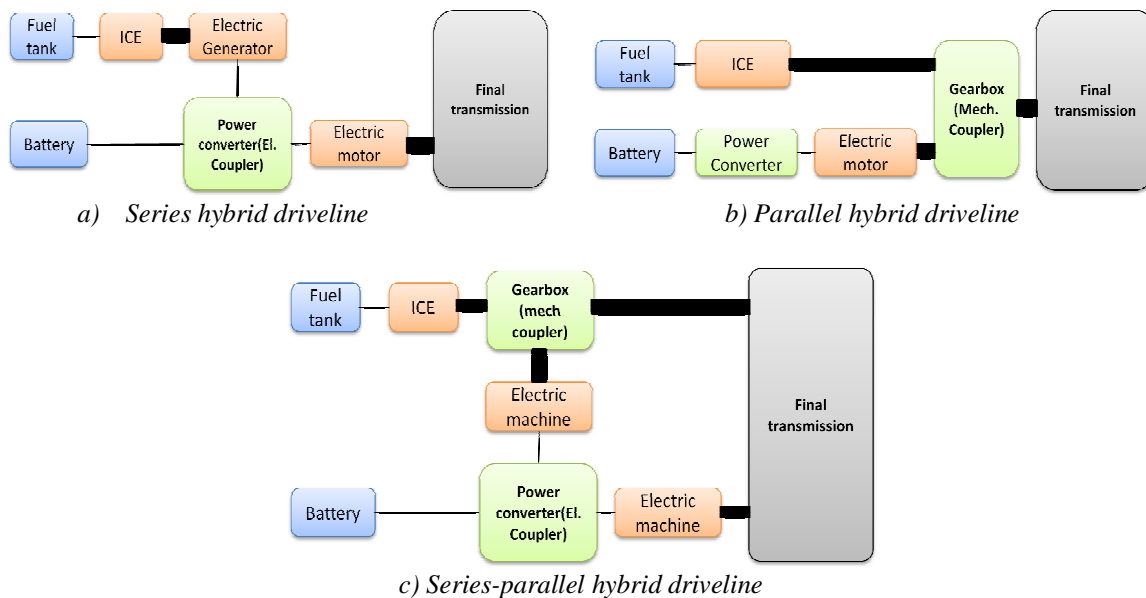


Fig. 1.6 – Classification of HEV

A hybrid vehicle drivetrain consists of two power sources. One is the primary power source and the other is the secondary power source. In order to recover part of the braking energy, hybrid drivetrain has at least one bidirectional energy source, usually an electrochemical storage system. Currently, fossil fuel IC engines are the first choice for the primary power source.

The architecture of a hybrid vehicle is approximately defined as the connection between the components defining the energy flow paths and control ports. Traditionally, HEVs were classified into two basic types: series and parallel. In the last 15 years, some newly introduced HEVs could not be classified into these kinds ; hereby, HEVs may currently be classified into three kinds [4]:

1. *Series hybrid;*
2. *Parallel hybrid;*
3. *Series-parallel hybrid.*

which are functionally shown in *Fig. 1.6*. In *Fig. 1.6*, a fuel tank-ICE and a battery-electric motor are taken as the examples of the primary power source (steady power source) and secondary power source (dynamic power source), respectively. Of course, the IC engine can be replaced by other types of power sources, such as fuel cells. Similarly, the batteries can be replaced by ultracapacitors, flywheels, or their combinations.

### 1.2.2 Series hybrid drivetrain

In a series hybrid drivetrain, two power sources feed a single electric machine that propels the vehicle, as shown in *Fig. 1.7* [4]. The typical primary power source is an ICE coupled to an electric generator. The output of the electric generator is connected to an electric power bus through an electronic converter (AC/DC). The secondary power source is a battery pack, which is connected to a DC link by means of a second power converter (DC/DC). The electric power bus is connected to the inverter supplying the electric traction motor. The traction motor can be controlled either as a motor or a generator, and either in forward or reverse motion. This configuration may include a battery charger to charge the batteries by wall plug-in from the power grid.

Series hybrid electric drivelines potentially have the following operation modes :

1. *Only electric mode*: The engine is turned off and the vehicle is propelled only from the batteries.
2. *Only ICE mode*: The vehicle traction power only comes from the ICE-generator, while the batteries do not exchange power with the drivetrain. The electric machines provide an electric transmission from the engine to the driven wheels.
3. *Hybrid mode*: The traction power is drawn from both the engine-generator and the batteries.
  - i. *Engine traction and battery charging mode*: The ICE-generator supplies power to charge the batteries and to propel the vehicle.

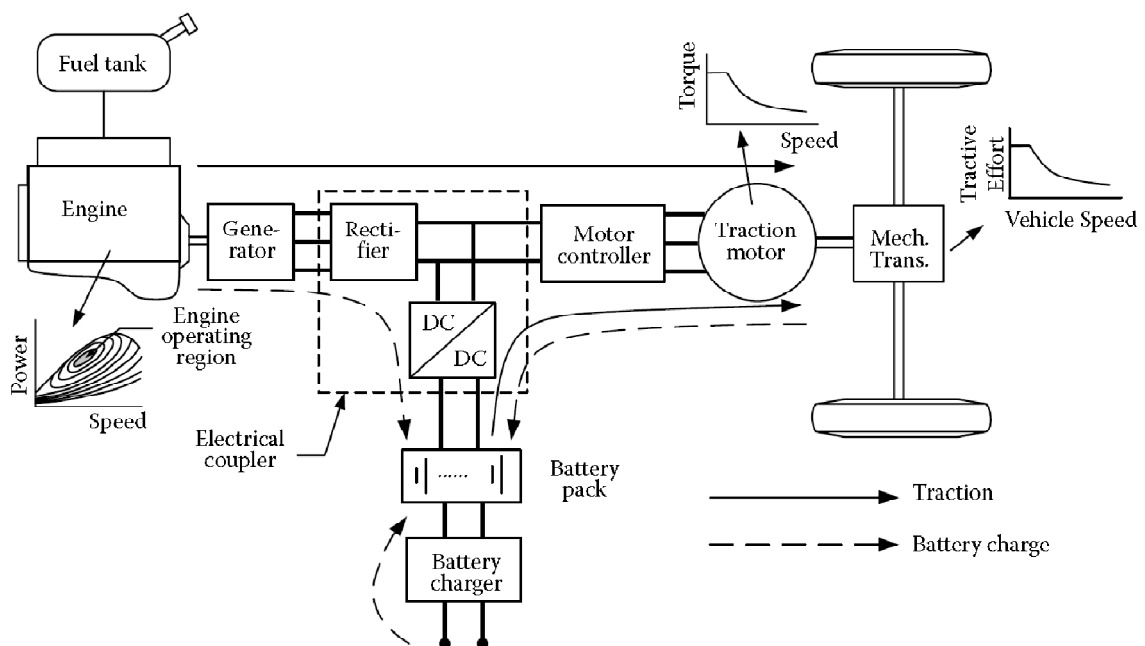


*Fig. 1.7 – Series hybrid drivetrain*

- ii. *Hybrid battery charging mode*: Both the engine-generator and the traction motor operate as generators to charge the batteries.
4. *Regenerative braking mode*: The gen-set is turned off and the traction motor is operated as a generator. The power generated is used to charge the batteries.
5. *Pure battery charging mode*: The traction motor receives no power and the engine-generator charges the batteries.

Series hybrid drivetrains offer several advantages:

1. The engine is fully mechanical decoupled from the driven wheels. Thus, it can be operated at any point on its speed-torque characteristic map. As a result, it can be potentially operated always within its maximum efficiency region as shown in *Fig. 1.7*. The efficiency and emissions of the engine can be further improved by optimal design and control in this narrow region, which is much easier and allows greater improvements than an optimization across the entire range. Furthermore, the mechanical decoupling of the engine from the driven wheels allows the use of a high-speed prime mover, such as gas turbines or with slow dynamics, like the Stirling engine.
2. Since electric motors have almost-ideal torque-speed characteristics, they do not need multi-gear transmissions. Therefore, the manufacturing is greatly simplified and the costs are reduced. Furthermore, instead of using one motor and a differential gear, two motors may be used, each powering a single wheel (all-wheel drive). This provides speed decoupling between the two wheels like a differential but also acts as a limited slip differential for traction control purposes.
3. Simple control strategies may be used as a result from the mechanical decoupling provided by the electrical transmission.

However, series hybrid electric drivetrains have some drawbacks:

1. The energy from the engine is converted twice, thus the losses may be significant.
2. The whole machines complex must be sized for the maximum power required, increasing cost and size of the transmission.
3. The traction motor must be sized for maximum torque requirement since it is the only propelling device.

### 1.2.3 Parallel Hybrid Drivetrains

While series hybrid drivetrain couples primary and secondary power sources together electrically, a parallel hybrid drivetrain couples them together mechanically; the engine supplies its power mechanically to the wheels like in a conventional fuel powered vehicle. It is assisted by an electric motor that is mechanically coupled to the transmission. The powers of the engine and electric motor are coupled together as shown in *Fig. 1.6(b)*, and this gives rise to several different architectures, in particular torque coupling and speed coupling [4].

#### Parallel hybrid drivetrains with torque coupling

In the torque coupling configuration, the torques of the engine and electric motor are added together in a mechanical torque coupler. *Fig. 1.8* conceptually shows a mechanical

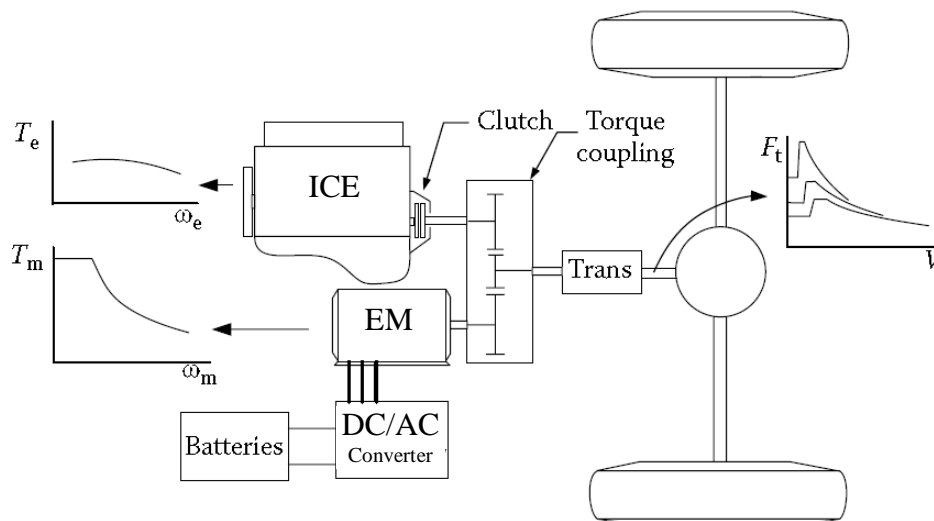


Fig. 1.8 –Parallel hybrid drivetrain (two shafts)

torque coupler, which has two input shafts (one is from the ICE, one is from the electric machine EM) and one output to a mechanical transmission.

If losses are ignored, the output torque and speed can be described by:

$$T_{out} = k_1 T_{in1} + k_2 T_{in2} \quad (1.48)$$

and

$$\omega_{out} = \frac{\omega_{in1}}{k_1} = \frac{\omega_{in2}}{k_2} \quad (1.49)$$

where  $k_1$  and  $k_2$  are the constants determined by the parameters of torque-coupling device. In the torque coupling configuration, the resulting torque at the output shaft is a linear combination of the input torques, while the speeds are related by fixed ratios.

The simplest architecture of the torque-coupled parallel hybrid drivetrain is the *single-shaft configuration*, where the rotor of the electric machine functions as the torque coupler ( $k_1=1$  and  $k_2=1$  in equations (1.48-49)), as shown in Fig. 1.9. A transmission may be placed between either the electric motor and drive shaft (“pre-transmission”, Fig. 1.9.a), or the engine and the electric motor (“post-transmission”, Fig. 1.9.b).

In the “pre-transmission” configuration, both the engine torque and motor torque are adapted by the transmission. The engine and motor must have the same speed range. This

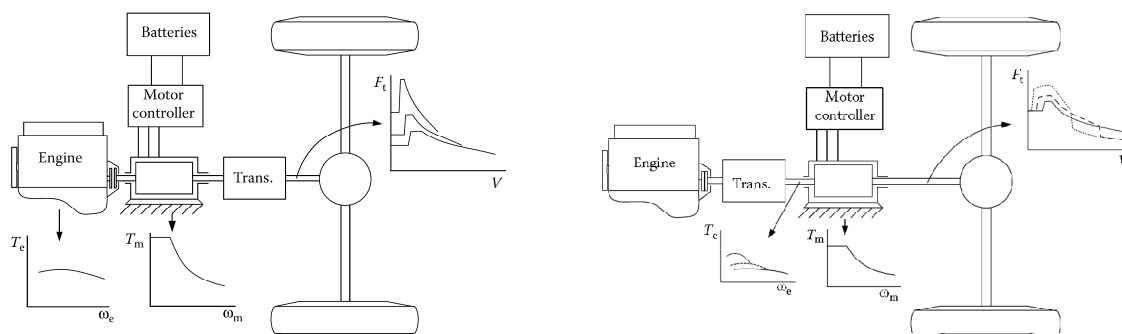


Fig. 1.9 –Parallel hybrid drivetrain- torque coupling – single shaft  
a. Before transmission b. After transmission

configuration is usually applied in the **mild hybrid drivetrains**, in which the electric drive functions as an engine starter, electrical generator (starter-alternator), engine power assistant, and regenerative brake. A recent example of this configuration is the *Honda Insight's* powertrain, which is equipped with a 13 kW electric motor on the main 98 hp ICE shaft [5]

In the post-transmission configuration as shown in *Fig. 1.9.b*, the transmission only modifies the engine torque while the motor torque is directly delivered to the driven wheels. This configuration may be used in the drivetrain where a large electric motor with a long constant power region is employed. The transmission is only used to change the engine operating points to improve the vehicle performance and engine operating efficiency. It should be noted that the batteries cannot be charged from the engine by running the electric motor as a generator when the vehicle is on standstill because the motor is rigidly connected to the driven wheels.

Another torque-coupling parallel hybrid drivetrain is the separated axle architecture, in which one axle is powered by the engine and another powered by the electric motor. The separated axle architecture offers some of the advantages of a conventional vehicle. It keeps the original engine and transmission unaltered and adds an electrical traction system on the other axle. It also is four-wheel-drive, which optimizes traction on slippery roads and reduces the tractive effort on a single tire. On the other hand, the electric machines and the eventual differential gear system take a lot of space and may reduce the payload volume. This problem may be solved if the ICE transmission is single-gear and the electric machine is replaced by two small-size electric machines placed within two driven wheels. It's worthy to note that the batteries cannot be charged from the engine when the vehicle is at standstill.

Parallel hybrid drivetrain with speed coupling

The power from two sources may be combined by coupling their speeds. A speed coupling device can be described by the following equations (the subscripts 1,2 and out indicates respectively the input shafts and the output shaft):

$$\omega_{out} = k_1\omega_{in1} + k_2\omega_{in2} \tag{1.50}$$

and:

$$T_{out} = \frac{T_{in1}}{k_1} = \frac{T_{in2}}{k_2} \tag{1.51}$$

where  $k_1$  and  $k_2$  are constants depending on the design of the speed coupling device.

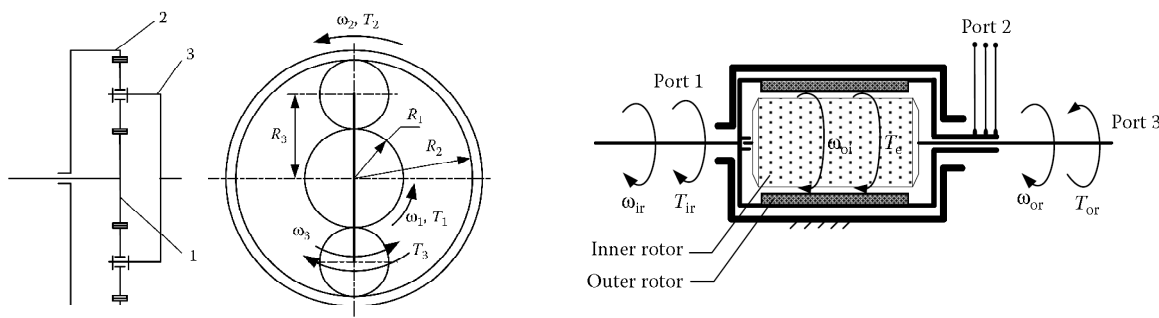


*Fig. 1.10 –Parallel hybrid drivetrain- speed coupling  
a. With planetary gear set b. With transmotor*

Figure 3.13 shows two typical speed couplers: One is a planetary gear unit and the other is an electric motor with a floating stator (called transmotor in this book).

The **planetary gear-set** unit has been described in detail in par. 1.1, and is the core of the e-CVT (electrical continuously variable transmission) power split device. As an example, comparing eq. 1.50 with eq. 1.4 (Willis formula), the following relationships can be written:

$$\begin{aligned}\omega_{out} &= \omega_C \\ \omega_1 &= \omega_R \\ \omega_2 &= \omega_S\end{aligned}\tag{1.52}$$

And the parameters  $k_1$  and  $k_2$  assume the values:

$$\begin{aligned}k_1 &= -\frac{\tau_0}{1-\tau_0} \\ k_2 &= \frac{1}{1-\tau_0}\end{aligned}\tag{1.53}$$

Another interesting device in speed coupling is the **electric transmotor**, in which the stator, generally fixed to a stationary frame, is released as a power-input port (floating stator). The other two ports are the rotor and the airgap, through which the electric power is converted into mechanical. The motor speed is intended to be the relative speed of the rotor to the stator. The torque on the stator and rotor is always the same (in steady state operation) and results in the constants  $k_1 = 1$  and  $k_2 = 1$ .

Similarly to the torque-coupling device, the speed-coupling units can be used to constitute various hybrid drive trains. *Fig. 1.11* and *Fig. 1.12* show two examples of hybrid drive trains with speed coupling using a planetary gear unit and an electric transmotor [4]. In *Fig. 1.11*, the engine supplies its power to the sun gear through a clutch and transmission. The transmission is used to modify the speed–torque profile of the engine so as to match the traction requirements. The electric machine supplies its power to the ring gear through a pair of gears. Lock 1 and lock 2 are used to lock the sun gear and ring gear to the stationary frame of the vehicle in order to implement different operation modes. The following operating

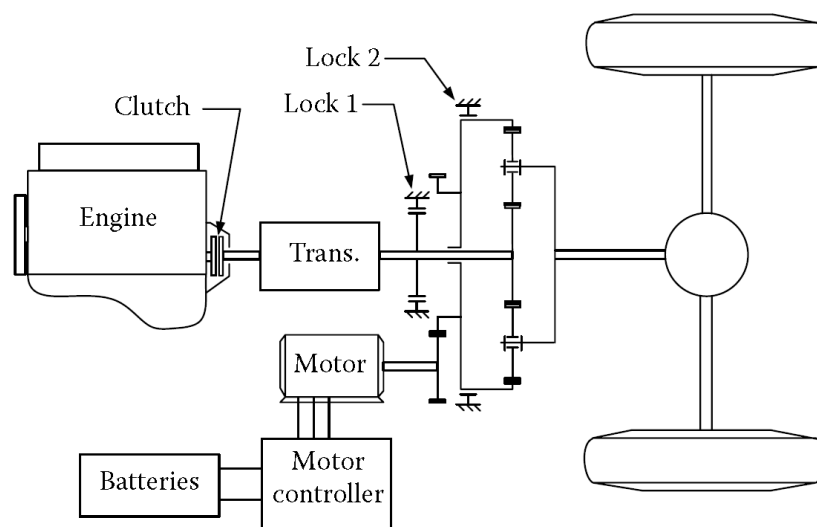


*Fig. 1.11 –Parallel hybrid driveline - speed coupling with planetary gear*

modes can be obtained:

1. *ICE pure traction*: When lock 2 locks the ring gear to the vehicle frame and lock 1 is released, the engine alone supplies power to the driven wheels.
2. *Electric pure traction*: When lock 1 engage the sun gear to the vehicle frame (engine is shut off and engine clutch is disengaged) and lock 2 is released, only the electric motor supplies its power to the driven wheels.
3. *Hybrid traction*: When lock 1 and lock 2 are released (the sun gear and ring gear can rotate), both the engine and electric machine supply positive speed and torque (positive power) to the driven wheels.
4. *Regenerative braking*: The states of lock 1 and lock 2 are the same as in motor-alone traction, the engine is also shut off, the engine clutch is disengaged, and the electric machine is controlled in regenerating mode (negative torque). The kinetic energy of the vehicle can be absorbed by the electric system.
5. *Battery charging from the engine*: The engine clutch and lock 1 and lock 2 are in the same state as in the hybrid traction mode. However, the electric motor is controlled to rotate in the opposite direction, negative speed. Thus, the electric machine operates with positive torque and negative speed (negative power) and absorbs energy from the engine and delivers it to the batteries. In this case, the engine power is split into two parts by decomposing its speed.

The drive train transmotor-based as shown in *Fig. 1.12*, has a similar structure as that in *Fig. 1.11*. Lock 1 and clutch 2 are used to lock the outer rotor to the vehicle frame and the outer rotor to the inner rotor, respectively. This drive train can perform all the operation modes mentioned above.

The main advantage of the hybrid drive train with speed coupling is that the speed of two power plants is decoupled from vehicle speed. Therefore, the speed of both power plants can be chosen freely. This advantage is important for efficiency of prime movers like the Stirling engine and the gas turbine engine, which are more speed-sensitive than torque-sensitive.

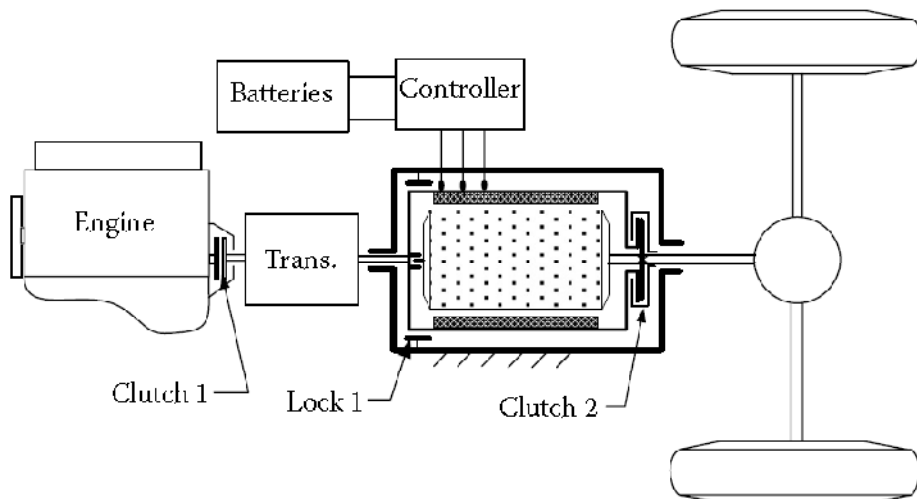


*Fig. 1.12 –Parallel hybrid driveline - speed coupling with transmotor*

### 1.2.4 Series/parallel Hybrid Drivetrains (power split driveline)

#### *Single mode power split driveline (input power split)*

Among full hybrid drivetrains, power split solutions are now considered a trade-off between sizing of the components (engine, electric machines, mechanical parts of the transmission) and performances. Regardless of the implementation, this solution requires two electric machines to be coupled each other, with the engine and with the differential gearbox.

The best known example is the system developed and implemented in the Toyota Prius by Toyota Motor Company (HSD, Hybrid synergy drive) [6]. Another drive line system of the input power split type is the Ford Hybrid System (FHS) [7].

This drive train type is schematically illustrated in *Fig. 1.13*. A planetary gear unit is used as the speed-coupling device and a set of fixed axle gears as the torque-coupling device. An IC engine is connected to the carrier of the planetary gear unit, and a small motor/generator (MG/1) is connected to the sun gear to obtain the speed-coupling configuration. The ring gear is connected to the driven wheels through an axle-fixed gear unit (torque coupler). Meanwhile, a traction motor (MG/2) is also connected to the fixed axle gear unit to constitute the torque-coupling configuration.

From Equation 5.11, the rotational speed of the ring gear or gear  $R$ , which is proportional to vehicle speed, is related to the rotational speed of the engine (carrier) and of the motor/generator (sun) and is expressed as

$$\omega_R = \frac{1-\tau_0}{\tau_0} \omega_{ICE} + \tau_0 \omega_{MG1} \quad (1.54)$$

where  $\tau_0$  is the gear ratio defined by eq. 1.1 and  $\omega_{ICE}$  and  $\omega_{MG1}$  are the rotational speeds of the engine and motor/generator, respectively. The load torque, acting on the ring gear of the planetary gear unit by final gear, is related to the engine torque and the motor/generator torque by:

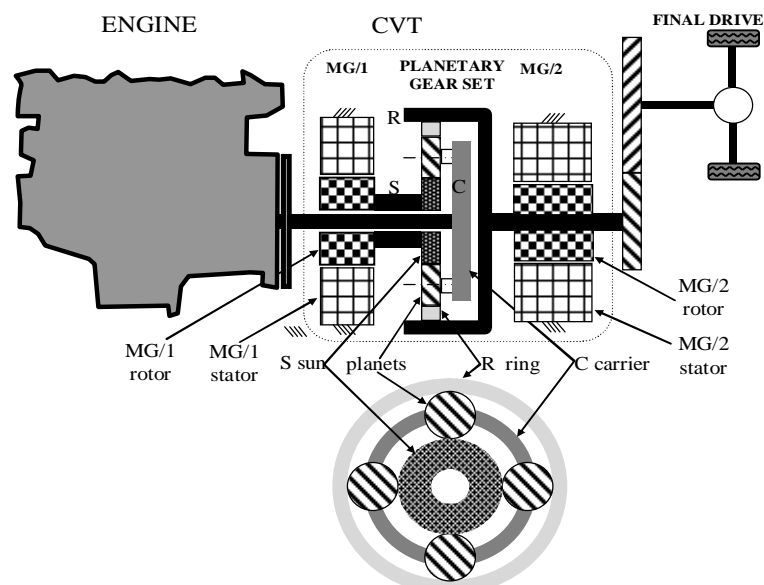


*Fig. 1.13 – Scheme of the input power split e-CVT*

$$\mathbf{T}_R = \frac{\tau_0}{1 - \tau_0} \mathbf{T}_{ICE} = -\tau_0 \mathbf{T}_{MG1} \quad (1.55)$$

Eq.(1.55) indicates that the torque acting on the sun gear, supplied by the motor/generator has opposite direction to engine torque and same direction as load torque on the ring gear ( $\tau_0 < 0$ ). With low vehicle speed (small  $\omega_R$ ) and a medium engine speed (larger than its idle speed), the motor/generator has to rotate in the positive direction (same direction as engine speed). In this condition, the motor/generator operates with a negative power, thus generating. The power of the engine is split into two parts: one part goes to the motor/generator and the other to the differential through the ring gear. This is how the drivetrain gets its name of **power-split e-CVT (electrical continuously variable transmission) hybrid drive train**. However, at high vehicle speed, while trying to maintain the engine speed below a given speed, for high engine operating efficiency, the motor/generator may be operated in negative speed, that is, rotating in the opposite direction of engine speed. In this case, the motor/generator delivers positive power to the planetary gear unit, that is, motoring. It becomes clear through the above analysis that the main function of a motor/generator is to control engine speed, therefore decoupling engine speed from wheel speed. The traction motor adds additional torque to the torque output from the ring gear of the planetary gear unit with a torque-coupling mode through the output gear, by which the engine torque is decoupled from the vehicle load. This transmission operates as a CVT, since the power that is fed electrically from one machine to another change the torque-speed operating point of the ICE, without delivering or drawing power. Of course the power balance is not always zero, e.g. in the pure electric and battery charging operations.

Another solution to obtain a power split device is shown in *Fig. 1.14*. This drive train is functionally very similar to the e-CVT drive train shown in *Fig. 1.13*, and is called **electrical variable transmission (EVT)**.

The EVT was conceived 75 years ago [8]: in this system the power-split effect is obtained by means of the combination of two electric machines[9]. Induction machines are usually proposed for this application. The first machine is coupled to the engine at the stator, which is rotating and supplied through slip rings by a first inverter. The rotor of this machine

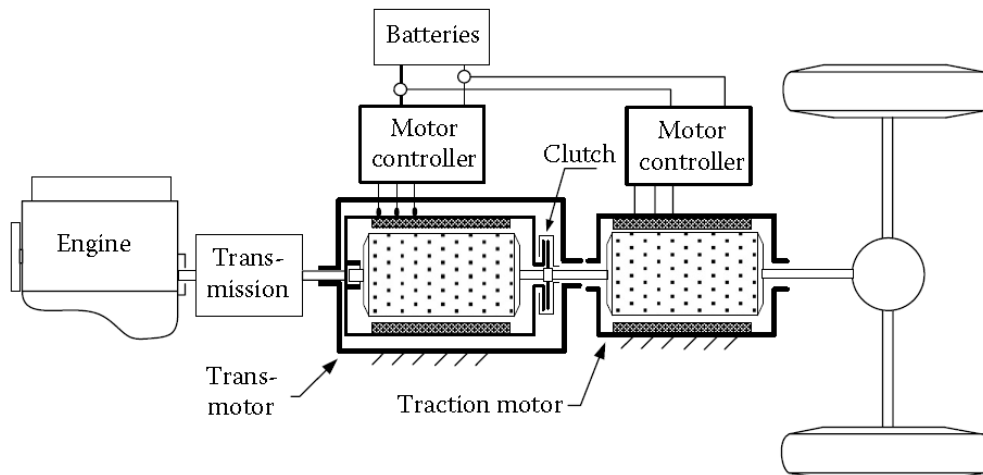


*Fig. 1.14 – Scheme of the input power split e-CVT with trans motor (EVT)*

is directly coupled to the rotor of the second machine, which stator is stationary and supplied by a second inverter connected at the same DC-bus. The output shaft is taken from the two-part rotor, often called inter-rotor. In this solution, the power from the engine to the wheels is split in the ‘direct’ fraction through the electromagnetic coupling at the air-gap of the machine and the ‘converted’ fraction through an electric path constituted by the electric machines and power electronics.

A great advantage of the EVT is the wide range of the speed regulation that can be obtained between the engine and the wheels. The main drawback of the EVT is the high torque sizing of the electric machines which must be sized for the engine maximum torque, leading to high volume and weight.

In the EVT, the two electric machines may be arranged concentrically [14] without using of mechanical gearing. Optimized solutions, with a very thin and saturated interrotor [15] or with PM machines [16] instead of induction machines have been proposed with the aim to reduce size and weight of the transmission.

#### Dual mode power split driveline (compound power split)

Beside the input power split e-CVT, there are several more complex solutions, based on the use of at least two epicyclical gear trains and one or more locking system. These solution can be classified as **compound type power split** such as the solution developed by Allison [17], Timken [18], Renault [19], Toyota [20], [21] and by the GM/Daimler/BMW joint project called Global Hybrid Cooperation [22].

In the second planetary gear unit (*Fig. 1.15*), one element (i.e the ring gear) can be kept stopped, or can be connected to one gear of input power split (i.e the sun gear and then the G/M1). This reconfiguration of the transmission is done through the use of mechanical clutches or hydraulic brakes. These devices are without slippage, and then are inexpensive and without losses. The two possible configurations of the second power split define the two operation modes of the transmission: low-range mode and high range mode.

*Low range mode:* R2 is stopped, the transmission is configured as the HSD (single

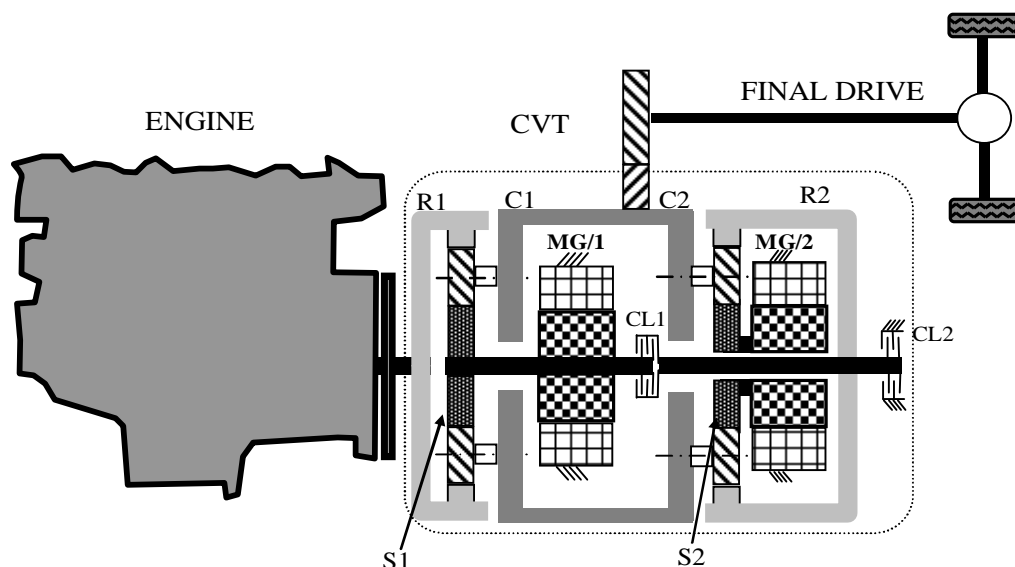


Fig. 1.15 – Scheme of compound power split e-CVT

mode, input split), with the second planetary gear set operating as ordinary gearing with a reduction ratio between S2 and C2 which multiplies the torque applied to the final drive. This mode allows maximum torque at the wheels and then best performance at low speed, combining the ICE and MG/2 torques in an output parallel torque coupling system.

*High range mode:* R2 rotates as S1 and MG/1. The second planetary gear set operates as true power split device and then both planetary gear sets are power split devices. MG/1 speed defines the differential ratio of both the power splits. The output torque at the final drive also contains the contribution of both the differentials. In this way, high operating speed for the final drive at decreasing torque can be obtained, due to the fact that the machine MG/2 can be slowed down by the second power split device, and thus its torque capability increased.

This solution yields to a minimum sizing of the electric components, and applies satisfactory torque level at the final drive both at low and high speed range, but is characterized by a relevant complexity of the mechanical layout. These solutions seem more suitable to be applied to heavier vehicles as big luxury cars, SUV (Sport Utility Vehicles) or trucks, than to small passenger cars. The performance now reached with these systems defines a benchmark for full hybrid drive-train future developments.

## References

- [1] Lynwander, P., 1983, Gear Drive Systems: Design and Application. Marcel Dekk
- [2] Smith, J. D., 1983, Gears and Their Vibration: A Basic Approach to Understand
- [3] Funaioli Ettore - Maggiore Alberto - Meneghetti Umberto, “Lezioni di meccanica applicata alle macchine”
- [4] X. Zhao e P. MaiBer, “A novel power splitting drive train for variable speed wind power generators,” *Renewable Energy*, vol. 28, Ott. 2003, pagg. 2001-2011.
- [5] G.Y. Ehsani M., Gao Y., e Ehmadi A., “Hybrid Electric Vehicles,” *Modern Electric, Hybrid Electric, and Fuel Cell Vehicles*, CRC Press, 2011, pagg. 123-150.
- [6] 2011 Honda Insight Hybrid - Specifications - Official Honda Site
- [7] S. Sasaki “Toyota's newly developed hybrid powertrain” Proc. of the 10th International Symposium on Power Semiconductor Devices and ICs, 1998. IEEE-ISPSD 98. Kyoto (JP) Jun 03-06 1998.
- [8] J. Yamaguchi, “Project G21 to Prius,” SAE Automotive Engineering International, March 2004, pp. 42-44\par
- [9] J. M. Miller “Hybrid electric vehicle propulsion system architectures of the e-CVT type” IEEE Transaction on Power Electronics, Vol. 21, No. 3, May 2006, page(s) 756-767.
- [10] J.M. Miller, P.J. McCleer, M. Everett, “Comparative assessment of ultra-capacitors and advanced battery energy storage systems in PowerSplit electronic-CVT vehicle powertrains” Proc. of IEEE International Conference on Electric Machines and Drives, IEEE-ICEM 2005 May 15-18 2005 page(s): 1513 - 1520 San Antonio, TX (USA).\par
- [11] K. Hefel, “Electric transmission gearing,” U.K. Patent 461 306, Jan. 1935..”
- [12] S. Eriksson and C. Sadarangani, “A four-quadrant hev drive system,” in Proc. 56th IEEE VTC—Fall, 2002, vol. 3, pp. 1510–1514.
- [13] F. Shibata, “Electric control system of an electric machine arrangement combining electromagnetic coupling with electric rotating machine,” U.S. Patent 3 789 281, Jan. 29, 1974.
- [14] M.J. [Hoeijmakers](#), J.A. [Ferreira](#) “The Electric Variable Transmission” [IEEE Transactions on Industry Applications](#), Publication Date: July-Aug. 2006 Vol. 42, [Issue 4](#) page(s): 1092 – 1100. ISSN : 0093-9994
- [15] G. T. Rodenhuis “Dynamoelectric gear,” EP Patent 1 154 551 A2, Jan. 2000.
- [16] E. Nordlund, P. Thelin, and C. Sadarangani “Four-quadrant energy transducer for hybrid electric vehicles,” in Proc. 15th ICEM, Brugge, Belgium, Aug. 25–28, 2002, CD-ROM.
- [17] G. Holmes and M. R. Schmidt, “Hybrid Electric Powertrain Including a Two-Mode Electrically Variable Transmission,” U.S. Patent 6 478 705 B1, Nov. 12, 2002.X. Ai
- [18] T. Mohr, and S. Anderson, “An electro-mechanical infinitely variable speed transmission,” presented at the Proc. SAE Congress Expo, 2004.
- [19] Villeneuve, “Dual mode electric infinitely variable transmission,” in Proc. SAE TOPTECH Meeting Continuously Variable Transm., 2004, pp. 1–11.
- [20] T. M. Grewe, B. M. Conlon, A. G. Holmes "[Defining the General Motors 2-Mode Hybrid Transmission](#)". [SAE Technical Paper Series](#) (SAE 2007-01-0273).
- [21] K.Muta, M. Yamazaki, J. Tokieda, “Development of New-Generation Hybrid System THS II – Drastic Improvement of Power Performance and Fuel Economy”, SAE Paper Number 2004-01-0064.
- [22] Kimura, I. Ando, K. Itagaki, “Development of Hybrid System for SUV”, SAE Paper Number 2005-01-0273.



---

# Chapter 2

## Hybrid E-CVT power split driveline for tractors

### 2.1 Introduction

This chapter presents a novel concept of power split transmission for off-road vehicles in the 100 HP range. It's based on the concept of e-CVT power split driveline of the input split type (presented in par. 1.2.4). The CVT concept has been considered in recent periods and applied in certain solutions, mainly equipped with hydrostatic actuators, and the research has been focused mainly on the control system performances over hardly irregular terrains [1]-[3].

A continuously variable transmission of electric type, similar to the HSD concept (*Fig. 1.13*) could introduce new important features and functionalities in the world of tractors. The developed transmission concept presents the following advantages over the classical solutions:

- Operation of the thermal engine on the maximum efficiency point;
- Possibility of pure electric propulsion at low power;
- Smoothed and fine speed regulation, by electrical machines control, particularly indicated for the so called “precision farming”;
- Utilization of a high speed, low torque commercial engine, cheaper and easy to gather on the market;
- Power over-boost by the electrical machines exploiting;
- Possibility of high vehicle speed obtained by a selectable high fixed ratio.

The operating modes of the transmission will be presented, and some simulations will be shown, to point out the main features of this newly introduced hybrid driveline concept.

### 2.2 Concept of the e-CVT driveline

The developed traction system is conceptually a variable structure hybrid driveline, based on a e-CVT system of the input power split type () and on two fixed ratio engine/wheels (for the highest speeds) selectable by appropriate clutches and brake devices.

As a tractor is equipped with a power-take-off device, directly driven by the combustion engine (by mean of a fixed ratio), and a selectable 4WD transmission.

The simplified mechanical layout is shown in *Fig. 2.1*, where the core of the system is focused. The following elements can be identified:

- **Internal combustion engine.** A high speed Diesel motor can be used, since the engine should not be sized for the maximum tractive effort, but just for the maximum required output power. This decreased torque capability reduces the on board dedicated space for the engine, with the possibility to introduce a very efficient variable speed cooling system, between the ICE and the driver cabinet.
- **E-CVT power split transmission,** composed by a planetary gearset with two electrical machines coupled. *Fig. 2.1* shows the mechanical layout of the E-CVT system, based on a concentric arrangement of the two electrical machines. The internal machine MG/1 on the sun wheel has an internal rotor structure, and is supplied by a four quadrant totally controlled inverter. Its control strategy has been conceived to adapt the required output speed to the engine goal speed, following the Willis relation (1.4).  
The external machine MG/2, on the ring wheel, has an external rotor structure, allowing the constitution of a single inter-stator shared by the two machines. It is also supplied by inverter, and it is controlled in order to adapt the required output torque to the ICE optimal working point; it is also requested to yield the most dynamic output torque requirements, and to regenerate the braking power.
- **The ICE shaft,** connected to the transmission of the vehicle and to the PTO device for supplying the working tools associated to the tractor. The main shaft supplies its power also to the hydraulic pumps of the auxiliaries and the remote tools, and the lubrication pumps. The ICE shaft is coupled to the planetary gear-train carrier.
- **The PTO mechanical port,** commanded by the engine shaft. It is the drive system for the agricultural working tools.
- **Clutches and selectors:**
  - *CL1* is the ICE clutch, which enables the power transmission from the engine to the transmission. Without ICE the all-electric drive is possible.
  - *B1* allows to block the sun shaft, imposing a fixed ratio between ICE and CVT

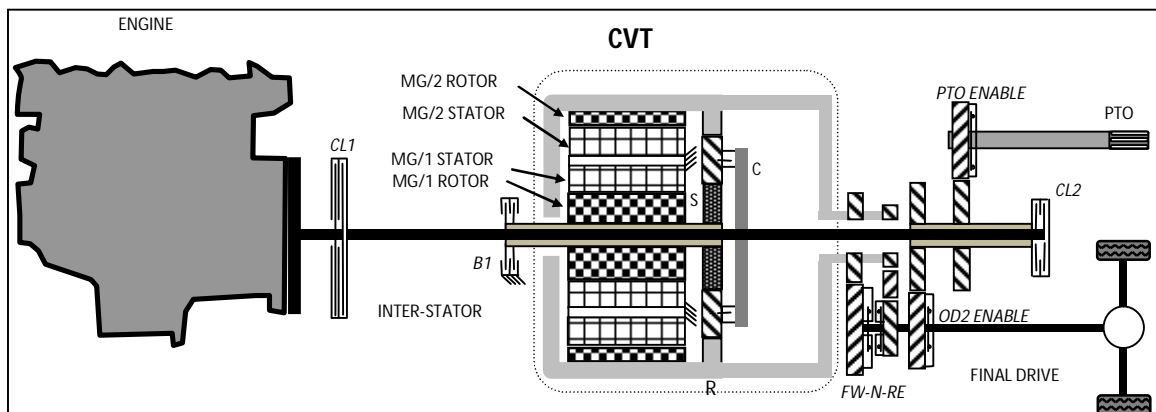


*Fig. 2.1- Conceptual scheme of a power split drive for tractor propulsion*



## 2.3 Case study

The case study considered in this chapter is a 120 HP rated power propeller equipped with a power split transmission based on a planetary gear set and two 25 kW rated power electrical machines.

- **IC Engine:** The Diesel engine is a 1,6 l FIAT MULTIJET 16 V 120 HP of brand new generation (2009), equipped with a variable geometry turbine and intercooler (Fig. 2.3).
- **Internal electrical machine M/G1** is a 4 quadrant inverter driven brushless AC machine, with a 80 Nm rated torque developed until a 3000 rpm rated speed. This machine is able to be controlled at constant power until 6000 rpm. The machine torque sizing has been chosen to match the ICE torque, in order to transmit the prime mover torque on steady state operation and in the dynamic phases.
- The **external machine M/G2** is a fully controlled induction machine, almost of the same power as the internal machine (27 kW 110 V) but developing a 220 Nm torque until 1160 rpm, and with a constant power region up to 6000 rpm. It is sized for developing a high driving torque on the output transmission, particularly at low speed.

## 2.4 Operating modes overview

The structure of the transmission has been conceived to operate the vehicle with the maximum flexibility and efficiency. The aim of the project is to realize a complete CVT transmission with the minimum size of the machines and with the finest controllability of the ICE performance and the vehicle speed.

Referring to fig. 3.1, the transmission layout can be changed by controlling the state of the following selectors:

	<b>FIAT 1,6 MULTIJET VGT 16V 120HP</b>	
	Displacement	1,6 l
	Bore x stroke	79,5 x 80,5 mm
	Weight	151 kg
	Max torque	300 Nm @ 1500 rpm
	Max power	87 kW @ 4000 rpm
	Intercooler and variable geometry turbine	
	EURO 5	

Fig. 2.3- The 1,6 120 HP Diesel engine

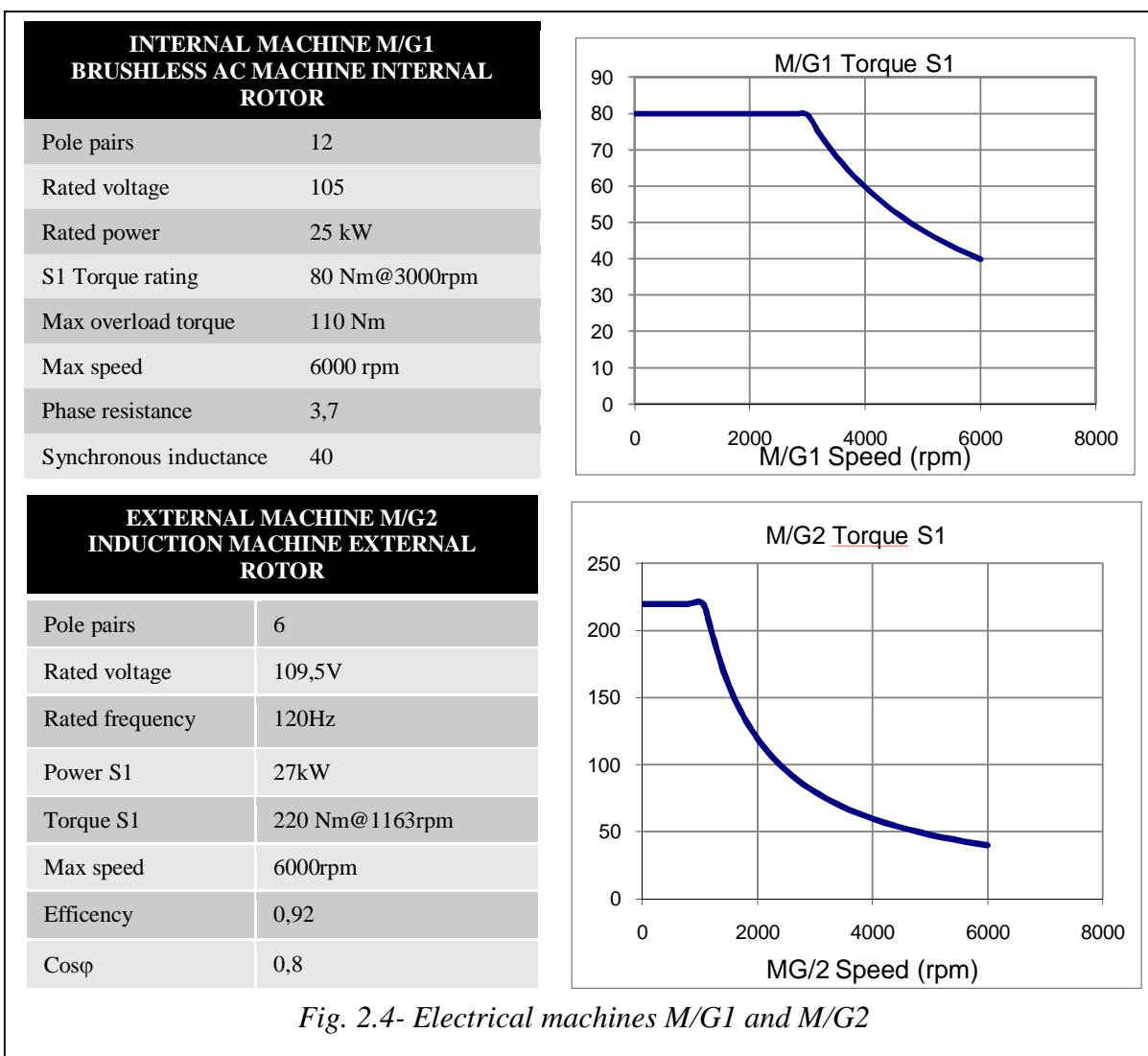


Fig. 2.4- Electrical machines M/G1 and M/G2

- *CL1*;
- *CL2*;
- *B1*;
- *FW-N-RE*;
- *OD2 ENABLE*;
- *PTO ENABLE*.

Among the different operating modes of the tractors, the following configuration can be distinguished:

**1. All electric traction mode;**

**2. Hybrid CVT traction mode:**

- ICE start-up;
- ICE optimal operation;
- ICE speed control by operator;
- PTO mode;
- Reverse way;

**3. Hybrid fixed ratio:**

- Over-drive 1;
- Over-drive 2;

A description of the different configurations will be given, focusing the relationship between torques and speeds in stationary conditions. The field of application of each driving mode in the maneuvering of the vehicle will be explained.

#### 2.4.1 All electric traction mode

The vehicle can be conducted for a short way with a pure electric propulsion, using the external electrical machine (M/G 2) as the main propeller, decoupling the ICE and keeping the M/G 1 machine stopped. Referring to *Fig. 2.1*, the following settings are applied:

<i>CL1</i>	<b>OPEN</b>
<i>CL2</i>	<b>OPEN</b>
<i>B1</i>	<b>CLOSED</b>
<i>FW-N-RE</i>	<b>FW</b>
<i>OD2</i>	<b>OPEN</b>
<i>PTO</i>	<b>OPEN</b>

*Tab. 2.1- All electric propulsion mechanical configuration*

The maximum output power in this case is limited by the external machine rated power, while the mileage is very low, depending on the battery pack sizing.

The principal features of this conduction phase are:

- High maneuverability and fine control of the ground speed;
- No pollutants emissions.

#### 2.4.2 Hybrid CVT traction mode

In the 90% of the working time, the tractor is controlled in the hybrid mode, with a synergy of control between ICE and electrical machines which allows the best performance for the whole system. The operator has two possible choices:

- The control system optimizes the working point of the Diesel Engine, deciding periodically its speed and torque employing, while the driver sets the ground speed setpoint.
- The driver set both the Diesel speed and the ground speed. This case is typical of the PTO operation, where the driver decide the PTO shaft speed.

#### ICE start-up

When the engine is started, the clutch C1 is kept open, the main shaft and the CVT are idle. Once the engine is launched to its minimum speed, the clutch C1 is released, and the ground speed setpoint (gs0) signal is enabled and fixed to zero. The CVT control system regulates the sun speed to keep the ring (output) speed equal to 0 (zero speed).

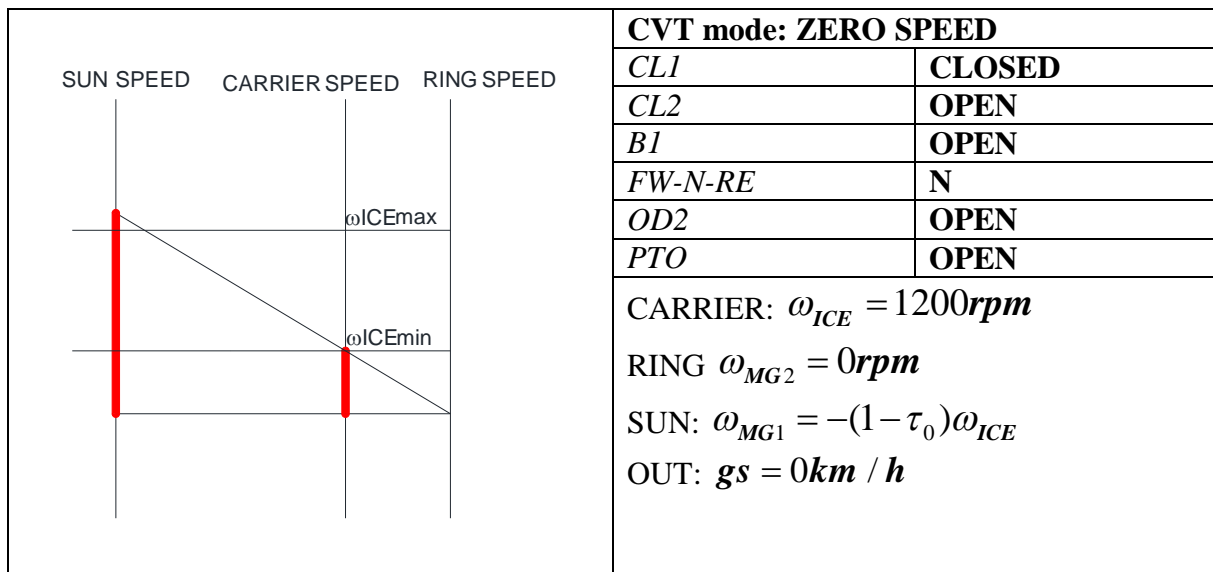


Fig. 2.6 - Zero speed ICE start-up: monogram, speed relationships and mechanical configuration

### ICE optimal operation

This operating mode is described by the Fig. 2.5 configuration. When the ICE is operated in its optimal operating point, it means that its torque is kept in the interval 70-80% of the maximum torque at the operating speed (Fig. 2.8). The control system checks at every cycle time the torque utilization of the engine, and adapt the working point to make it laying between the two red lines of Fig. 2.8. When the maximum power is required by the driver, the engine is operated to yield the maximum power, and thus the maximum available torque. The control system, in strongly dynamic conditions, such as fast accelerations, can increase the engine torque demand above the efficiency limit, in order to enhance the vehicle dynamic.

At low speeds the engine is maintained minimum, and the ground speed setpoint is

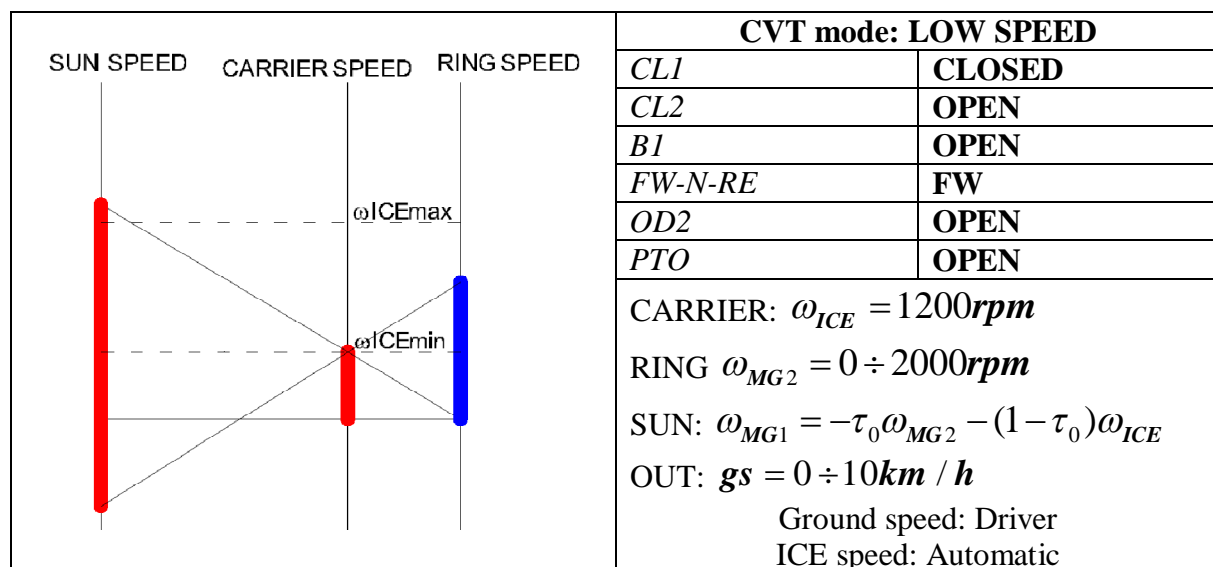


Fig. 2.5 – CVT mode, low output speed, cinematic nomogram, speed relationships and mechanical configuration

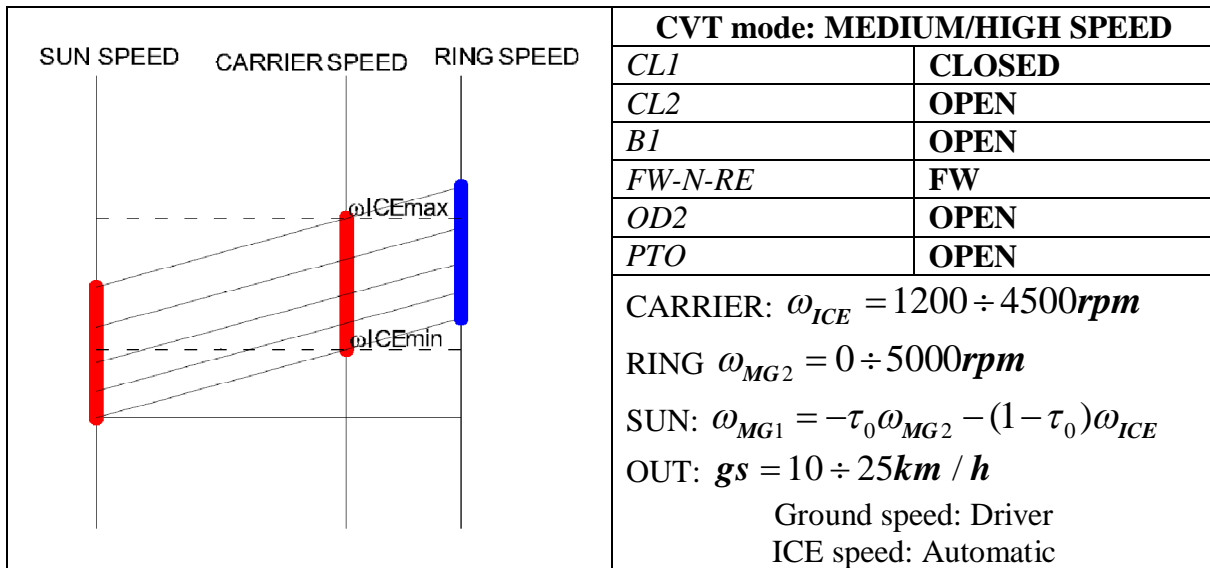


Fig. 2.7 – CVT mode, medium/high output speed, cinematic nomogram, speed relationships and mechanical configuration

satisfied by regulating the speed of the sun machine, behaving as a motor or as a generator. This field of operation is represented by the nomogram of Fig. 2.5, where the sun speed is varied, fixing the speed of the ICE (carrier), to change the output speed. As the sun speed increase, its torque is no longer enough to transmit the engine required torque, and the ICE speed is increased by the control, which takes care of the engine efficiency as well.

In the nomogram of Fig. 2.7, the output (ring) speed is regulated by mean of the combined speed control of the engine and sun machine. The output machine M/G2 is controlled to add its torque to the output shaft, allowing the ICE to be operated within its optimal region.

The ground speed available is limited by the rated power of the engine, and by the electrical machines torque capability.

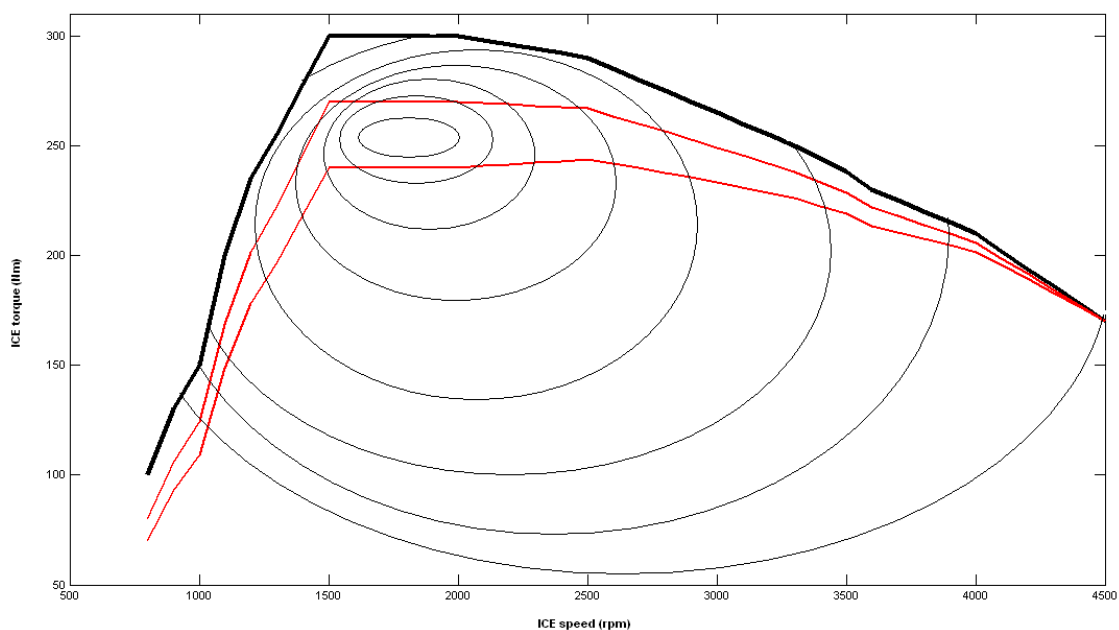


Fig. 2.8- ICE torque characteristic and efficiency map

### ICE speed control by driver

The driver is allowed to take the control of the engine speed: in this case both the ground speed and the engine speed are manually controlled. The ICE speed setpoint has the priority over the ground speed, which is limited by the available power of the engine at the current speed. The operator is notified of the eventual reached speed limit, and can increase the engine speed, so as to get the desired speed setpoint.

A limitation for the ICE speed is provided by the control system in order to keep the M/G1 machine (internal) below its maximum speed, and below its torque limit, for a certain ground speed.

### PTO mode

When the PTO clutch is engaged (*Tab. 2.2*), the ICE speed control is manual, in order to give the farmer the control of the PTO speed. This is necessary to control the functionality of the tools commanded by the PTO shaft. The control priority is given to the ICE speed over the ground speed, meaning that the thrust force and the PTO load torque has to be satisfied in any case. If the speed setpoint is too high (saturated) and the traction load is suddenly missing, the control system increase the speed gradually (e.g. 1 km/h/s).

Two particular options may be provided to the operator when spraying products, in order to have a constant product concentration when the engine is overloaded and the vehicle is slowing down:

- PTO PROP: The ICE speed is proportional to the ground speed, i.e. if the tractor slow down, also the PTO shaft, commanding the spray fan, slow down and the pesticide concentration is maintained constant.
- PTO CONST: The ICE speed is always constant (and so the fan speed), and the product flow is regulated by controlling the spray valve proportionally to the effective ground speed, obtaining the desired effect.

### Reverse way

The driver has two selectable options when going in reverse way:

- Quick reverse way (quick shuttle) RE1;
- Power reverse way RE2;

The selection of the **RE1** mode doesn't change the position of the mechanical inverter FW-N-RE, but exploit the acceleration of M/G1 in the positive sense, so as to invert the ring motion, thus the ground speed (*Fig. 2.9*). In this modality the negative speed can be obtained very quickly, without attending the electro-valve to switch the mechanical selector. Of course the ICE speed should be minimized, in order to obtain higher negative speeds (although no more than 5 km/h).

The selection of the **RE2** mode implies that the tractor speed needs to be zero until the mechanical inverter FW-N-RE is switched to RE. Afterwards the transmission works in the hybrid mode, but the ground speed is inverted. The highest rearward speeds can be reached by selecting this modality.

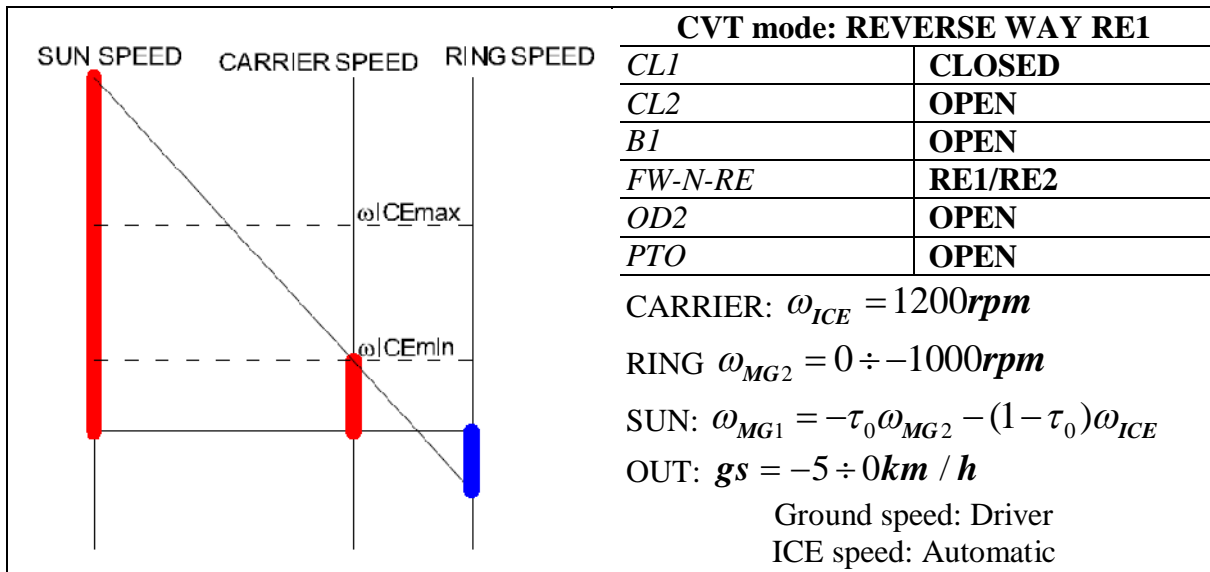


Fig. 2.9 – CVT mode, reverse way RE1, cinematic nomogram, speed relationships and mechanical configuration

Downhill or uphill zero speed maintenance

The transmission is capable of keeping the zero speed without using the brake or the park lock, for time intervals no longer than almost 1 minute.

In the forward mode, the following considerations can be made:

**Uphill:** The zero speed is maintained by the internal machine, which function as a generator, moved by the engine (Fig. 2.6). The external machine is supplied as a motor, and develops torque at zero speed. The M/G1 generated power should balance the M/G2 drawn power.

**Downhill:** The zero speed is still kept by the internal machine, which functions as a motor, developing negative torque at the ring. The external machine is supplied as a motor, developing no mechanical power. At this time the ICE functions as a brake.

The same functionality is possible in the reverse mode. Obviously, after some ten seconds, the driver is invited to switch on the park lock brake.

**2.4.3 Hybrid fixed ratio traction mode**

Two fixed ratios between Diesel engine and output shaft are provided, in order to allow

CL1	CLOSED
CL2	CLOSED
B1	OPEN
FW-N-RE	FW
OD2	OPEN
PTO	CLOSED

Tab. 2.2- CVT mode, PTO inserted: mechanical configuration

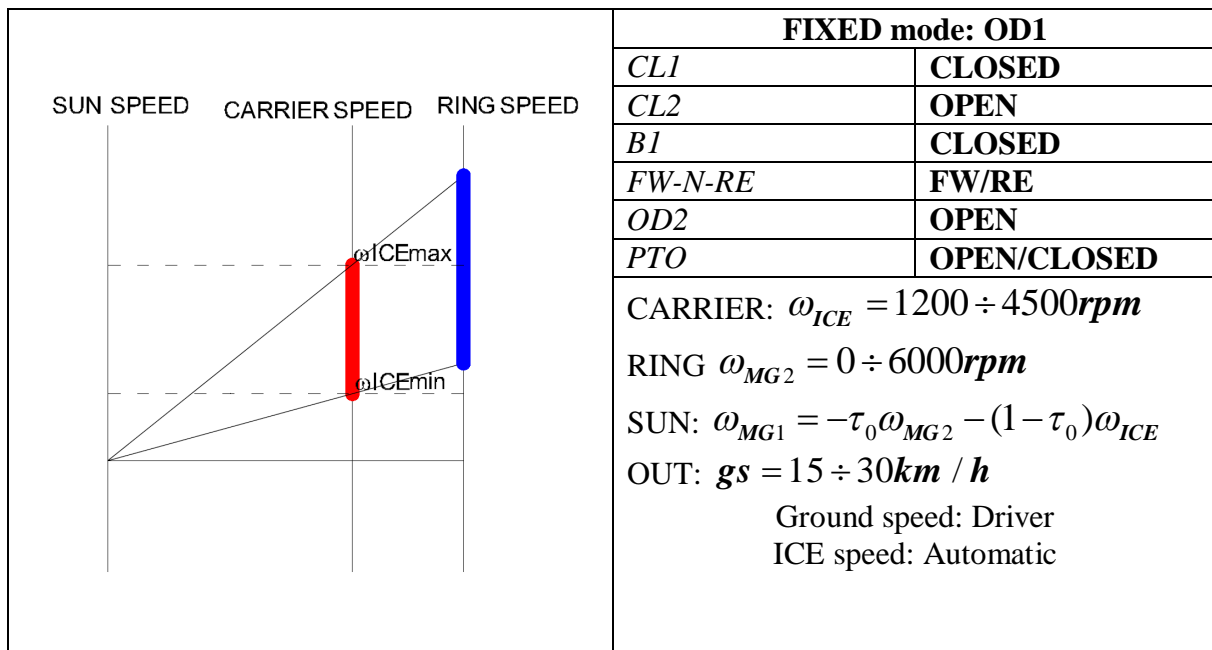


Fig. 2.10 – FIXED mode, OD1, cinematic nomogram, speed relations, mechanical configuration

the maximum ground speed in particular conditions. These two operating modes are called Over-drive 1 (OD1), and Over-drive 2 (OD2).

#### Over-drive 1 (OD1)

This first fixed ratio is obtained when the internal machine is stopped and locked by the brake B1 engagement. The OD1 insertion is manual, and can be selected by the driver under some particular conditions:

1. The M/G1 speed is below a certain limit.
2. The utilized torque is below the maximum available torque.

In this operating mode, the ICE speed is proportional to the ground speed, thus, by controlling the tractor speed, the operator controls also the engine speed (Fig. 2.10). OD1 mode can be disabled directly by the user, or automatically by the control system, when at least one of the following conditions subsist:

1. ICE speed falls below the minimum ICE speed.
2. ICE torque rate is 100% and the engine speed derivative is high and negative (fast deceleration of the ICE).

The PTO mode is possible in OD1 configuration.

#### Overdrive 2 (OD2)

The over-drive 2 mode (OD2) is a second fixed ratio between ICE and wheels, which can be used only in on-road transfer operations, where high speed and low tractive effort are required. The clutch CL2 is engaged, and the OD2 selector is enabled: such a configuration provides a direct coupling of the ICE shaft to the output shaft, realizing the longest engine/wheels ratio.

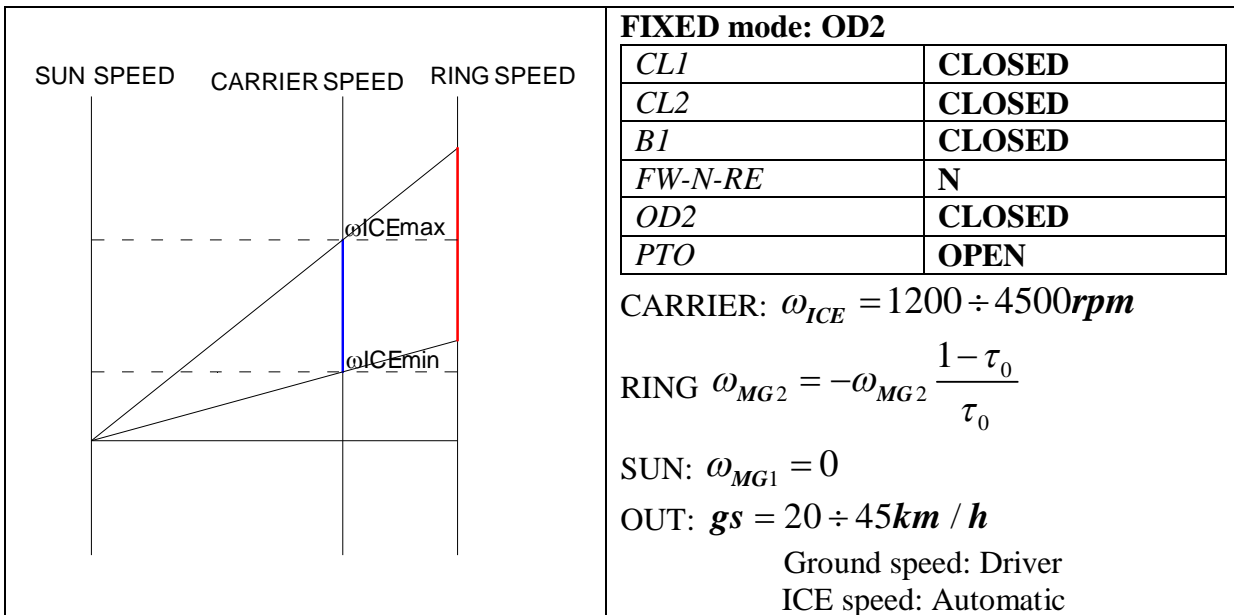


Fig. 2.11 – FIXED mode, OD2, cinematic nomogram, speed relations, mechanical configuration

The OD2 insertion is left up to the driver, but the control system switches automatically to the CVT mode as (at least) one of the following condition is verified:

1. The ICE torque rises above a fixed limit.
2. The ICE speed drops with a high time derivative.
3. The ICE speed falls below a fixed minimum speed.
4. The ground speed goal falls below the limit for the OD2 ratio (20 km/h).

The necessary condition to enable OD2 is the **deactivation of the PTO** supply.

In Fig. 2.11 the cinematic nomogram of the OD2 configuration shows that the output is now the carrier shaft, and the two electrical machines can be left free. If batteries need some recharge, the two machines can be controlled as generators: e.g. the sun machine can be blocked by the brake B1 and the ring machine can rotate and generate power, like in a pure parallel hybrid transmission.

## 2.5 The drivetrain control strategy

The overall control system has a function of coordination among the different devices taking part at the drive transmission.

In this paragraph a general description of the control scheme model will be given, as it has been conceived till now, keeping in account the following limitations of the model:

- It's an ideal model (no losses).
- The CVT hybrid mode operation is represented only.

Three different control schemes can be distinguished, each one communicating with the remainders:

- The ICE control system;

- The MG/1 drive control system;
- The MG/2 drive control system.

The main task of the control unit is to regulate the ground speed at the setpoint value given by the driver, under the different traction load conditions and operating states of the thermal engine, and to maintain the power balance of the electrical system, recharging when necessary the battery.

### 2.5.1 The ICE control system

The ICE speed goal can be determined in two ways:

- Directly by the driver
- By the control system in order to maximize the ICE efficiency and to follow the ground speed reference.

The first case is obvious, and it's typical of the PTO mode, when the driver needs to control the ICE shaft speed, since its speed is directly related to the PTO shaft speed. This case will not be dealt with.

In Fig. 2.12 the control scheme layout is represented, where two setpoint speeds are generated by two different paths: the engine efficiency optimization path ( $\omega_{ICE,1}^*$ ) and the ground speed feed forward path ( $\omega_{ICE,2}^*$ ). These two contributions are added together to constitute the ICE speed setpoint.

The *engine efficiency optimization path* implements the task to maintain the motor operating where its efficiency is maximum, compatibly with the power requirements of the driveline. This means that the torque employing of the engine should be kept in the range 70%-80% (cfr. par. 2.4.2). In Fig. 2.13 a flowchart describes the control strategy:

1. A **first routine** checks if the internal machine M/G1 is saturated (torque employing above 90%). If not, the algorithm continues with a second routine, regarding the efficiency of the ICE. If M/G1 torque is close to the limit torque, two actions are possible: if the machine is in the constant torque region, the algorithm attempts to increase the ICE speed, in order to reduce the torque applied to the planetary gear

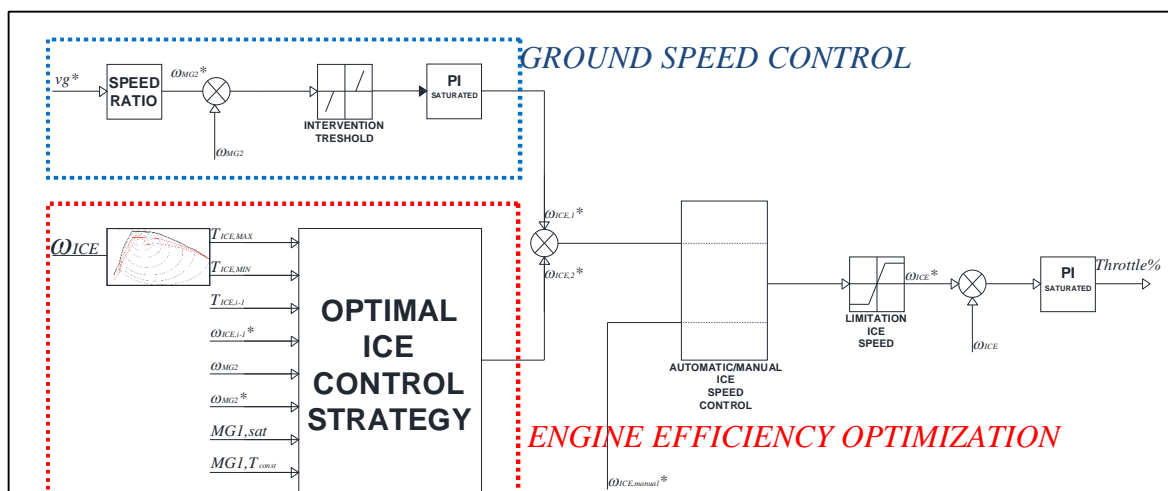


Fig. 2.12 – ICE control system

train, and get it away from the saturation. If the machine is in constant power region, the algorithm tries to reduce the ICE speed, in the attempt to reduce also the machine speed, and increase its torque limit. Of course no speed modification can be done if the ICE speed is near to its lower or upper limit.

2. A **second routine** changes the engine speed setpoint, so as to maintain the engine torque between the lower limit and the upper limit (cfr. par. 2.4.2). This means that the engine is operated efficiently. No interventions on the ICE speed are made if the ground speed (M/G2 speed) setpoint is not respected: of course the engine can be required to develop the maximum power, regardless its efficiency.

In optimization mode, the speed setpoint is decreased as the torque falls below the lower limit, and it is increased as the torque rises above the upper limit. No actions are provided if the torque limits are respected.

The *ground speed feed forward path* is fundamentally made up by a PI regulator,

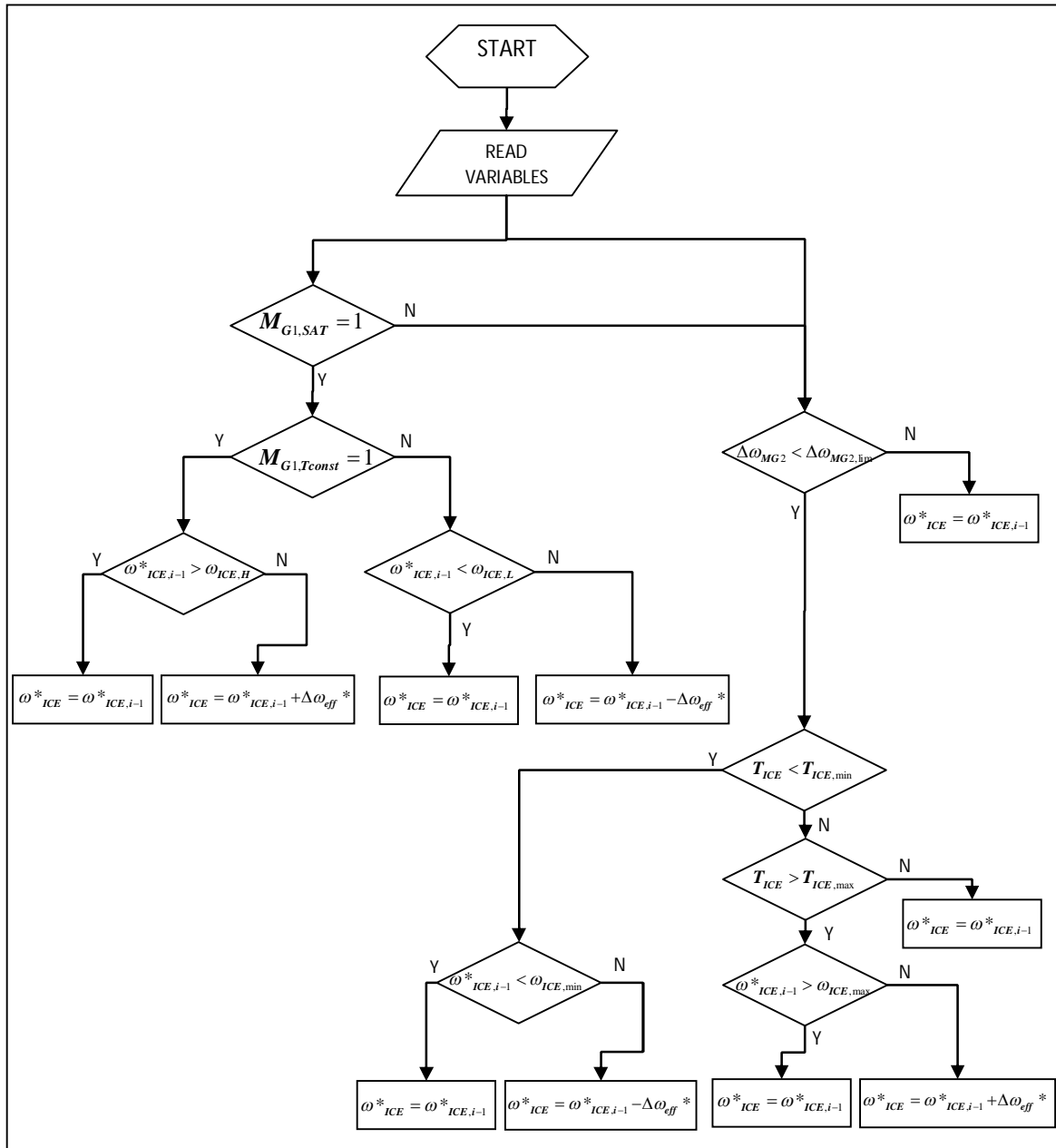


Fig. 2.13 –Optimal ICE control strategy flowchart

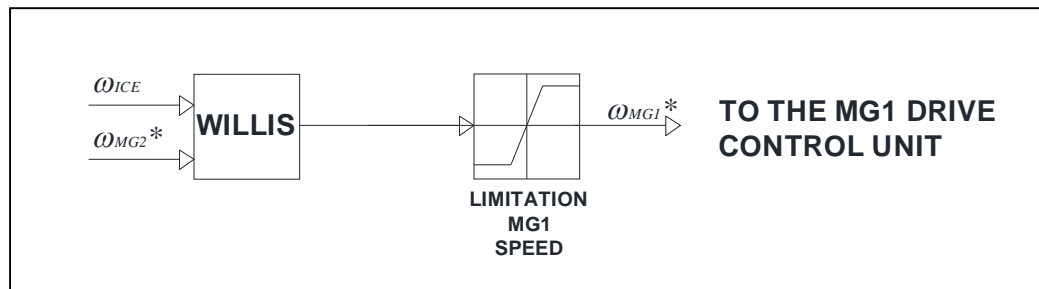


Fig. 2.14 – MG/1 control system

sensitive to the ground speed error, which starts to get involved only if the error rise above a certain threshold (e.g. 10 rpm on the MG/2 shaft). This path allows to get from the engine its maximum power, until the maximum vehicle speed.

### 2.5.2 The MG/1 machine control system

The internal machine has the main task to control the ground speed, compensating the variations of the ICE speed, which is controlled responding to efficiency criteria. By the Willis formula, the MG/2 setpoint speed (proportional to the vehicle speed) is converted into a MG/1 setpoint speed, respecting the current ICE speed.

In Fig. 2.14 the control scheme is represented, where also the M/G1 speed limitation has been inserted.

### 2.5.3 The MG/2 machine control system

Another important task of the control system is to keep the power balance between the electrical power sources, allowing unbalances only in dynamic conditions (accelerations or regenerative braking), batteries charging or pure electric traction mode. This function is implemented by the MG/2 drive controller (Fig. 2.15)

The power error, resulting from the algebraic sum of the internal machine and external

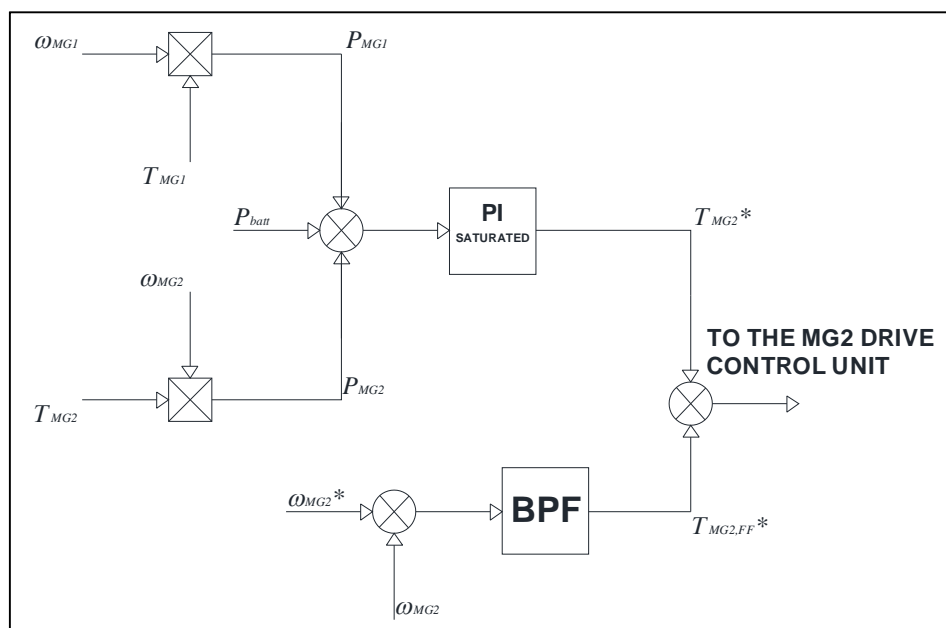


Fig. 2.15 – MG/2 control system

machine, enables a PI regulator, which gives a torque setpoint for the M/G2 drive control unit ( $T_{MG2}^*$ ). Also the battery power setpoint is involved in this control loop: a part of the current produced by the electrical machines can be used to recharge the battery pack. In the followings the hypothesis of zero battery current will be made.

A further torque setpoint can be generated by a feed forward action, sensitive to the ground speed error. The external machine should accelerate the output shaft only when strong accelerations are required, that's why a band pass filter has been inserted between the ground speed error and the feed forward torque setpoint ( $T_{MG2,FF}^*$ ).

In every moment the control system should not apply to the wheels a torque above the adherence limit, in order to avoid wheels slip.

## 2.6 Simulations

The control system has been tested by way of numeric simulations. The vehicle transmission model has been implemented in MATLAB/Simulink, as well as the control algorithm, in order to adjust the regulators parameters and to verify the stability and performances of the system.

The CVT hybrid mode has been considered only, due to its originality. The following transient conditions have been simulated:

<b>Drivetrain parameters</b>			
<i>Diesel Engine</i>		<i>M/G1 electrical machine</i>	
Rated power @ 4000 rpm [kW]	88	Rated power [kW]	25
Rated torque @ 2000 rpm [Nm]	300	Rated speed [rpm]	2800
Torque loop time constant [s]	0,01	Max speed [rpm]	6000
Inertia [kgm <sup>2</sup> ]	1,5·10 <sup>-3</sup>	Torque loop time constant [s]	0,005
Speed range [rpm]	800÷4400	Inertia [kgm <sup>2</sup> ]	1,5·10 <sup>-3</sup>
<i>M/G2 electrical machine</i>		<i>Vehicle data</i>	
Rated power [kW]	25	Mass [kg]	2700
Rated speed [rpm]	1050	Dynamic rolling friction coefficient [N/kg]	0,06
Max speed [rpm]	6000	Aerodynamic friction coefficient [Ns <sup>2</sup> /m <sup>2</sup> ]	0,7
Torque loop time constant [s]	0,005	Front surface [m <sup>2</sup> ]	2,5
Inertia [kgm <sup>2</sup> ]	1,5·10 <sup>-3</sup>		
<i>Transmission data</i>			
Planetary gear fund. speed ratio	2,19	Engine/carrier ratio	0,857
REAR TRAIN		FRONT TRAIN	
Differential/ring ratio FW	0,39	Differential/ring ratio FW	0,48
Differential/ring ratio RE	0,354	Differential/ring ratio RE	0,44
Wheels/differential ratio (rear)	0,30	Wheels/differential ratio (front)	0,393
Wheels radius (rear)	0,65	Wheels radius (front)	0,425

*Tab. 2.3- Drivetrain parameters used in simulations*

<b>Control system parameters</b>			
<i>ICE control system</i>		<i>M/G1 control system</i>	
Speed loop PI proportional gain	0,001	Speed loop PI proportional gain	1
Speed loop PI integral gain	0,005	Speed loop PI integral gain	1
Ground speed controller proportional gain	0,01		
ICE torque controller proportional gain	0,1		
<i>M/G2 control system</i>			
Power loop PI proportional gain	0,001		
Power loop PI integral gain	0,1		
BPF zero frequency (ground speed FF action) [Hz]	50		
BPF pole frequency (ground speed FF action) [Hz]	1000		
<i>Tab. 2.4- Control system parameters used in simulations</i>			

- ICE start-up;
- Speed transients;
- Tractive load transients;
- Battery power transients;
- PTO mode insertion.

In the *Tab. 2.3* the parameters of the simulated drive train have been reported, related to the main components of the system:

- ICE;
- Electrical machines;
- Vehicle;
- Transmission.

In the succeeding table (*Tab. 2.4*), the control algorithm parameters have been listed, with their associated values derived from the tuning of the system, defining accurately the three control systems described in par. 2.5.

The ICE torque controller is sensitive to the ICE torque error, to the ground speed error, and to the MG/1 machine saturation.

The MG/1 torque controller is sensitive to the ground speed error (it is the main speed regulator).

The MG/2 torque controller is sensitive mainly to the power balance error, but also to the high frequency components of the ground speed error.

### 2.6.1 Simulation results

In the next pages, various simulation results will be shown, so as to demonstrate the performances and the stability of the driveline system.

Particularly the following simulations will be examined:

- Simulation 1 – Speed variations at fixed load
- Simulation 2 - Speed variations at fixed load
- Simulation 3 – Load variations at fixed speed
- Simulation 4 – Load variations at fixed speed
- Simulation 5 – Start up at high load
- Simulation 6 – Battery recharge at constant speed

### Simulation 1 – Speed variations at fixed load: 2000 N

This simulation shows the behavior of the vehicle system when the speed setpoint is changed by the driver, the tractive effort is 2000 N constant and the battery recharge power is maintained to zero.

#### Setpoint signals:

- Ground speed setpoint: Variable.
- ICE speed setpoint: Max efficiency
- Battery power setpoint: Zero.

**Description:** The ground speed is varied by the driver, between zero and the maximum speed (29 km/h), following the profile of *Fig. 2.16*. As can be noted in *Fig. 2.17* the ICE speed is controlled with the goal to maintain the torque within the 70-80% interval. This is not always possible, due to the M/G1 torque limit (saturation): the transmittable torque decreases when the speed increases. Whenever the internal machine reaches its torque limit, the ICE

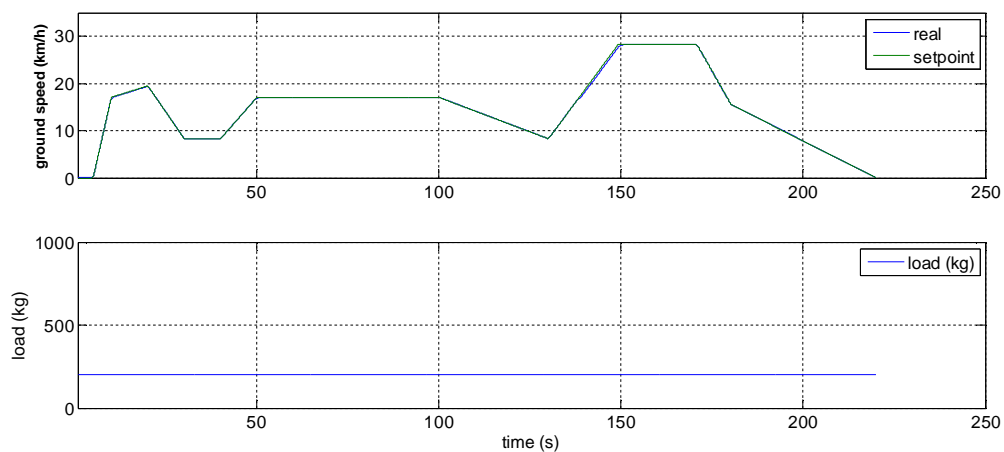


*Fig. 2.16 - Simulation 1, ground speed and load*

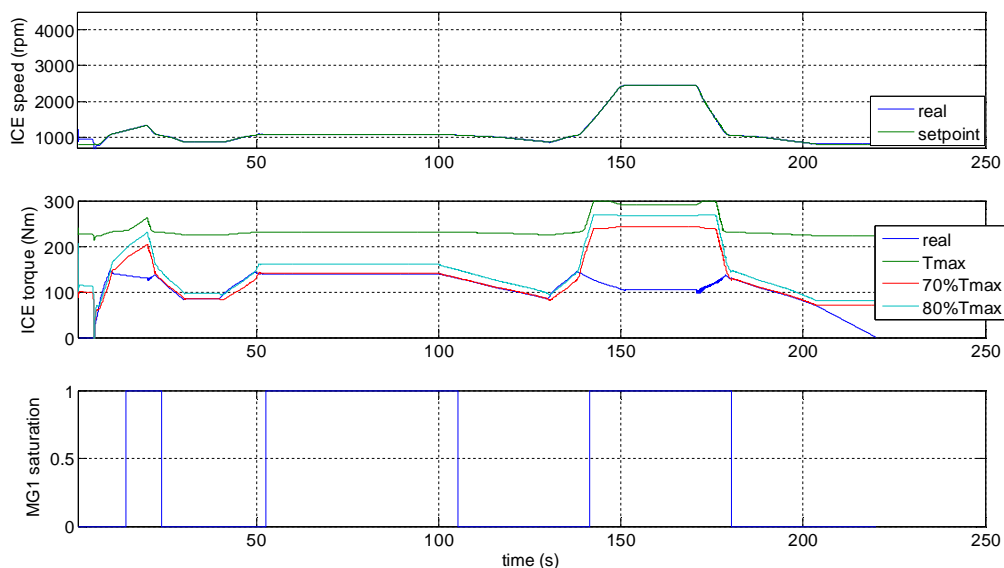


*Fig. 2.17 – Simulation 1, ICE speed and torque, M/G1 saturation*

speed must be increased to follow the output speed setpoint (150 s to 170 s). This is clear from the graph of Fig. 2.18, where M/G1 torque and speed are represented. It can be seen that also the maximum speed limit is reached (6000 rpm at 150 s), and that's why the ICE speed cannot be further kept in the minimum consumption range. The M/G2 machine torque is controlled in order to keep the power balance (Fig. 2.19): the real torque is filtered respected to the setpoint one, allowing transitory power unbalance, covered by the battery (Fig. 2.21). It's interesting to note that, at small load conditions (200 N) the M/G2 machine behaves almost always as a generator, and M/G1 as a motor. This happens because the required output torque is low compared to the ICE torque, consequently the external machine reacts pulling off a part of the torque and generating power. The power balance is represented evidently in Fig. 2.20 and Fig. 2.21: the MG/1 and MG/2 powers are equal and opposite, the whole ICE power is transferred to the wheels, and the battery has only a function of energy buffer.

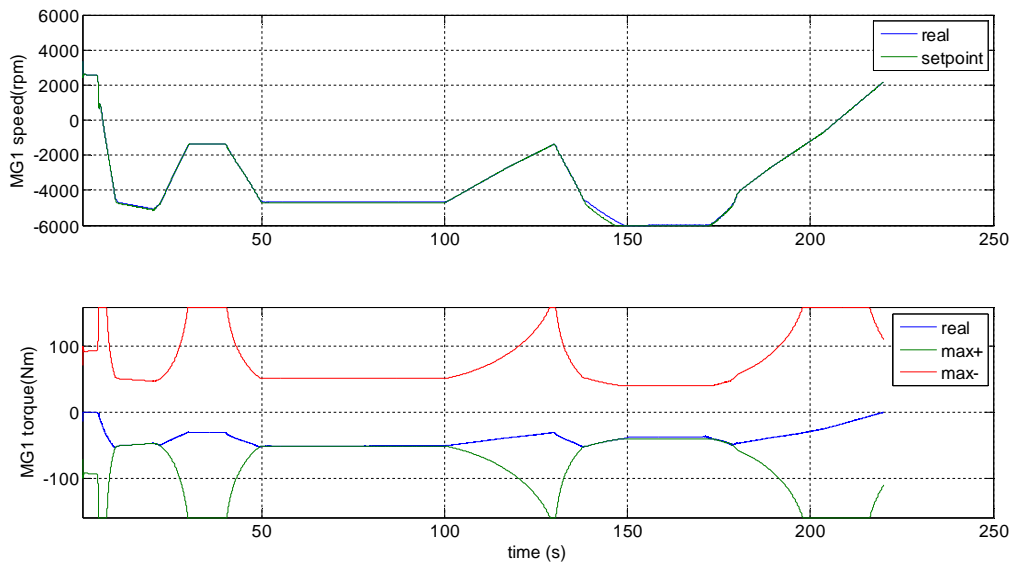


Fig. 2.18 – Simulation 1, MG/1 speed and torque

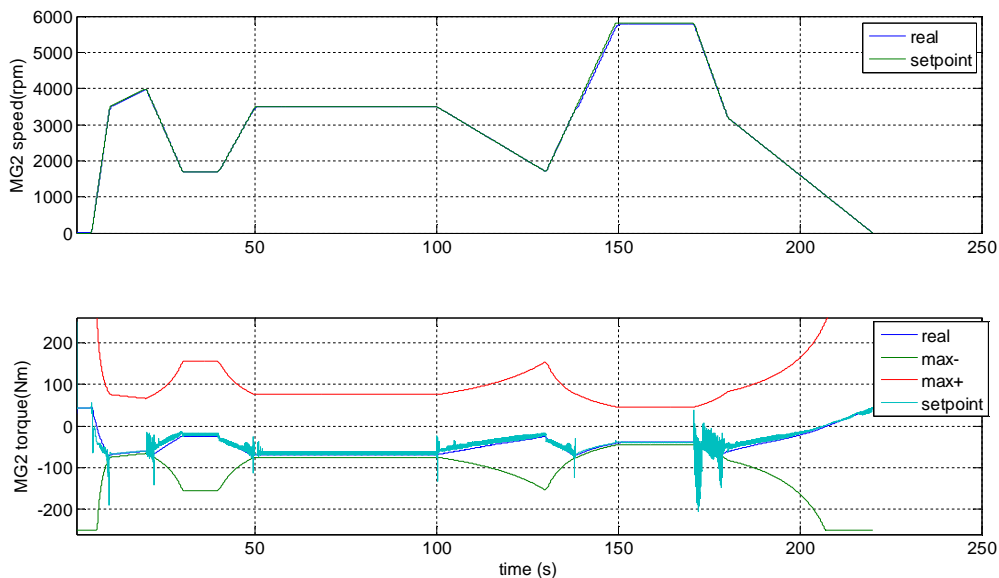


Fig. 2.19 – Simulation 1, MG/2 speed and torque

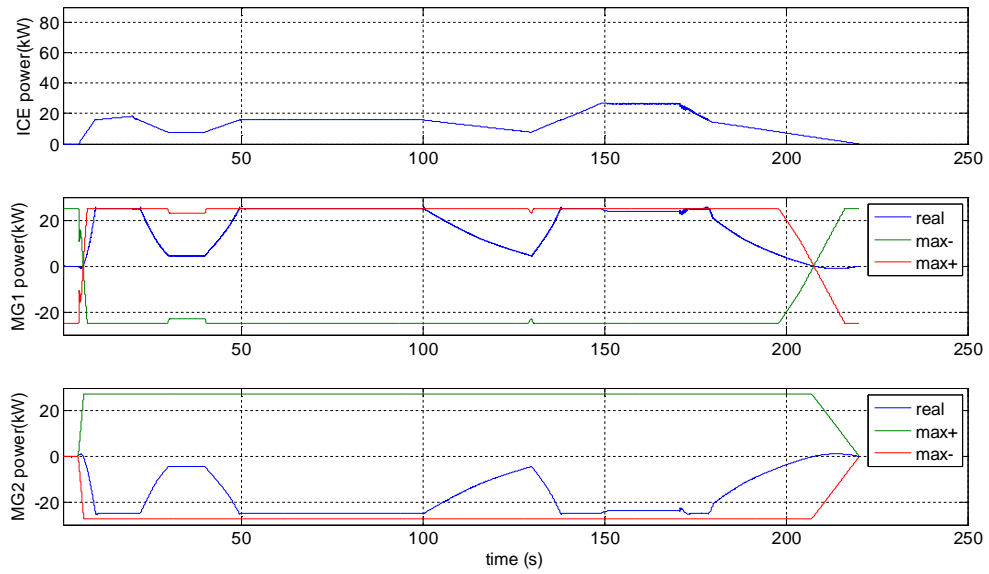


Fig. 2.20 – Simulation 1, Machines power

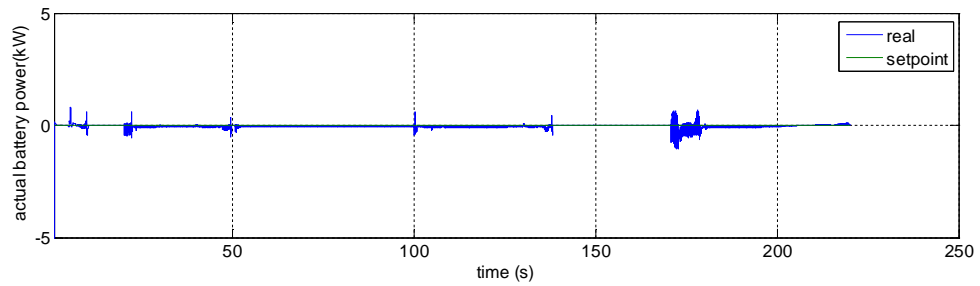


Fig. 2.21 – Simulation 1, Battery power

**Simulation 2 – Speed variations at fixed load: 6000 N**

This simulation shows the behavior of the vehicle system when the speed setpoint is changed by the driver, the tractive effort is 6000 N constant and the battery recharge power is maintained to zero.

**Setpoint signals:**

- Ground speed setpoint: Variable.
- ICE speed setpoint: Max efficiency
- Battery power setpoint: Zero

**Description:** The situation is similar to the simulation 1, but in this case the load is higher (600 kg), as shown in Fig. 2.22. As Fig. 2.23 demonstrates, the ICE speed is controlled with the goal to maintain the torque within the 70-80% interval, but this goal is less respected than before, due to the increased load. This is clear particularly in the intervals 50-100s and 150-170 s, where the internal machine is at the torque limit. Compared to the simulation 1

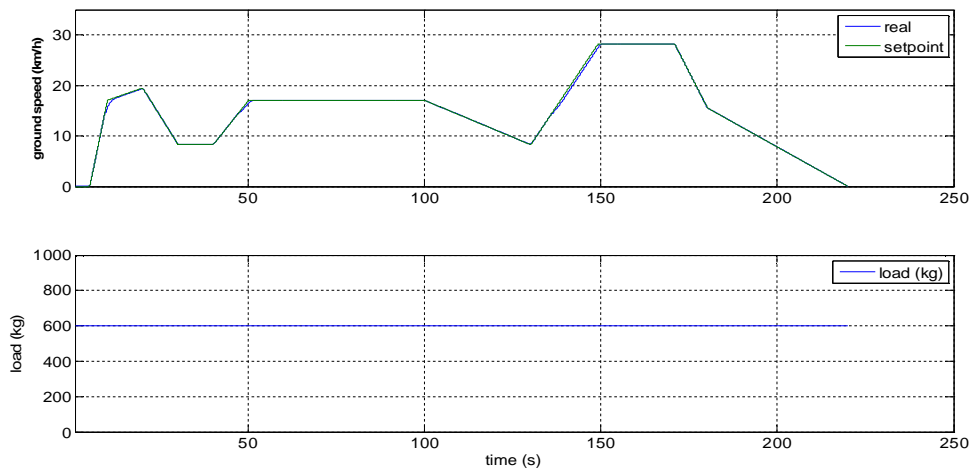


Fig. 2.22 – Simulation 2, ground speed and load

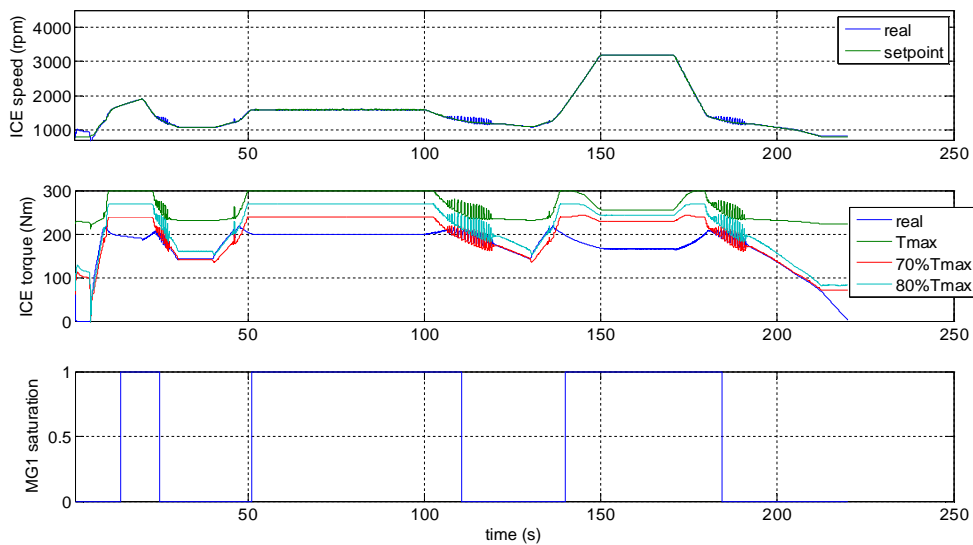


Fig. 2.23 – Simulation 2, ICE speed and torque, M/G1 saturation

here the ICE speed is higher, to achieve the setpoint output speed, that's why the torque is lower than that required for efficiency. In the interval 100 s and 150 s, when the speed is lower than 15 km/h, the ICE is operated at the best efficiency. In Fig. 2.24 the internal machine transient is depicted: in particular the speed is slower than in sim. 1, because the higher load take the machine in saturation at a low speed. The M/G 2 machine operates as a generator in the whole simulation interval, except when the speed is very low (>200s). This can be seen also in the diagrams related to machines power (Fig. 2.26, Fig. 2.27).

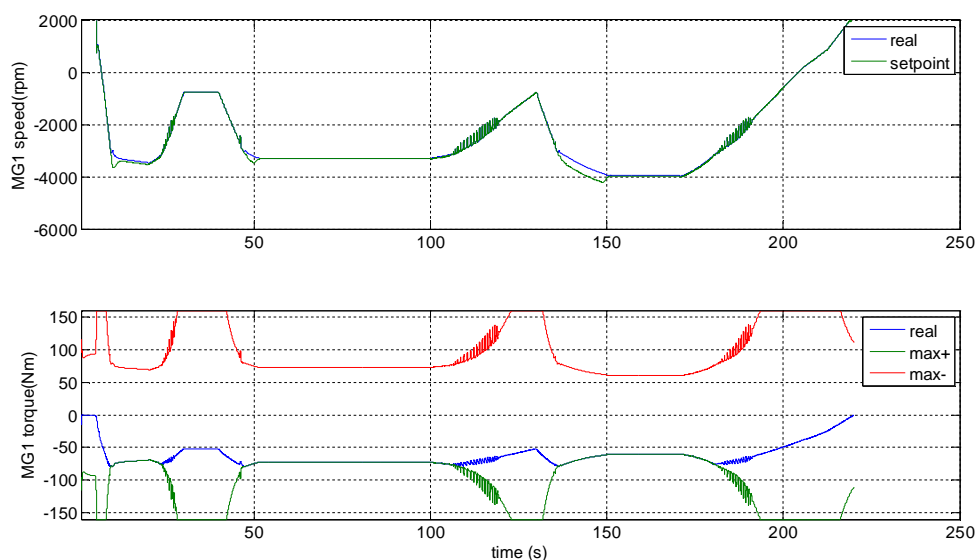


Fig. 2.24 – Simulation 2, MG/1 speed and torque

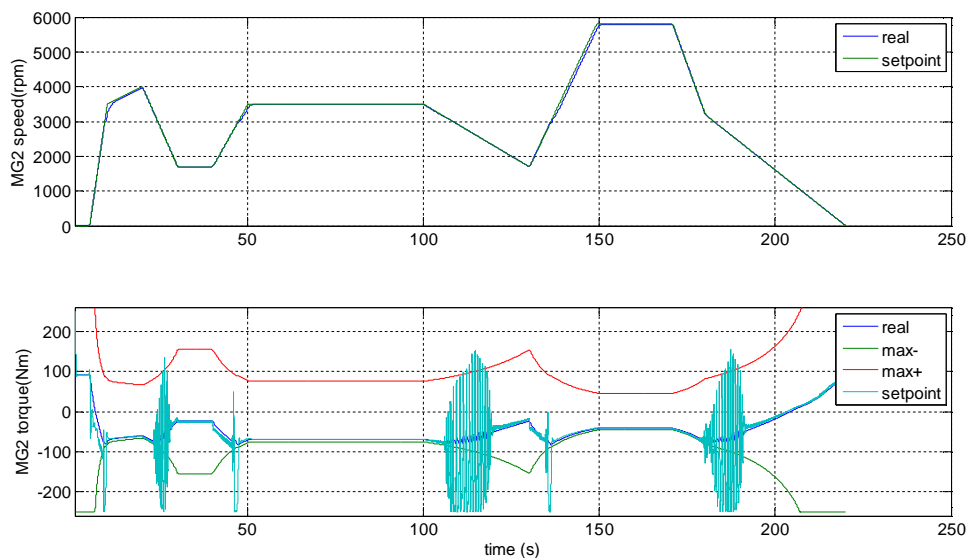


Fig. 2.25 – Simulation 2, MG/2 speed and torque

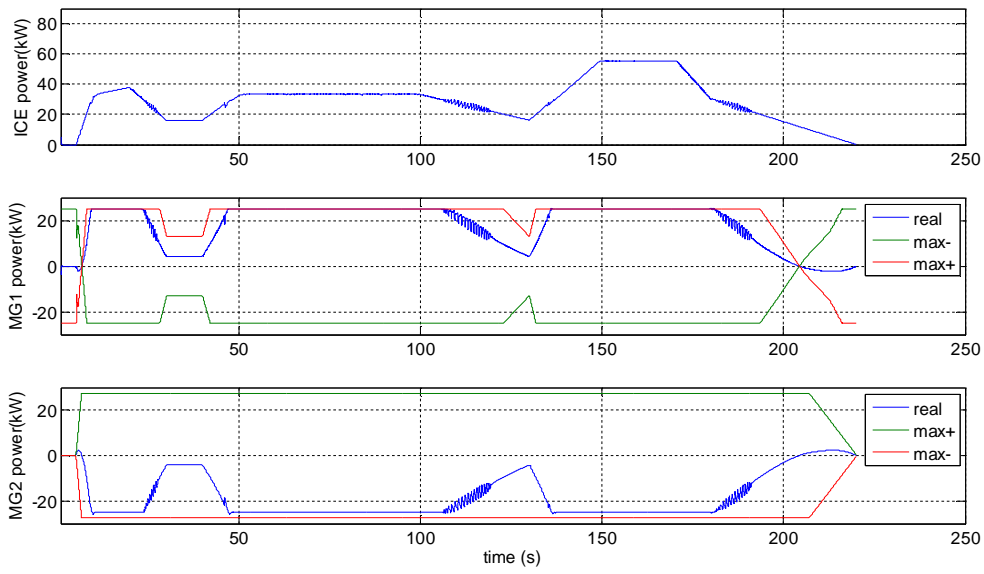


Fig. 2.26 – Simulation 2, Machines power

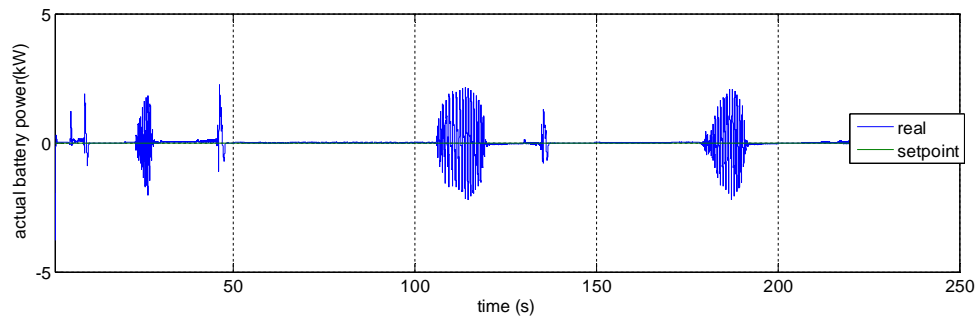


Fig. 2.27 – Simulation 2, Battery power

### Simulation 3 – Load variations at fixed speed: 15 km/h

This simulation shows the behavior of the vehicle system when the speed setpoint is kept constant by the driver, while the tractive effort is step varying. The battery recharge power is maintained to zero.

#### Setpoint signals:

Ground speed setpoint: Constant.

ICE speed setpoint: Max efficiency

Battery power setpoint: Zero

**Description:** The speed is controlled to 25 km/h and two load steps are introduced during the simulation interval (). The first step is from 0 to 600 kg: the ICE torque is kept

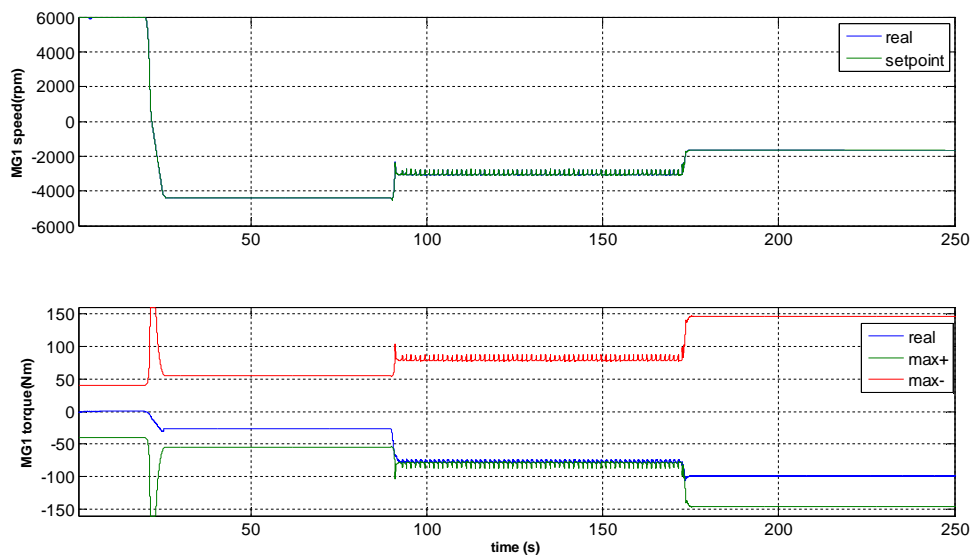


Fig. 2.30 – Simulation 3, MG/1 speed and torque

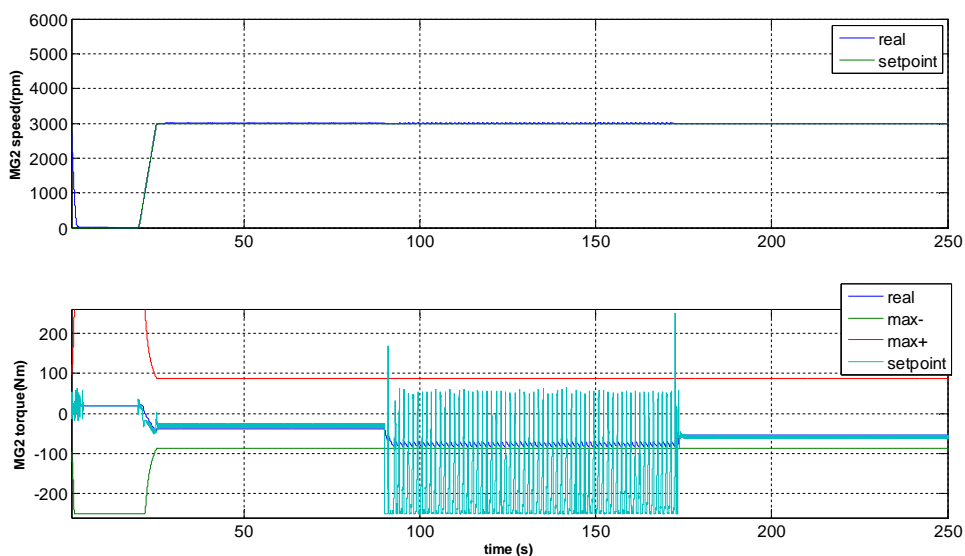


Fig. 2.31 – Simulation 3, MG/2 speed and torque

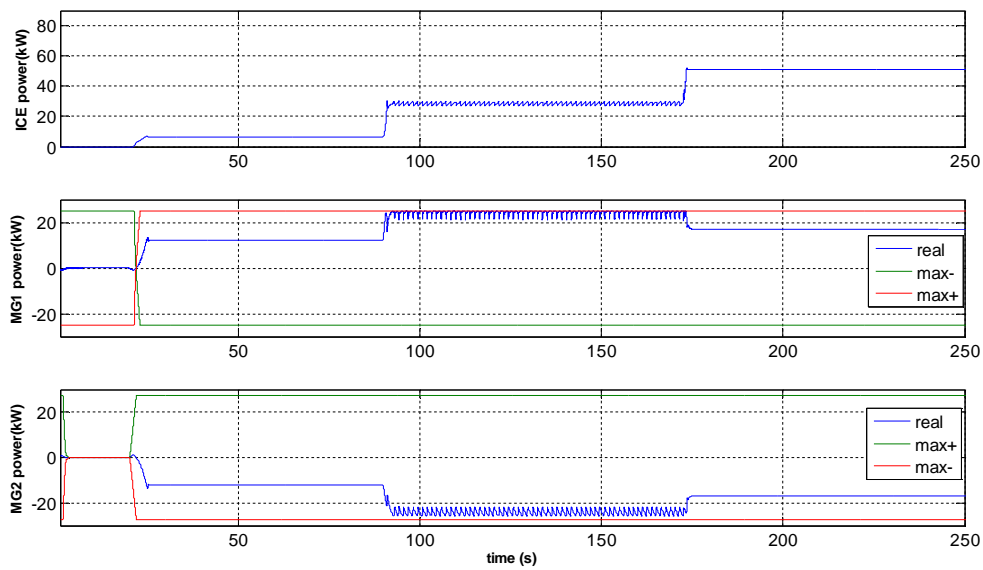


Fig. 2.32 – Simulation 3, Machines power

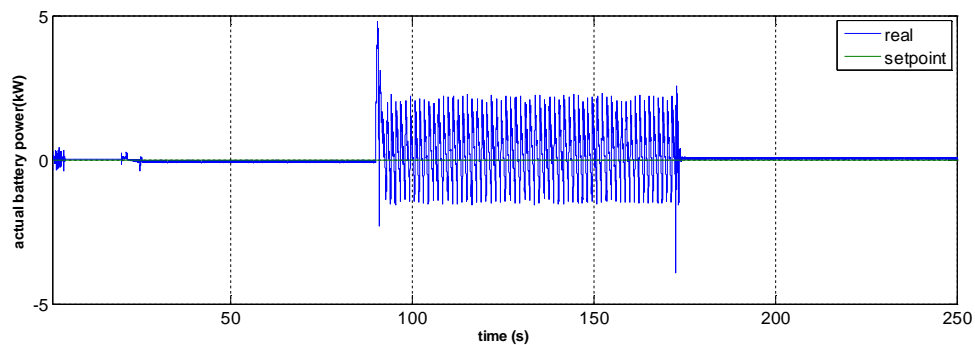


Fig. 2.33 – Simulation 3, Battery power

within the optimal efficiency interval, by way of a raise of the speed (from 800 to 1400 rpm). This ICE acceleration yields to a M/G1 deceleration, to keep the goal output speed (Fig. 2.30). The deceleration increase the torque availability of M/G1, which consequently can sustain the increased load. The same happens in the following load transient (600 to 1200 kg), where the M/G1 torque reach the 100 Nm level: this implies a current overload condition, which can be maintained for a limited time (rated torque is 80 Nm). The two machines are close to their rated power in the central interval only, but the internal machine is torque overloaded in the third interval. As results from Fig. 2.32 and Fig. 2.33, the power balance is correctly preserved by the action of M/G2. The battery is employed as a buffer, to soak up the transitory power unbalances between the machines. It's remarkable how the system tries to keep the Diesel engine as more loaded as possible, increasing its speed only when the internal machine join the torque limit. Its working point can be shifted compatibly with the power requirements and the electrical machines limits.

### Simulation 4 – Load variations at fixed speed: 25 km/h

This simulation shows the behavior of the vehicle system when the speed setpoint is kept constant by the driver, while the tractive effort is step varying. The battery recharge power is maintained to zero.

#### Setpoint signals:

Ground speed setpoint: Constant.

ICE speed setpoint: Max efficiency

Battery power setpoint: Zero.

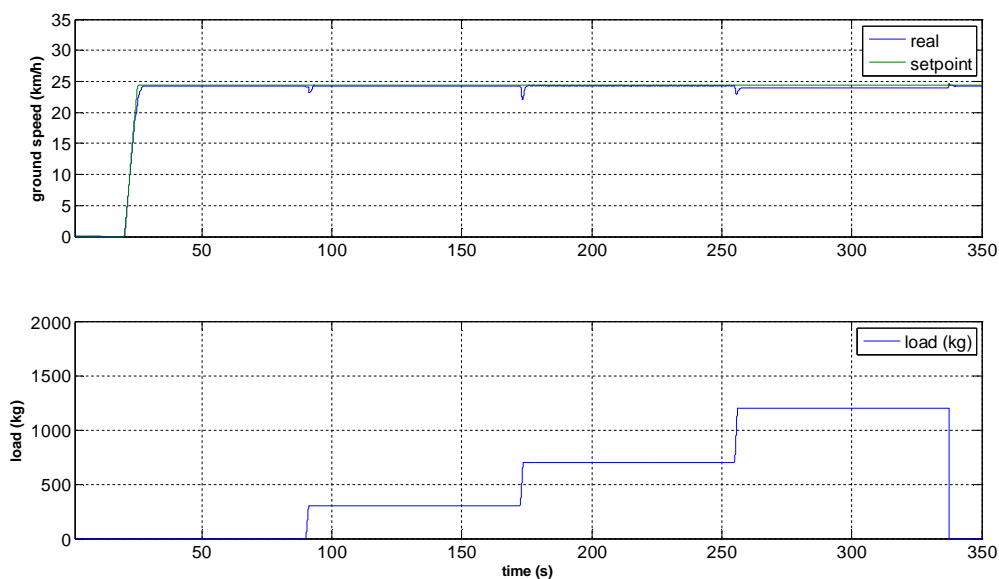


Fig. 2.34 – Simulation 4, ground speed and load

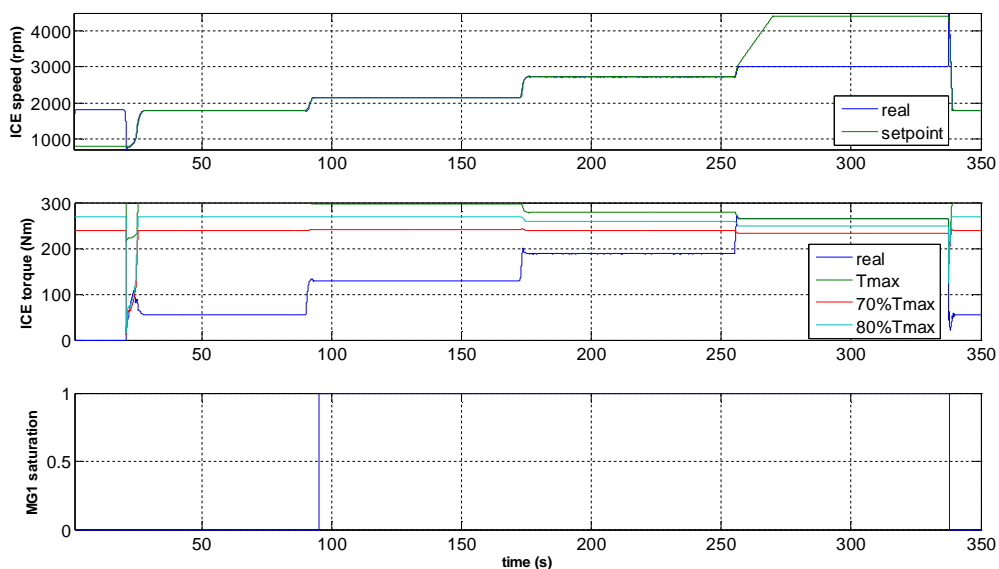


Fig. 2.35 – Simulation 4, ICE speed and torque, M/G1 saturation

**Description:** The speed is controlled to 25 km/h and three load steps are introduced during the simulation interval (). The first step is from 0 to 300 kg, then to 600 kg, and finally to 1200 kg. The ground speed is high, for this reason the ICE speed must be increased both at no load because the speed limit of M/G1 is reached, and with load because of reached torque limits. In this case the torque employment is out of the efficiency bounds, being the required ICE speed too high. In the last step, although the ICE is required to deliver its maximum torque, its speed can't reach the setpoint: the engine yields almost its maximum power. The required speed is not reached in this phase, being the power limits of the system overridden. It's worthy to observe in () how the battery drains power at rising load, and is recharged by load falling.

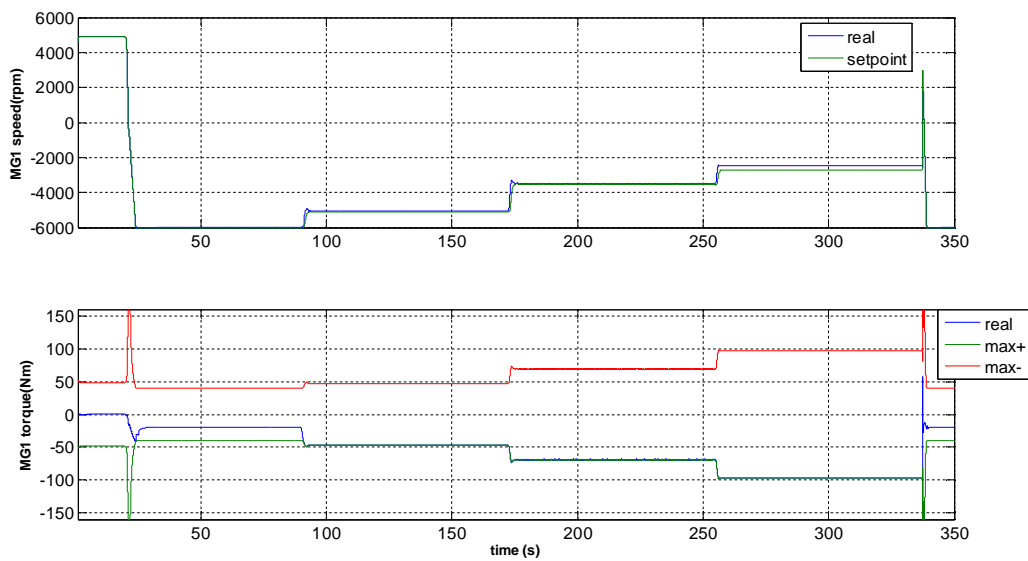


Fig. 2.36 – Simulation 4, MG/1 speed and torque

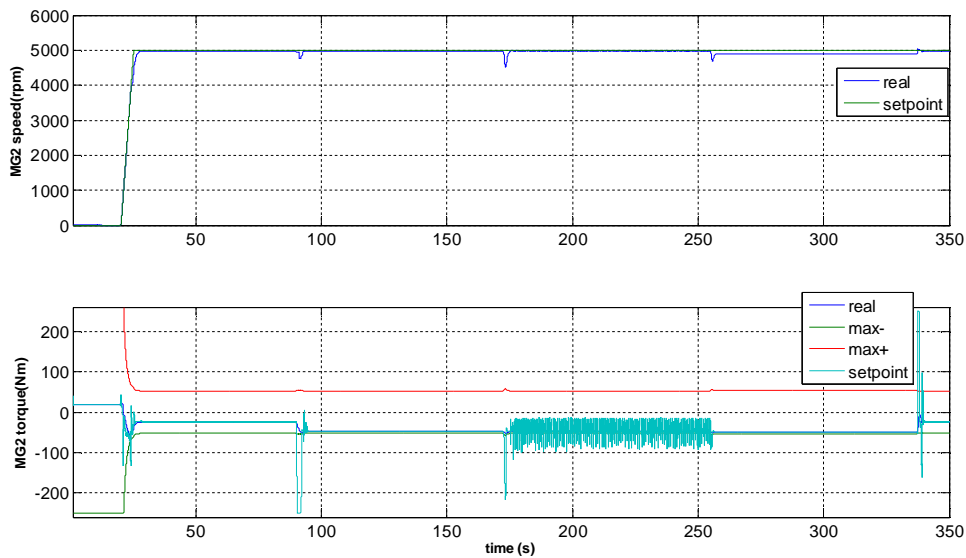
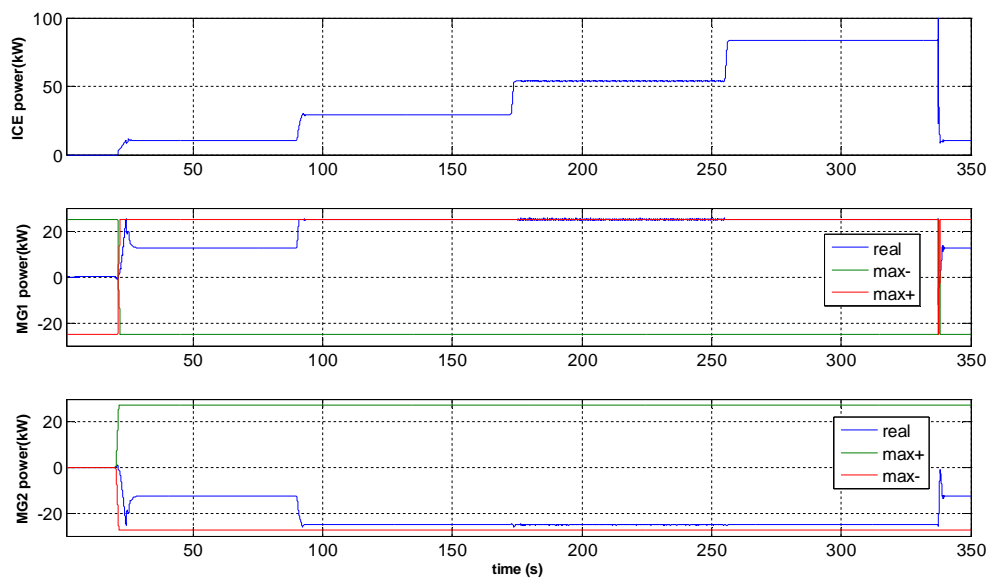
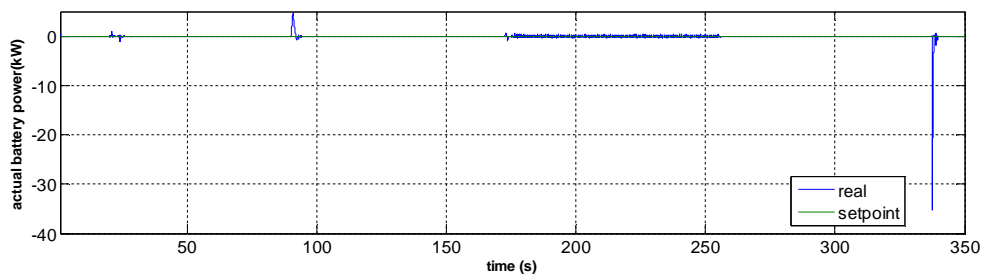


Fig. 2.37 – Simulation 4, MG/2 speed and torque



*Fig. 2.38 – Simulation 4, Machines power*



*Fig. 2.39 – Simulation 4, Battery power*

**Simulation 5 – Start-up at high load: 25000 N**

This simulation shows the behavior of the vehicle system when it is started by the driver, under a high traction load: 25000 N. The ICE speed is controlled by the operator, while the battery recharge power is maintained to zero.

**Setpoint signals:**

Ground speed setpoint: Variable.

ICE speed setpoint: Set by the driver

Battery power setpoint: Zero

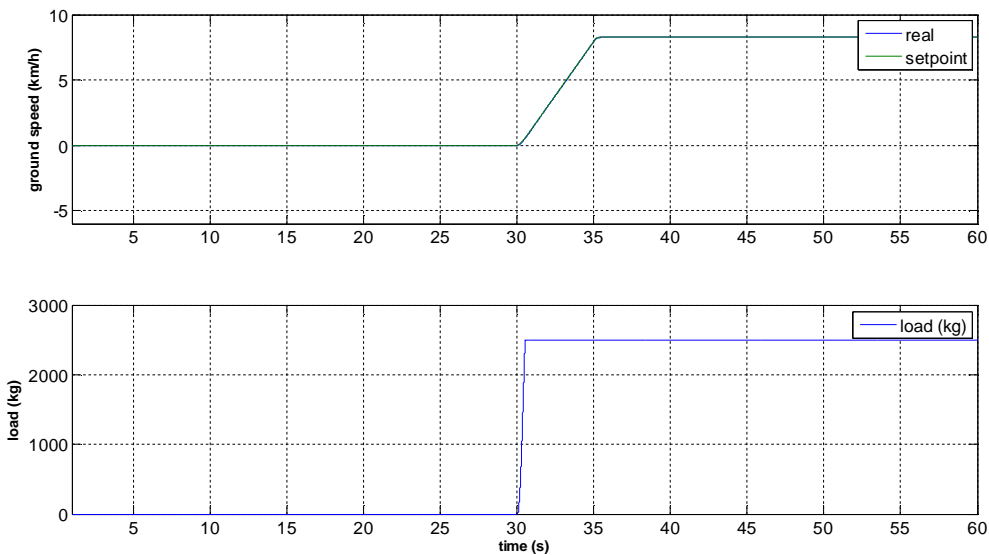


Fig. 2.40 – Simulation 5, Ground speed and load

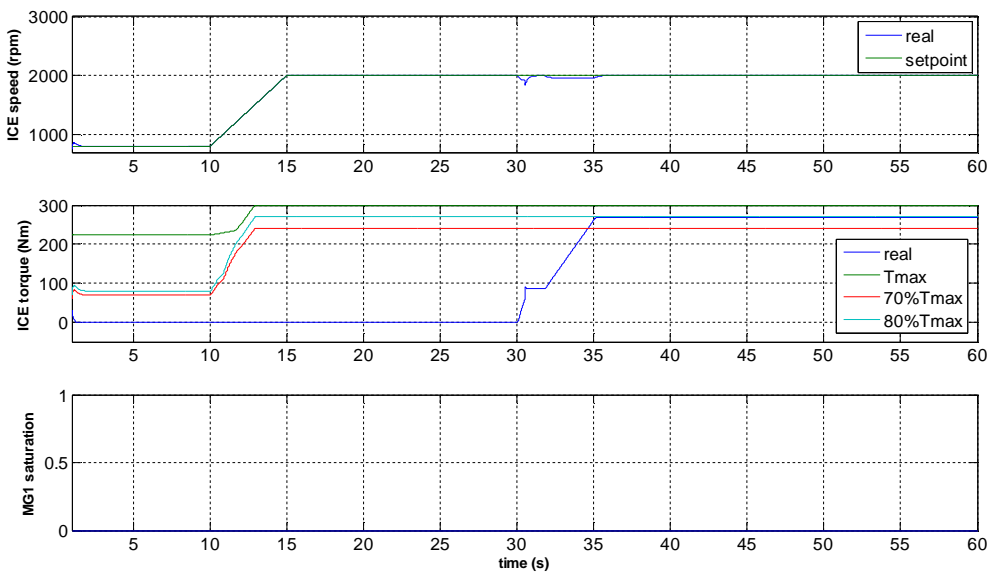


Fig. 2.41 – Simulation 5, ICE speed and torque, M/G1 saturation

**Description:** The vehicle is started under a very high load, and the engine speed is controlled by the driver. At 30 s the ground speed setpoint start to rise, and the engine speed is maintained constant by the driver at 2000 rpm. The tractor starts to pull the 2500 kg load until a speed of 8 km/h: the ICE is close to the maximum torque, while the M/G1 is already in overload, 100 Nm, which means that this condition can't be sustained permanently, but only for few minutes. The M/G2 machine drains the power generated by M/G1, developing a 250 Nm torque, necessary to accelerate the vehicle. In this situation the CVT acts like a very short gear ratio providing a very high output torque, with a high developed power (about 60 kW). The power generated by M/G1 is not entirely transformed in output power by M/G2, a part is absorbed by the battery, which plays its energy buffer role, for a few seconds.

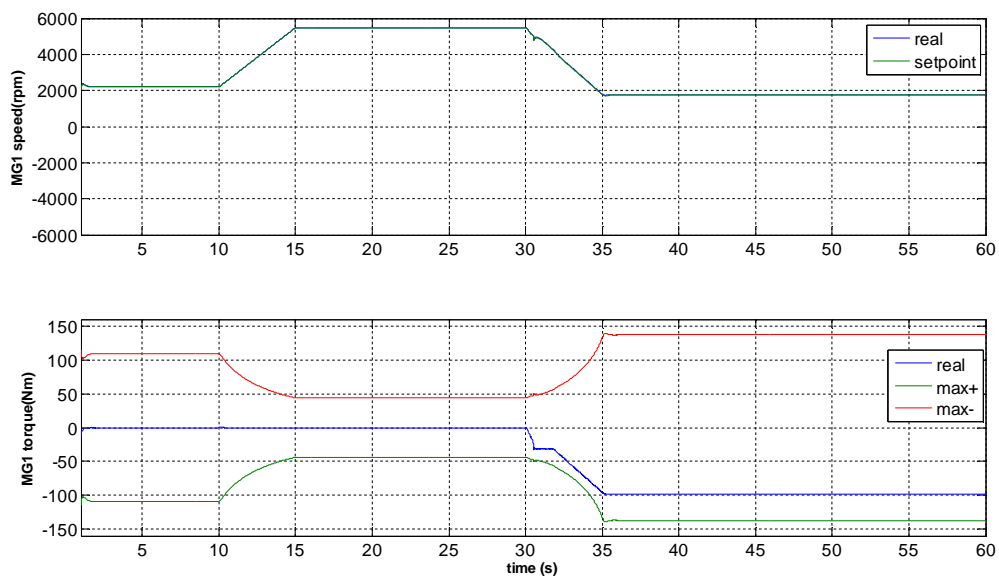


Fig. 2.42 – Simulation 5, MG/1 speed and torque

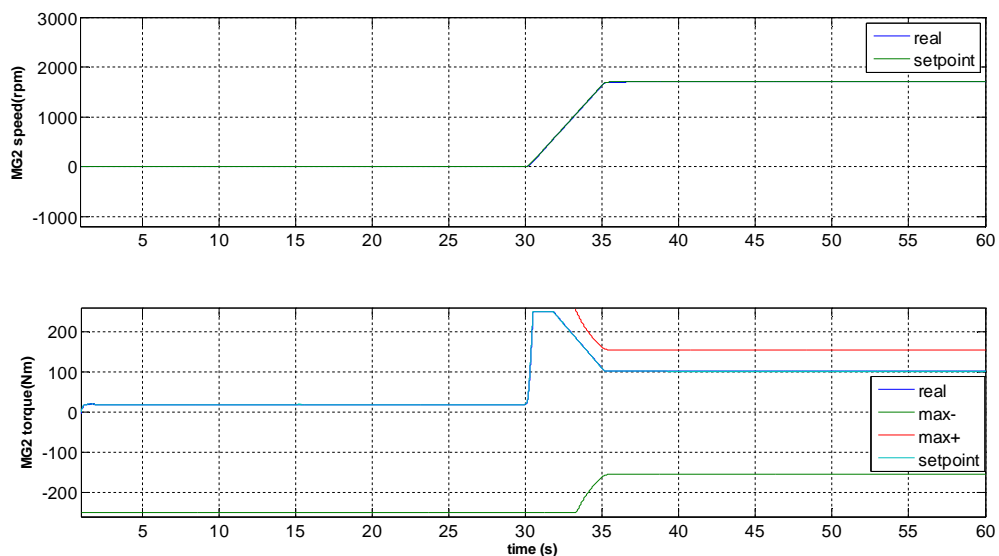


Fig. 2.43 – Simulation 5, MG/2 speed and torque

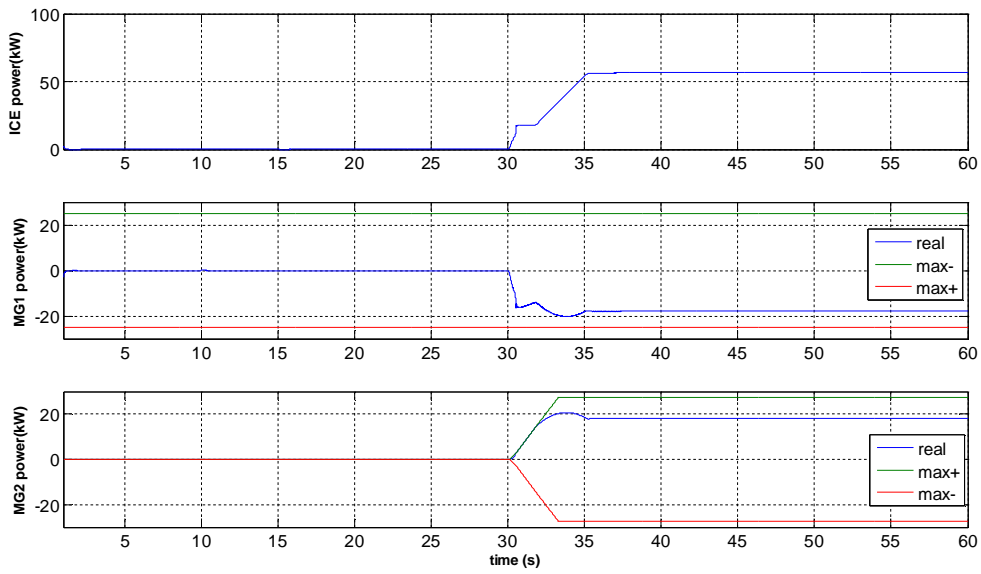


Fig. 2.44 – Simulation 5, Machines power

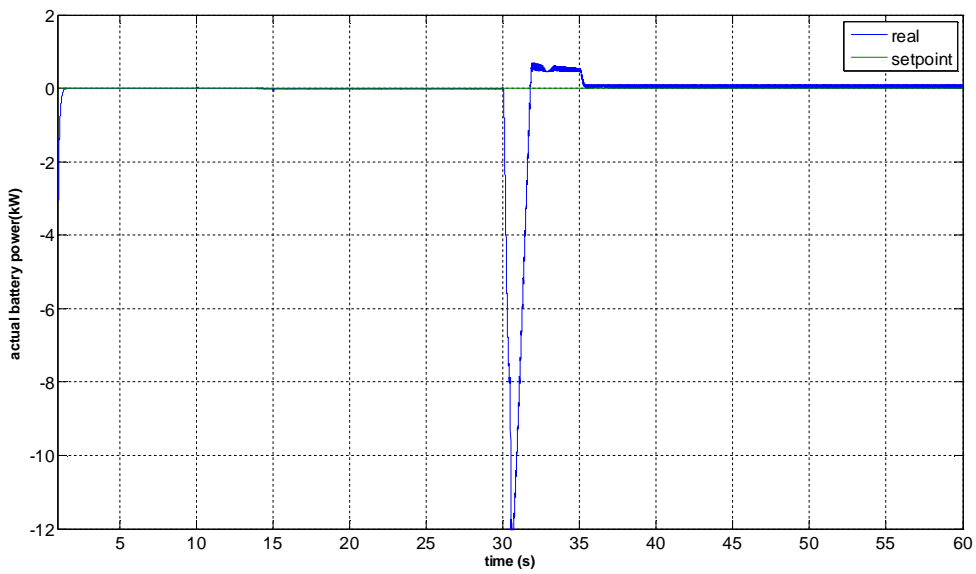


Fig. 2.45 – Simulation 5, Battery power

### Simulation 6 – Battery recharge at constant speed

This simulation shows the behavior of the vehicle system when the speed is constant and fixed by the driver, under a zero traction load. The ICE speed is controlled by the maximum efficiency strategy, while the battery recharge power setpoint is varied by the battery management system (e.g. to enhance or maintain the state of charge).

#### Setpoint signals:

Ground speed setpoint: Constant

ICE speed setpoint: Max efficiency

Battery power setpoint: Variable

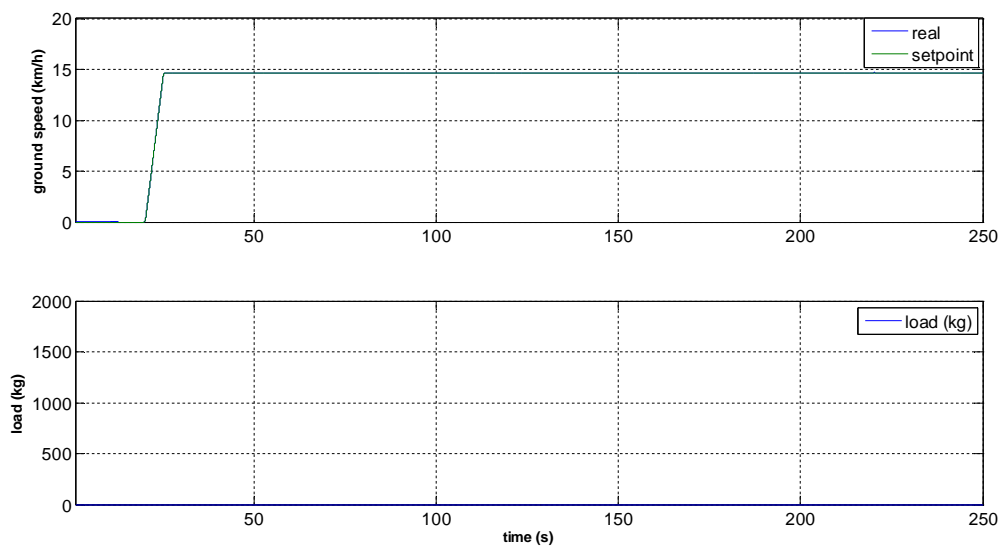


Fig. 2.46 – Simulation 6, Ground speed and load

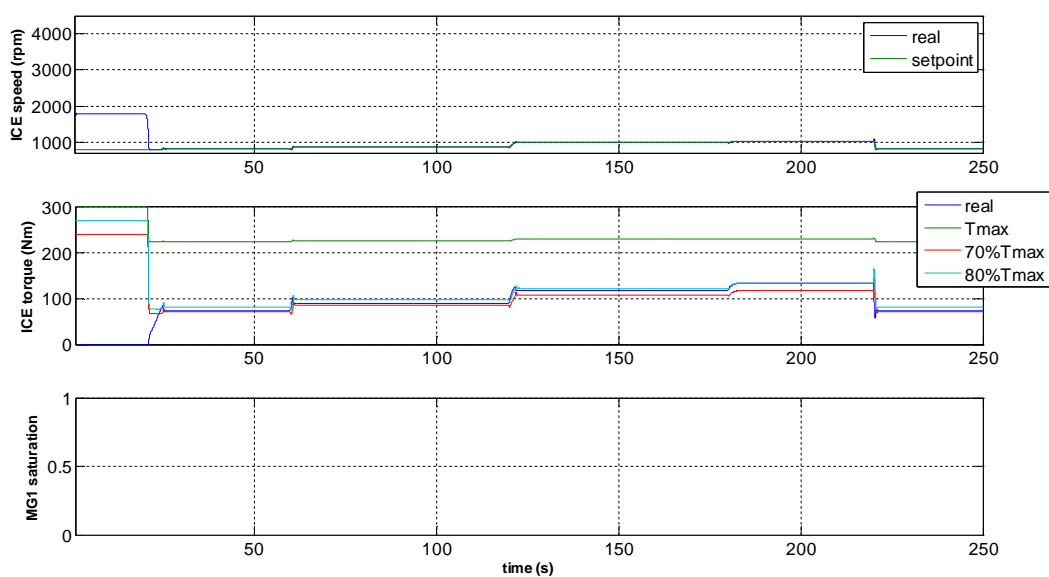


Fig. 2.47 – Simulation 6, ICE speed and torque, M/G1 saturation

**Description:** Three recharge power steps have been required, while the vehicle is proceeding at constant speed (15 km/h) and no load is present. As the graphs show, all the control goals are respected, except the last step of battery regenerating power (10 kW). In this conditions the maximum power is limited by the M/G2 power, which cannot be overridden. Another control strategy would permit to generate more power, controlling the M/G1 machine also as a generator, but losing the possibility of choose the torque employing of the ICE. It's worthy to say that the optimal condition to recharge batteries is at high speed, with stopped MG/1 and regenerating MG/2 (OD1 mode), having all the available power from the external machine.

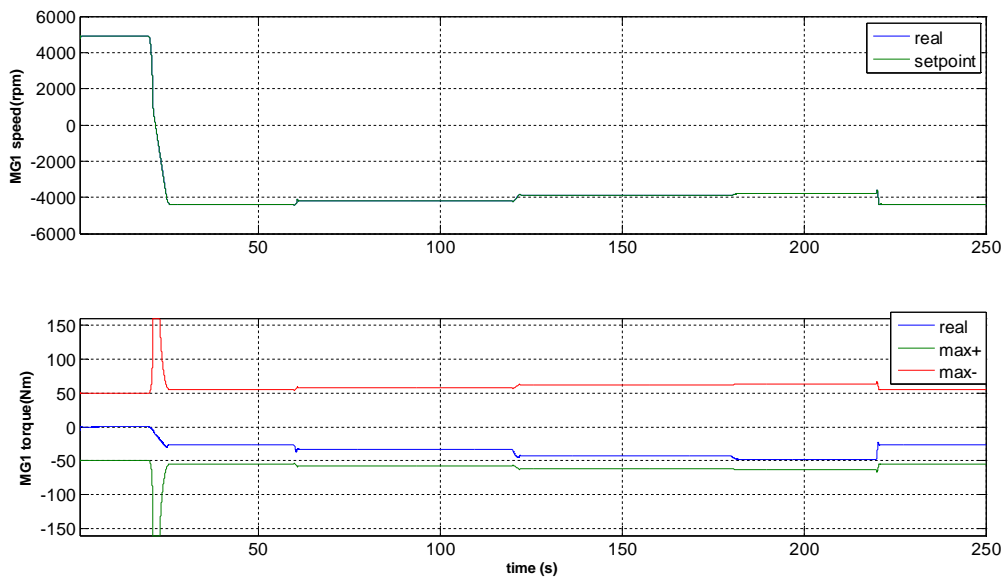


Fig. 2.48 – Simulation 6, MG/1 speed and torque

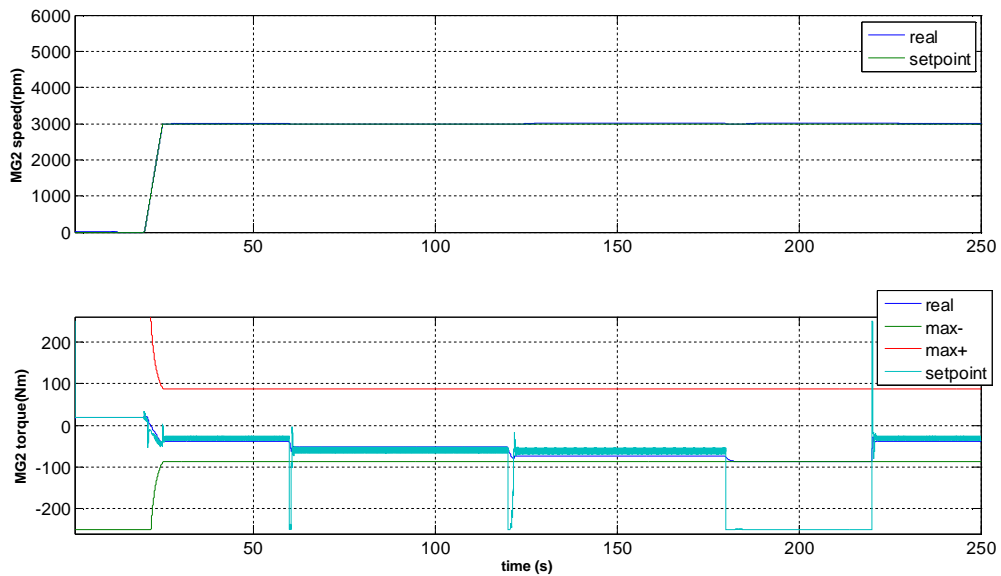
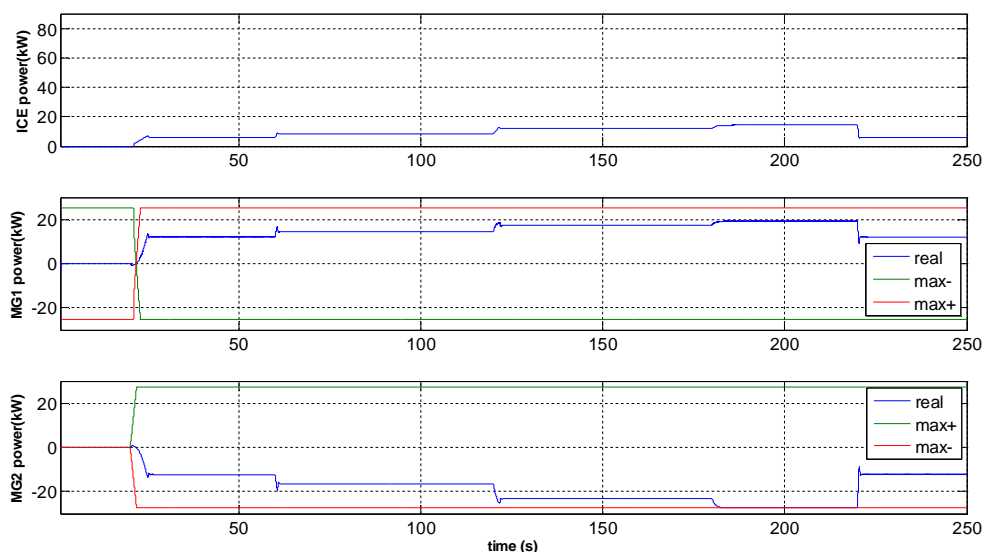
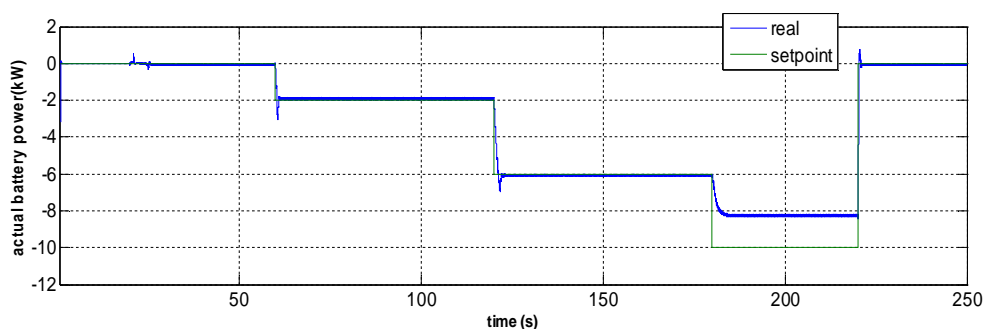


Fig. 2.49 – Simulation 6, MG/2 speed and torque



*Fig. 2.50 – Simulation 6, Machines power*



*Fig. 2.51 – Simulation 6, Battery power*

## 2.7 Conclusions

A new tractor transmission based on the e-CVT power split device has been proposed. The operating modes and functionality of the new vehicle have been presented, together with the vehicle control system.

The simulations of the hybrid mode operation have shown a good dynamic and steady state behavior, in the following situations:

- Fixed load and variable speed;
- Fixed speed and variable load;
- High load startup;
- Varying battery power request.

The tractor is in a prototypal phase, the hardware is almost completed and the testing phase should be started in the next months.

## **References**

- [1] S.M. Savaresi; F.L. Taroni; F. Previdi; S. Bittanti; “Control system design on a power-split CVT for high-power agricultural tractors”. *Mechatronics, IEEE/ASME Transactions on*. Issue Date: Sept. 2004.
- [2] Liyou Xu, Zhili Zhou, Fuyi Cao, Mingzhu Zhang, “Research of Speed Ratio Matching Strategies of Hydro-Mechanical Continuously Variable Transmission System for Tractor”. *Intelligent Computation Technology and Automation, 2009. ICICTA '09. Second International Conference on*. Issue Date: 10-11 Oct. 2009.
- [3] Zhang Mingzhu, Zhou Zhili, Xie Jinfa, Xi Zhiqiang, “Modeling and control simulation for farm tractors with hydro-mechanical CVT”, *Automation and Logistics, 2008, ICAL 2008. IEEE International Conference on*. Issue Date: 1-3 Sept. 2008.

---

# Chapter 3

## Hybrid e-CVT ship propulsion

### 3.1 Introduction

In the naval sector there is a growing interest in new operating mode of a ship that can be summarized as follows:

- pure electric propulsion in a low-medium speed range, without any pollution in the point of use (docking, endangered environment, etc.);
- high maneuverability and high control capability of the propulsion thrust at low speed either in forward or backward direction (docking, position holding, pulling, thrusting);
- combined production of energy for the on board electric power system and for the propulsion system;
- reduction of fuel consumption and emissions over a mission characterized by different operating condition both for the propulsion and for the electric power system;
- supplying the on board electric power system in silent mode, without using thermal engines.

Even if these features could be realized by pure series driveline [1], in several categories of ships it is desirable to maintain the more traditional configuration of the driveline constituted by thermal engine coupled to the propeller shaft through a fixed ratio reduction gearbox.

The driveline proposed in this chapter is installed between the engine flywheel and the propeller shaft, and substitutes the traditional gearbox with almost the same volume and the same mechanical couplings. It can be targeted to small vessels, in the 1MW power range. The categories of ships which could take advantage from this new hybrid propulsion system are: leisure boats, tugs, passenger ships like that for inner water lines and also some simpler configuration of war crafts.

The developed drivetrain concept is based on the power split E-CVT (electrically continuously variable transmission) configuration which realizes a real hybrid propulsion

system with several advantages of a series naval driveline configuration, but with a significant size reduction of the electric and power electronic components of the driveline.

The operation of the analyzed e-CVT based HySP (Hybrid ship propulsion) requires an energy storage device (battery pack) for management of the energy exchanged by the e-CVT with the rest of the electric vessel power system. Choice of the type, and sizing of these batteries depends mainly on the power/energy requirements of the vessels and on performance demanded in pure electric propulsion. Battery technology is now booming, because it is supported by the expansion of hybrid and electric vehicles and actually does not represent a technical limit for this application.

### 3.2 Concept of the HySP e-CVT driveline

The core of the power split electric continuously variable transmission (E-CVT) shown in *Fig. 3.1* is a planetary gear set. The outer part is the ring which is connected to the thermal engine (ICE), the intermediate part is the carrier, coupled to the propeller shaft, the inner part, the third element of the planetary gear (sun) is connected to an electric machine, called also ‘**driver**’, operating over four quadrants.

The mechanical layout of the transmission is shown in *Fig. 2.1*, where the three planetary gear’s components are pointed out by three different colors:

- **SUN WHEEL** (green): the sun is coupled to the electrical machine EM, which is integrated within the transmission. The internal disc brake is also put in evidence.
- **CARRIER WHEEL** (blue): it’s coupled to the output shaft, going to the propeller. The output disc brake is also pointed out.
- **RING WHEEL** (red): the ring is coupled to the ICE shaft.

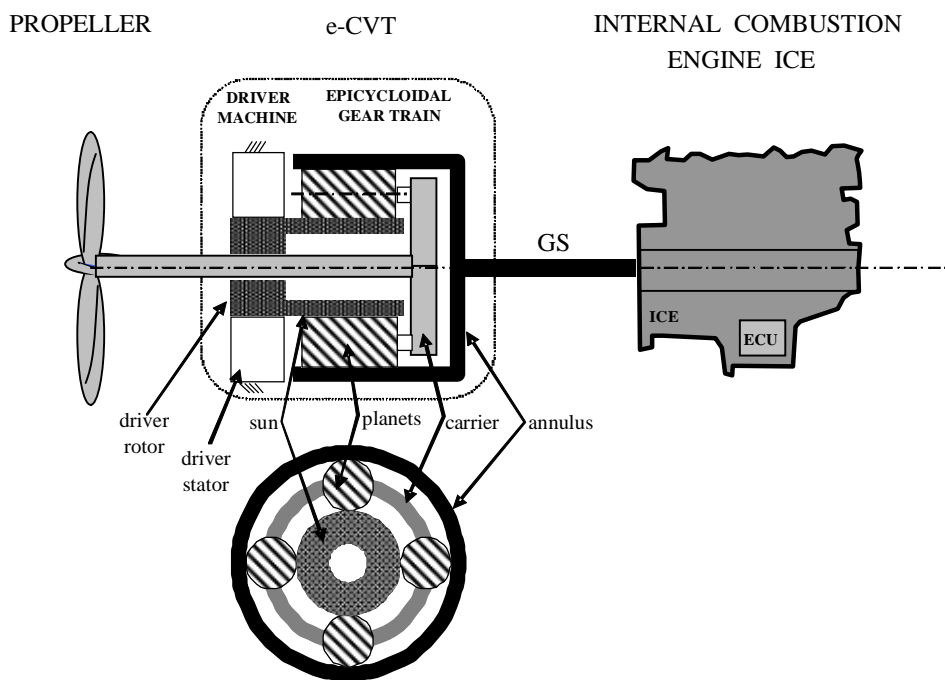


*Fig. 3.1- Scheme of the power split e-CVT for hybrid ship propulsion*

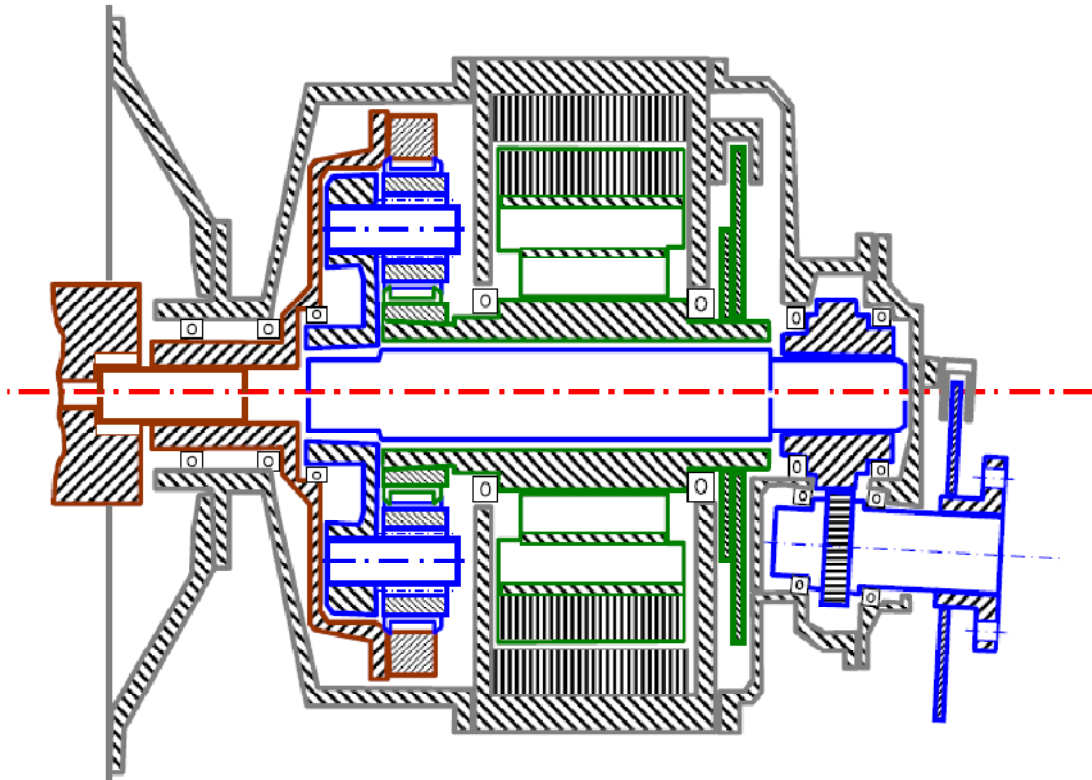


*Fig. 3.2- Mechanical layout of the power split e-CVT for hybrid ship propulsion*

The remaining parts (gray) are fixed to the chassis. The bearings position has also been pointed out. The transmission box is intended to replace the original and traditional gearbox, with no modifications in the vessel structure.

In this application of the planetary gear set as power split, each of the three elements of the epicyclic gear set can be configured as power input or output, or can be held stationary. Choosing which part plays which role, a fixed or variable speed ratio between input and output and the consequent power flow can be determined [3]. In the par. 3.3 the different functional modes will be dealt with, remarking the above mentioned aspects.

The electrical layout of the hybrid drivetrain equipped vessel is essentially made up by the following elements:

- **Battery pack:** The battery system should be sized in order to supply the on board electric system, for a determined time. Another criteria could be the desired mileage in pure electric propulsion. In this case the battery pack is not only an energy buffer, but becomes an energy source, since it must have enough capacity to power the loads (utility or propulsion) for a certain time.
- **Inverter EM:** The power converter supplying the electrical machine is a fully controlled four quadrants inverter, bidirectional in voltage and current. It must be sized for the maximum current required by the control system.
- **ICE, electric drive and vessel control units:** The different control units must be capable of controlling and automate the drive train system in the different operating modes, to supply the batteries and the on board electric loads, and to guarantee the operation safety, and the diagnostic standards for the ship.

- **On board electric system:** The on board loads can be supplied silently by the battery/inverter system, until the battery is discharged, afterwards the ICE can be started to recharge battery without propelling the vessel. An additional gen-set system is not required to supply the electric loads.

### 3.3 Operating modes overview

In order to achieve the goals described in par. 3.1, the developed transmission has three possible operating modes, to be switched one upon the other by the control system, depending on the vessel speed requirement and the battery state of charge.

The three operating mode are:

- Pure electric propulsion
- Pure thermal propulsion
- Hybrid propulsion

#### 3.3.1 Pure electric propulsion

In this operating mode, the ICE is switched off and braked ( $n_{RICE}=0$ ). The propeller shaft is driven only by the electric machine integrated within the transmission. In Fig. 3.3 the speed nomogram, and the speed relationships of this modality are shown.

Pure electric propulsion consists of controlling the propeller shaft at medium-low speed, in both direction, with an accurate and smoothed speed control, which is proper of electric drives connected to the sun of the planetary gear train.

For example, if the sizing of ICE, propeller and hull are well matched, meaning that the full propeller load is given at the maximum speed of the ICE, and at the maximum speed of the vessel (for a displacing hull) a realistic power sizing of the EM integrated in the E-CVT is about 10% of the engine rated power. With this sizing it is possible to drive the propeller up to about the 50% of its rated speed, meaning driving the vessel up to 30% of its maximum speed. Of course the size of the batteries influences the mileage of the ship operated in this

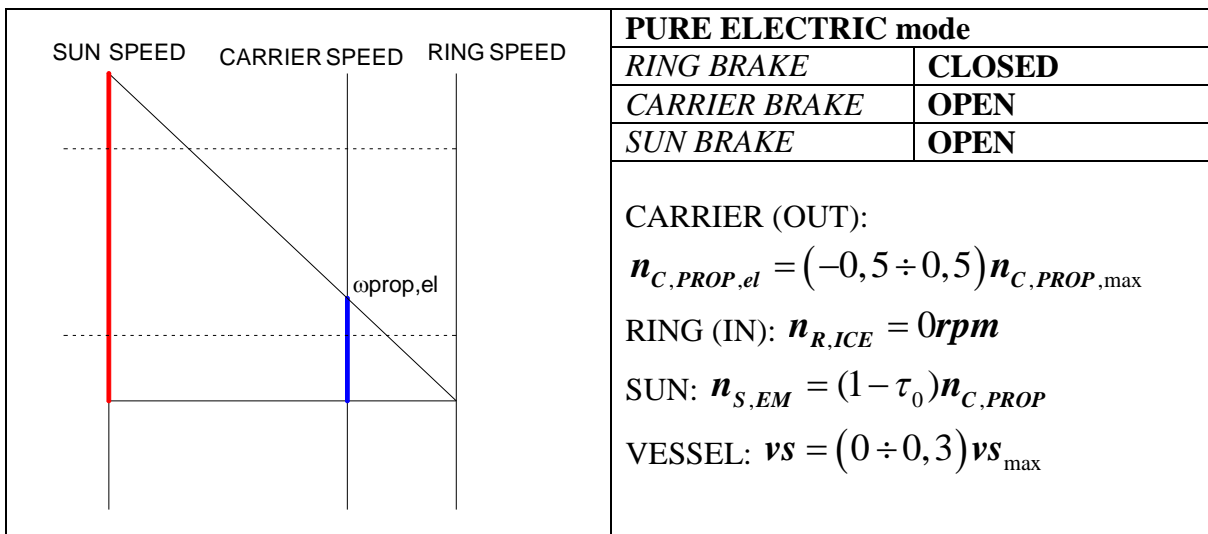


Fig. 3.3- Pure electric mode - Speed nomogram, mechanical configuration and speed relationship

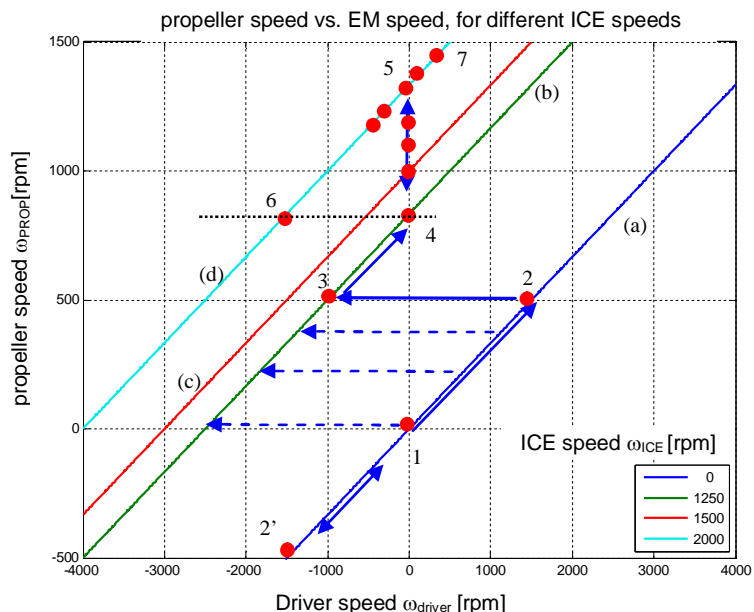


Fig. 3.4- Relationships between speeds in E-CVT power split

way.

In the example of Fig. 3.4, by considering the ICE switched off and stopped, the relationship between the propeller and the EM speed is represented by curve (a) between point (2) and (2'). The diagram of Fig. 3.4 represents the propeller speed as a function of the EM speed, for fixed ICE speeds.

### 3.3.2 Pure thermal propulsion

In this operating condition the EM integrated with the transmission is switched off and kept stopped by a mechanical brake. The ICE is coupled to the propeller shaft through a fixed reduction ratio, as shown in the scheme of Fig. 3.5.

In this way the E-CVT operates as a traditional pure mechanical transmission delivering all the engine power to the propeller shaft. This operating mode will be preferred at the maximum power. In the example of Fig. 3.4 pure thermal operation mode is represented by

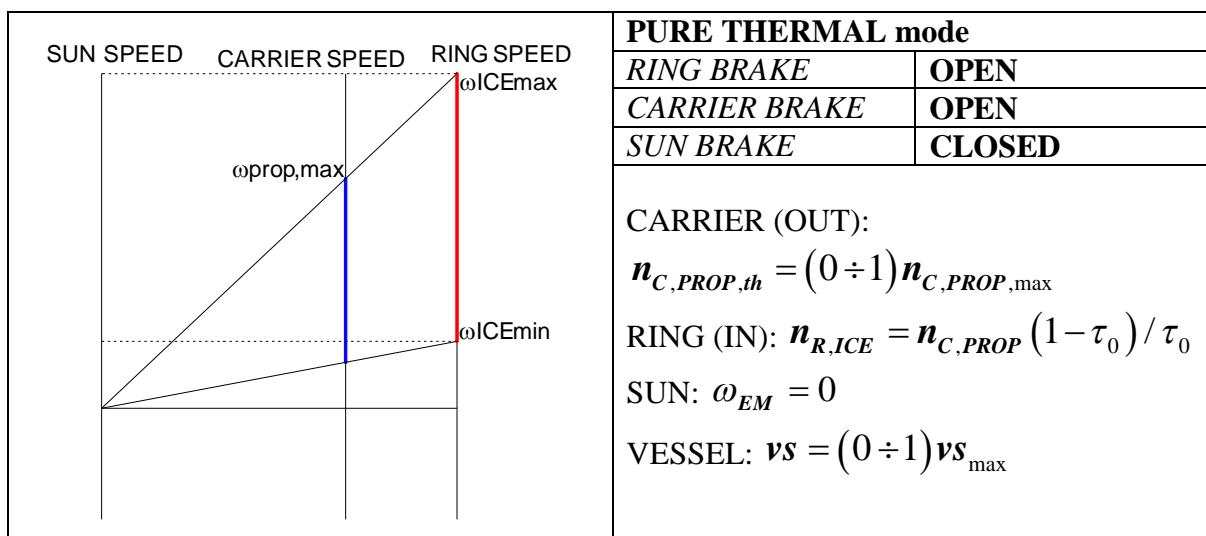


Fig. 3.5- Pure thermal mode - Speed nomogram, mechanical configuration and speed relationship

points aligned from 4 to 5 in the vertical axis ( $n_{S/EM}=0$ ).

### 3.3.3 Hybrid mode

In hybrid mode both the ICE and the EM are operated for controlling the propeller speed and the electric power flow between the transmission and the on board energy system.

A given propeller speed  $n_{C,PROP}$  can be obtained by operating the engine at a speed  $n_{R,ICE}$ , depending on the speed of the driver  $n_{S,EM}$  (Willis formula, cfr. eq. 1.4). In steady state conditions, the torque applied by the EM  $T_{S,EM}$  and by the engine  $T_{R,ICE}$  are related to the load torque  $T_{C,PROP}$  by means of eq. (1.7). In other words, in stationary condition, for a given propeller load operating point ( $n_{C,PROP}, T_{C,PROP}$ ), it is possible to regulate the power of the driver machine ( $P_{S,EM} = \omega_{S,EM} T_{S,EM}$ ), by selecting the corresponding value of  $n_{S,EM}$  and than by (1.4) the corresponding speed of the engine  $n_{R,ICE}$ . The operating limits of the system are defined by the limit mechanical characteristics ( $T_{MAX,n}$  curves) of the three elements of the transmission (load, engine, electrical machine). Anyway, the use of the cinematic diagram of Fig. 3.4 is useful to understand the regulation capability of the transmission in hybrid mode: a given propeller speed, for example  $\omega_C=800$ rpm (the dotted line between point 4 and 6), can be obtained for engine speed ranging from 1250 and 2000 rpm, by regulating the driver speed from 0 to 1500rpm (negative) respectively. Each EM speed value corresponds to an electric power level generated. That power value depends only by the driver speed at fixed carrier speed, because the driver torque is fixed (at steady state).

The nomogram of Fig. 3.6 shows a fixed ICE speed condition, where the carrier speed is varied by changing the driver/sun speed: the three colored zones represents the different

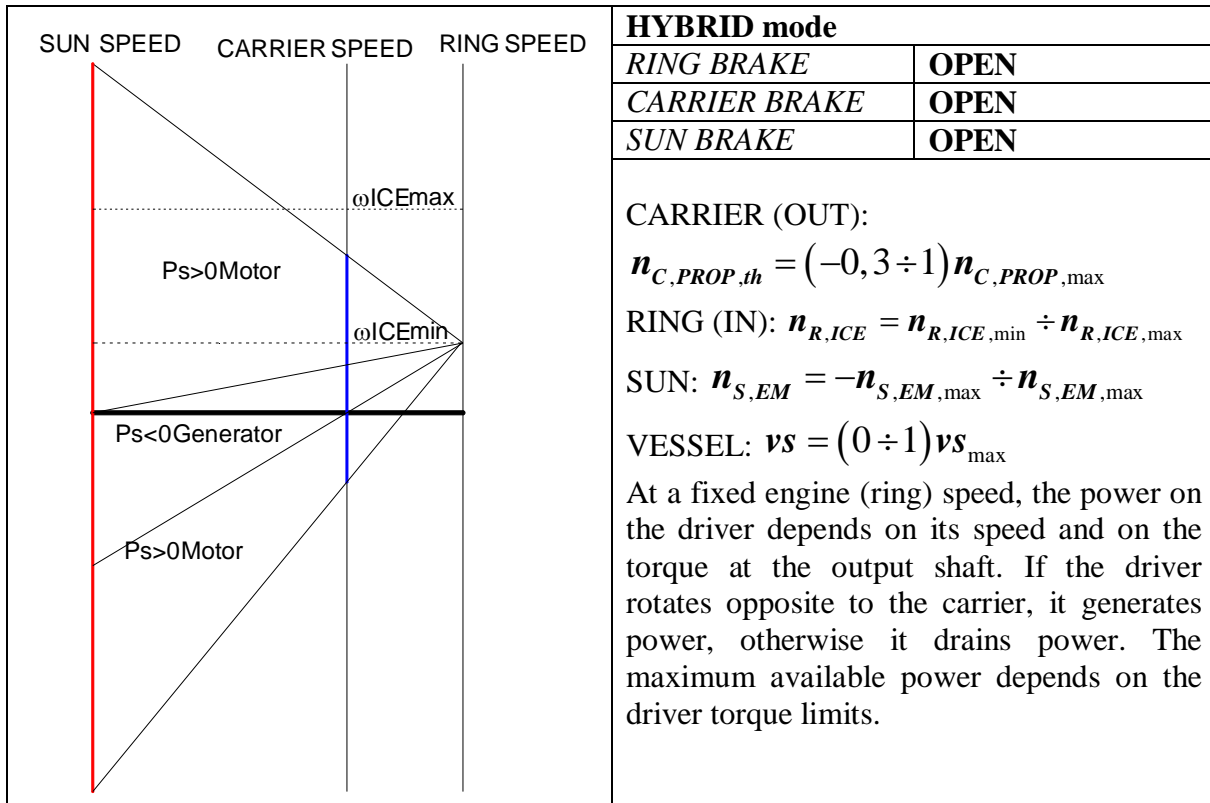


Fig. 3.6- Hybrid mode - Speed nomogram, mechanical configuration and speed relationships

operating modes of the driver. When the output (carrier) speed (thus the output torque) and the driver speed have the same sign, the EM is a motor, otherwise it is a generator. Choosing adequately the driver speed it's possible to generate the desired power, of course respecting its torque limits. It's worthy to observe that the propeller can be taken to negative speeds even with a finite ICE speed, obtaining a fast and smooth vessel reverse way operation.

In the case electric power  $P_S$  goal is not assigned, the transmission earns a degree of freedom that can be exploited in certain operating conditions. This is the case of assigning the engine speed as in the following cases:

#### Start up of the ICE

Engine start up is obtained in the traditional way, by using its starter electric motor coupled to the flywheel of the engine. In *Fig. 3.4* this phase is represented by horizontal dashed lines connecting points from curve (a) to curve (b). During the start up of the engine, according to (1), the propeller speed can be kept constant at its initial value, by varying the speed of the driver as a function of the variation of the engine speed. Otherwise the propeller speed can be briefly reduced, helping the ICE start-up, as will be shown by the simulations.

#### Regulation at low speed

At medium-low propeller speed, for a given constant speed of the ICE, it is possible to implement a precise and smoothed speed regulation of the propeller shaft in both direction by controlling the speed of the driver. For example in *Fig. 3.4*, assuming the ICE rotating at low and constant speed, for example  $n_{R,ICE} = 1250$  [rpm], the EM integrated with the transmission is used to regulate the speed of the propeller along curve (b) in both direction.

#### Boost at high speed

For a given value of the engine speed it is possible to increase the propeller speed from the speed with the driver stopped (pure thermal propulsion). In this condition, shown in *Fig. 3.4* along the curve d) between points 5 and 7, the driver adds power to the system.

## 3.4 Case study: analysis of the operating limits

A 800 HP propulsion system for a yacht have been considered as case study. After choosing the components for the examined propeller, ICE and electrical machines, a methodology to size the planetary geartrain will be shown. Finally, the operating limits of the system will be analyzed.

### 3.4.1 Propeller (CARRIER)

The propeller load is modeled as a cubic power curve [7] as a function of the rotating speed (*Fig. 3.7*). This is a simplification of the real propeller load curve that does not take into account the vessel speed and the aging of the propeller blades. The propeller maximum power matches the thermal engine maximum power in pure thermal propulsion operating mode.

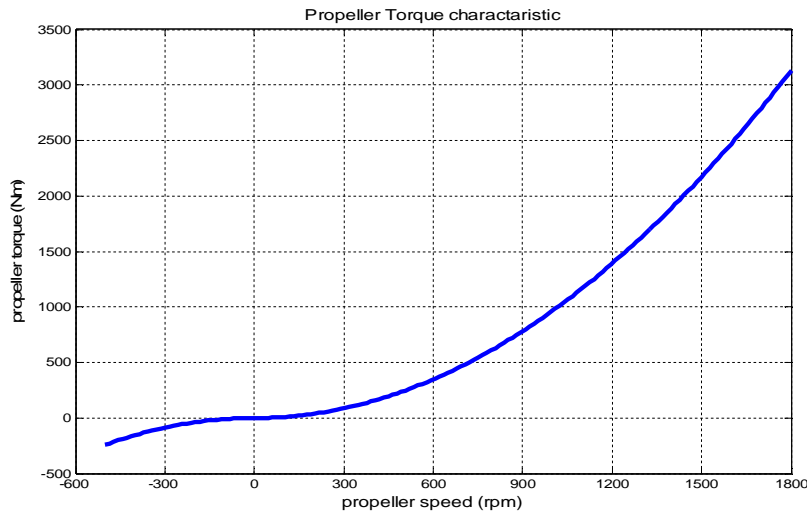


Fig. 3.7- Propeller torque curve

### 3.4.2 Diesel Engine (RING)

The selected ICE is a marine 800 hp Diesel engine (MAN R6-800), which is commonly used in propulsion of ships like pleasure crafts, escort boats, patrol or police boats, ambulance boats. It's a very efficient propeller, equipped with a ultimate marine propeller common rail. Thanks to this technology, this marine motor respects all of the limits introduced by the severe anti-pollutants legislations at world level.

The MAN R6-800 engine has the technical features listed in *Tab. 3.1*.

The full load mechanical characteristic of the engine is released by the manufacturer, and is represented in *Fig. 3.8*.

It's remarkable that the ICE has the possibility to operate with a braking torque when carried by an external torque: this is one of the possible operating conditions of the vessel drivetrain. The maximum torque developed by the motor in brake mode is about 1/3 of the maximum torque in motoring mode. The curve of *Fig. 3.8* has been used in the model of the engine, which has been used to simulate the control system of the drive train.

### 3.4.3 Electrical machine (SUN)

The *driver* connected at the sun is an electric drive supplied by a battery pack, operating over four quadrants. Induction machine IM and internal permanent magnet synchronous machine IPM-SM are the best candidates for this application. The very best sizing of this system can be reached if the driver is able to generate higher torque at low speed and to

Type of engine	R6-730	R6-800
Displacement (l)	12.82	12.82
Maximum output to DIN ISO 3046-1 kW (mhp)	537 (730)	588 (800)
Rated speed (rpm)	2,300	2,300
Maximum torque (Nm)	2,512	2,700
at speed (rpm)	1,200 - 2,100	1,200 - 2,100
Weight (dry) (kg)	1,305	1,305
Fuel consumption at rated power (l/h)	145	158

(1) The ratings are only for operation of private yachts.

Tab. 3.1 – Technical data of the MAN engines

Rated torque $T_r$ (Nm)	300
Rated speed $n_r$ (rpm)	2000
Pole pairs	6
Rated frequency (Hz)	200
Max speed (rpm)	8000
Max frequency (Hz)	700
Max overload torque (Nm, overload)	600
Speed at max torque (rpm)	1000

Tab. 3.2 – Technical data of the driver machine

operate at constant power over a wide speed range.

The electric machine should be controlled in maximum torque per current MTC, all over the speed range. In this application the dynamic response demanded to the electric drive is not very fast, being comparable with that of an ICE. Best control technique recommended for this application are the rotor flux oriented vector control for IM [4] - [5] and segmented magnets rotor design combined with an optima flux weakening trajectory for IPM-SM [6].

In this paper a very simplified model of this electric drive is considered. The dynamic response of the electric drive is modeled as a torque follower with a first order response applied between the reference and the applied torque all over the speed range. The mechanical output limits of the electrical drive are represented by assuming a speed range operating at constant rated torque  $T_r$  from 0 to rated speed  $n_r$ , constant rated power from  $n_r$  to  $2n_r$ , and a speed range operating at decreasing power from  $2n_r$  to  $4n_r$ . Torque overload can reach  $2T_r$ , up to a speed corresponding about to  $1/2 n_r$ . A closed loop regulation system based on a simple PI regulator has been implemented for the speed control of this electric drive.

For the case analyzed in this chapter, the electrical machine has been rated to 10÷15% of the maximum propeller power, reporting the technical features of Tab. 3.2.

The driver torque limit is shown in Fig. 3.9, where the blue line represents the rated torque, and the dashed line the overload torque, which can be maintained until the thermal stress on the machine is acceptable. The torque limits of the driver represents the limits of the transmission in hybrid mode, as will be shown in the next paragraph.

#### 3.4.4 Choice of the planetary gear set

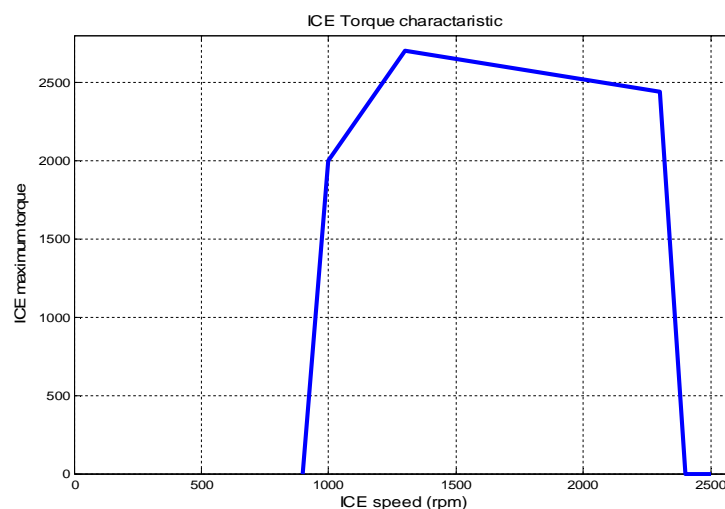


Fig. 3.8- MAN R6-800 full load torque curve

The sizing of the planetary gear set is made by considering the available machines (ICE and electrical machine) characteristics, the propeller load characteristic and fixing the desired performances of the transmission:

- Getting at least  $n_{C,PROP}=800$  rpm in pure electric;
- Getting at least  $n_{C,PROP}=1200$  rpm in hybrid mode;
- Getting the max speed  $n_{C,PROP}=1800$  rpm in pure ICE mode.

The desired propeller/ICE speed ratio is thus determined by:

$$\tau_{C/R} = \frac{n_{C,max}}{n_{R,max}} = \frac{1800}{2200} = 0,8181 \quad (3.1)$$

Which determines a  $\tau_0$  ratio:

$$\tau_0 = \frac{n_S}{n_R} = \frac{\tau_{C/R}}{\tau_{C/R} - 1} = -4,2631 \quad (3.2)$$

Obtainable for example choosing the teeth number of the sun and the other wheels:

- S=39
- P=68
- R=175

This choice give  $\tau_{C/R} = 0,8178$ , thus very close to the goal.

Now the condition 1) in pure electric mode must be verified, considering the torque at the propeller at 800 rpm:  $T_{C,PROP}(800rpm)=618Nm$ . This operating point corresponds to the following point of the electrical machine in pure electric:

$$\begin{aligned} n_S(n_C = 800rpm) &= (1 - \tau_0)n_C = 4309rpm \\ T_S(T_C = 618Nm) &= T_C / (1 - \tau_0) = 112Nm \end{aligned} \quad (3.3)$$

This operating point is possible because the maximum torque of the EM at 4309 rpm is 139 Nm. The torque necessary to brake the ring shaft during this operating mode is 505 Nm.

Now the condition 3) in pure ICE mode must be verified. The propelling torque at 1800 rpm must be:  $T_{C,PROP}(800rpm)=618Nm$ . The ICE operating point should be:

$$\begin{aligned} n_R(n_C = 1800rpm) &= [(1 - \tau_0) / \tau_0]n_C = 2200rpm \\ T_S(T_C = 3110Nm) &= T_C [\tau_0 / (1 - \tau_0)] = 2560Nm \end{aligned} \quad (3.4)$$

The max ICE torque at 2200 rpm is slightly lower than this value, but this is considered acceptable.

In case the sun is controlled by the electric drive, it should develop the max torque of the ICE reported at the sun, which can be developed by ICE in dynamic conditions:

$$T_{S,max} = -T_{R,max} / \tau_0 = 601Nm \quad (3.5)$$

This is obtainable by overloading the EM two times in the constant torque region, which is possible for the electrical machine, within the limits imposed by the thermal strength.

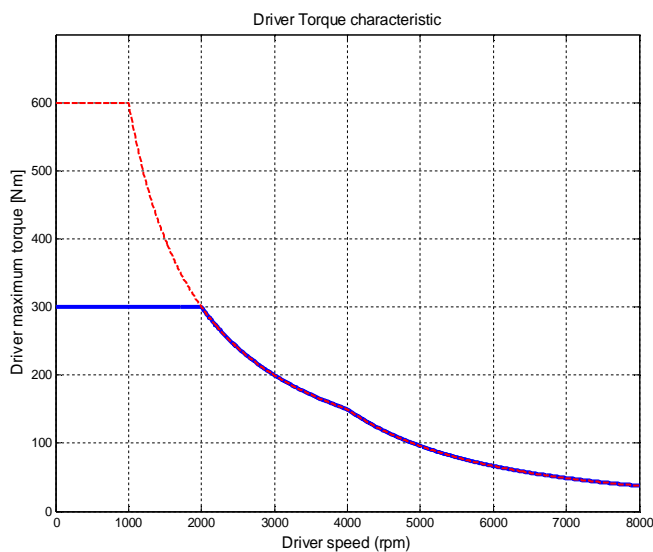


Fig. 3.9- Driver machine torque limit curve

### 3.4.5 Operating limits of the driveline in Hybrid mode

In order to realize the operating capability of the power split E-CVT transmission in hybrid mode the system is analyzed by considering the thermal engine operating at a given constant speed, and the driver output torque limited at the rated curve given in Fig. 3.9.

In the following example the ICE is controlled at constant speed  $\omega_{R,ICE}=1000$  rpm. For this low speed operation of the ICE, Fig. 3.10 shows the output maximum torque it is possible to apply at the propeller shaft all over the speed range of the driver. In this diagram the upper limits for positive and negative rotating speed are determined by the equilibrium between output and load torque. The output torque at the propeller shaft and then the operating range is limited by the driver torque. Fig. Fig. 3.10 demonstrates that by keeping the ICE at  $\omega_{R,ICE}=1000$  [rpm], it is possible to control the propeller speed in both rotating sense in the speed range:  $-550\div 1200$  [rpm]. Higher positive operating speed could be obtained by overloading the driver.

Fig. 3.12 represents the torque of the driver while operating along the transmission output characteristic presented in Fig. 3.10. By comparing the two diagrams, the possible operating quadrants of the driver for this example are classified as follows:

- first quadrant, motoring mode: for positive rotating sense of the propeller at a speed higher than  $\omega_{C,PROP}=820$ rpm.
- second quadrant, generating mode: for positive rotating sense of the propeller at speed lower than  $\omega_{C,PROP}<820$  [rpm].
- third quadrant, motoring mode: for negative rotating speed of the propeller.

For the same rotating speed of the ICE ( $\omega_{R,ICE}=1000$  [rpm]), Fig. 3.11 represents the maximum output torque at the engine shaft while operating along the transmission output characteristic presented in Fig. 3.10. It is shown that for negative rotating speed of the propeller the ICE output torque is negative and then the ICE operates in braking mode.

The diagram of Fig. 3.13 represents the maximum power in the three elements of the transmission, when the ICE rotates at  $\omega_{R,ICE}=1000$  [rpm], along the speed range of the propeller shaft shown in Fig. 3.12.

It's clearly shown the important feature of the power split E-CVT to be used as electric power source for supplying the on board power system. This operating condition is obtained by accelerating the driver EM in negative direction ( $\omega_{S,EM}<0$ ,  $T_{S,EM} >0$ , driver in generating mode), meaning the propeller speed is decreased with respect to the value obtained for  $\omega_{S,EM} = 0$ .

The main regulation capability in hybrid mode should be given in terms of electric power  $P_{S,EM}$  that can be generated at the driver for any given rotating speed  $\omega_{C,PROP}$  of the propeller. This analysis is carried out by taking into account the torque limits of the driver and of the ICE, as given in Fig. 3.8 and Fig. 3.9 respectively, and by considering the system in stationary condition with the load torque applied at the propeller shaft as given in Fig. 3.7. The electric power generation capability of the power split e-CVT all over the operating range of the system is represented by the diagrams of Fig. 3.14. In these two diagrams, for any given speed of the propeller  $n_{C,PROP}$ , it is possible to generate an electric power from the driver  $P_{S,EM}$ , by setting the engine speed  $n_{R,ICE}$  as given in Fig. 3.14(a) and by setting the

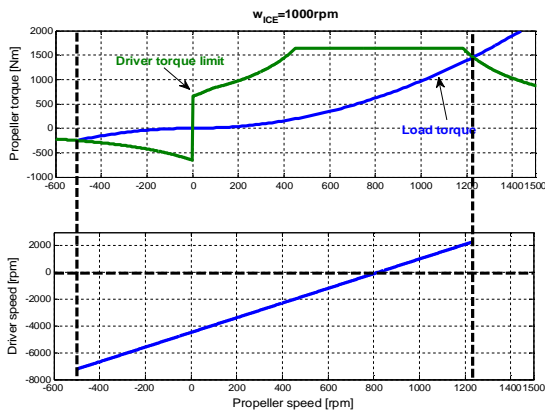


Fig. 3.10. Upper: Output torque of the transmission and load propeller torque vs. propeller shaft speed. Bottom: speed of the driver vs. propeller shaft speed.  $\omega_{R,ICE}=1000$  [rpm].

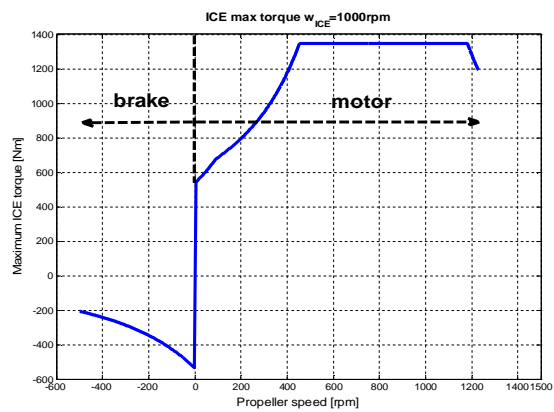


Fig. 3.11 - Output torque of the ICE vs. propeller speed for  $\omega_{R,ICE}=1000$  [rpm]

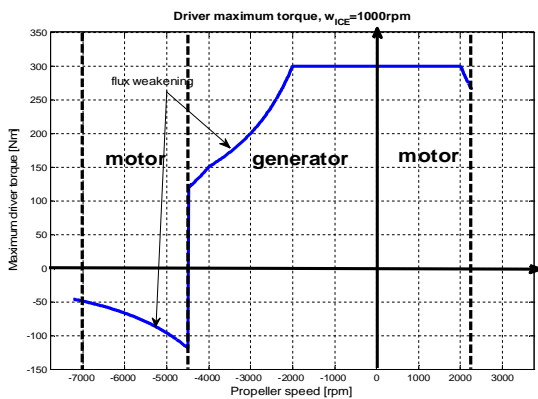


Fig. 3.12 Output torque of the driver EM vs. driver speed for  $\omega_{R,ICE}=1000$  [rpm]

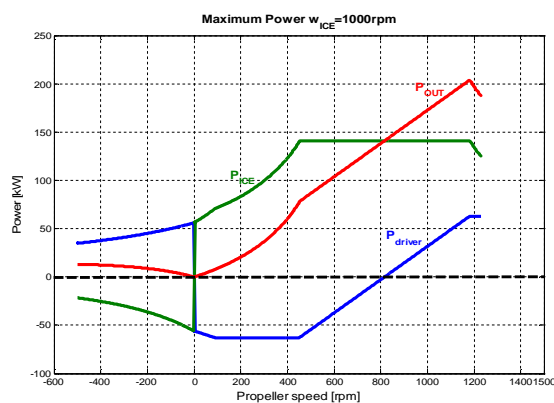


Fig. 3.13 - Maximum power in the three element of the transmission vs. propeller speed for  $\omega_{ICE}=1000$  [rpm].  $P_{ICE}$ : output power of the ICE;  $P_{driver}$ : output power of the driver;  $P_{out}$ : output power at the propeller shaft.

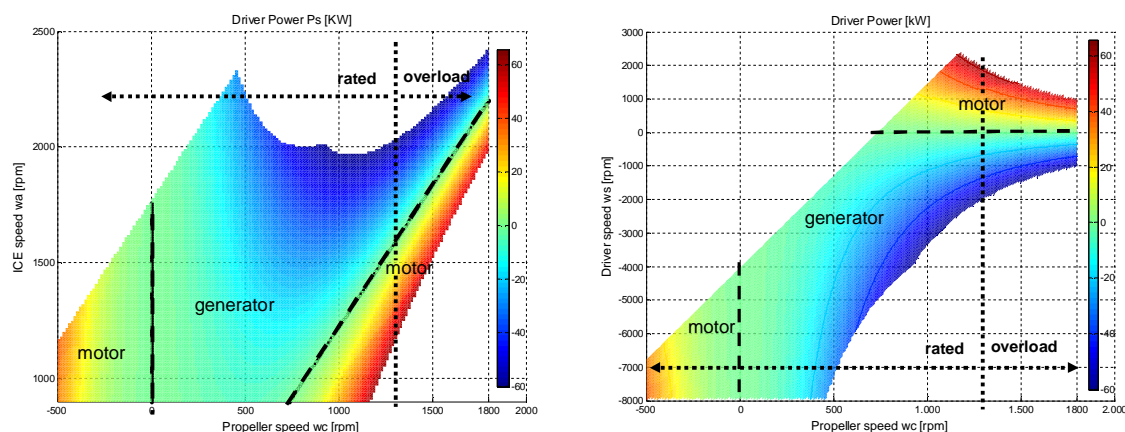


Fig. 3.14- Mapping of the controlled variables (prop. speed and EM power) as functions of a) ICE speed, b) EM speed.

driver speed  $n_{S,EM}$  as given in Fig. 3.14(b). These figures demonstrate the possibility to generate electric power up to a maximum value of about 60kW over a wide range of the propeller speed (with a maximum in the region  $n_{C,PROP}=1091rpm$ ).

In these diagrams, positive driver power values, obtained for positive rotation of the propeller, means the driver adds power to the transmission contributing to accelerate the propeller with respect to the pure thermal propulsion ( $n_{S,EM}=0$ ,  $P_{S,EM}=0$ ). This is the so-called 'power boost' operating mode of the transmission.

Diagrams of Fig. 3.14 include operation of the driver in torque overload condition, as given by the dashed curves in Fig. 3.9. It means that operating points obtained by overloading the driver can be reached during transients or for a limited time only. Permanent operating conditions, corresponding to keeping the driver below the rated torque given in Fig. 3.9 are represented by the cluster of points obtained for propeller speed lower than 1350 rpm (at the left side of the dotted lines in Fig. 3.14). The hybrid mode operation is possible permanently only for  $n_{C,PROP} < 1350rpm$ .

## 3.5 The control algorithm

The control strategy of the E-CVT hybrid ship propulsion system has been conceived starting from an hypothesis: the propelling torque is known as a function of the propeller speed. This assumption may not reflect the reality, but can be very useful to select the operating points of the machines and satisfy the speed and power setpoints.

### 3.5.1 Layout of the control system

The goal of the control system is basically to generate the control signals for the ICE and for the driver control units:

- ICE torque setpoint ( $T^*_{R,ICE}$ );
- Driver torque setpoint ( $T^*_{S,EM}$ ).

starting from the following inputs:

- Propeller setpoint speed ( $n^*_{C,PROP}$ );

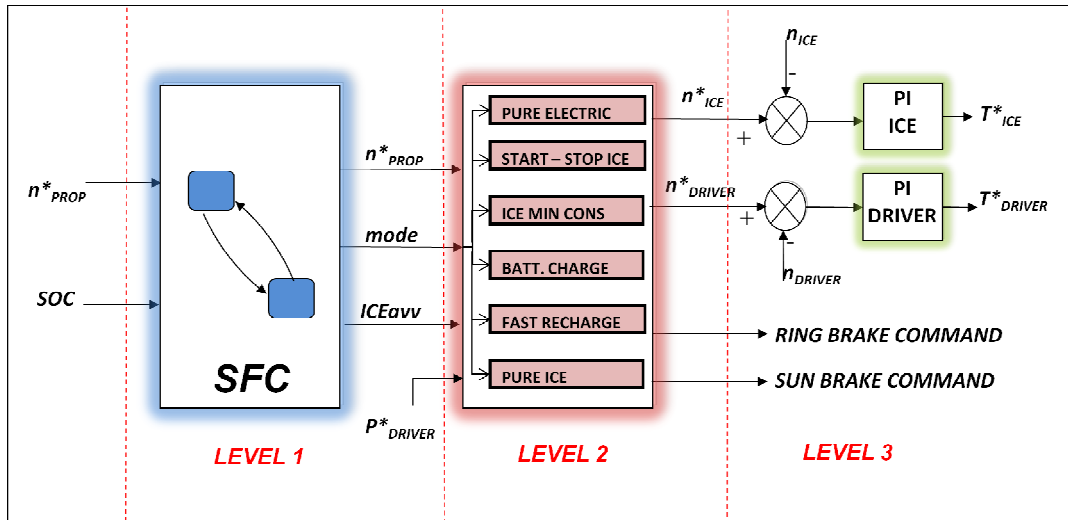


Fig. 3.15- Layout of the HySP E-CVT power split control system

The Sequence control takes as inputs the desired propeller speed and the state of charge of the battery. Its outputs are basically the operating mode and the signal of start and stop of the ICE. The operating mode depends fundamentally on the required output speed and on the battery SOC, and realizes different goals, such as pure electric propulsion, battery recharging, minimization of fuel consumptions. For each operating mode, the parameters of the speed control loop (level 3) are modified, as shown in *Tab. 3.3*, where all of the operating modes are described in detail. The ten operating modes are the following:

1. ONLY\_EM: Pure electric propulsion (low speed, high battery charge)
2. START\_ICE: Starting of the ICE (medium speed or medium battery charge)
3. MIN\_CONS\_1: ICE max efficiency (medium/high speed, high battery charge)
4. ONLY\_ICE\_1: Pure Diesel propulsion (highest speeds)
5. RECHARGING\_MODE\_1: Generated power setpoint (medium/high speed, medium battery charge)

°	MODE	CONDITIONS	DESCRIPTION	EM PARAM			ICE PARAM		
				T <sub>LPF</sub> (s)	P	I	T <sub>LPF</sub> (s)	P	I
1	ONLY_EM	$n_{C/PROP} < 800$ SOC=1	ICE stopped and braked $n_{R/ICE}^* = 0$ $n_{S/EM}^* = n_{C/PROP}^* (1 - \tau_0)$	0,1	10	1	$10^{-5}$	1	$10^3$
2	START_ICE	$n_{C/PROP} > 800$ SOC=1,2,3	ICE brake disengaged $n_{C/PROP} = 0.55 * n_{C/PROP}$ to allow the ICE start-up by mean of the driver machine.	0,1	1	4	10	1	$10^4$
3	MIN_CONS_1	$n_{C/PROP} = 800 \div 1200$ SOC=1	$n_{C/PROP}$ is followed and the fuel cons. are minimized. $n_{S/EM}$ e $n_{R/ICE}$ from the matrix Cluster_rif	0,1	10	1	50	1	10
4	ONLY_ICE_1	$n_{C/PROP} > 1200$ SOC=1	Reached from state 3, as the propeller speed setpoint rises above 1200 rpm and SOC=1. EM braked. ICE respects Willis.	$10^{-5}$	10	$10^{-4}$	$10^{-5}$	1	1
5	RECHARGING_MODE_1	$n_{C/PROP} = 800 \div 1200$ SOC=2	From phases 1,2,3,8, if SOC=2, this mode is activated. The propeller speed setpoint is satisfied, the EM power is taken as close as possible to the setpoint (by Cluster_rif)	0,1	10	1	50	1	$10^3$
6	RECHARGING_MODE_2	$n_{C/PROP} > 1200$ SOC=2,3	This mode is activated if, from phase 4, SOC falls to 2 or 3. The maximum power production is activated, after operator's command. $n_{C/PROP} = 1081$ ; $n_{R/ICE} = 1950$ ; $n_{S/EM} = Willis$	0,1	10	1	50	1	$10^3$
7	RECHARGING_MODE_3	$n_{C/PROP} = 800-1200$ SOC=3	This mode is selected when, from phase 5, the SOC falls to 3. The maximum power production is activated (after operator OK). $n_{C/PROP} = 1081$ ; $n_{R/ICE} = 1950$ ; $n_{S/EM} = Willis$	0,1	10	1	10	1	$10^3$
8	MIN_CONS_2	$n_{C/PROP} = 800-1200$ SOC=1	This mode is activated if, from 7, the battery is at SOC=1. The speed setpoint is respected, and the consumptions are minimized, selecting the correct Cluster_rif row.	0,1	1	1	3	1	10
9	ONLY_ICE_2	$n_{C/PROP} > 1200$ SOC=1	This mode is entered if, from 6, SOC=1 and $n_{C/PROP} > 1200$ . EM is braked and ICE respects Willis formula.	0,1	10	0,1	3	0.5	$10^4$
10	OFF_ICE	$n_{C/PROP} < 800$ SOC=1	Whenever a transition to 1 is commanded, the ICE must be decelerated and then stopped by this mode.	$10^{-5}$	10	20	10	1	1

*Tab. 3.3 – Operating modes conditions and control parameters value*

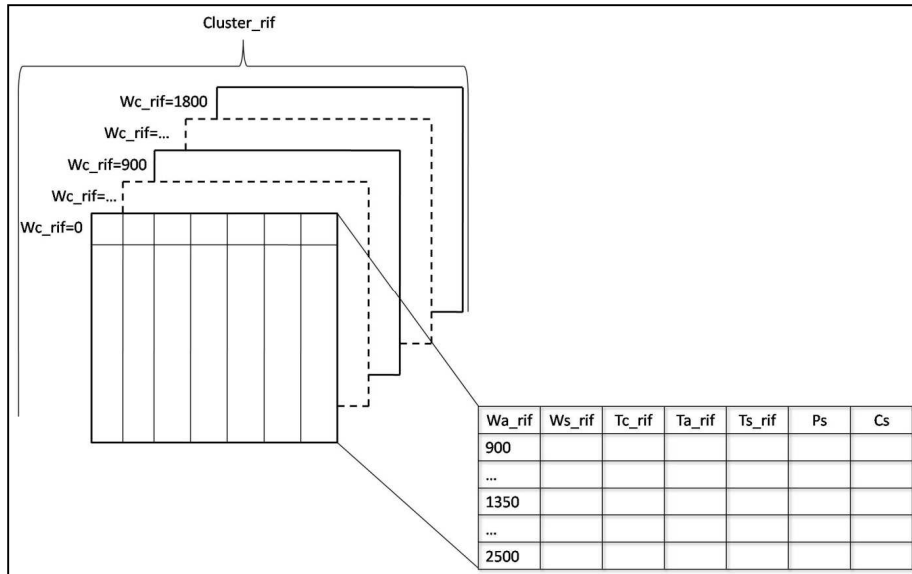


Fig. 3.16- 3D matrix Cluster\_rif for the determination of the speed setpoints

6. RECHARGING\_MODE\_2: Maximum producible power (low battery charge)
7. RECHARGING\_MODE\_3
8. MIN\_CONS\_2
9. ONLY\_ICE\_2
10. OFF\_ICE: Stop of the engine (back to low speed, high battery charge).

The variable SOC can assume three values:

1. SOC=1, High battery charge.
2. SOC=2, Medium battery charge.
3. SOC=3, Low battery charge.

### 3.5.3 LEVEL 2: Determination of the speed references

Once the operating mode has been determined, the ICE and driver speed setpoint have to be determined.

The operating interval of propeller/carrier speed has been discretized, yielding to the creation of a 3D matrix, as shown in Fig. 3.16. For each value of propeller speed  $n^*_{C/PROP}$ , the main system variables have been tabled, utilizing the planetary gear set relationships (1.4), (1.7), (1.8) and assuming to know the steady state propeller torque at the setpoint speed:

- $n^*_{RICE}$ : ICE/ring setpoint speed (varying in the [min,max] range);
- $n^*_{SEM}$ : Driver/sun setpoint speed;
- $T_{C/PROP}$ : Carrier/propeller torque;
- $T_{RICE}$ : ICE/ring torque;
- $T_{SEM}$ : Driver/sun torque;
- $P_{SEM}$ : Driver mechanical power;
- $C_S$ : fuel spec. cons. of the ICE.

By way of the over cited table, the control system is able to realize the propeller goal speed, choosing e.g. the desired power produced by the driver, or the minimum engine consumption, depending on the current operating mode.

Operating mode 1: ONLY EM

When  $enable=1$ , the ONLY\_EM mode is selected, and the following operations are performed (Fig. 3.18):

- Ring brake engagement;
- Sun brake dis-engagement;
- ICE speed set to 0.
- Driver speed setpoint calculated by the Willis formula.

Operating mode 2: START ICE

Normally, the thermal engine is started from 0 rpm to the minimum speed by the use of an electrical starter motor. In the studied application, the starter motor should have a rated torque sufficient to start the ICE at a determined propeller speed. For this reason, in this study a possibility have been examined: when the transmission is operating in mode 1 (all electric), and mode 2 is selected, the driver speed is immediately inverted, and the ring brake disengaged, so as to carry the ICE shaft towards its idle speed. This operation allows the ICE to start and the control system to shift to another operating mode. A transient reduction of the carrier speed must be tolerated if this start up modality is adopted, and this is computed in the control system, which adapts the carrier setpoint speed, by means of a constant  $k_{avv}$ :

$$\begin{aligned} n_{R/ICE}^* &= n_{ICE,min} \\ n_{S/EM}^* &= k_{avv} n_{C/PROP}^* (1 - \tau_0) + n_{R/ICE}^* \tau_0 \end{aligned} \quad (3.1)$$

In synthesis, the following operations are performed:

- Ring brake disengagement;

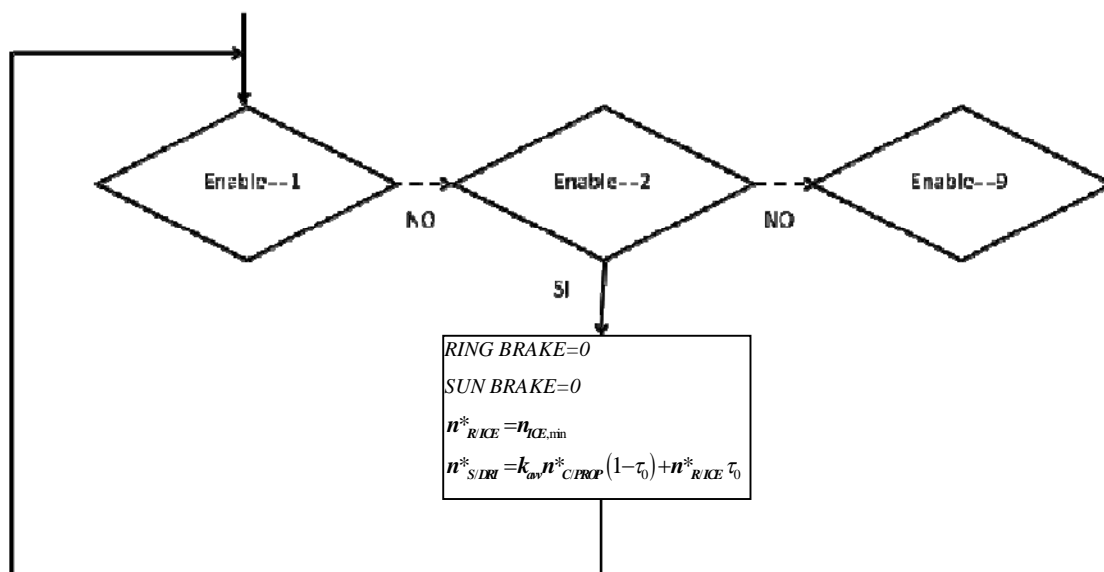


Fig. 3.17- Flow chart for operating mode 2: START\_ICE

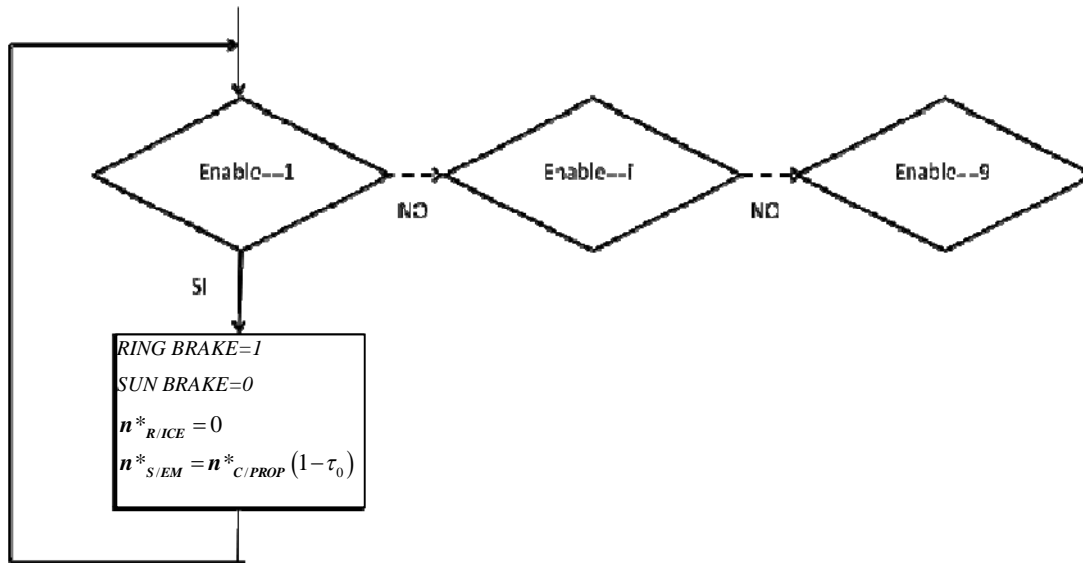


Fig. 3.18- Flow chart for operating mode 1: ONLY\_EM

- Sun brake disengagement;
- ICE speed set to the minimum;
- Reduction of the propeller speed (by the constant  $k_{avv}$ );
- Driver speed setpoint calculated by the Willis formula.

Operating mode 3: MIN CONS 1

When this state is chosen, the ICE is operated at the speed which minimizes the consumptions, thus the following variables must be controlled:

- The ICE specific consumption  $C_s$ .
- The generated power  $P_{DRI}$ .

As shown in Fig. 3.20 the operating mode 3 ( $enable=3$ ) executes the following operations:

- Disengagement of the sun and ring brakes;
- Selection of the “Cluster\_rif” matrix corresponding to the propeller setpoint speed  $n^*_{C/PROP}$
- Selection of the admissible rows of the matrix (without NaN values)
- Extraction of the matrix row corresponding to the minimum specific consumption ( $C_s$ ).

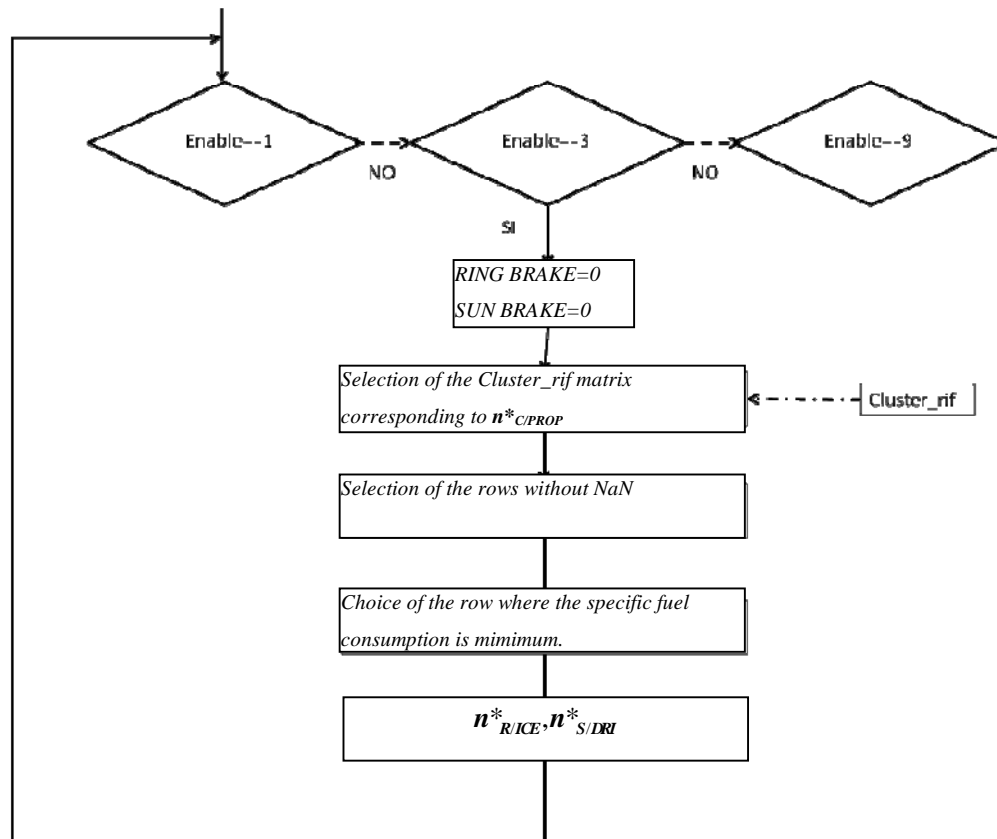


Fig. 3.19- Flow chart for operating mode 3: MIN\_CONS\_1

- Output of the ring speed and sun speed setpoints ( $n^*_{R/ICE}, n^*_{S/DRI}$ ) of the chosen row.

It's worthy to say that the matrix "Cluster\_rif" contains a finite number of points: the discretization step has been chosen as a compromise among the algorithm execution speed and the control accuracy.

#### Operating mode 4: ONLY ICE 1

This operating mode ( $enable=4$ ), as shown in Fig. 3.20 executes the following operations:

- Disengagement of the ring brake;
- Engagement of the sun brake;
- Setting of the driver speed to zero.
- Determination of the ICE speed by mean of the Willis formula, given the propeller speed setpoint.

#### Operating mode 5: RECHARGING MODE 1

This operating mode ( $enable=5$ ) is selected by the sequence control when the battery must be recharged. Thus the following variables must be controlled:

- The propeller speed  $n_{C/PROP}$ .

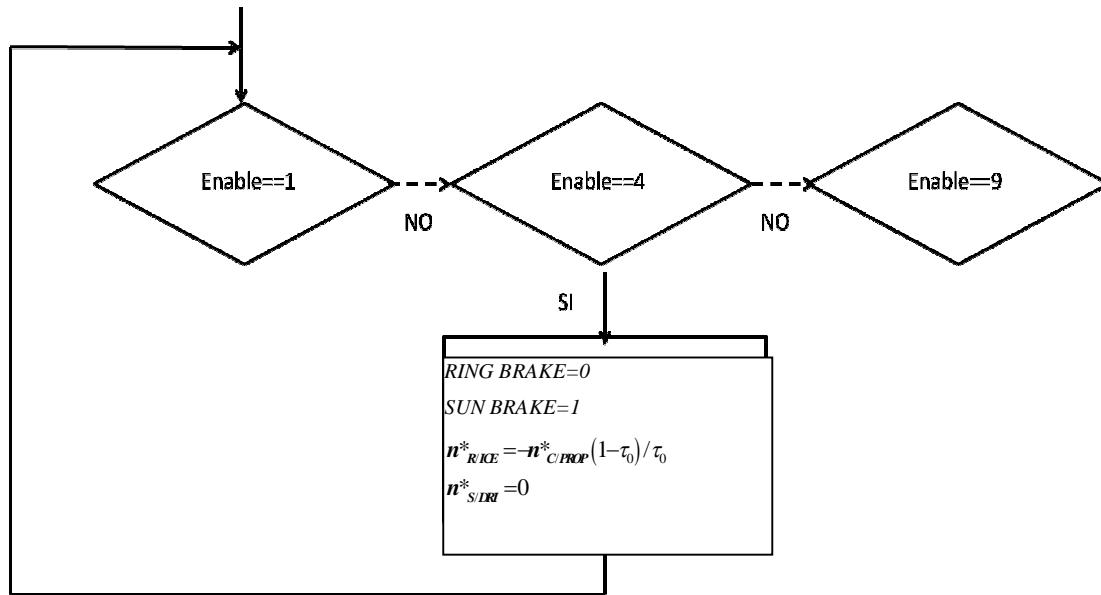


Fig. 3.20- Flow chart for operating mode 4: ONLY\_ICE\_1

- The generated power  $P_{S,EM}$ .

The operations are similar to the MIN\_CONS\_1 mode, with the difference that the parameter to be controlled is no longer the ICE fuel consumption, but the generated power ():

- Disengagement of the sun and ring brakes;
- Selection of the “Cluster\_rif” matrix corresponding to the desired propeller setpoint speed  $n^*_{C/PROP}$ ;
- Selection of the admissible rows of the matrix (without NaN values);

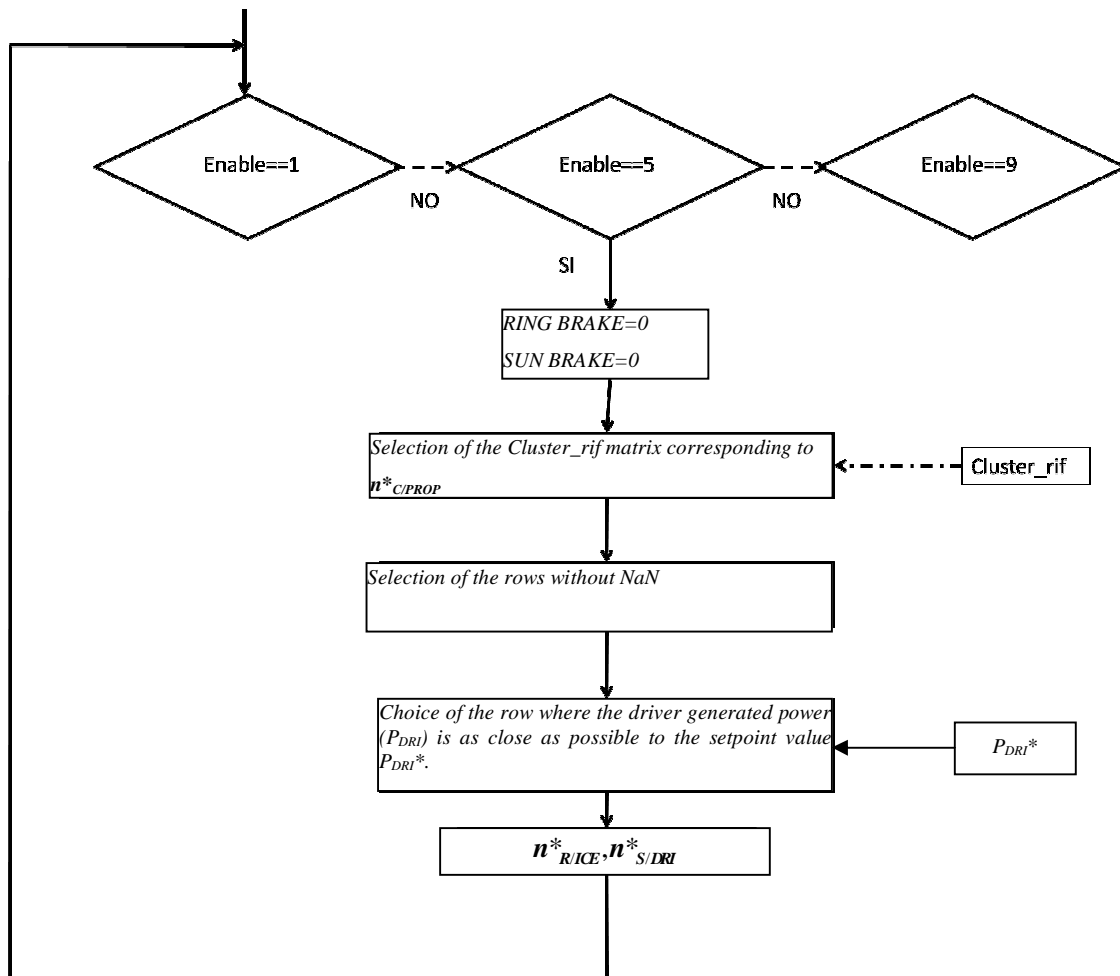


Fig. 3.21- Flow chart for operating mode 5: RECHARGING\_MODE\_1

- Extraction of the matrix row corresponding to the driver power setpoint  $P_{S,EM}^*$ , or which is as close as possible to this value;
- Output the ring speed and sun speed setpoints  $(n_{R/ICE}^*, n_{S/EM}^*)$  of the chosen row.

#### Operating mode 6: RECHARGING MODE 2

This operating mode ( $enable=6$ ) is contemplated to give the priority to the battery recharge over the propeller speed setup, whenever the battery state of charge should fall below a certain limit (e.g. below 50%). As seen in par. 3.4.5, the maximum producible power ( $P_{DRI}=60kW$ ) is obtained in a particular zone:

- $n_{C/PROP}=1081$  rpm
- $n_{R/ICE}=1950$  rpm

Of course this modality must be left to the operator choice.

The diagram of Fig. 3.22 shows the operational sequence of this modality:

- Disengagement of both the sun and ring brakes
- Setting of the ICE speed and driver speed at the maximum power generation point.

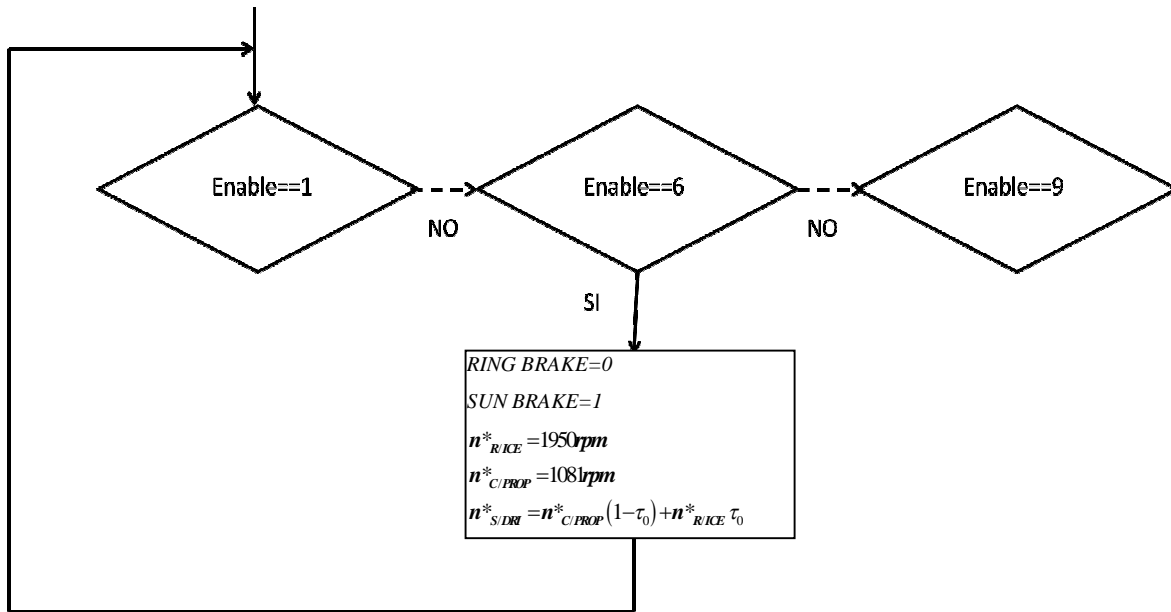


Fig. 3.22- Flow chart for operating mode 6: RECHARGING\_MODE\_2

Operating mode 10: OFF ICE

Whenever a transition to *ONLY\_EM* is commanded (the output speed falls below a certain limit e.g. 800 rpm), the ICE must be arrested and braked.

The operational sequence is the following (*enable=10*) as shown in Fig. 3.23:

- Disengagement of the sun brake;
- Disengagement of the ICE brake;
- Set the ICE speed to zero, so as to decelerate the thermal engine;
- Set the driver speed setpoint by the Willis formula, known the setpoint propeller speed.

The OFF\_ICE mode is just a transitory phase, when the ICE speed falls below a determined value (e.g. half the minimum speed), the *ONLY\_EM* mode is selected and the

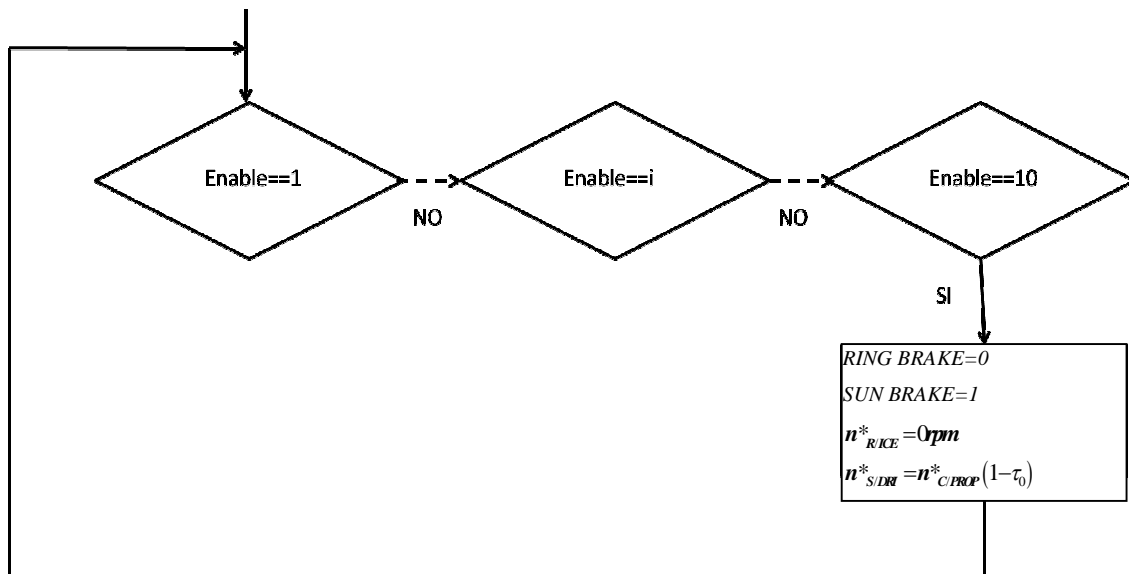


Fig. 3.23- Flow chart for operating mode 10: OFF\_ICE

ICE brake system is engaged.

### Operating mode 7,8,9

The other operating modes are basically identical to the previously described (RECHARGING\_MODE\_3, MIN\_CONS\_2, ONLY\_ICE\_2 are equal respectively to RECHARGING\_MODE\_2, MIN\_CONS\_1, ONLY\_ICE\_1), the only reason of their presence is the different control parameters setting respect to their twins (see *Tab. 3.3*). These difference of settings have been provided in order to have a good response in the operating mode shifting transients.

### 3.5.4 LEVEL 3: Speed control loops

The 3<sup>rd</sup> and last level is the low level speed control loop, made up by PI controllers and low pass filters, to smooth the speed setpoint transitions between the operating modes. The layout is shown in *Fig. 3.24*. The parameters of the filters and of the PI regulators have been tuned for each operating mode, as can be observed in *Tab. 3.3*.

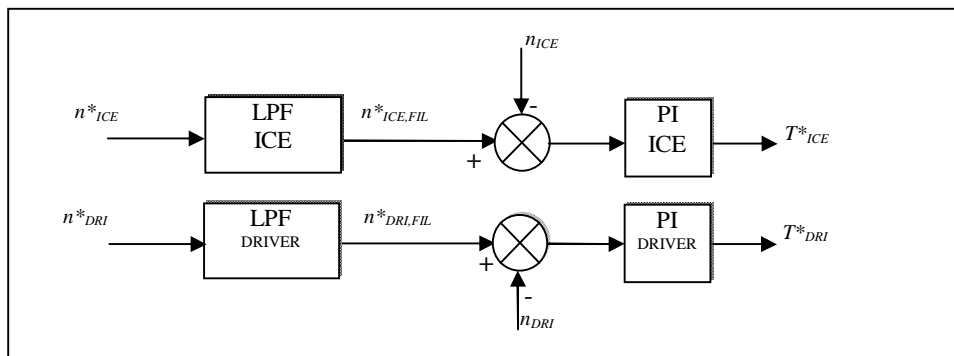


*Fig. 3.24- Speed control loop*

### 3.6 Simulations

In this paragraph the numerical simulations of the HySP E-CVT driveline are shown, in order to understand the behavior of the system, in steady state and in transient conditions. The parameters of the simulated system are resumed in *Tab. 3.4*.

<i>Parameters of the System</i>			
<b>Electric machine (Driver)</b>		<b>ICE (Diesel engine)</b>	
Rated power [kW]	62.8	Rated power @ 2200 rpm [kW]	590
Rated torque [Nm]	300	Max torque @ 1300 rpm [Nm]	2700
Rated speed [rpm]	2000	Torque in brake operation	1/3
Proportional gain PI speed	Tab	Proportional gain PI speed	Tab
Integral gain PI speed	Tab	Integral gain PI speed	Tab
Time constant of the torque loop [s]	0.05	Time constant of the torque loop [s]	0.052±0.14
Inertia [Kgm <sup>2</sup> ]	0.1	Inertia [Kgm <sup>2</sup> ]	0.5
<b>Load (propeller)</b>		<b>Planetary gear train</b>	
Max speed [rpm]	1800	Sun teeth number (S)	39
Max torque [Nm]	3130	Planets teeth number (P)	68
Inertia [Kgm <sup>2</sup> ]	3.6	Ring teeth number (R)	175
Max power [kW]	590	Ratio P/S	1,74
Shaft stiffness coefficient	500	Fundamental ratio $\tau_0$ (-R/S)	-4.49
Shaft damping coefficient	500		

*Tab. 3.4 – Parameters of the E-CVT system for HySP*

For each simulation, the profiles of propeller speed setpoint, battery state of charge, and power generation request have been defined. The simulations have been carried out to test the different features of the system:

- Verify the correct operating mode shifting by the level 1 control algorithm.
- Verify that the propeller speed profile is correctly followed, with acceptable dynamic performances and low regime error.
- Verify that the power generation setpoint is respected as far as possible in recharging mode.
- Verify that the operating torque limits of ICE and EM are respected every time.
- Verify the stability of the system during mode shifting and setpoints variations.

The simulations can be divided in three types:

- a) The battery SOC is always medium (SOC=2), and a variable propeller speed setpoint is required at fixed power gen level, or a variable power gen setpoint is required at a fixed propeller speed.

- b) The battery SOC is fixed at high (SOC=1), and the propeller speed is varied.
- c) The battery SOC is variable, and the propeller speed is varied.

Among the three simulation typologies, different cases will be presented, in order to show advantages and limits of the system as it has been conceived since now.

### 3.6.1 Simulations (a)

Test n°	Test type (a)
1	Battery recharge at SOC=2 with variable power gen setpoint (low prop. speed).

#### Test description

The propeller speed is maintained at a very low value (190 rpm), the power generation request at the EM is varied, the capability of the system to follow both the requests is evaluated.

**SOC level:** 2. The system is always in battery recharge mode.

**Operating mode:** 5 (Recharge\_mode\_1)

**Propeller speed setpoint:** Constant at 190 rpm.

**Power generation setpoint:** Variable from 2.2 KW to 10 KW.

The power producible at the fixed propeller speed of 190 rpm is variable with the ICE speed, and it is characterized by the  $P_{S,EM} - n_{R,ICE}$  curve of Fig. 3.25.

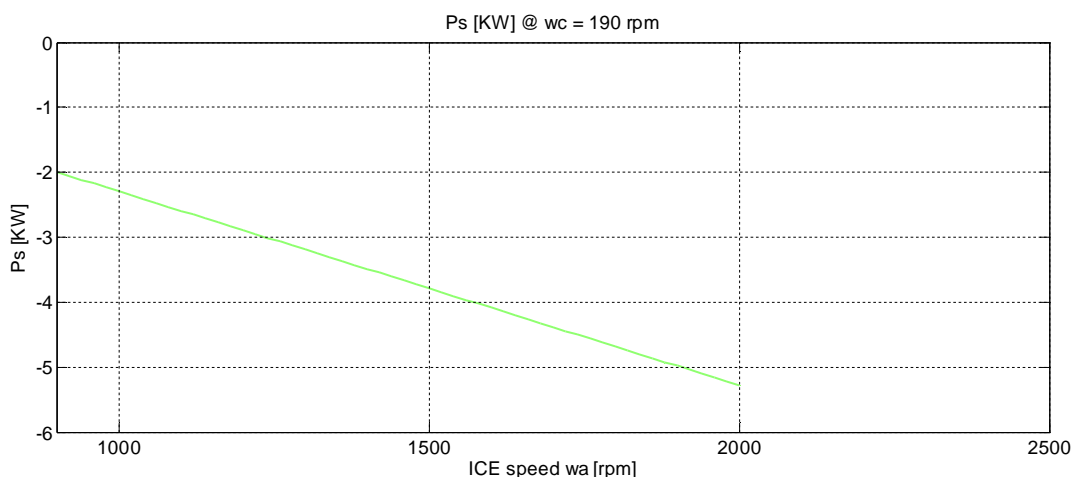


Fig. 3.25- Power producible by the EM varying the ICE speed (propeller at 190 rpm)

As it's possible to observe, the system is able to supply a max 5,5 kW power, with the ICE rotating at 2000 rpm and the EM at the maximum speed (8000 rpm).

#### Analysis of the simulation results

Looking at the Fig. 3.26 graph, it's clear that the propeller speed is disturbed by the power transients at the EM. This happens because the propeller torque is low, due to its low speed, and so the reaction to the EM accelerations is weak. Although these dynamic

disturbances, the speed reference is followed almost perfectly in steady state.

Moving to the EM power (Fig. 3.29), the setpoint is followed with good precision, except during the transients, where the EM speed grows up (Fig. 3.28), adsorbing power and behaving as a motor. The oscillatory phenomena are also stressed by the decreasing available torque in the EM field weakening region.

In the last part of the simulation, the required power is too high for the available EM speed range, and for this reason the power setpoint cannot be followed.

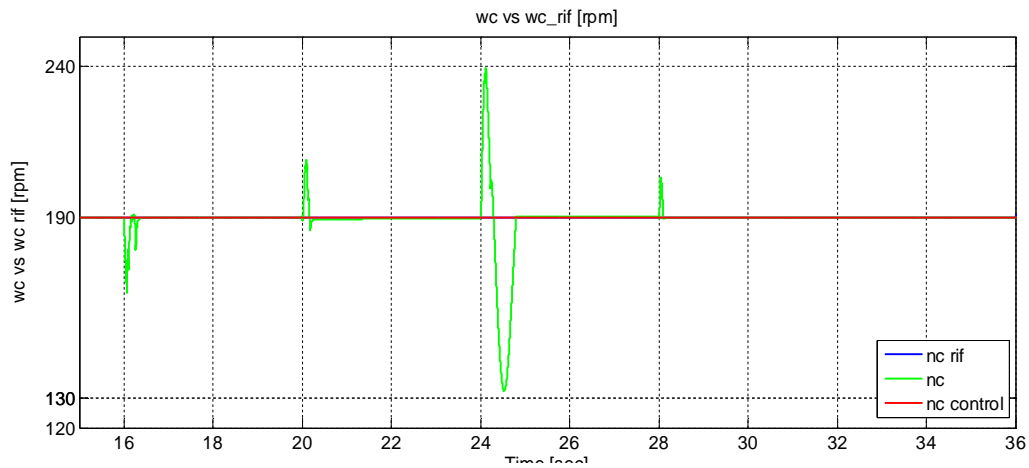


Fig. 3.26- Actual propeller speed nc (green), propeller speed setpoint nc\_control (red)

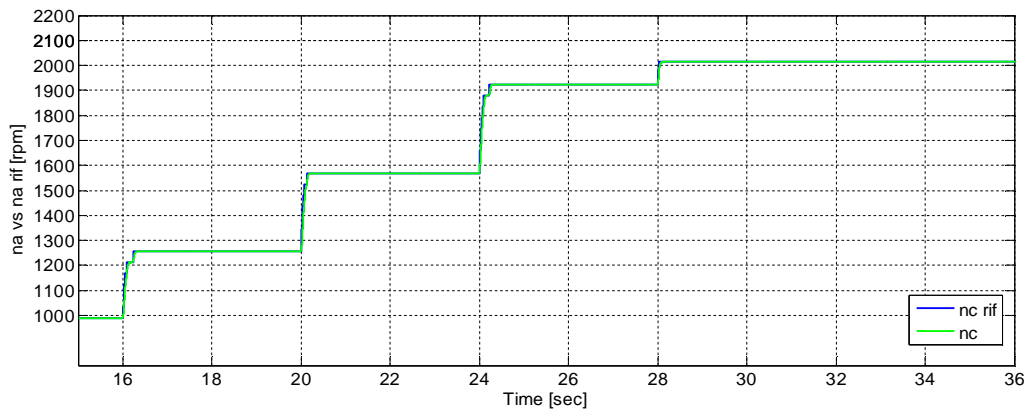


Fig. 3.27- Ring/ICE speed na (green), and its setpoint (blue)

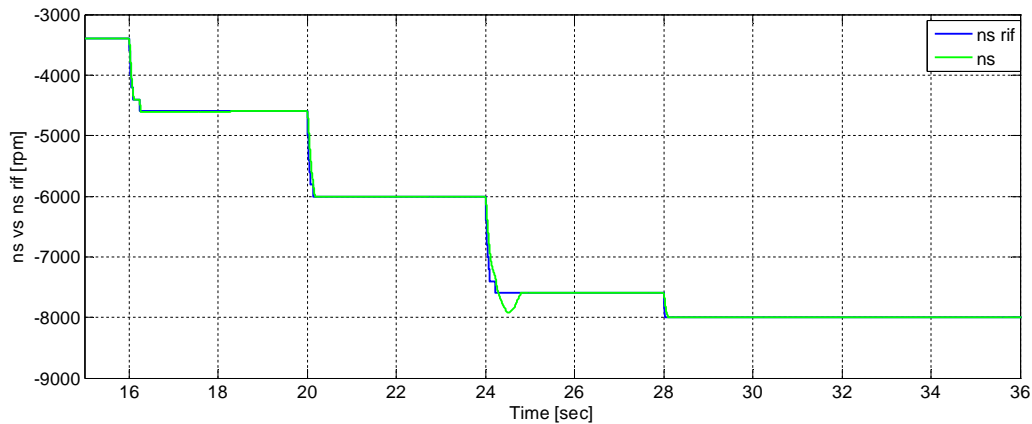


Fig. 3.28- Sun/EM actual speed (green), and its setpoint value (blue)

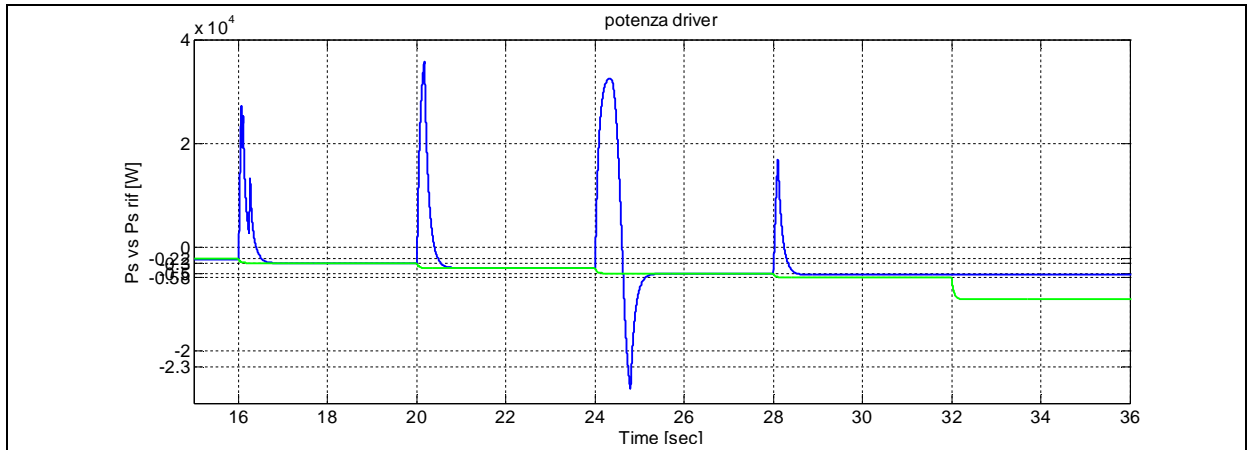


Fig. 3.29- EM generated power (negative)

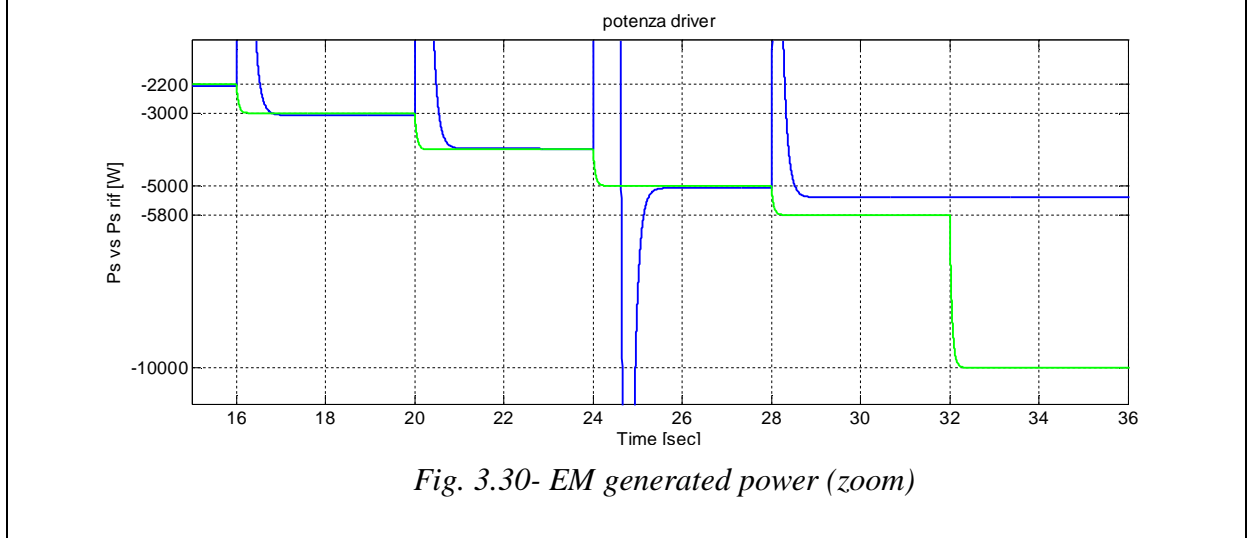


Fig. 3.30- EM generated power (zoom)

Test n°	Test type
2	Battery recharge with variable power gen setpoint (high prop. speed).

**Test description**

The propeller speed is maintained at a high value (995 rpm), the power generation request at the EM is varied: the capability of the system to maintain both the requests is evaluated.

**SOC level:** 2. The system is always in battery recharge mode.

**Operating mode:** 5 (Recharge\_mode\_1)

**Propeller speed setpoint:** Constant at 995 rpm.

**Power generation setpoint:** Variable from 10 kW to 60 kW.

The power producible at the fixed propeller speed of 995 rpm is variable with the ICE speed, and it is characterized by the  $P_{S,EM} - n_{R,ICE}$  curve of Fig. 3.31.

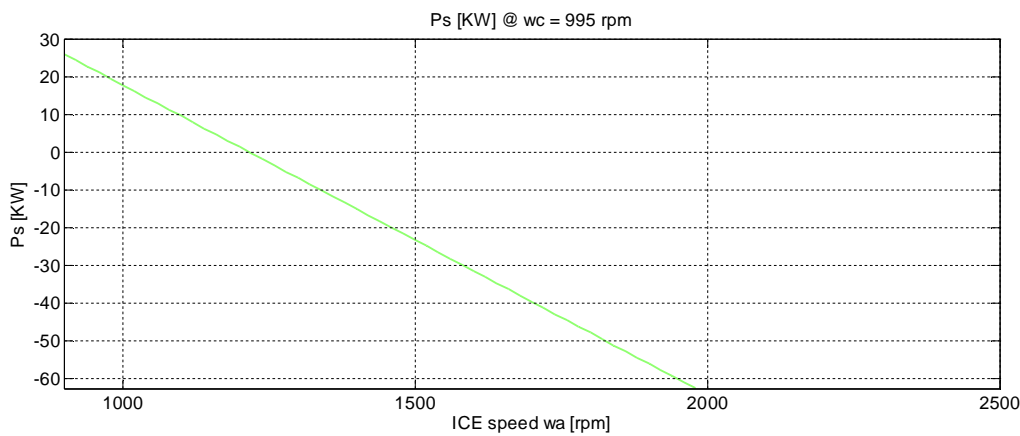


Fig. 3.31- Power producible by the EM varying the ICE speed (propeller at 995 rpm)

From Fig. 3.31 it's clear that the system is able to supply a max 60 kW power, thanks to the fact that the operational speed is in the the max production speed zone (1081 rpm).

**Analysis of the simulation results**

The torques transmitted through the planetary gearbox are stronger than the previous simulation, consequently the speed and power transients are lighter. The speed setpoint is still followed with dynamic disturbances (Fig. 3.32), like the generated power (Fig. 3.35), caused by the dynamic operation of the planetary gear train.

It is important to observe the steady state error of the EM power, caused by the discretization of the high level control system, which takes the value of the power which is closer to the reference in the Cluster\_rif table.

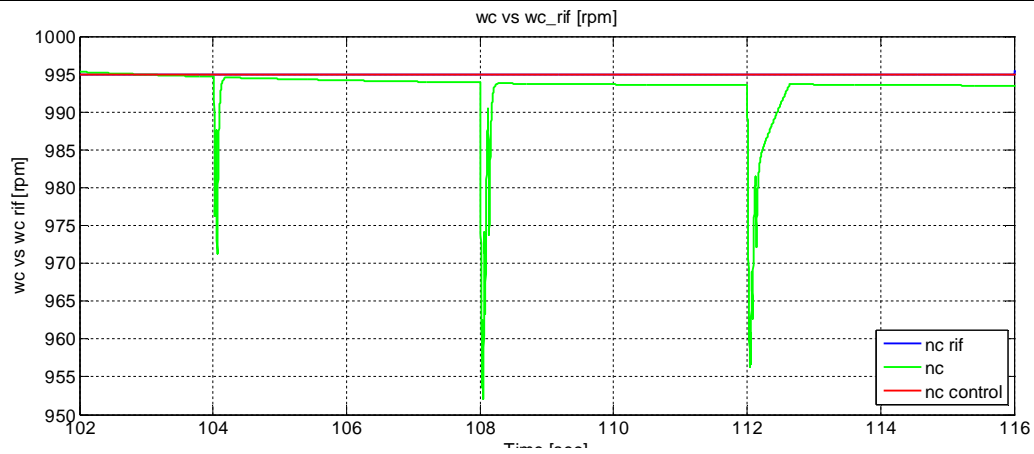


Fig. 3.32- Actual propeller speed  $nc$  (green), propeller speed setpoint  $nc\_control$  (red)

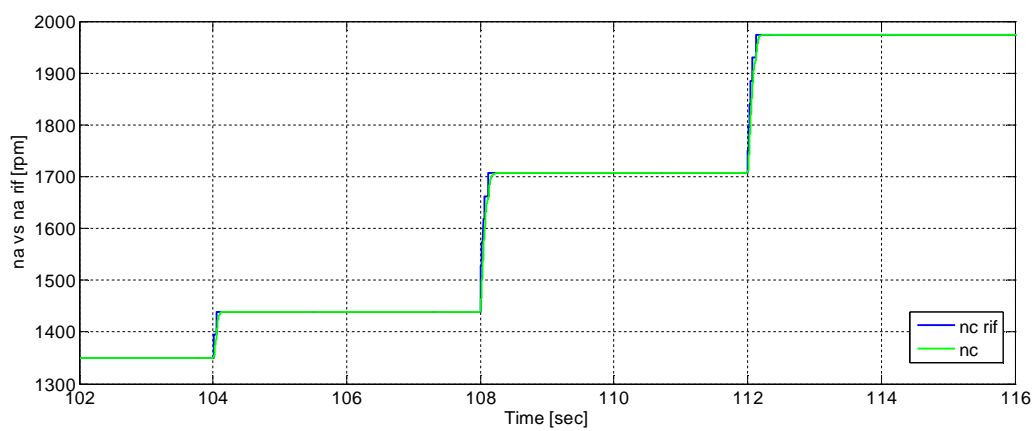


Fig. 3.33- Ring/ICE speed  $na$  (green), and its setpoint (blue)

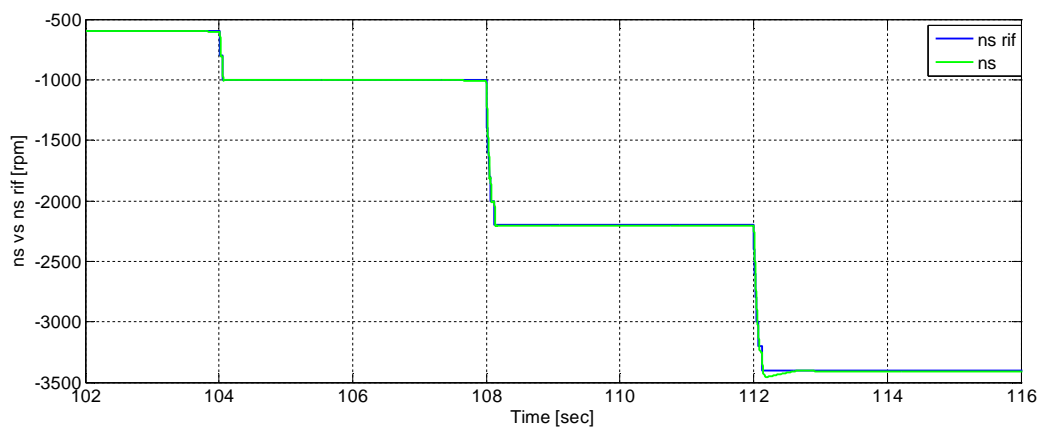
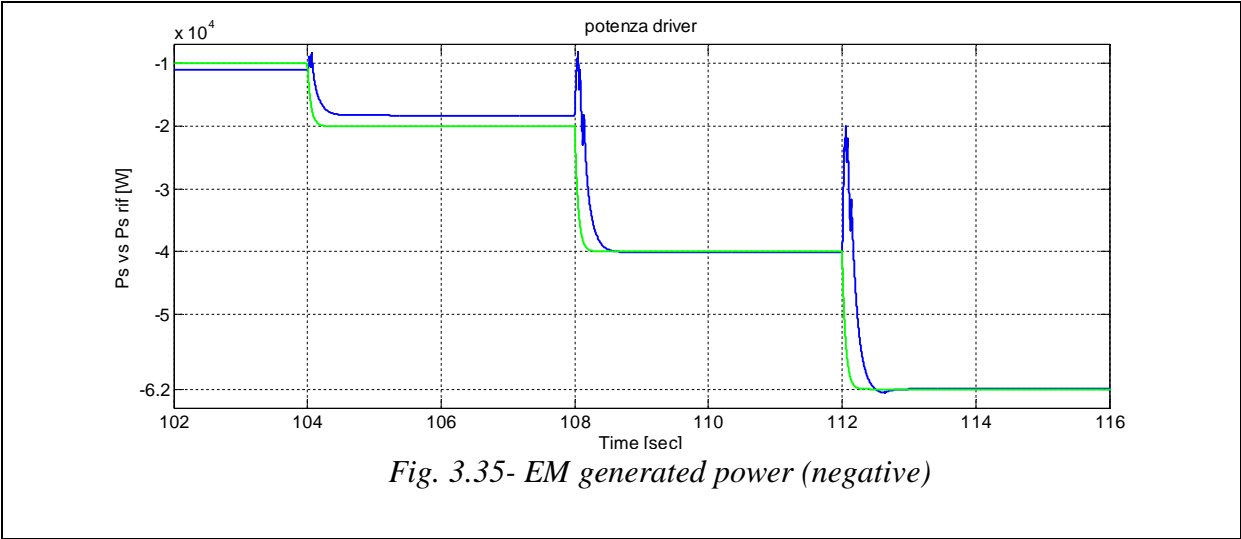


Fig. 3.34- Sun/EM actual speed (green), and its setpoint value (blue)



Test n°	Test type (b)
3	Battery recharge at SOC=2 with constant power gen setpoint and variable propeller speed.

### Test description

This simulation shows the capability of the control system to make the system following a variable propeller speed setpoint, when the generated power is maintained at a constant value.

**SOC level:** 2. The system is always in battery recharge mode.

**Operating mode:** 5 (Recharge\_mode\_1).

**Propeller speed setpoint:** Step variable (in the range 800÷1200rpm).

**Power generation setpoint:** Constant at 20 kW.

The power producible at each propeller speed is always inside the limits shown in *Fig. 3.14*.

### Analysis of the simulation results

Looking at the speed profile (*Fig. 3.36*), it's clear that the setpoint is followed correctly, until  $n_{C,PROP}=1200$  rpm, to increase the speed it would be necessary to pass at the only ICE mode, or to overload the EM, because it's giving the limit torque. Also the power setpoint is followed with good precision, excluding the effects of the discretization, which shifts the power setpoint. Some peaks occurs when the speed changes by step variations, they are caused by EM torque reactions to ICE speed variations.

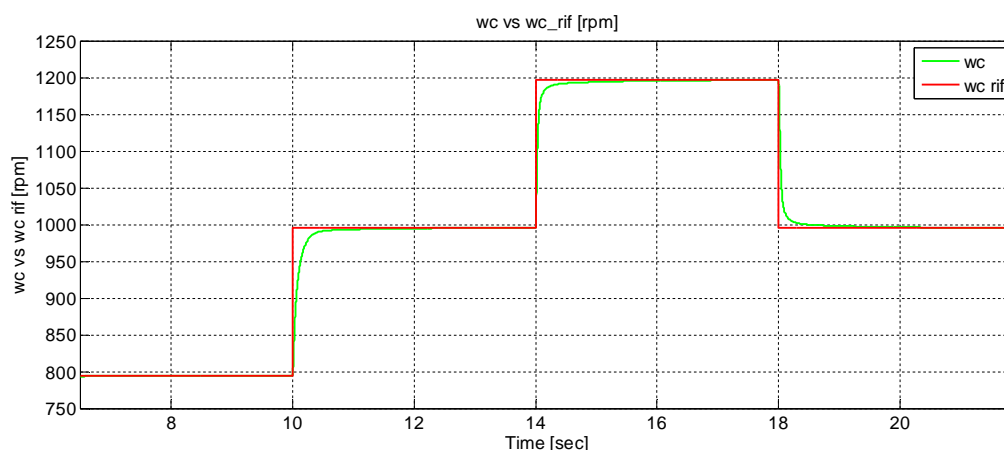


*Fig. 3.36- Actual propeller speed  $wc$  (green), propeller speed setpoint  $wc\_rif$  (red)*

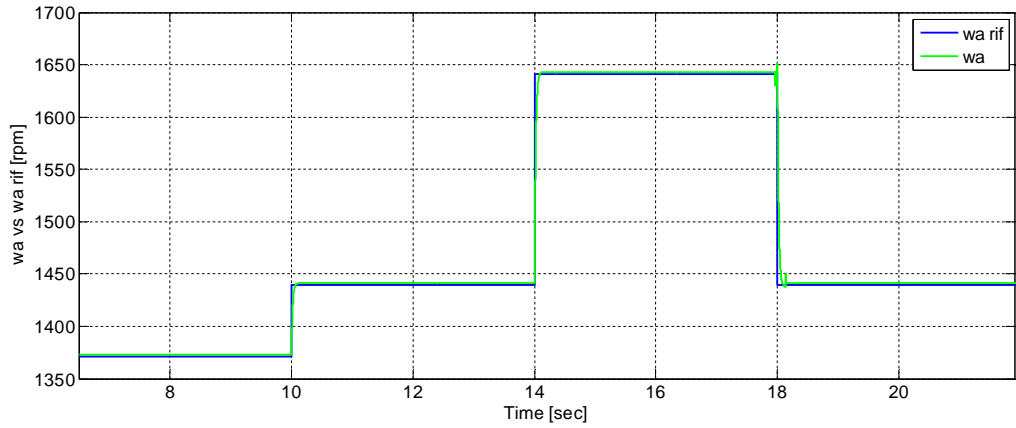


Fig. 3.37- Ring/ICE speed  $n_a$  (green), and its setpoint (blue)

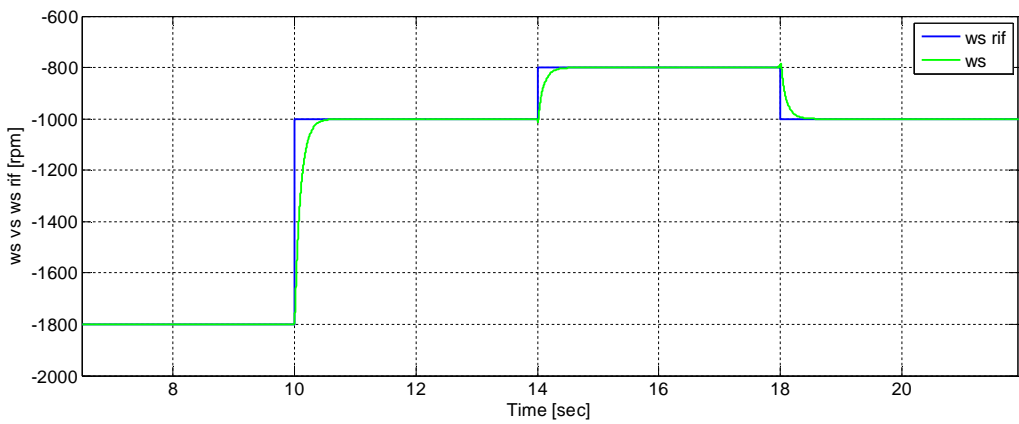


Fig. 3.38- Sun/EM actual speed (green), and its setpoint value (blue)

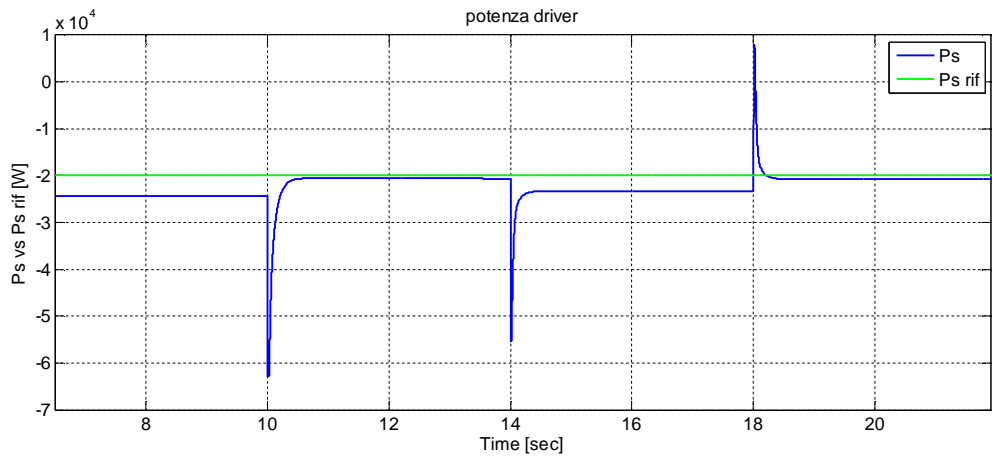
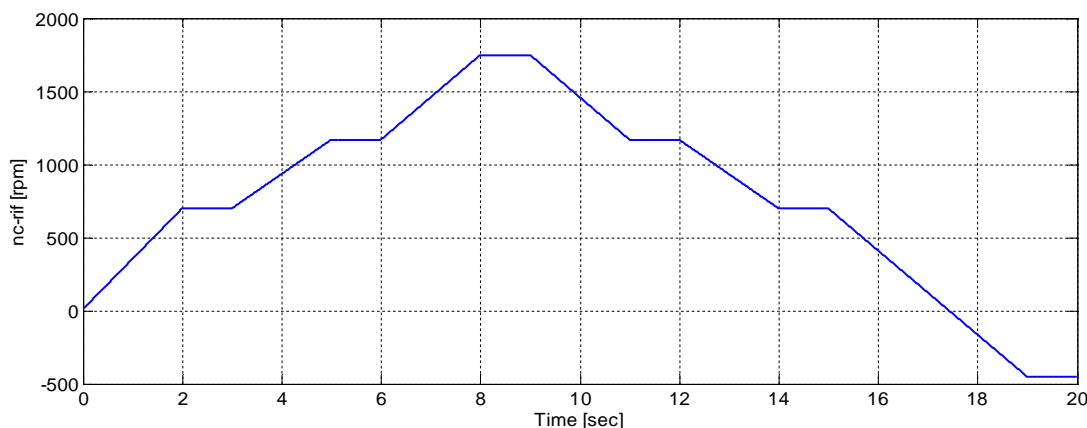


Fig. 3.39- EM generated power (negative)

### 3.6.2 Simulations (b)

The simulations of type (b) are carried out in order to verify the operating mode shifting transients. The following settings are applied:

- The propeller speed setpoint profile of *Fig. 3.40*.
- The state of charge of the battery is constant and high ( $SOC=1$ ).



*Fig. 3.40- Propeller speed profile*

The speed setpoint variations make the control system to switch from one modality to another, in particular the battery charge is considered to remain high during the simulation time. In this way, the control system will give the order to maximize the ICE efficiency, taking no care about the power produced by the electrical machine.

Test n°	Test type (b)
4	Analysis of the low speed at high battery charge, $SOC=1$ .
<p><b>Test description</b> This simulation shows a propeller startup, from 0 rpm to 700 rpm.</p> <p><b>SOC level:</b> 1. <b>Operating mode sequence:</b> 1 (Only_EM). <b>Propeller speed setpoint:</b> Ramp variable (in the range 0÷700rpm). <b>Power generation setpoint:</b> Constant at 8 kW.</p> <p><b>Analysis of the simulation results</b></p> <p>The EM power is always positive, it's operating as a motor, in fact the operating mode is always mode 1 ONLY_EM (<i>Fig. 3.41</i>). The battery give the power for this start-up, discharging itself. The ring speed is maintained at zero by the action of the brake (<i>Fig. 3.43</i>), while the propeller speed setpoint is followed with good precision (<i>Fig. 3.42</i>).</p>	

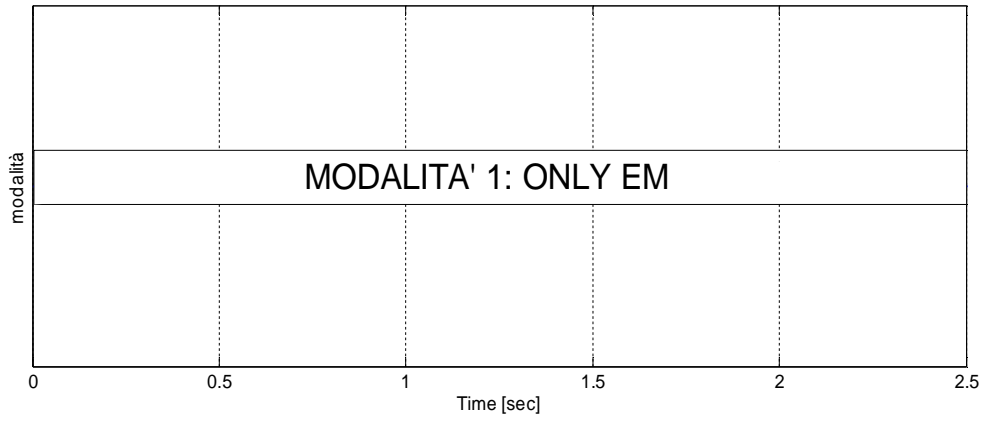


Fig. 3.41- Operating mode sequence

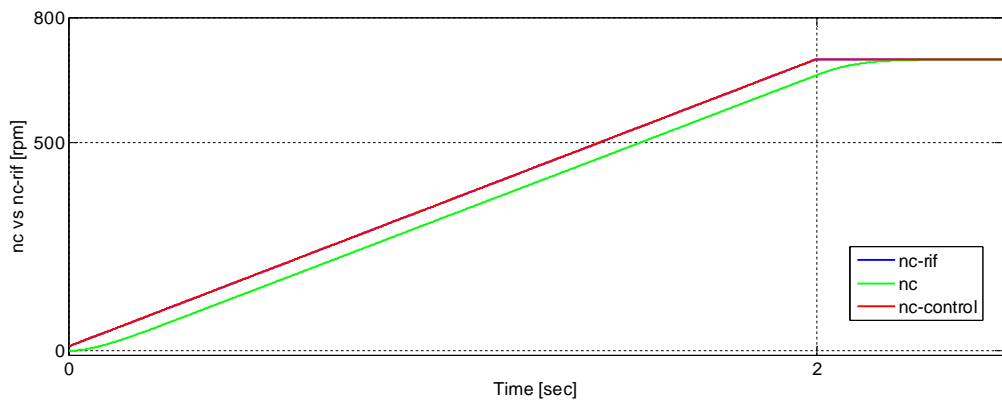


Fig. 3.42- Actual propeller speed nc (green), propeller speed setpoint nc\_control (red)

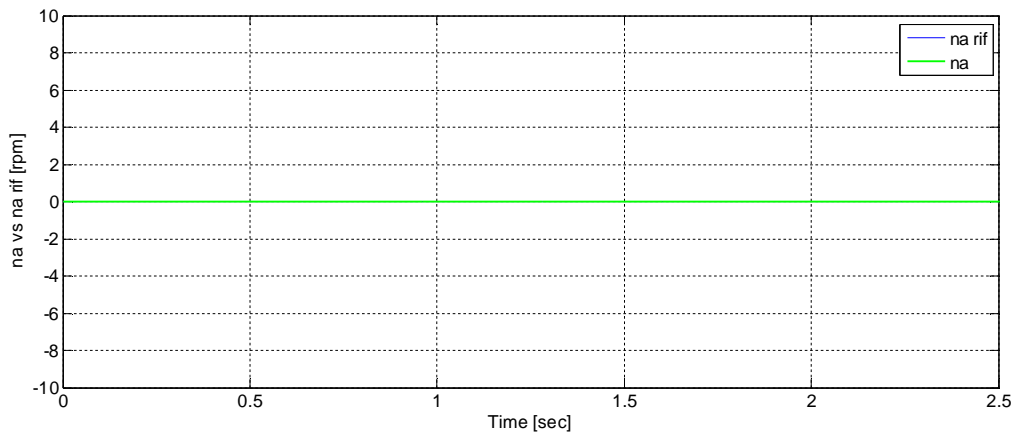


Fig. 3.43- Ring/ICE speed na (green), and its setpoint (blue)

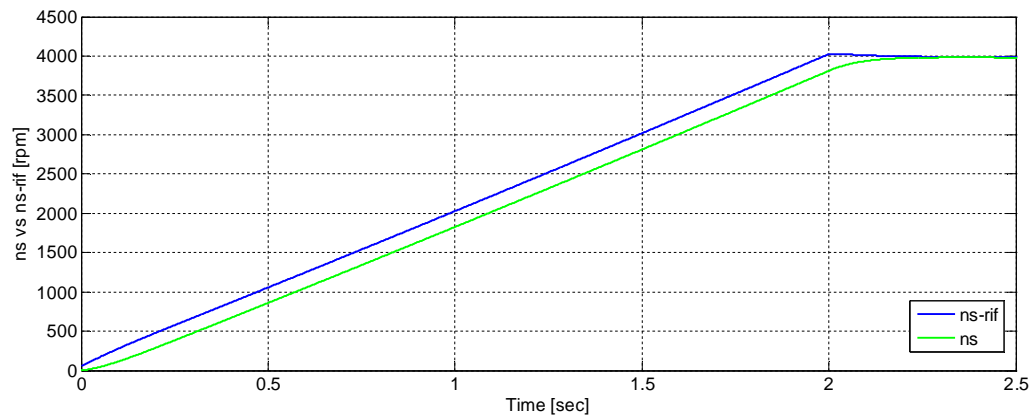


Fig. 3.44- Sun/EM actual speed (green), and its setpoint value (blue)

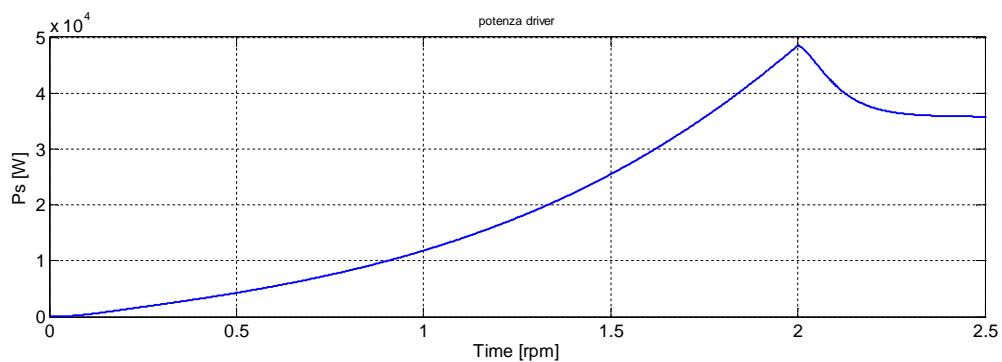


Fig. 3.45- EM generated power (negative)

Test n°	Test type
5	Analysis of the medium speed at high battery charge, SOC=1.
<p><b>Test description</b></p> <p>This simulation shows a transient of the propeller speed, from 700 rpm to 1170 rpm. The ICE is started and a hybrid mode operation is selected.</p> <p><b>SOC level:</b> 1.</p> <p><b>Operating mode sequence:</b> 1 (Only_EM) → 2 (ICE_start) → 3 (Min_cons)</p> <p><b>Propeller speed setpoint:</b> Ramp variable (in the range 700÷1170rpm).</p> <p><b>Power generation setpoint:</b> Constant at 8 kW.</p> <p><b>Analysis of the simulation results</b></p> <p>During the simulation, the propeller speed setpoint is taken above 800 rpm. This is the switching point from only electric mode to ICE startup mode. The propeller speed setpoint is temporary slowed down at 50%, to help the ICE starting. After the ICE have reached the idle speed, it contributes to follow the propeller speed setpoint, in synergy with the EM. The step varying speed setpoint is due to the discretization of the high level control algorithm, which</p>	

aims to take the ICE to the minimum consumption working point, that is  $\omega_{R,ICE}=1320$  rpm. Finally the propeller speed is stabilized to the setpoint value 1170 rpm. It's worth underlying that in MIN\_CONS\_1 mode the driver machine drain power from the battery, yielding to its discharge. (about 10 kW).

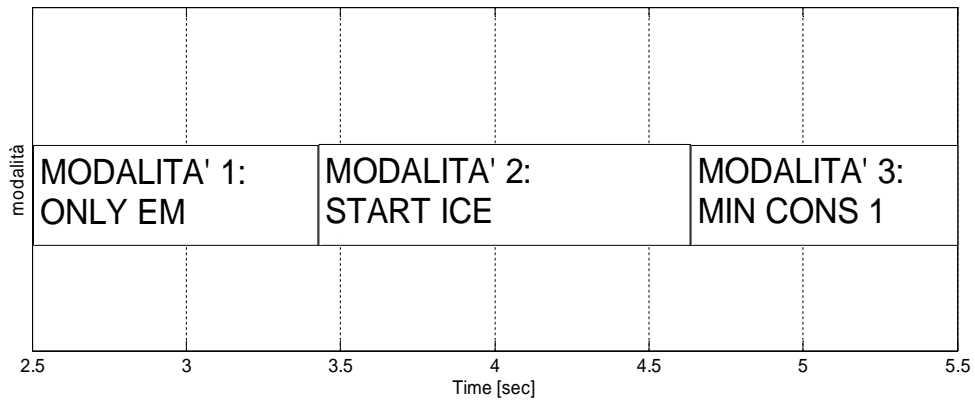


Fig. 3.46- Operating mode sequence

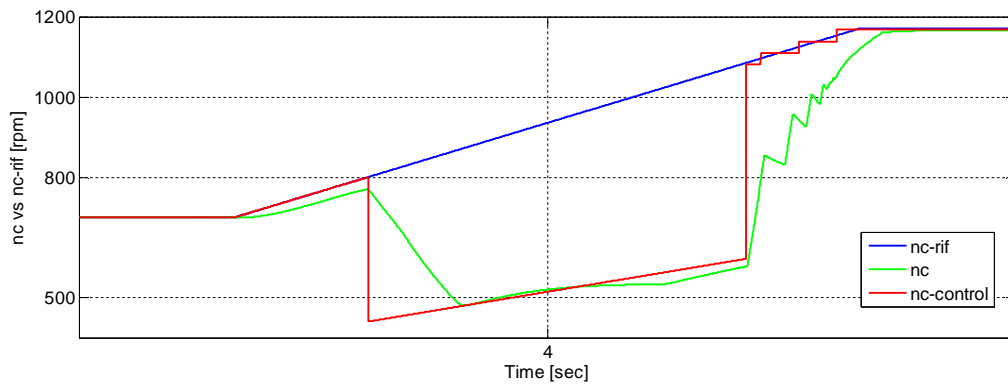


Fig. 3.47- Actual propeller speed  $nc$  (green), propeller speed setpoint  $nc\_control$  (red)

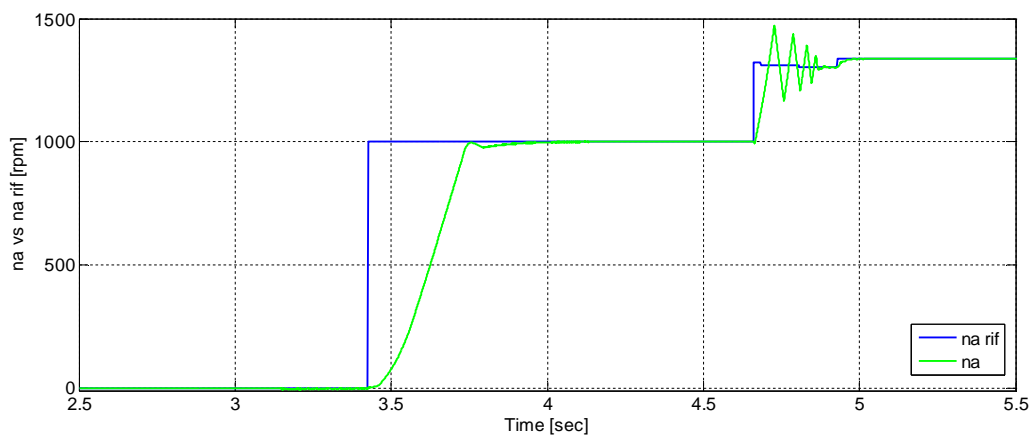


Fig. 3.48- Ring/ICE speed  $na$  (green), and its setpoint (blue)

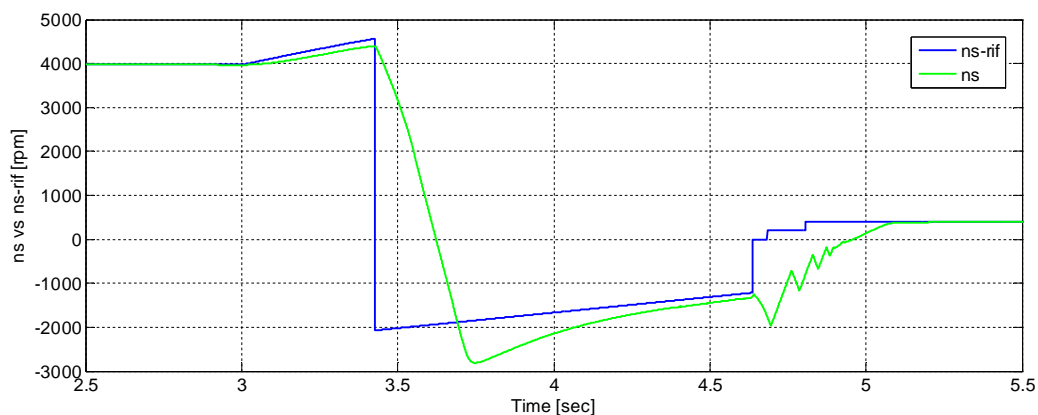


Fig. 3.49- Sun/EM actual speed (green), and its setpoint value (blue)

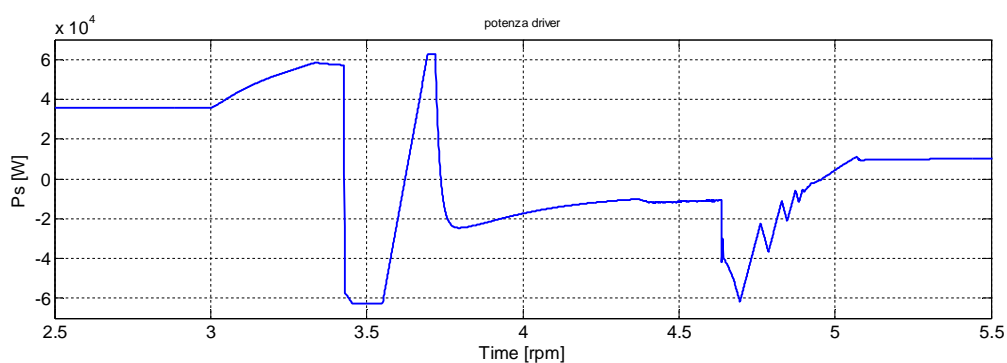


Fig. 3.50- EM generated power (negative)

Test n°	Test type
6	Analysis of the high speed at high battery charge, SOC=1. Positive acceleration.
<p><b>Test description</b></p> <p>This simulation shows a transient of the propeller speed, from 1170 rpm to 1750 rpm. The EM is stopped and a pure thermal mode operation is chosen.</p> <p><b>SOC level:</b> 1.</p> <p><b>Operating mode sequence:</b> 3 (Min_cons) → 4 (Only_ICE)</p> <p><b>Propeller speed setpoint:</b> Ramp variable (in the range 1170÷1750rpm).</p> <p><b>Power generation setpoint:</b> Constant at 8 kW.</p> <p><b>Analysis of the simulation results</b></p> <p>Once the propeller speed setpoint overcomes the 1200 rpm threshold, the driver machine is switched off, to avoid overloading, and the ONLY_ICE mode is selected by the control system. By Fig. 3.53 it's noticeable the EM stopping, which causes a transitory drop of the propeller speed, but after almost 0,2 s the increasing speed setpoint is followed correctly. The ICE passes from a minimum consumption speed (1320 rpm) to a traditional propulsion, where its speed is related to the propeller speed goal.</p>	

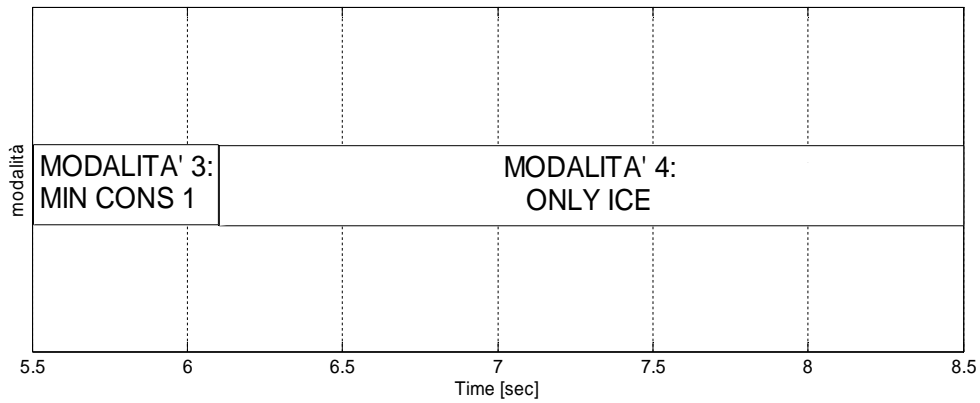


Fig. 3.51- Operating mode sequence

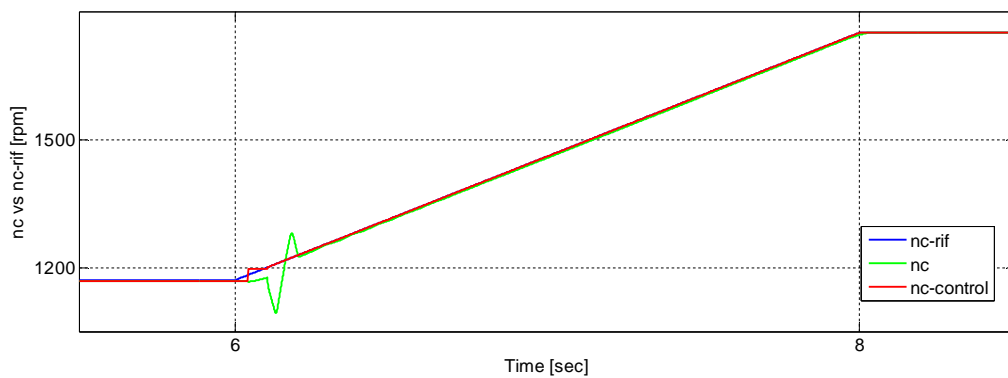


Fig. 3.52- Actual propeller speed *nc* (green), propeller speed setpoint *nc\_control* (red)

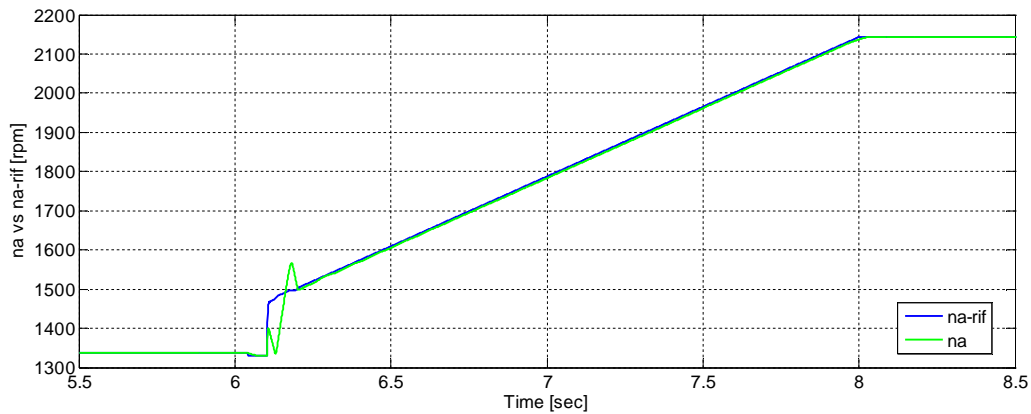


Fig. 3.53- Ring/ICE speed *na* (green), and its setpoint (blue)

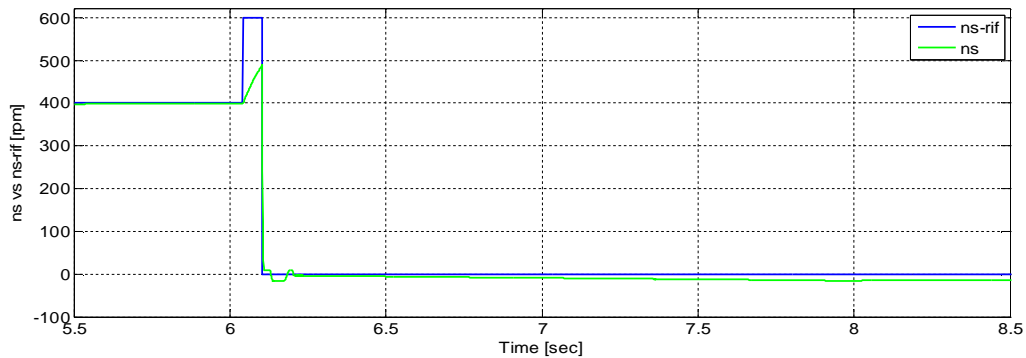
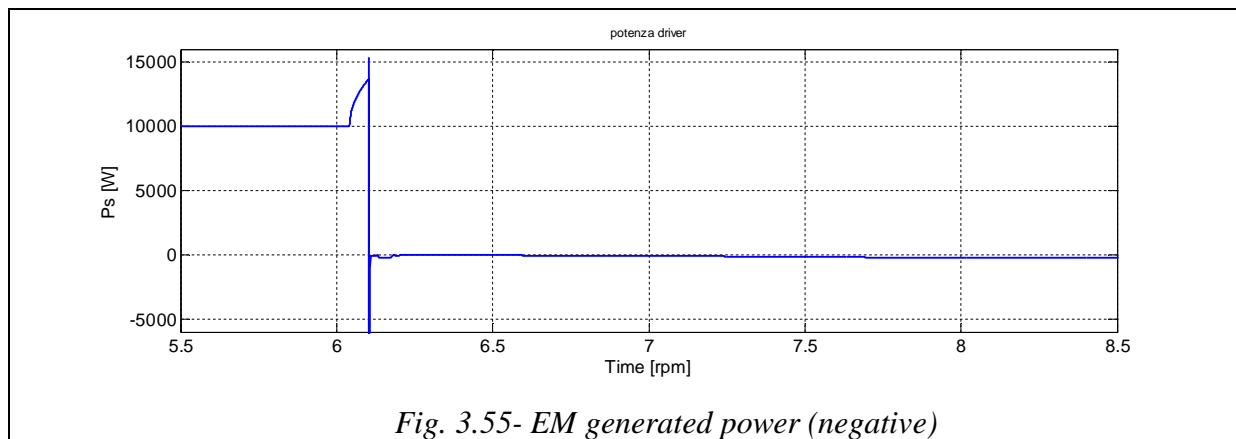


Fig. 3.54- Sun/EM actual speed (green), and its setpoint value (blue)



Test n°	Test type
6	Analysis of the medium speed at high battery charge, SOC=1. Negative acceleration.

### Test description

This simulation shows a transient of the propeller speed, from 1170 rpm to 700 rpm. The ICE is stopped and a pure electric mode operation is provided.

**SOC level:** 1.

**Operating mode sequence:** 3 (Min\_cons) → 10 (Off\_ICE) → 1 (Only\_EM)

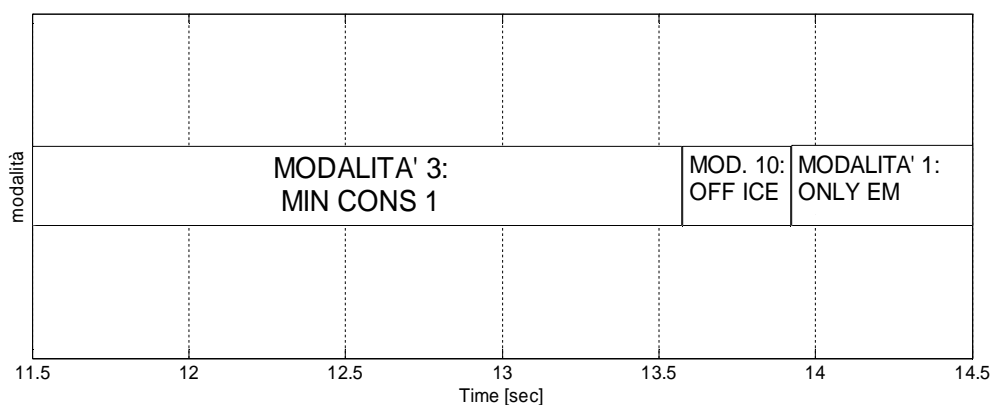
**Propeller speed setpoint:** Ramp variable (in the range 1170÷700rpm).

**Power generation setpoint:** Constant at 8 kW.

### Analysis of the simulation results

When the MIN\_CONS1 mode is selected, and the propeller speed is decreasing, the system always search for the minimum consumption point, but the discretization of the propeller speed range introduce a step variation of the speed setpoint (*Fig. 3.57*).

When the speed setpoint falls below the 800 rpm threshold, the ICE is stopped and braked (*Fig. 3.58*): this operation introduce a decreasing of the propeller speed respect to the reference, due to the delay of the driver to accelerate to the setpoint speed (*Fig. 3.59*). Anyway, the regime propeller speed is followed by a pure electric propulsion.



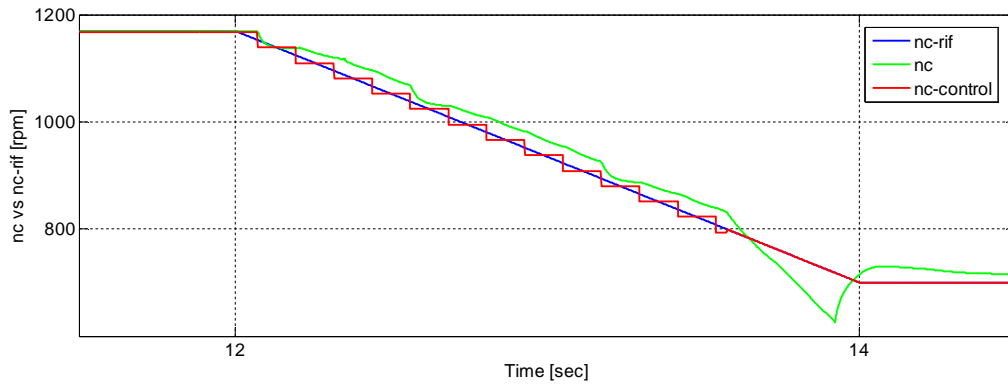


Fig. 3.57- Actual propeller speed nc (green), propeller speed setpoint nc\_control (red)

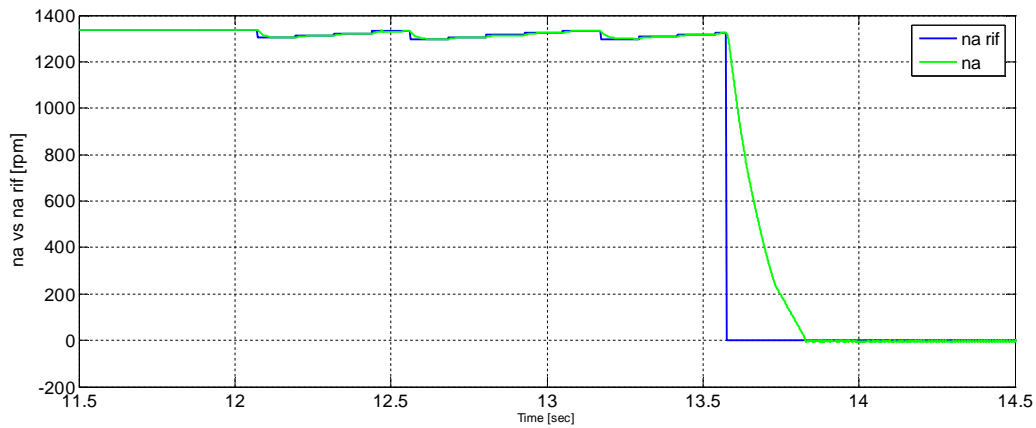


Fig. 3.58- Ring/ICE speed na (green), and its setpoint (blue)

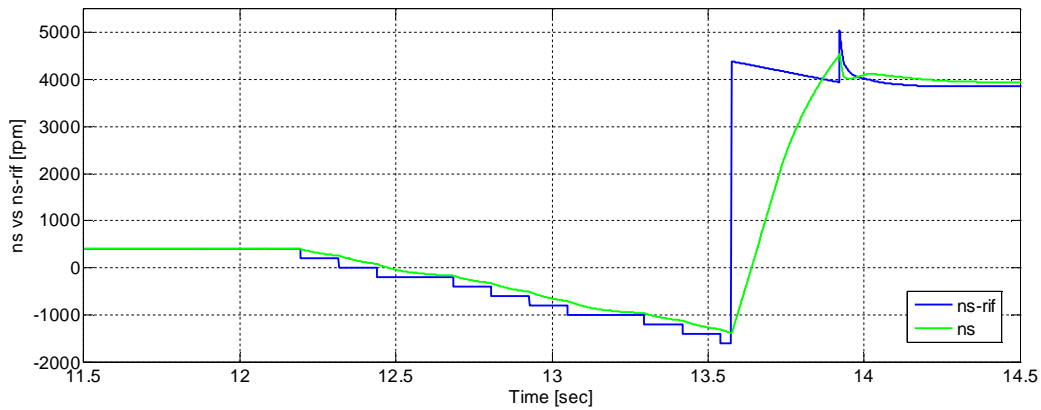


Fig. 3.59- Sun/EM actual speed (green), and its setpoint value (blue)

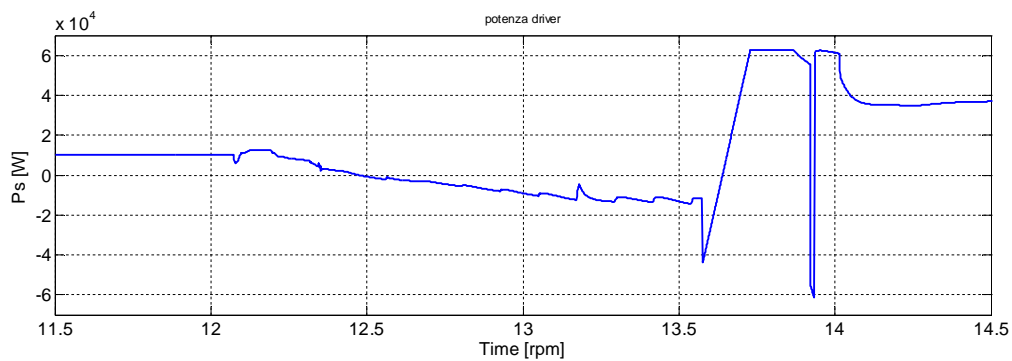


Fig. 3.60- EM generated power (negative)

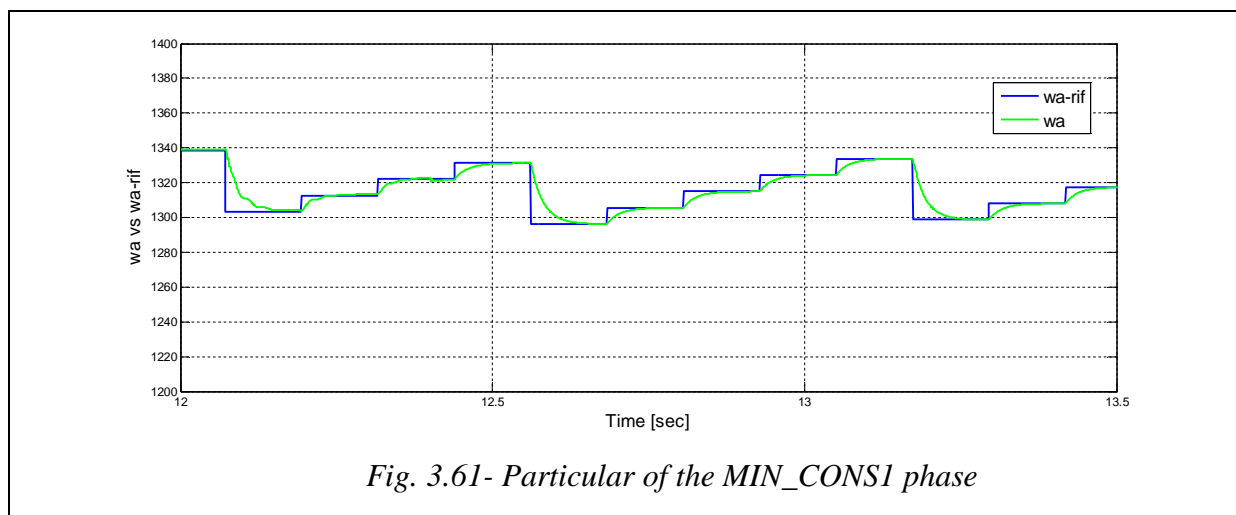


Fig. 3.61- Particular of the MIN\_CONS1 phase

### 3.6.3 Simulations (c)

In the following simulations of type (c), the speed setpoint is varied, under a variable battery state of charge. The goal of these simulations is to show the possibility of the system to satisfy the different requests changing automatically the operating mode. No battery model has been implemented at this level, for simplicity, thus the SOC profile is completely arbitrary. The following inputs have been used:

- The propeller speed profile of Fig. 3.62.
- The three level SOC profile of Fig. 3.63.
- The generated power setpoint in simple battery recharging mode is constant at 8 kW.

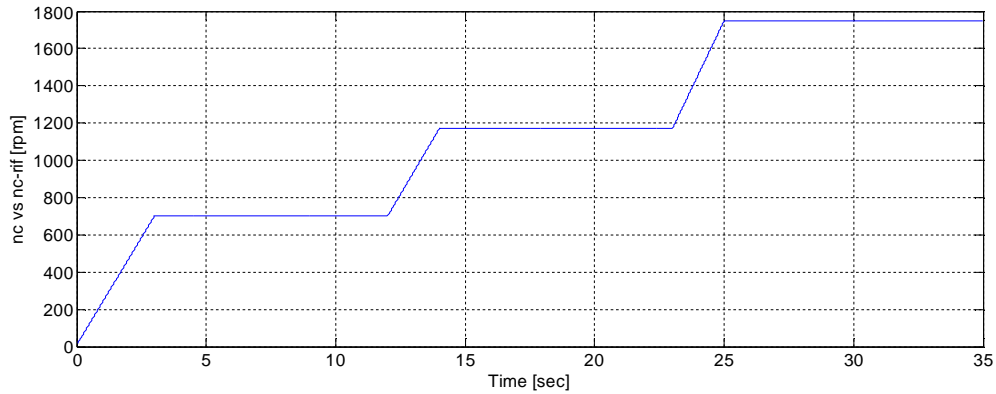


Fig. 3.62- Propeller speed profile

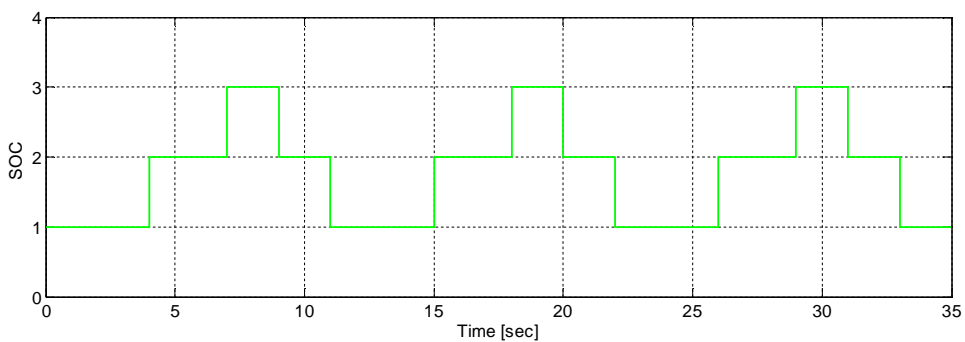


Fig. 3.63- Battery state of charge profile

Test n°	Test type
7	Analysis of the vessel low speed on battery recharge regime, SOC=2.
<p><b>Test description</b>                      This simulation shows a propeller startup in pure electric, followed by a state of charge transition, which enables the battery recharge.</p> <p><b>SOC level:</b> Step variable 1→2.</p> <p><b>Operating mode sequence:</b> 1 (Only_EM) →2 (Start_ICE) →5 (Recharging_mode_1)</p> <p><b>Propeller speed setpoint:</b> Ramp variable (in the range 0÷700rpm).</p> <p><b>Power generation setpoint:</b> Constant at 8 kW.</p> <p><b>Analysis of the simulation results</b></p> <p>After a pure electric startup, the battery SOC falls from 1 to 2, authorizing the control system to switch over a ICE startup and then on a simple recharging mode. This startup implies a temporary propeller speed derating (1 s) as shown in Fig. 3.65.</p> <p>During the RECHARGING_MODE_1 the driver speed is regulated to generate the required power (in this case 8 kW). The final oscillations on the generated power (Fig. 3.68) is due to the continuous research by the control system of the correct operating point.</p>	

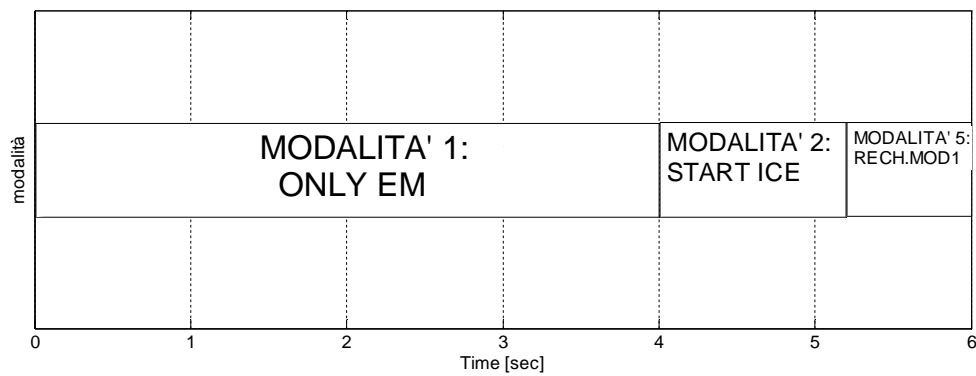


Fig. 3.64- Operating mode sequence

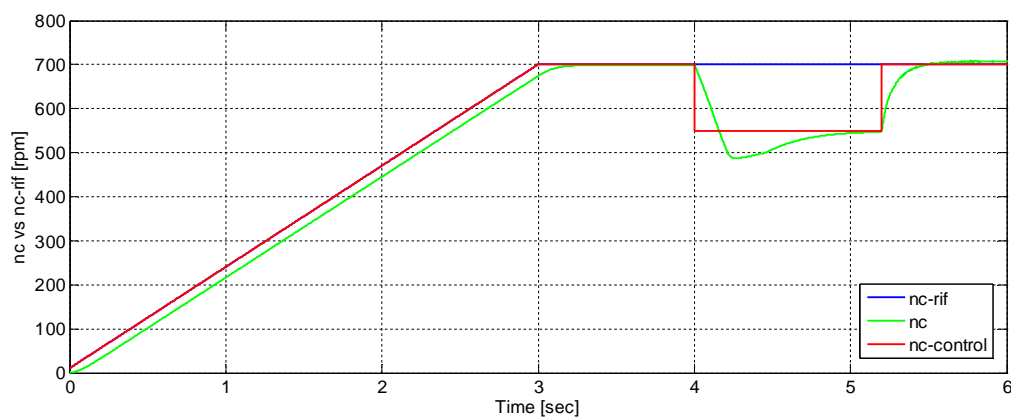


Fig. 3.65- Actual propeller speed  $nc$  (green), propeller speed setpoint  $nc\_control$  (red)

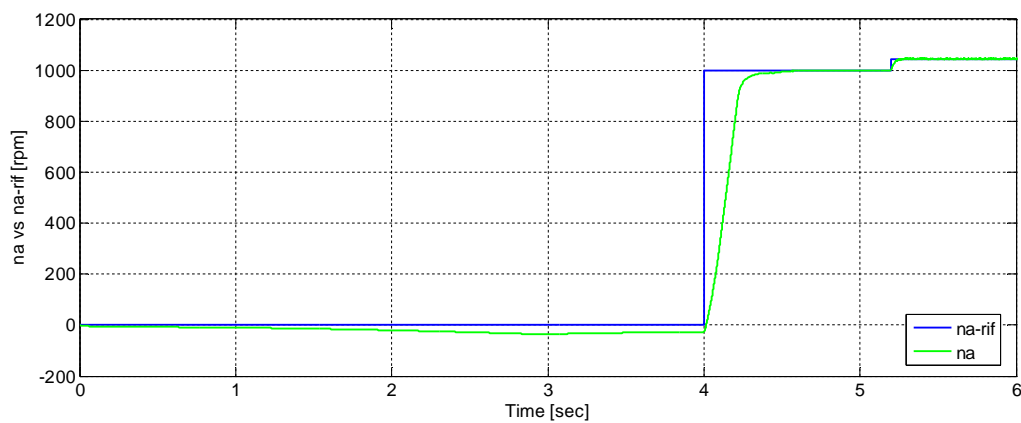


Fig. 3.66- Ring/ICE speed  $na$  (green), and its setpoint (blue)

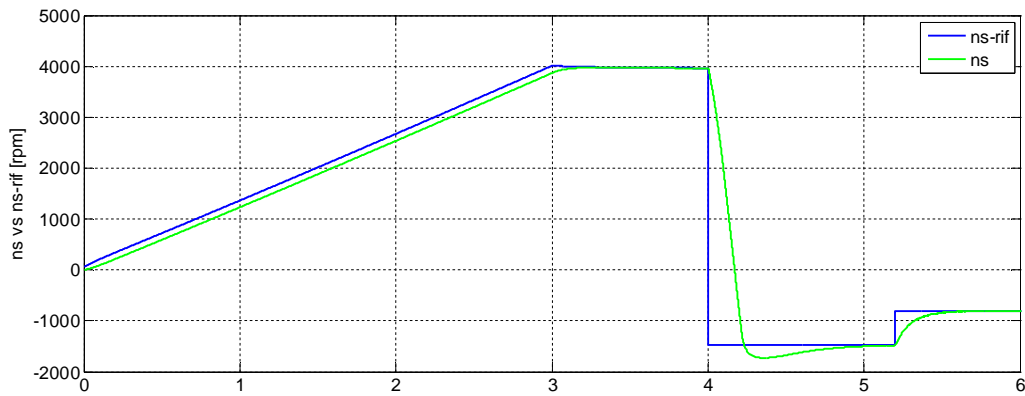


Fig. 3.67- Sun/EM actual speed (green), and its setpoint value (blue)

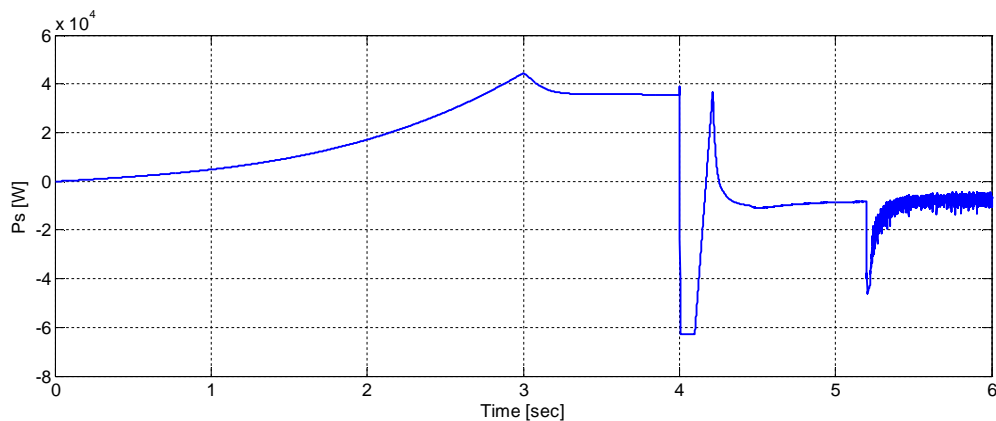
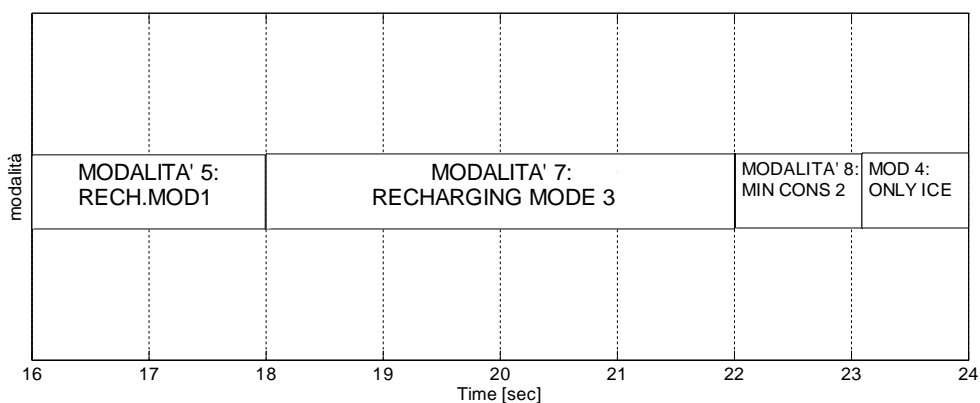


Fig. 3.68- EM generated power (negative)

Test n°	Test type
8	Analysis of the vessel medium speed on battery recharge regime, SOC=2,3.
<p><b>Test description</b></p> <p>This simulation shows a SOC level transient, from medium to low. The propeller speed is automatically reduced, with the operator approval, in order to supply the maximum electrical power (emergency battery recharge).</p> <p><b>SOC level:</b> Step variable 1→2.</p> <p><b>Operating mode sequence:</b> 5 (Recharging_mode) →7 (Emergency_recharging_mode) →8 (Min_cons)→4 (Only_ICE)</p> <p><b>Propeller speed setpoint:</b> Constant, reduced for the emergency recharge, and finally increased at the pure thermal level.</p> <p><b>Power generation setpoint:</b> Constant at 8 kW (in the simple recharging mode). The maximum power (60kW) in the emergency recharging mode).</p> <p><b>Analysis of the simulation results</b></p> <p>The simulation shown below wants to put in evidence the capability of the system to</p>	

respond at a sudden discharge of the battery. When the SOC falls at 3, the power setpoint is taken to the maximum possible, and this means that the speed should be decreased a little. If the operator wants, it can take the system to the optimal recharging point (mode 7). When the battery changes status again, as it has been charged, the system restart to follow the propeller speed setpoint (*Fig. 3.70*), on best ICE efficiency and then on only ICE mode. Oscillations on the propeller speed are mainly due to the operation of the driver machine at high speeds, where the torque is limited by the flux weakening operation.



*Fig. 3.69- Operating mode sequence*

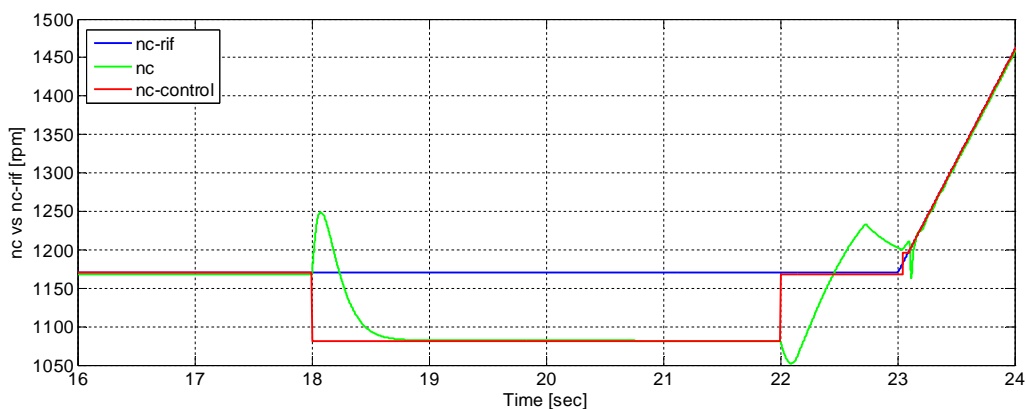


*Fig. 3.70- Actual propeller speed nc (green), propeller speed setpoint nc\_control (red)*

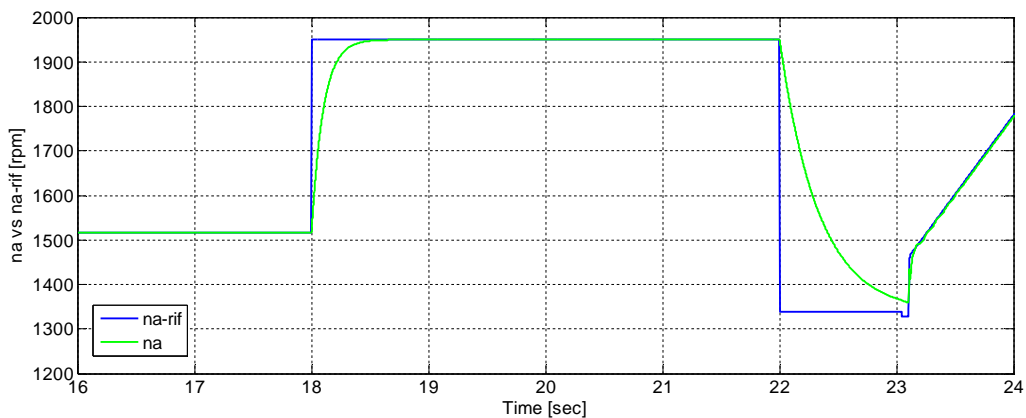


*Fig. 3.71- Ring/ICE speed na (green), and its setpoint (blue)*

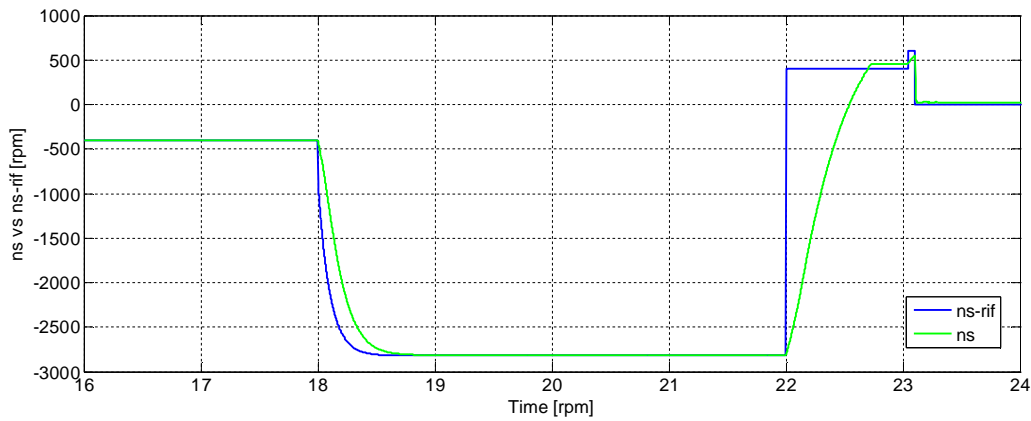


Fig. 3.72- Sun/EM actual speed (green), and its setpoint value (blue)

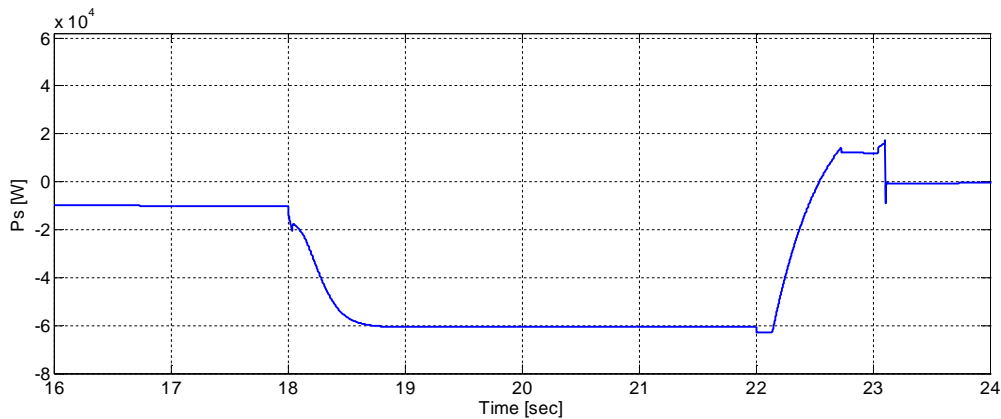


Fig. 3.73- EM generated power (negative)

### 3.7 Conclusions

The e-CVT power split system applied on a 590 kW vessel driveline system has been characterized and designed, the control system has been shown and the numerical simulations carried out. The control strategy has shown good properties of stability, even if some further work can be done, particularly on the problem of the discretization, which affects the modality transitions.

The analyzed system allows the following functionalities:

- Pure electric propulsion at low speed;
- Power production integrated in the driveline;
- Power boost or fine regulation of the propeller speed;
- Operation of the ICE at the max efficiency speed;
- Max power in all ICE propulsion with no electric power exchange.

---

## References

- [1] F. Feudale, P. Bordignon, C. Ferrero, P. Castangia, 'Tradition and innovation in ship electric components and systems' Proc. of Ship Propulsion and Railway Traction Sytems SPRTS, 4-6 October 2005, Bologna, Italy.
- [2] L. Guzzella, A. Sciarretta, "Vehicle propulsion systems, Introduction to modeling and optimization", Springer 2007
- [3] D. Hermance, "Toyota hybrid system," presented at the SAE TOPTEC Conf., Albany, NY, May 1999.
- [4] L. Harnefors, K. Pietilainen, L. Gertmar, "Torque-maximizing field-weakening control: design, analysis, and parameter selection," IEEE Trans. on Ind. El., vol. 48, no. 1, Feb. 2001, pp. 117 122.
- [5] D. Casadei, G. Serra, A. Tani, Luca Zarri, "A Robust Method for Field Weakening Operation of Induction Motor Drives with Maximum Torque Capability", IAS 2006, Tampa, Florida, 8 12 Oct. 2006, Paper N.IAS03P5, ISBN: 1-4244 0365-0.
- [6] M. Sanada, S. Morimoto, Y. Takeda: "Advantages of IPMSM with Adjustable PM Armature Flux Linkage in Efficiency Improvement and Operating Range Extension". Proc. of PCC. Osaka, 5 April 2002, Pages: 136 - 141 vol.1.
- [7] G. Messina, L. Susat "La potenza propulsiva dei veicoli navali", Vol. I, Ancona 1993,



# Chapter 4

## Power split E-CVT driveline for WECS

### 4.1 Introduction

The Wind Energy Conversion System (WECS) is considered one of the most important application of variable speed constant frequency (VSCF) system. The integration of the WECS with the grid requires to generate electric power at constant electrical frequency. The need to maximize power with wind fluctuating requires regulation of the turbine mechanical speed.

Among the possible combinations of converter, generator, and gearbox for WECS in the power range 100kW - 5MW, the use of a Wound Rotor Induction Generator WRIG coupled to a fixed ratio gearbox represents the most common solution [1]- [6]. Up to now a minor interest seems to be paid to the gearless solutions based on the use of a multipole synchronous generators. Only few manufacturers of WECS based on Permanent Magnet Synchronous Generators PMSG or Wound Rotor Synchronous Generator WRSG are reported. These direct drive solutions are still very expensive due to the full scale AC/AC converter for the integration with the grid of the generated power [7]-[9][10].

WRIG for WECS are based on a 4 or 6 poles machine with stator phases directly connected to the grid, and rotor phases connected through slip rings to a bidirectional power converter. This configuration allows the WRIG to operate both in subsynchronous and supersynchronous conditions. During subsynchronous operation, the rotor drain a fraction of the power generated from the stator, whereas during supersynchronous operation both stator and rotor inject power to the grid [11]. In a WRIG if  $\omega_s$  is the synchronous speed of the generator, and  $P_{sr}$  is the rated power of the stator, a regulation of the generator speed in the range  $(1-s)\omega_s < \omega < (1+s)\omega_s$  requires a power rating of the rotor converter  $P_R = sP_{sr}$ . Usually the maximum slip is around  $s = 0.2 \div 0.3$ , and then the sizing of the bidirectional rotor converter is  $0.2 \div 0.3P_{sr}$ . For example, assuming  $s = 0.3$  (and then  $P_R = 0.3P_{sr}$ ), it is possible to regulate the speed from 53% to 100% of the maximum speed  $\omega_{MAX} = (1+s)\omega_s$ . Once the rotor power rating is defined, the current rating of the bidirectional rotor converter is chosen by selecting a proper value of the rotor and stator turn ratio. Usually less turns are put on the rotor side and than a transformer for feeding the rotor converter is required.

This chapter deals with a driveline for WECS based on a Continuously Variable Transmission (CVT) placed at the high speed end of the step up gear train. The CVT decouples the variable speed of the gear train output from the fixed (or quasi fixed) speed of the generating machine. In this way the electric generator can be a conventional wound rotor synchronous machine or a squirrel cage induction machine with 4 or 6 pole, directly connected to the grid.

The CVT is constituted by a mechanical differential gearbox integrated with an additional electric machine called driver. A variable speed control of this driver machine allows to adjust the step up ratio of the CVT in a speed range which is larger than that obtained with traditional WRIG drive systems.

This solution was proposed for the first time 25 years ago [12], but the early development stage of variable speed drive did not allow to obtain satisfactory results. More recently the use of a CVT transmission for WECS based on a differential gearbox appeared again [13], [14] but in these cases the transmission is driven by a hydrodynamic system. These hydrodynamic CVTs are based on a complex torque converter, constituted by a variable geometry pump and turbine actuator which drives one element of a differential gearbox. The experience recently gathered with hydrodynamic CVT have demonstrated the possibility to use conventional synchronous or asynchronous generator, and the possibility to smooth the oscillations in the grid injected power through the control of the transmission. Unfortunately, the use of a fluid-machine determines a high level of complexity and decreases the efficiency of the transmission.

In the following paragraphs a detailed description of a CVT based power transmission for WECS is given, including the possible design criteria, the layout of the control system and a set of simulations obtained by the developed model. In the last chapter the experimental results obtained in LEMAD lab on a scale prototype will be shown.

## 4.2 Description of the system

### 4.2.1 Wind turbine characteristic

For analyzing electric generation capabilities of a WECS, wind turbines are usually modeled by using the following relationship between the wind speed and the mechanical power extracted from the turbine shaft [15], [16]:

$$P_{WT} = \frac{1}{2} \rho A_R c_p (\lambda, \theta) v_w^3 \quad (4.1)$$

Where:

- $P_{WT}$ : aerodynamic power extracted from the wind [W]
- $\rho$ : air density [ $\text{kg}/\text{m}^3$ ]
- $A_R$ : cross section of the rotor swept area [ $\text{m}^2$ ]
- $c_p$ : power coefficient
- $\lambda$ : tip speed ratio (ratio between the blade tip speed [m/s] and the upstream wind speed [m/s])
- $\theta$ : pitch angle of the blade [deg].

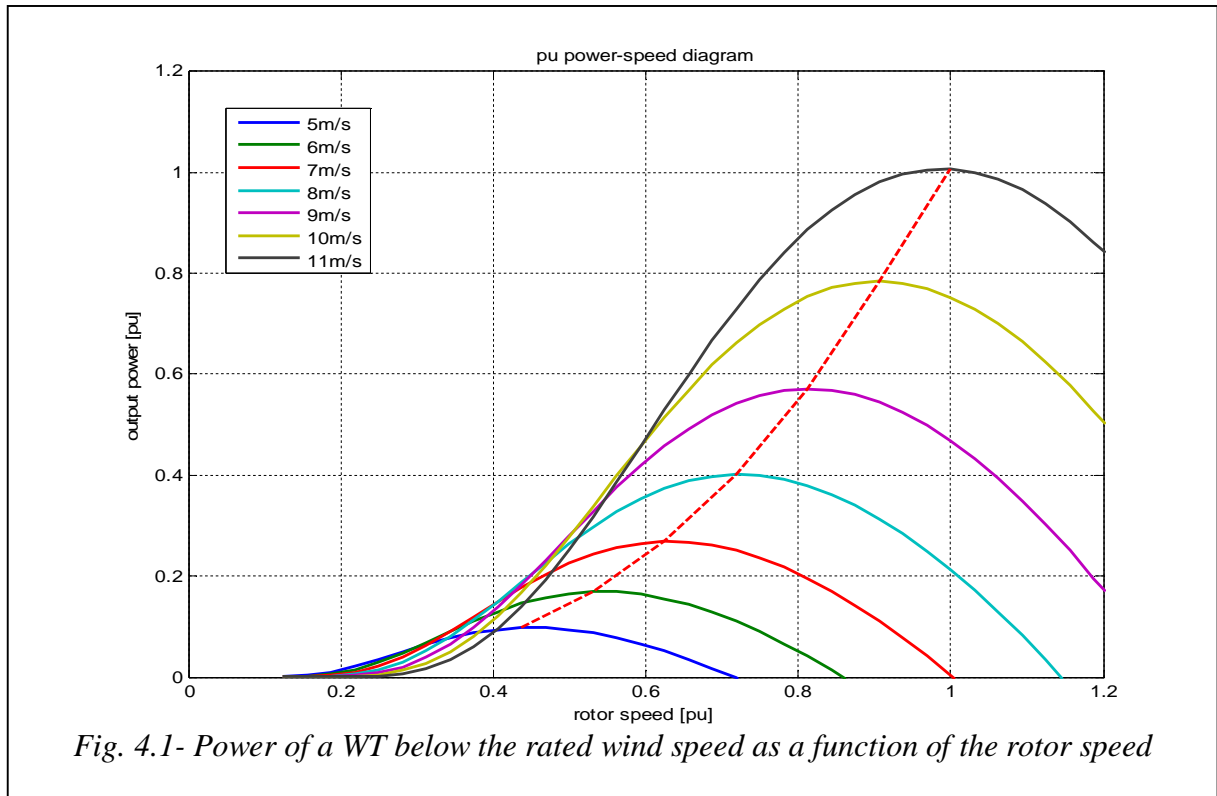


Fig. 4.1- Power of a WT below the rated wind speed as a function of the rotor speed

- $v_w$ : actual upstream wind speed [m/s]

Several numerical representation for  $c_p(\lambda, \theta)$  have been given depending on the turbine geometry [17]-[20]. In this paper the approximation and coefficients introduced in [21] have been used:

$$c_p(\lambda, \theta) = 0,73 \left( \frac{151}{\lambda_i} - 0,58\theta - 0,002\theta^{2,14} - 13,2 \right) e^{-18,4/\lambda_i} \quad (4.2)$$

Where:

$$\lambda_i = \frac{1}{\frac{1}{\lambda - 0,02\theta} - \frac{0,003}{\theta^3 + 1}} \quad (4.3)$$

The difference between turbine models are very small and are not relevant for the scope of this essay to show the CVT technology applied to wind turbines.

With respect to the wind speed range, in order to optimize energy extraction and to comply with system power rating, a simplified mode of operation of the WECS is the following:

- in the **low wind** speed range, from the minimum wind speed to the rated wind speed, the regulation of rotor speed represents the key point in order to optimize the power capture from the wind.
- In the **high speed** range, from the rated wind speed to the maximum wind speed, the WECS should operate at constant rated rotating speed, the blade pitch angle is controlled to cut the wind power from the rotor (pitch to feather or pitch to stall mode) and the system generates the rated power from the generator.

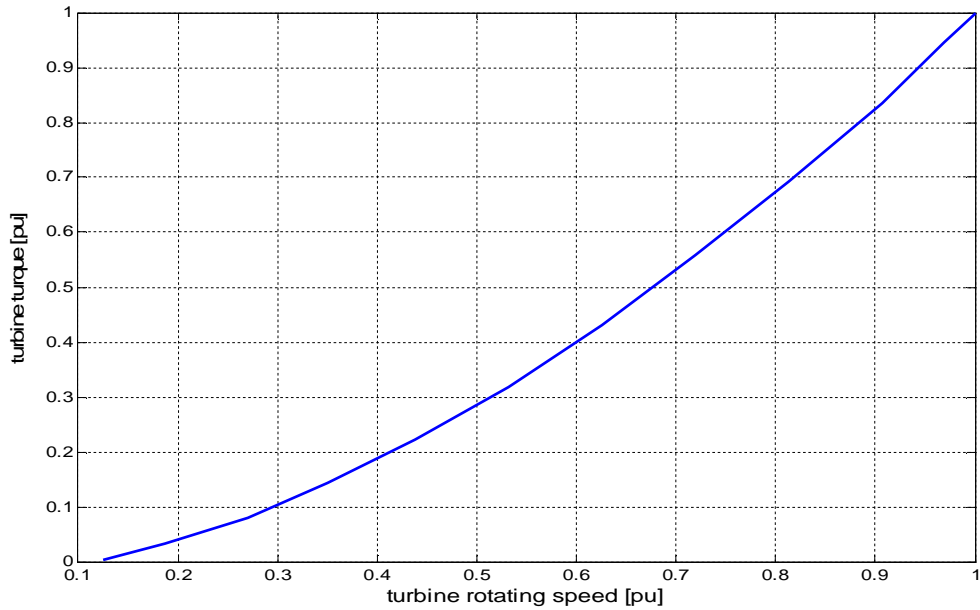


Fig. 4.2- Torque of a WT in the MPPT operation

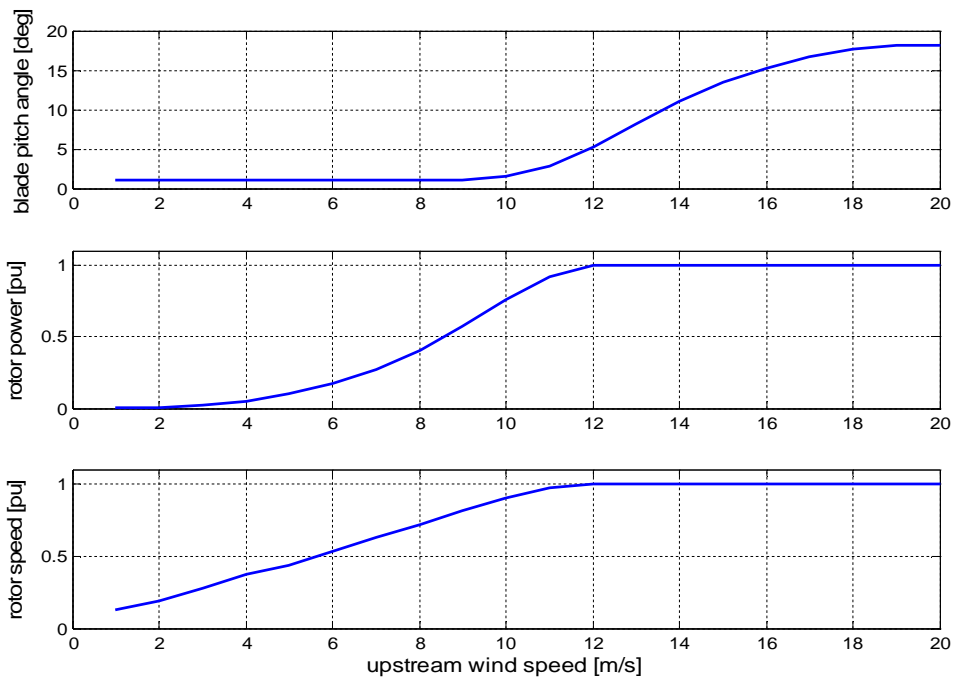


Fig. 4.3- a. Pitch angle, b. Rotor power, c. Rotor speed at a variable wind speed

Fig. 4.1 shows the extracted power vs. rotating speed for a turbine by considering a wind range speed from 5 to 12 [m/s]. In this turbine, for any given wind speed, the maximum power tracking (MPPT) is obtained on the dashed curve.

Assuming the correct operation of the maximum power point tracking shown in Fig. 4.1, the corresponding mechanical characteristic at the turbine shaft is given by the curve shown in Fig. 4.2. More complex control strategy based on the combination of pitch control and regulation of the rotating speed are often used to smooth the generated power. In these cases the turbine output torque is always below the curve of Fig. 4.2. By considering the

whole operating range of a modern WECS the power curve resulting from an optimal control of the system is represented in *Fig. 4.3b*.

#### 4.2.2 E-CVT WECS mechanical configuration

A schematic drawing of the CVT presented in this paper is shown in *Fig. 3.1*. The CVT is constituted by a **planetary gear stage**, in the following configuration:

- the input power from the high speed end (HS) of the step up gear train is supplied to the CARRIER,
- the output power delivered to the electric generator is taken by the RING shaft (GS);
- the SUN is driven by an adjustable speed electric drive (ASD). In this way the sun behaves as **driver**, adjusting the speed ratio between the carrier and the ring.

In this system the speed control of the driver machine determines the capability to regulate the speed of the turbine across a wide range, by maximizing the power extraction of the turbine for wind speed below the rated speed. As it will be shown, an electric drive is a particularly indicated solution for implementing the driver machine on the sun.

The complete model of the planetary gear train has been explained in Chapter 1, referring to absolute quantities. It has been useful to introduce the steady state equations of the gear train expressed in normalized values, in order to better understand the different design possibilities of the planetary gear set.

Assuming as base quantities the rated WT speed and torque after the step up gear train,  $\omega_{Cr}$  and  $T_{Cr}$ , the following p.u. representation can be given for the speeds:

- $\hat{\omega}_C = \frac{\omega_C}{\omega_{Cr}}$  is the p.u. carrier speed;

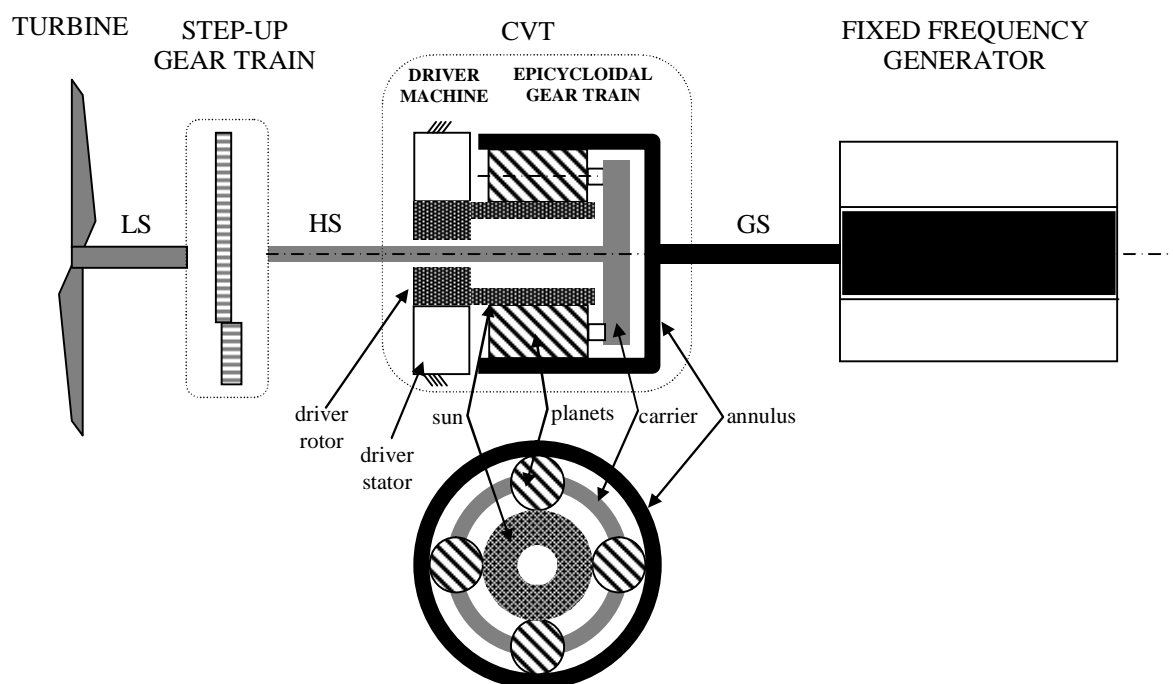


*Fig. 4.4- Mechanical layout of the power split e-CVT for Wind Turbine*

- $\hat{\omega}_R = \frac{\omega_R}{\omega_{Cr}}$  is the ring p.u. speed;
- $\hat{\omega}_S = \frac{\omega_S}{\omega_{Cr}}$  is the sun p.u. speed;
- $\hat{\omega}_{C0} = \frac{\omega_{C0}}{\omega_{Cr}}$  is the carrier speed when the sun is stopped ( $\omega_S=0$ )

From (1.4), the speed  $\omega_{C0}$  of the carrier, when the sun is at zero speed is:

$$\hat{\omega}_{C0} = -\hat{\omega}_R \frac{\tau_0}{1-\tau_0} \quad (4.4)$$

Eq. (4.4) can be used to set the epicyclic gear ratio  $\tau_0$  on the base of the required  $\omega_{C0}$ . By normalizing with respect to maximum torque at the carrier  $TCr$ , the torque at the ring and sun are given from the normalized torque at the carrier  $TC$ , by using eq. (1.7),(1.8):

$$\hat{T}_R = \hat{T}_C \frac{\tau_0}{1-\tau_0} \quad (4.5)$$

$$\hat{T}_A = -\hat{T}_C \frac{1}{1-\tau_0} \quad (4.6)$$

The application of the CVT to the WECS is based on the control of the driver speed  $\hat{\omega}_S$  in order to keep the generator speed  $\hat{\omega}_R$  (quasi)constant all over the operating speed range of the turbine  $\hat{\omega}_C$ . In this way, for a given value of the gear ratio  $\tau_0$ , the speed required to the driver is given from (1.4) as a function of the turbine speed only, and the torque applied by the turbine to the driver  $T_S$  and to the generator  $T_R$  are then calculated from (4.5) and (4.6).

From the mechanical characteristic  $(\hat{\omega}_c, \hat{T}_c)$ , of the wind turbine operating in MPPT, represented in *Fig. 4.2*, by applying Willis, and (4.5), (4.6) it is possible to determine torque and power curves in both the driver and the generator.

#### 4.2.3 E-CVT WECS electrical configuration

The electrical layout of the proposed WT-CVT system is exposed in *Fig. 4.5*, where also the principle scheme of the control system is shown.

The core of the electrical system is the power converter for the driver machine supply. This machine is controlled by the EM control system, which takes at every instant the EM torque setpoint by the WT-CVT control system. This high level control unit knows at every instant the power injected to the grid by the system, the WT speed, and optionally the current wind speed (measured by anemometers). Its main tasks are basically two:

- Regulate the WT speed at the MPP (MPPT as shown in *Fig. 4.1*), below the rated power, independently of the fixed generator speed;

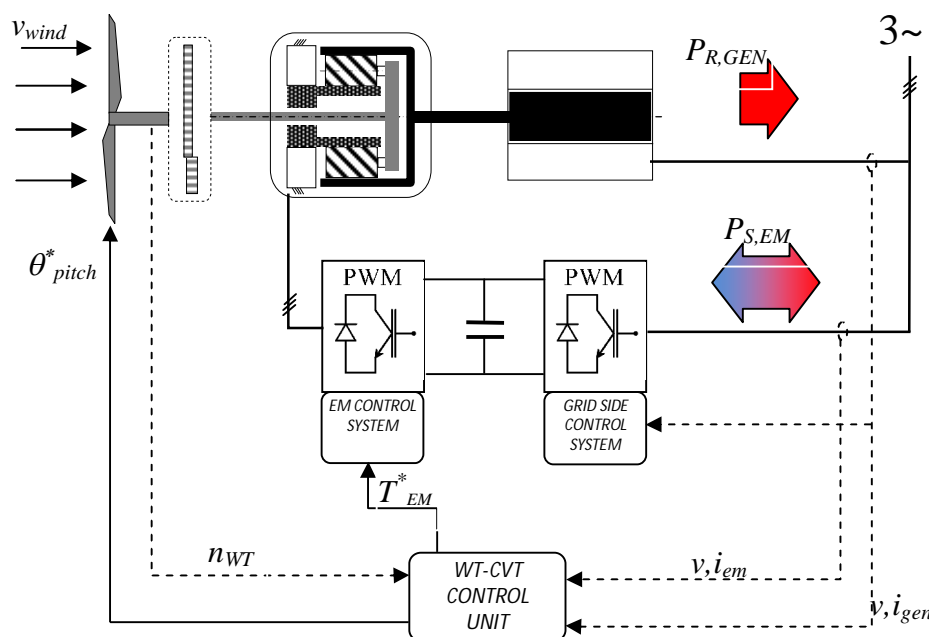


Fig. 4.5- Electrical layout of the power split e-CVT for Wind Turbine (back to back converter)

- Limit the grid injected current when it overcomes the rated value, or the turbine power when the wind speed rise above the rated speed, by controlling the EM torque and by regulating the blade pitch angle ( $\theta_{pitch}$ ).

The grid side converter represented in Fig. 4.5 is a totally controlled PWM converter (active front end), which allows the bidirectional power flow on the driver machine. This kind of power converter, in back to back configuration, requires a grid side control system, which basically has the task to balance the power flow, controlling the DC-link voltage, and could also have power factor control purposes, or active filter functions. This is not the topic of this chapter, because, as the next paragraph will demonstrate, this is not the optimal E-CVT design configuration.

The electrical configuration which will be referred to is the one depicted in Fig. 4.6, where the PWM grid converter is replaced by a simple diode rectifier, which allows the driver only to drain power from the grid. This mode of operation is possible if the planetary/step-up gearbox complex is correctly designed.

The unidirectional power converter do not permit the current flow from the EM to the grid: in particular conditions, when the driver must convert the WT incoming energy, functioning as generator, this power must be supplied to a dissipative load, to preserve the DC link capacitor.

In the next paragraph two possible strategies of design will be examined, corresponding at the two configurations of Fig. 4.5 and Fig. 4.6, and their main advantages and drawbacks will be pointed out and commented.

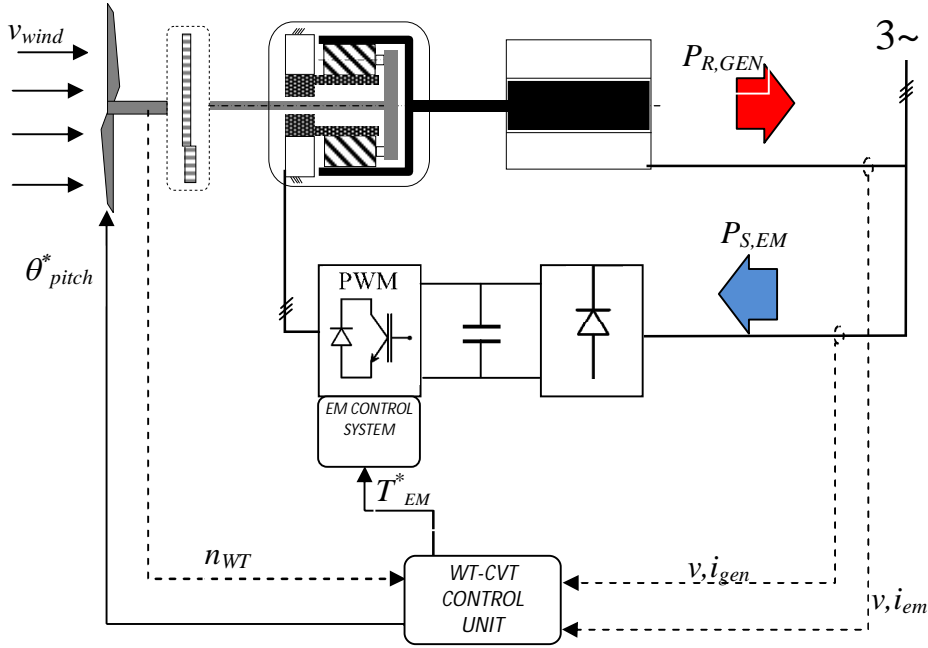


Fig. 4.6- Electrical layout of the power split e-CVT for Wind Turbine (diode rectifier/inverter)

### 4.3 Design criteria

For analyzing torque and power curve at the CVT elements it is necessary to fix the epicyclic gear ratio as defined in (1.3). Two cases have been considered. In the first case study, it has been chosen in order to have  $\hat{\omega}_{c0} = 1$ , meaning that, when the driver is at zero speed, the turbine is at its maximum speed  $\omega_c = \omega_{c0}$ . In the second case it is selected in order to have  $\hat{\omega}_{c0} < 1$ , meaning that when the driver is at zero speed, the rotating speed of the turbine is lower than its maximum speed  $\omega_c < \omega_{c0}$ :

CASE 1  $\hat{\omega}_{c0} = 1$

By considering the condition  $\hat{\omega}_{c0} = 1$  and then, the power at the carrier, at the ring and at the sun, applying eq. (1.15) and (1.16) become:

$$\hat{P}_C = \hat{\omega}_c \hat{T}_C \quad (4.7)$$

$$\hat{P}_R = \hat{\omega}_R \hat{T}_R = -\hat{T}_C \quad (4.8)$$

$$\hat{P}_S = \hat{\omega}_S \hat{T}_S = \hat{T}_C (1 - \hat{\omega}_c) \quad (4.9)$$

where  $\hat{T}_C$  is given from the turbine characteristic and for this case study is given in p.u. in the diagram of Fig. 4.2. The three power curves in p.u. are shown in Fig. 4.7.a. The dashed line is the input power at the carrier, the blue line is the output power at the ring (generator)

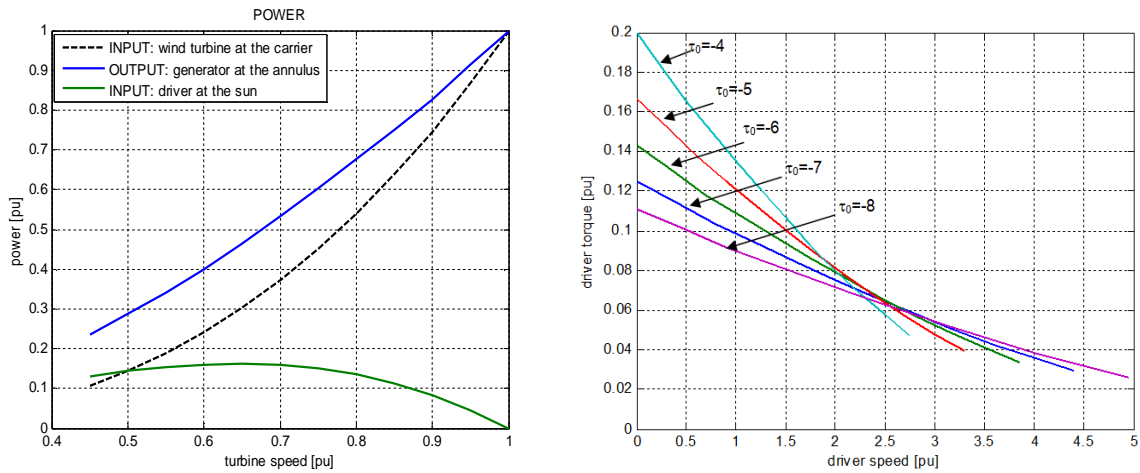


Fig. 4.7 – a) p.u. power curves at MPPT - b) driver torque characteristics at a variable  $\tau_0$  for  $\hat{\omega}_{C0} = 1$  and  $\hat{\omega}_R = 1,143$

and the green line is the input power at the sun (driver) . From the analysis of eq. (4.7)-(4.9) and of Fig. 4.7 it is possible to underline the following aspects:

- The generator is sized for the full power. When turbine speed and power are lower than the rated values, the driver increases its speed from zero, by absorbing a fraction of the generated power from the grid.
- The driver machine on the sun operates as motor all over the speed range. It means that this drive system needs for an unidirectional (one quadrant) converter (Fig. 4.6).
- The driver power is a small fraction of the turbine power. For the given input curve  $(\hat{\omega}_c, \hat{T}_c)$ , the maximum of the driver input power is  $\hat{P}_{S,max} = 0,16$ . This value represents the power rating of the static converter supplying this machine.
- The power sizing of the driver machine depends only by eq. (4.10). In other words it does not depend from gear ratio , and then from the rated speed of the carrier. This consideration means that the power sizing of the CVT is the same, regardless of the stage of the step-up gear where it is inserted.

The capability of the system to regulate the turbine speed at lower values depends on the value of the gear ratio , and on the possibility to operate the driver at higher speed. In Fig. 4.7.b is represented an example of the required speed-torque characteristic demanded at the driver for several values of  $\tau_0$ . In this diagram it is assumed regulation range of the turbine speed in the range  $0.45 \div 1$ .

#### CASE 2 $\hat{\omega}_{C0} < 1$

By considering the condition  $\hat{\omega}_{C0} < 1$  and then  $\tau_0 < 1/(1-\hat{\omega}_R)$ , for a fixed value of  $\hat{\omega}_R$  the power at carrier, ring and sun are determined directly from the fundamental equations of the planetary gear set, and can be written as follows:

$$\hat{P}_C = \hat{\omega}_C \hat{T}_C \quad (4.11)$$

$$\hat{P}_R = \hat{\omega}_R \hat{T}_R = T_C \omega_R \frac{\tau_0}{1-\tau_0} \quad (4.12)$$

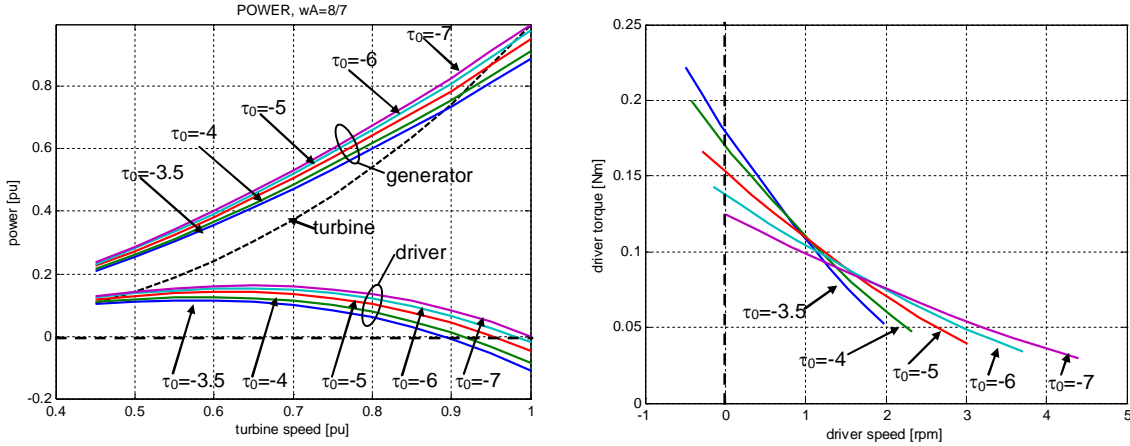


Fig. 4.8 – a) p.u. power curves at MPPT - b) driver torque characteristics at a variable  $\tau_0$  for  $\hat{\omega}_{C0} < 1$  and  $\hat{\omega}_R = 1,143$

$$\hat{P}_S = \hat{\omega}_s \hat{T}_s = -\hat{T}_C \hat{\omega}_C - \hat{T}_C \hat{\omega}_R \frac{\tau_0}{1 - \tau_0} \quad (4.13)$$

These three power curves in p.u. are shown in Fig. 4.8 for a given value of the ring (generator) speed:  $\hat{\omega}_R = 1,143$  as function of the speed of the turbine speed and for different values of the planetary gear fundamental ratio ( $\tau_0 = -3.5, -4, -5, -6, -7$ ).

The condition  $\hat{\omega}_{C0} < 1$ , means that the speed of the turbine when the driver is at zero speed is lower than the turbine maximum speed. From Fig. 4.8 it is clearly shown that the driver operates either as motor for  $\hat{\omega}_{C0} < 1$  or as generator for  $\hat{\omega}_{C0} < \hat{\omega}_C < 1$ . In particular, when the driver operates as generator, both the generator and the driver itself inject power into the grid determining the following main consequences:

- A reduction of the power sizing of the main generator to less than 100% of the rated power of the turbine;
- A reversible power flow in the driver that requires a bidirectional power electronic converter (back to back) for driver grid interface (Fig. 4.5);
- A reduction of the driver power sizing.

In particular these last features can be appreciated on Fig. 4.8.a by observing that the minimum power sizing of the driver is obtained with the epicyclic gear ratio  $\tau_0 = -3.5$ . By this sizing, the maximum power of the driver is about 0.11 p.u. which is reached in motoring mode at a speed 0.6 p.u. and in generating mode at the maximum turbine speed  $\hat{\omega}_C = 1$ .

Even though the case 2 design of the CVT transmission is convenient in terms of power sizing, both for the generator and the driver machine, this option must be further investigated. For the complete analysis of this case, it is required to calculate the torque demanded at the driver for different values of the epicyclic gear ratio. By using Eq. 7b the output torque of the driver is represented in Fig. 4.8.b. In this diagram it is shown that when the driver operates in generating mode (for  $\hat{\omega}_s < 0$ ) the maximum demanded torque is increased with respect to the case  $\hat{\omega}_{C0} = 1$ , here represented by the curve  $\tau_0 = -7$ .

	$\hat{\omega}_{C0} = 1$	$\hat{\omega}_{C0} < 1$
minimum driver power $\hat{P}_S _{MAX}$	16%	11%
maximum driver torque $\hat{T}_S _{MAX}$	minimized by the choice of $\tau_0$	always larger than with $\hat{\omega}_{C0} = 1$
generator power $\hat{P}_G _{MAX}$	100%	89%
power converter for the driver	unidirectional	bidirectional (back-to-back)

Tab. 4.1 – Summary of the WT-CVT sizing possibilities

In other words the increased torque size of the driver yields to enlarge the weight of the E-CVT device and then could not probably be accepted, even if accompanied by an under sizing of the main generator.

The relevant aspects of both the design choice are summarized in Tab. 4.1.

The steady torque characteristics shown in Fig. 4.7 and Fig. 4.8 are easily implementable by an electric drive, which usually has three operational zones: constant torque until the rated speed, constant power for a variable speed range, and decreasing power at higher speeds. The characteristics of an induction machine controlled above the rated speed [25], or an internal permanent magnet machine (IPM) controlled in MTC and by an optimal flux weakening technique [23][24] seem to be the most indicated for this application.

## 4.4 System modeling and control algorithm

### 4.4.1 Model of the system

A model of the above explained system has been developed using MATLAB/Simulink, the scheme of the model is depicted in Fig. 4.9.

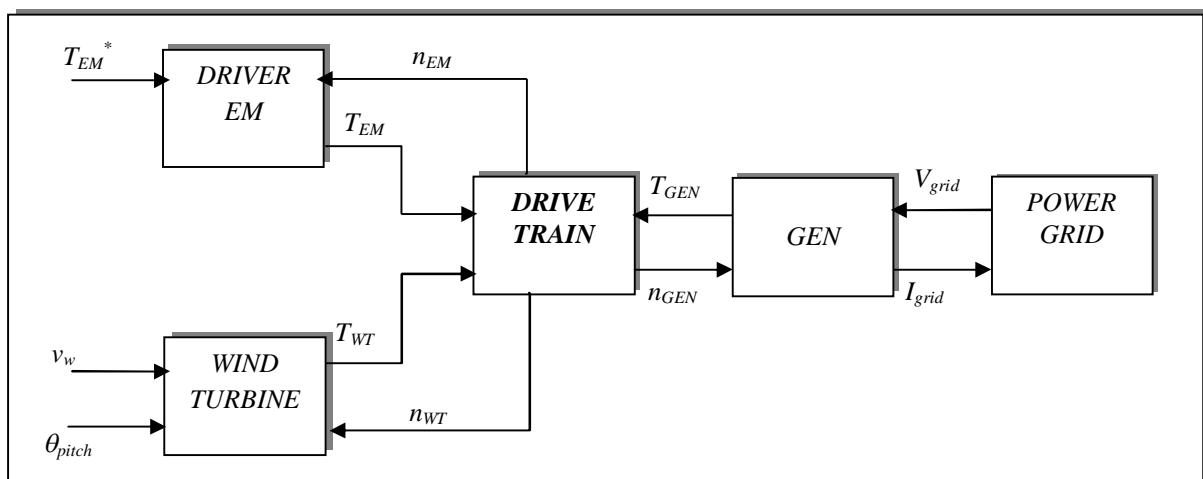


Fig. 4.9 – Block scheme of the WT-CVT system model

### Wind turbine model

The model of the wind turbine has been developed on the basis of the equations (5.1)-(5.3): the model takes as inputs the wind speed, the blade pitch angle and the turbine speed, and outputs the wind turbine developed torque.

### Generator model

In the considered case study the generator is a squirrel cage induction generator (SCIG), which has been modeled by using the space vector theory, writing the equations on the [d,q] stationary reference frame, according to [Mohan]. The model inputs are the line voltage and the shaft speed, while the outputs are the injected current and the shaft torque.

### Driver electrical machine

The driver machine model has been extremely simplified, in order to have a general model, regardless of the machine type, in fact the goal is to verify the operation of the system, and not of the singular machine. The torque characteristic of the machine is shown in *Fig. 4.10*. The dynamic model is represented by the torque loop time constant, which introduces a delay in the torque actuation, and depends on the machine electrical parameters.

### Power grid

The power grid has for simplicity been considered a constant voltage, infinite power source.

### Drivetrain

The drivetrain is constituted by a step up gear train and a planetary gearset, as shown in *Fig. 3.1*. The model of this system has been treated in detail in chapter 1. This model intakes the torques coming from turbine, generator and driver machine, and outputs the speeds of the

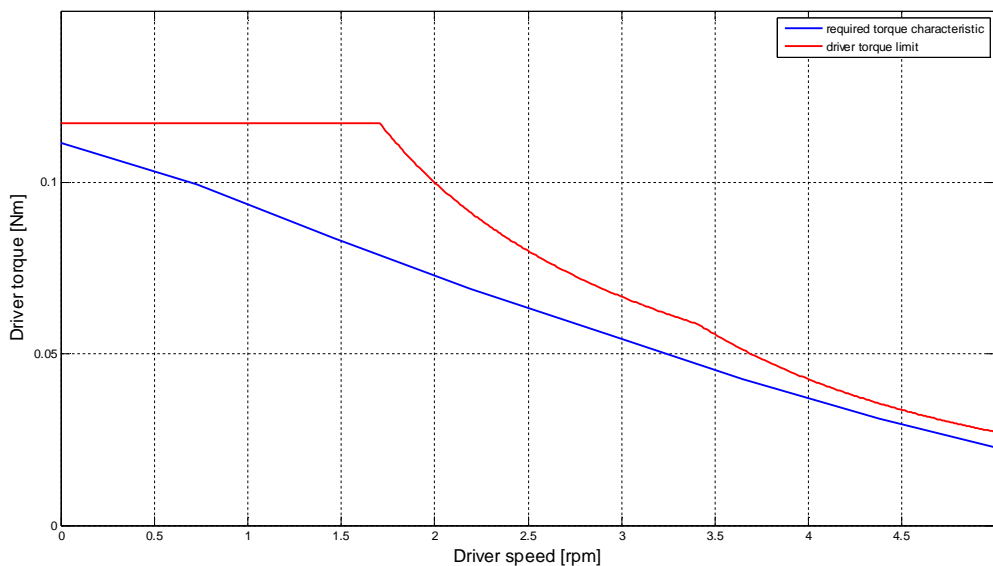


*Fig. 4.10 – Driver torque characteristic ( $\tau_0=-8$ )*

three parts.

#### 4.4.2 Model of the control algorithm

The control scheme, shown in *Fig. 4.11* is basically made up by two parts:

- The EM torque control system
- The blade pitch angle control system

The first one has the goal to maximize the efficiency of the turbine, regulating its speed at a variable wind speed, and at fixed generator speed: its output is the torque setpoint for the driver machine. The MPPT block calculates the setpoint speed of the turbine, then the setpoint speed of the driver is obtained by applying the Willis formula. The PI speed regulator calculates then the torque reference for the EM.

The driver torque setpoint can be limited by the block “Torque limiter”, which has the only task to reduce the driver applied torque whenever the current injected on the grid by the generator becomes higher than the maximum possible. This may enhance the system capability to resist at wind gusts, or more generally to over torques caused by various factors, like grid fault overcurrents.

The pitch control system has a role of aerodynamic power limiter, turning the blades off wind at over rated wind speeds, allowing setpoint power generation at high wind speeds. The pitch actuators may be electrical or hydraulic, allowing a maximum regulation rate variable in the range  $3\div 10$  deg/s, depending on the turbine size. It’s worthy to point out that, under wind gusts, the pitch actuator cannot instantaneously cut the incoming power, and for this reason the driver acceleration (by the torque limiter) permits the turbine to accelerate and not to overload the generator.

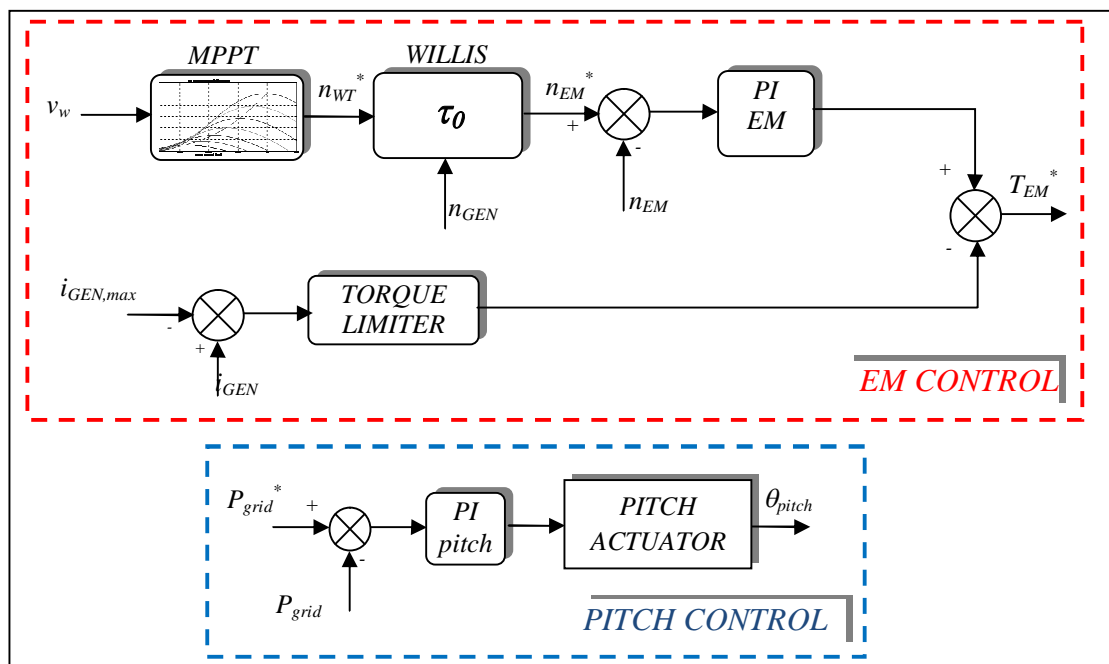


*Fig. 4.11 – WT-CVT control system layout*

The simulation carried out on the presented system will be shown in the next paragraph, where the main features and advantages of the analyzed system will be focused, underlining also the possible future development strategies.

## **4.5 Simulations**

The simulations which have been carried out are essentially of two types:

- a) Normal WT operation, below or above the rated wind speed;
- b) Operation of the WT during wind gusts.

The parameters of the model for the case studied are represented in *Tab. 4.2*.

It has been supposed to apply the E-CVT concept transmission to a classic 2 MW wind turbine, 690 V rated voltage. The simulations results are shown below.

<b>WT – CVT power split model parameters</b>					
<b>Wind turbine</b>			<b>Drive – train</b>		
$P_n$	Rated power [MW]	2	$\tau_0$	Planetary gear ration	-8
$T_n$	Rated torque [MNm]	1,032	$r$	Step up gear ratio	48,45
$n_n$	Rated speed [rpm]	18,5	$k$	Low speed shaft rotational stiffness [Nm/rad]	5,8 E+3
$R_b$	Rotor radius [m]	41	$c$	Low speed shaft stiffness [Nm*s/rad]	2,79 E+8
$J_r$	Inertia [kgm <sup>2</sup> ]	5 E+6			
$T_p$	Pitch actuator time constant [s]	0,03			
$\frac{d\theta}{dt}$	Pitch actuator slew rate [deg/s]	3			
<b>Driver machine</b>			<b>Driver speed control</b>		
$n_{dr,n}$	Rated speed [rpm]	1530	$K_p$	Proportional gain	5
$T_{dr,n}$	Rated torque [Nm]	2500	$K_i$	Integral gain	1
$J_c$	Inertia [kgm <sup>2</sup> ]	7	$T_d$	Time constant of the torque control loop [s]	0,02
$P_{dr,n}$	Rated power [kW]	400			
<b>Generatore asincrono</b>					
$P_n$	Rated power [MW]	2			
$V_n$	Rated voltage [V <sub>rms</sub> ]	690			
$P$	Pole pairs	3			
$J_g$	Inertia [kgm <sup>2</sup> ]	82			
$R_s$	Stator resistance [ $\Omega$ ]	1,748 E-3			
$R_r$	Rotor resistance [ $\Omega$ ]	3,253 E-3			
$L_s$	Stator inductance [H]	2,589 E-3			
$L_r$	Rotor inductance [H]	2,604 E-3			
$L_m$	Mutual inductance [H]	2,492 E-3			

Tab. 4.2 – Parameters of the model

Test n°	Test type (a)
1	Turbine operation below the rated 12 m/s wind speed
<p><b>Test description</b></p> <p>This simulation shows the capability of the control system to regulate the turbine speed at a step variable wind speed, below the rated one.</p> <p><b>Wind speed:</b> Variable in the range 6÷12 m/s.</p> <p><b>Turbine speed setpoint:</b> Regulated by MPPT control.</p> <p><b>Pitch blade angle:</b> Fixed at the minimum, to maximize the power extraction.</p> <p><b>Power generation setpoint:</b> Constant at 2 MW.</p> <p><b>Analysis of the simulation results</b></p> <p>The wind speed is considered variable with finite steps, from 12 m/s to 6 m/s and then again to 12 m/s, as shown in <i>Fig. 4.12</i>. The pitch regulator is not involved by these transients, because the power is always below the setpoint of 2 MW.</p> <p>As shown in <i>Fig. 4.13</i>, the turbine speed is varied following the wind speed profile, in order to get the maximum power exploitation by the turbine. The speed graph shows the real speed compared to the setpoint one, and it is correctly followed.</p> <p>Contextually, looking at the graphs of <i>Fig. 4.15</i>, it's evident that the generator speed is almost constant, varying only of few %, due to the induction machine slip, which makes the speed varying proportionally to the input torque. It is clear now the CVT operation of the proposed transmission, which makes of the WT-CVT system a variable speed-fixed frequency application, coupling together generator and turbine with the maximum efficiency.</p> <p>In <i>Fig. 4.16</i> the driver operation is shown, with a speed variable in the range 0÷4000 rpm, then also in flux weakening region, where the torque is decreasing with speed. Particularly in the time range 80→100 s, the speed dynamic is affected by torque limitation, especially during transients. The acceleration of the EM is slower than in higher wind regions, even if the turbine torque is decreasing. Although this high speed limitation, the speed follows the setpoint with no regime error.</p> <p>By <i>Fig. 4.17</i> the mechanical power profile on the system components can be observed. The electrical power is the same neglecting losses. The following consideration can be made:</p> <ul style="list-style-type: none"> <li>• The grid power (violet) is the same of the generator (red) and the turbine (blue), only at the rated power (2 MW).</li> <li>• The grid power transients are 'sweeter' than the turbine mechanical power transients, due to the driver power draining (green line), which absorbs the turbine</li> <li>• The driver always adsorbs power, until a maximum of almost 300 kW in the 60→80 s interval, which means that the 0,16 power rating is correct for this machine, with an overloading possibility during transients.</li> </ul>	

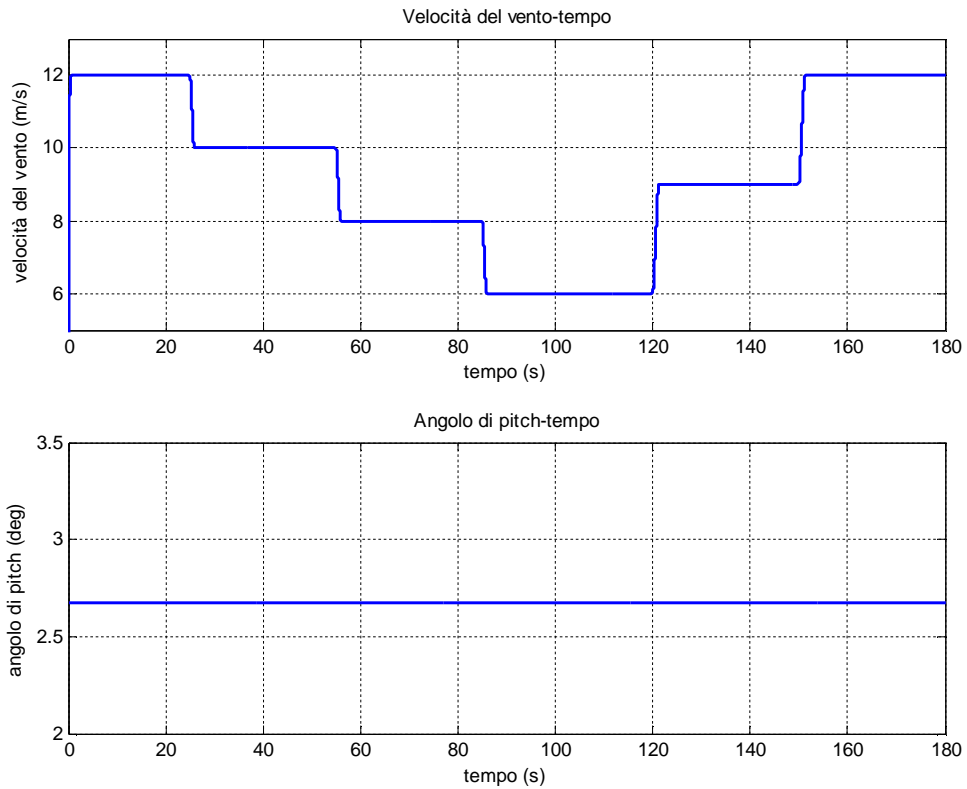


Fig. 4.12 – Simulation 1 – Wind speed and pitch angle

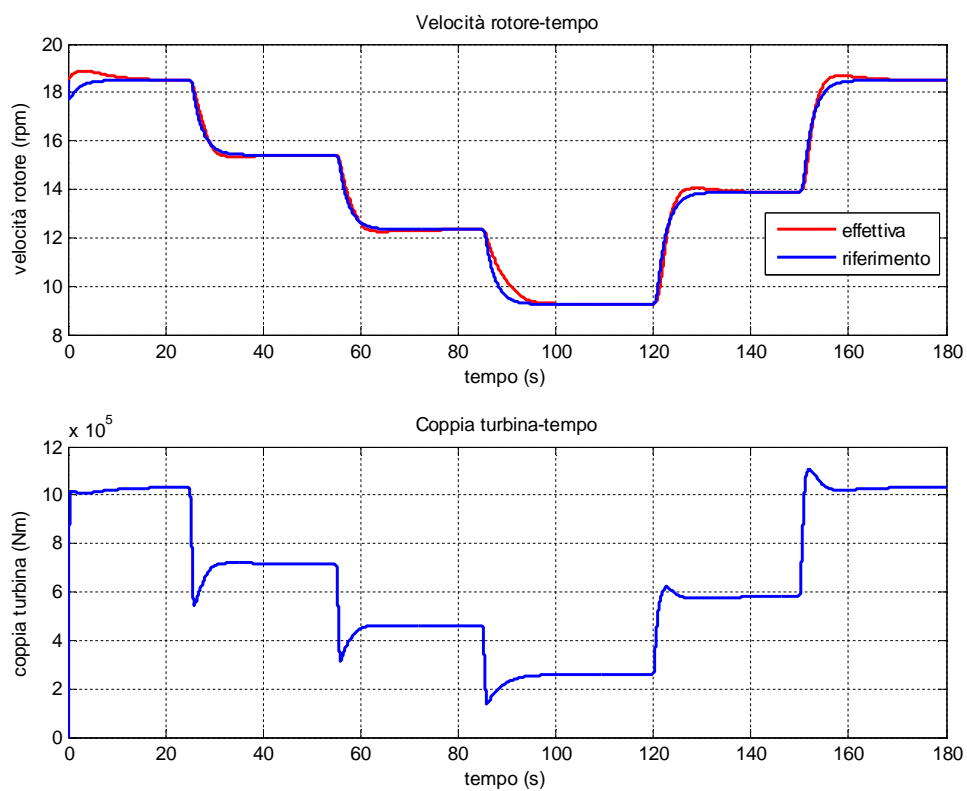


Fig. 4.13 – Simulation 1 – Turbine speed and torque

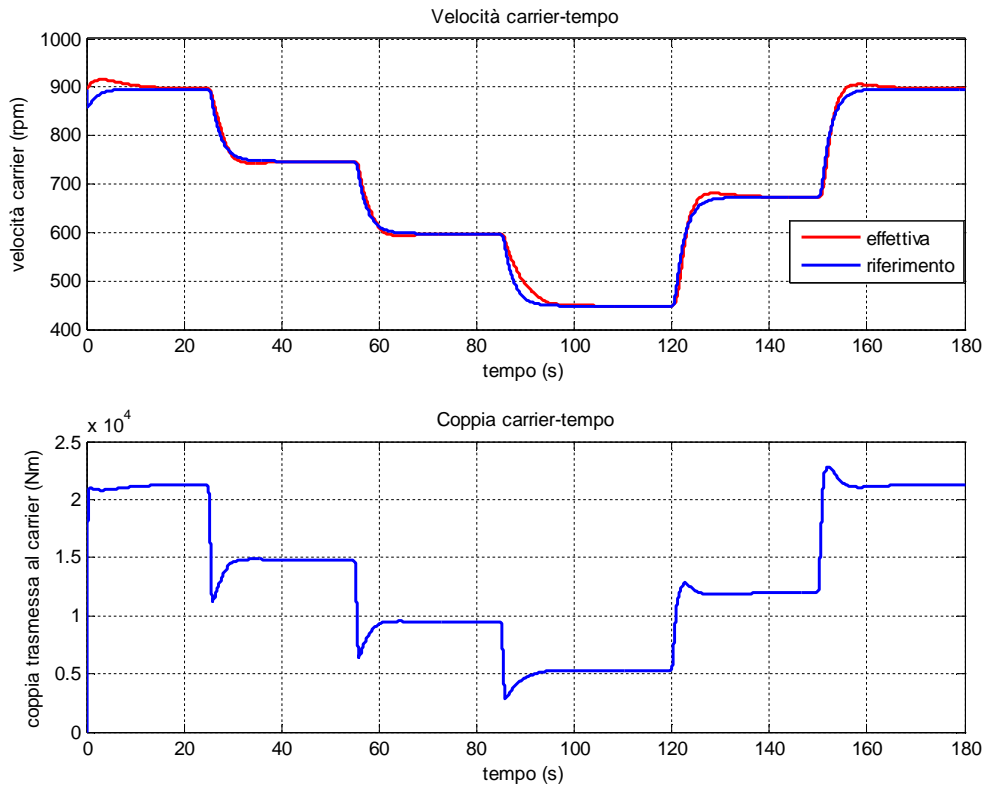


Fig. 4.14 – Simulation 1 – Carrier speed and torque

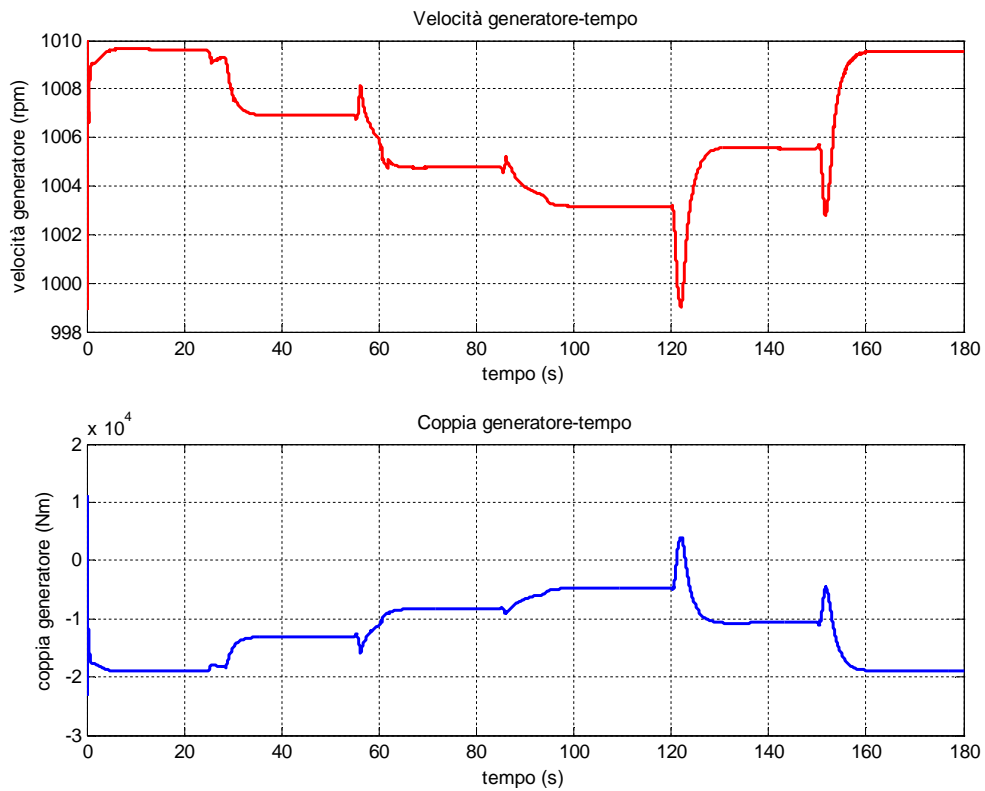


Fig. 4.15 – Simulation 1 – Generator speed and torque

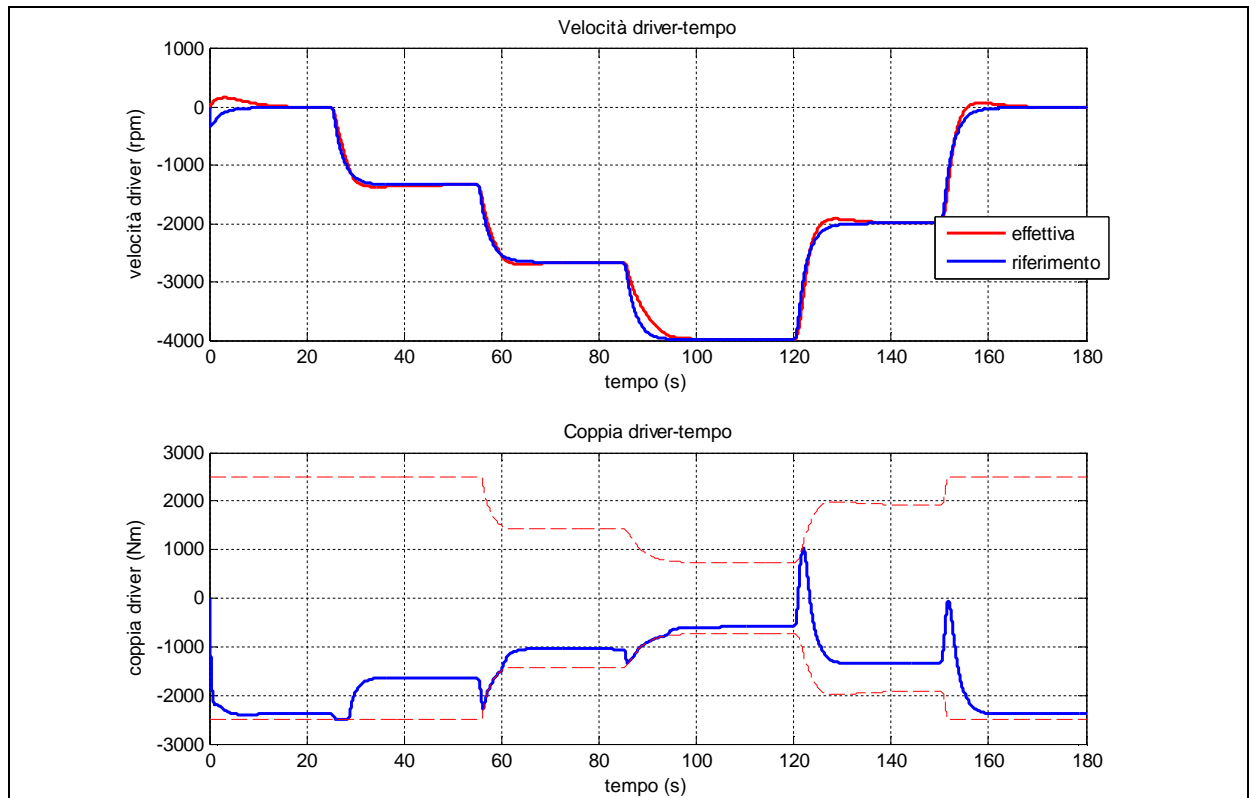


Fig. 4.16 – Simulation 1 – Driver speed and torque

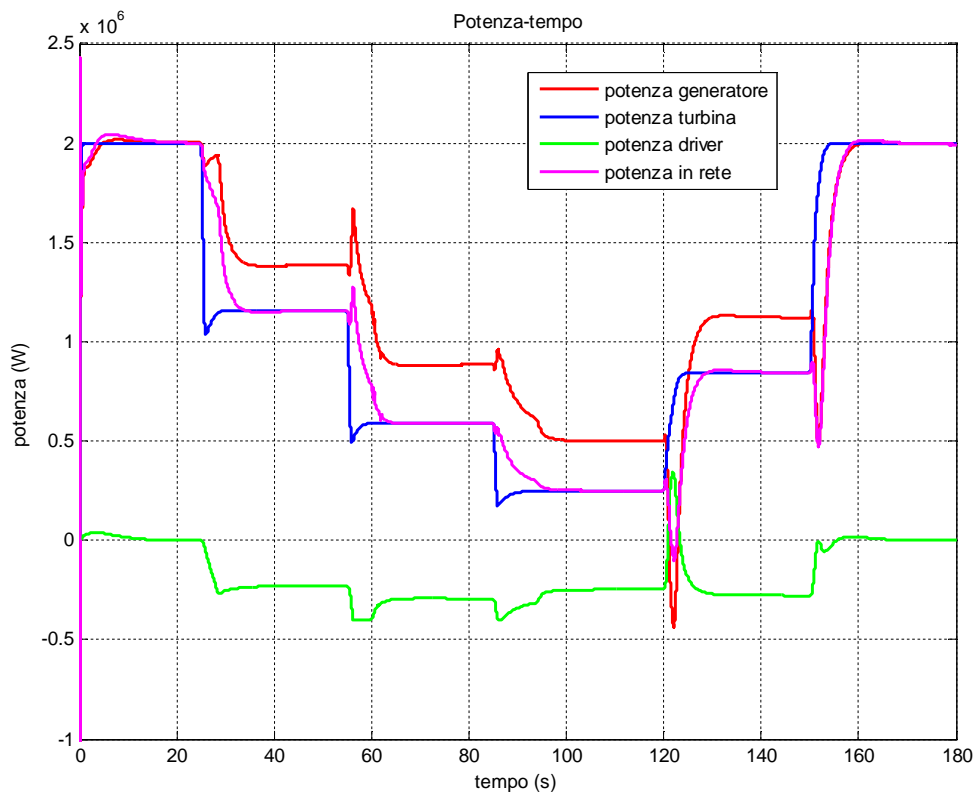


Fig. 4.17 – Simulation 1 – Power (negative is adsorbed)

Test n°	Test type (b)
2	Turbine operation above the rated 12 m/s wind speed, under wind gust

**Test description**

This simulation shows the capability of the control system to limit the torque transmitted from the turbine rotor to the generator at high wind gusts either with a torque limiting action or without.

**Wind speed:** Variable in the range 12÷19 m/s.

**Turbine speed setpoint:** Regulated by MPPT control at rated speed.

**Pitch blade angle:** Rises up on wind gust, trying to limit the incoming power

**Power generation setpoint:** Constant at 2 MW.

**Analysis of the simulation results**

1) In this simulation, a constant wind speed of 12 m/s is considered, until the 40 s instant. At this point a wind pulse of 7 m/s and 3 seconds long happens (Fig. 4.18.a), the turbine torque instantaneously increases (Fig. 4.19.b), giving rise to a rotor acceleration, which only is permitted by the driver torque limitation. In fact the EM is not capable to transmit all the incoming rotor torque, thus its speed rises above the null speed, inverting the power flow (Fig. 4.22.b and Fig. 4.23 green). The acceleration of the driver permits the turbine to accelerate (Fig. 4.19.a) and to avoid transmitting an excessive torque at the generator shaft (Fig. 4.21.b). In this phase, the driver machine operates as a generator, therefore its power must be injected onto the grid (if a back to back configuration is used, Fig. 4.5) or has to be dissipated on a passive load (if a one quadrant rectifier is used, Fig. 4.6). In this test no torque limiting action was introduced.

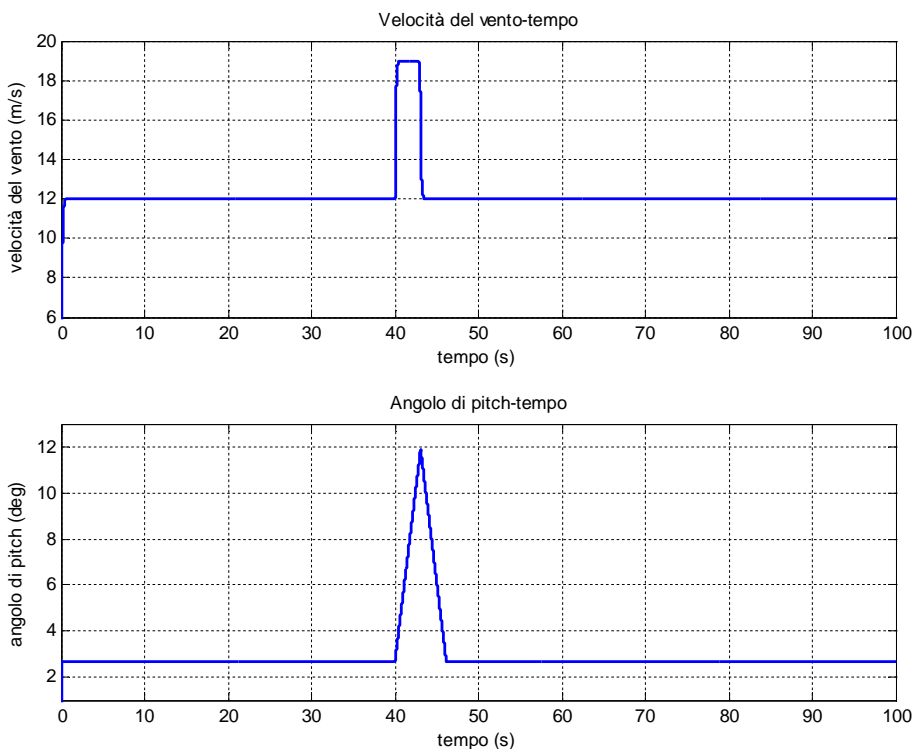


Fig. 4.18 – Simulation 2 – Wind speed and pitch angle

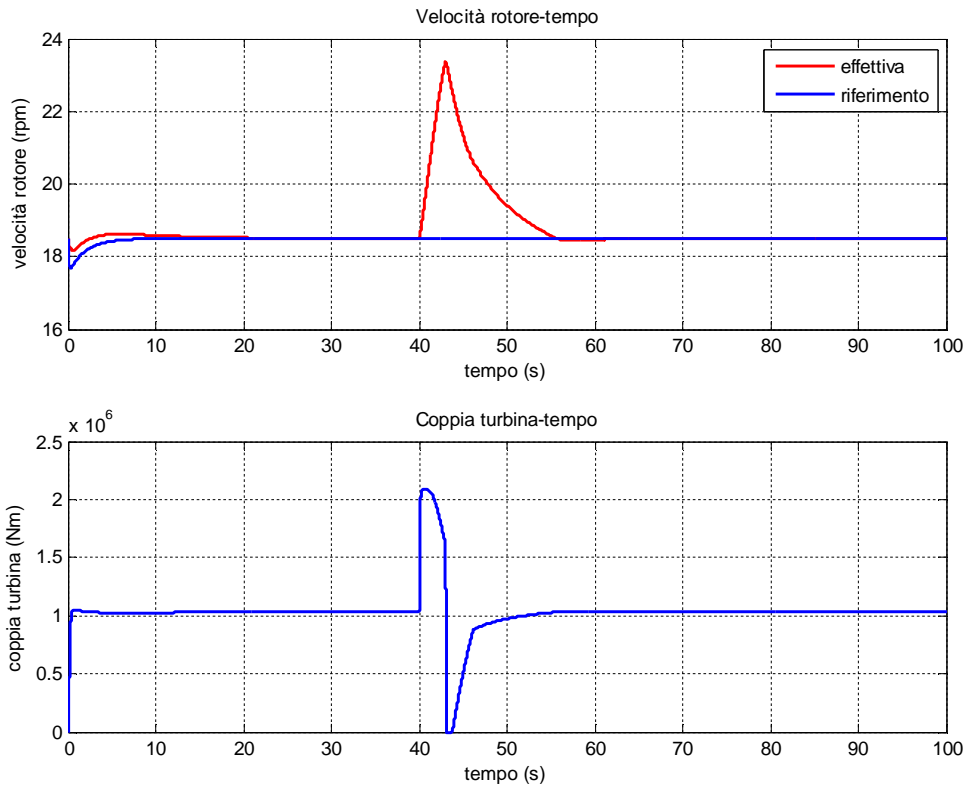


Fig. 4.19 – Simulation 2 – Turbine speed and torque

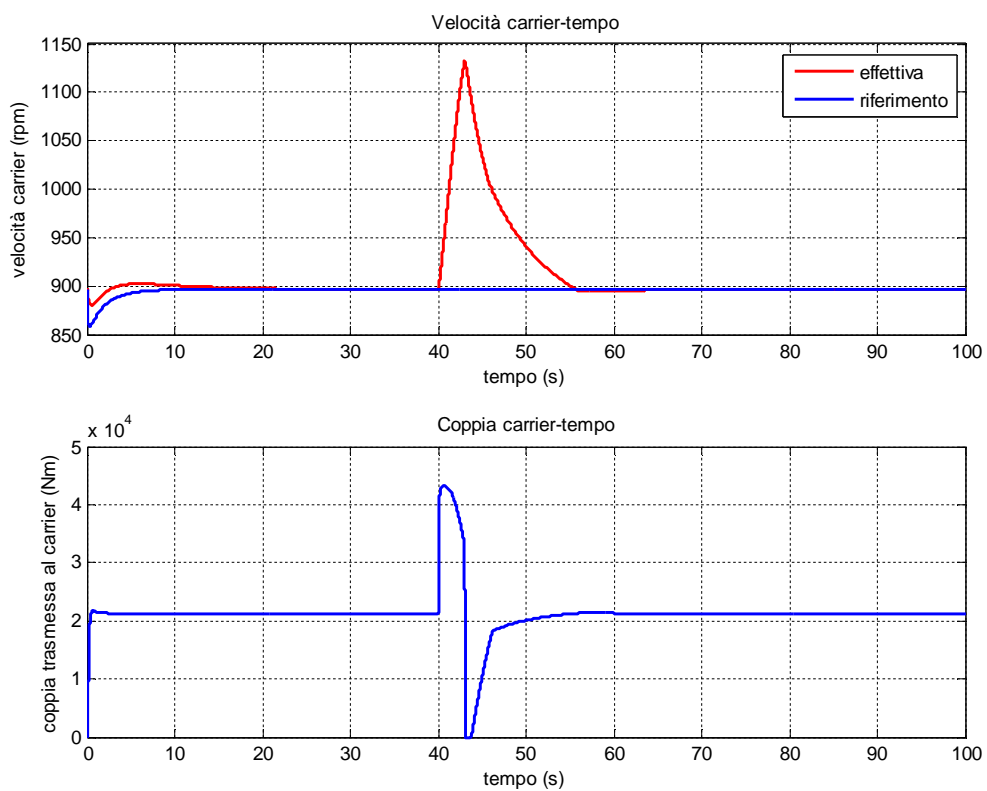


Fig. 4.20 – Simulation 2 – Carrier speed and torque

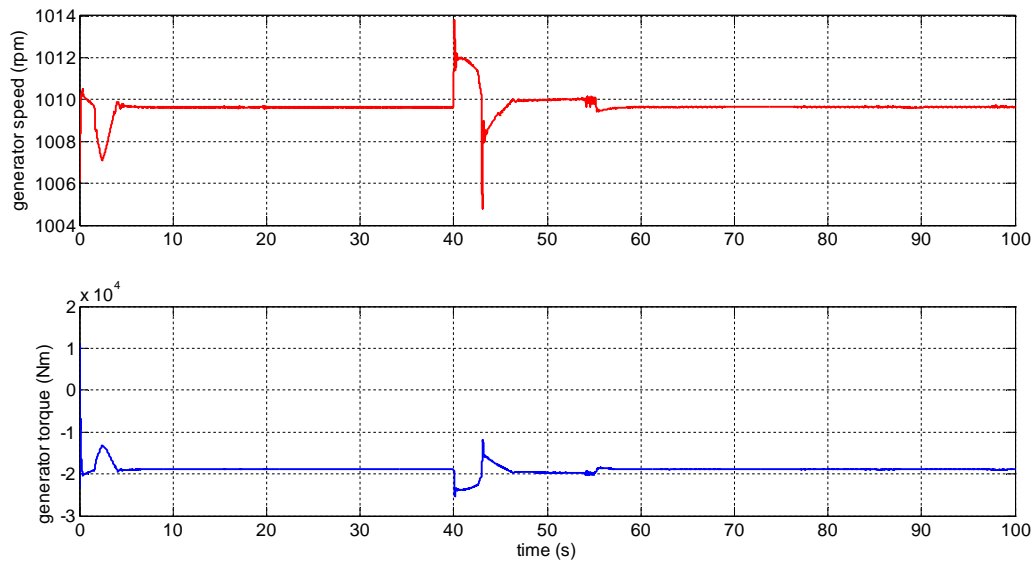


Fig. 4.21 – Simulation 2 – Generator speed and torque

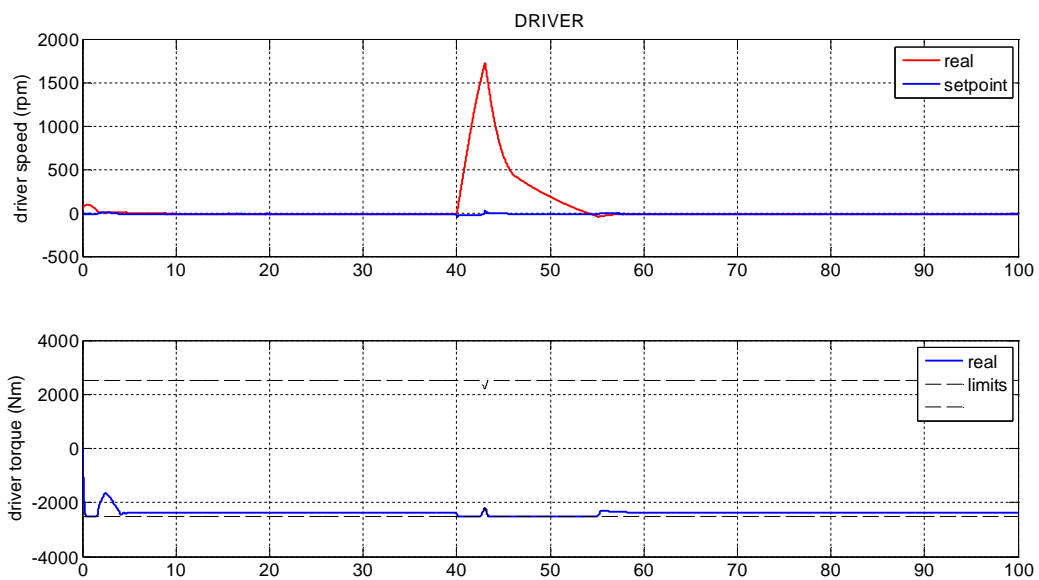


Fig. 4.22 – Simulation 2 – Driver speed and torque

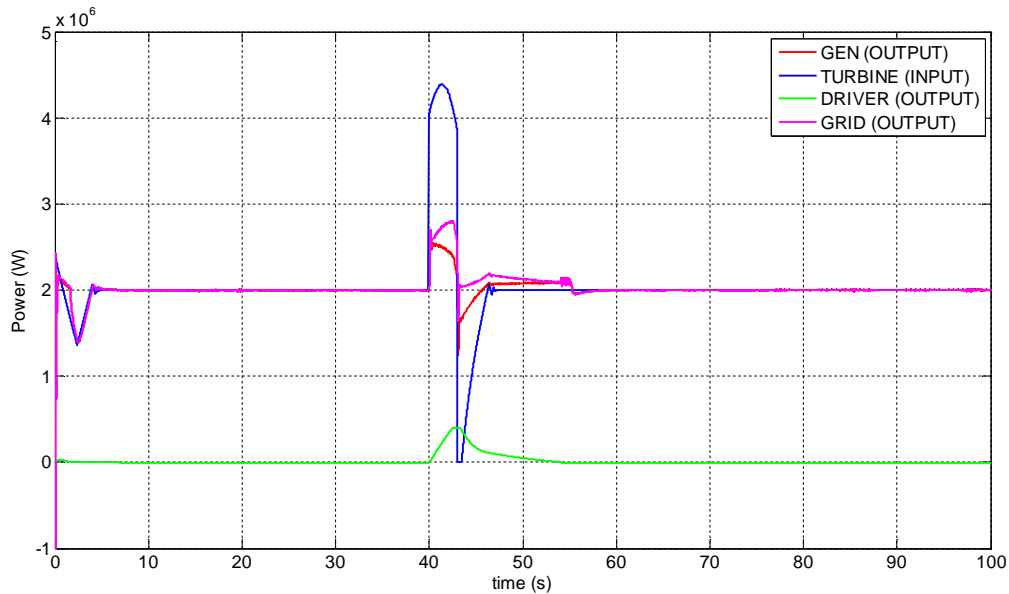


Fig. 4.23 – Simulation 2 – Power (negative is adsorbed)

2) If a torque limiting action is adopted, as shown in Fig. 4.11, the driver torque can be further limited, by using a PI controller on the estimated generator torque, or the generator current. The results of this introduction can be appreciated on the following graphics. In Fig. 4.24.b, the generator reaction to the wind gust is compared to that without torque limiter, and a reduction is visible. This is due to the limitation of the driver torque (Fig. 4.25.b), which is able to accelerate more than in the previous case (cfr. Fig. 4.22.a). The torque limitation effect is evident in Fig. 4.25.

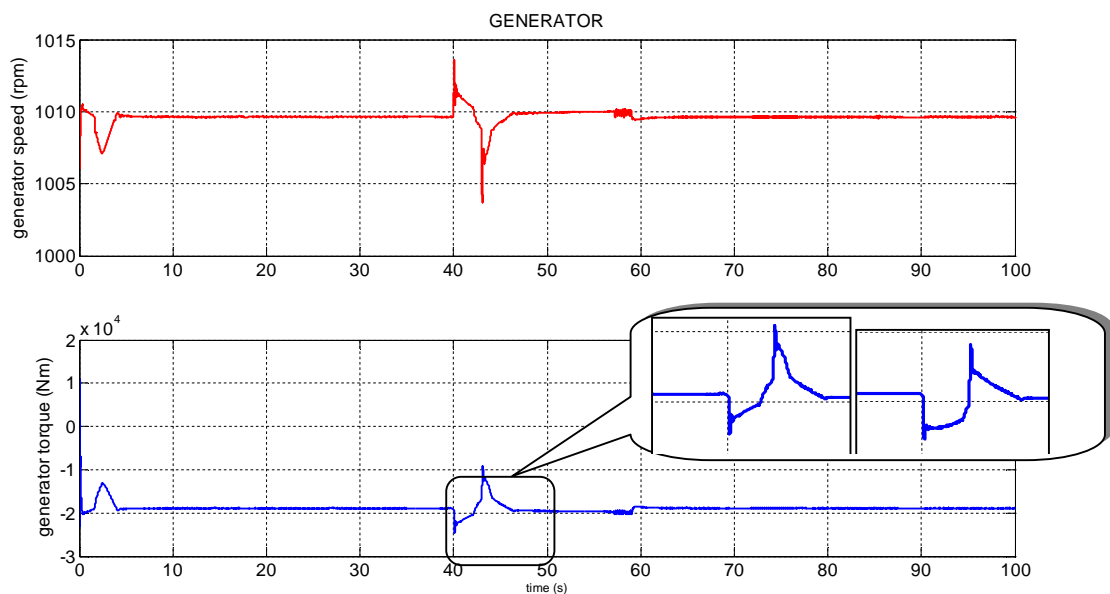


Fig. 4.24 – Simulation 2/bis – Generator speed and torque. In the particular, the reduction of the overload torque compared to the unlimited case.

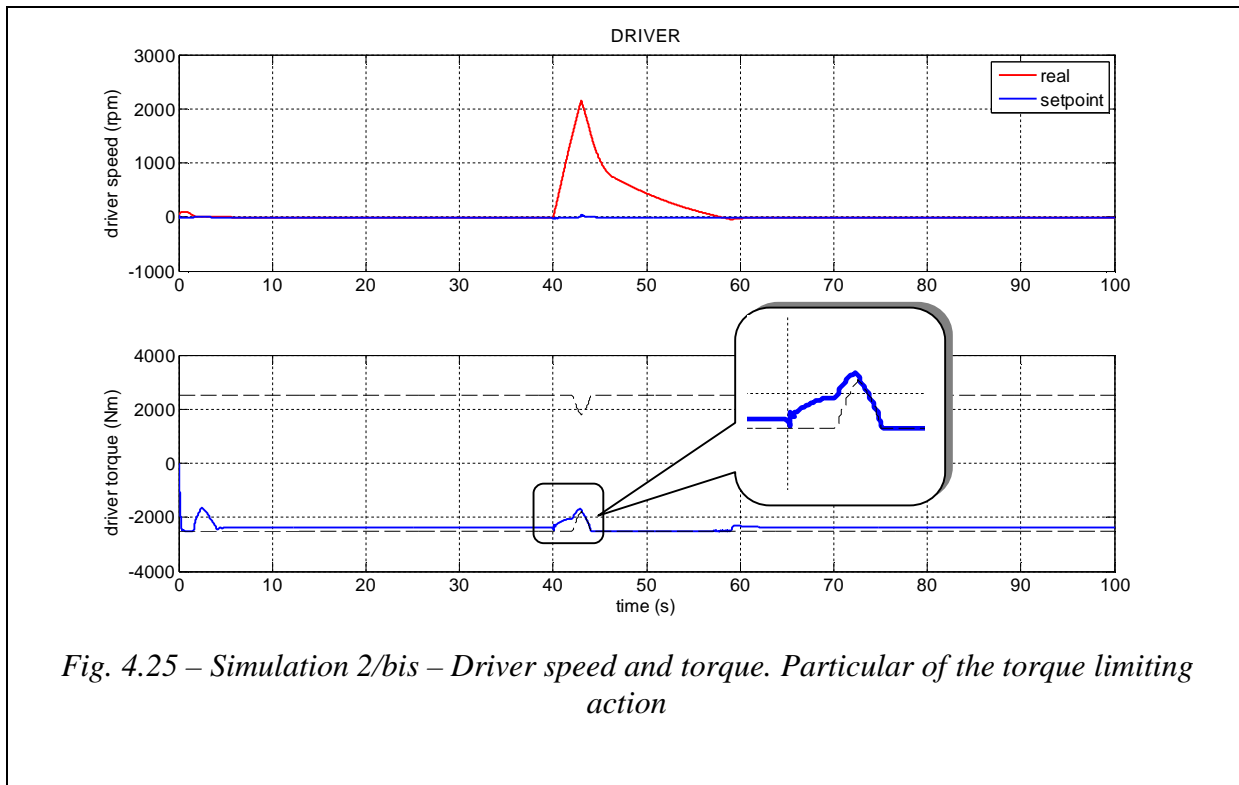


Fig. 4.25 – Simulation 2/bis – Driver speed and torque. Particular of the torque limiting action

## 4.6 Conclusions

The power split applied to a wind energy conversion system has been examined, in the steady state operation and in transient simulations, where the main features of the system has been put in evidence, e.g. the low power rating of the driver converter (16% of the turbine power). MPPT operation below rated wind speed and transmitted torque limitation on wind gusts reaction have been found on simulation results.

Experimental results will be shown on the next chapter, to validate the simulation results.

## References

- [1] E.S. Abdin, W. Xu, —Control Design and Dynamic Performance Analysis of a Wind Turbine-Induction Generator Unit|| IEEE Trans. On Energy Conversion, Vol. 15, No. 1, pp. 91-96, March 2000.
- [2] M.Y. Uctug, I. Eskandarzadeh, H. Ince, —Modeling and Output Power Optimization of a Wind Turbine Driven Double Output Induction Generator,|| IEE Proc. Electric Power Applications, Vol. 141, No. 2, pp. 33-38, March 1994.
- [3] R. Pena, J.C. Clare, G.M. Asher, —Doubly Fed Induction Generator Using Back-to-Back PWM Converters and its Application to Variable-Speed Wind-Energy Generation,|| IEE Proc. Electric Power Applications, Vol. 143, No. 3, pp. 231-241, May 1996.
- [4] B. Rabelo, W. Hofmann, —Optimal Active and Reactive Power Control with the Doubly-Fed Induction Generator in the MW-Class Wind-Turbines,|| Proc. of 4th IEEE International Conference on Power Electronics and Drive Systems, Vol. 1, pp. 53-58, Oct. 2001.
- [5] Z. Chen, E. Spooner, —Wind Turbine Power Converters: A Comparative Study,|| 7th International Conference on Power Electronics and Variable Speed Drives, No. 456, pp. 471-476, Sept. 1998.
- [6] I. Cadirci, M. Ermis, —Double-Output Induction Generator Operating at Sub-synchronous and Super-Synchronous Speeds: Steady-State Optimization and Wind-Energy Recovery,|| IEE Proc. B Electric Power Applications, Vol. 139, No. 5, pp. 429-442, Sept. 1992.
- [7] E. Spooner, A.C. Williamson, —Direct coupled, permanent magnet generators for wind turbine applications|| Proc. of Electric Power Applications, IEE - Vol. 143, Issue 1, Jan. 1996 Page(s):1 - 8
- [8] M. Popesci, M. V. Cistelecan, L. Melcescu, M. Covrig, —Low Speed Directly Driven Permanent Magnet Synchronous Generators for Wind Energy Applications|| Proc. of Int. Conf. on Clean Electrical Power, 2007. ICCEP '07. 21-23 May 2007 Page(s):784 - 788
- [9] L. Hui, C. Zhe —Design optimization and comparison of large direct-drive permanent magnet wind generator systems|| Proc. of International Conference on Electrical Machines and Systems, 2007. ICEMS. 8-11 Oct. 2007 Page(s):685 - 690
- [10] A. Binder, T. Schneider, —Permanent magnet synchronous generators for regenerative energy conversion - a survey|| Proc. of European Conference on Power Electronics and Applications, 2005 11-14 Sept. 2005 Page(s):10 pp.
- [11] R. Datta, V. T. Ranganathan, —Variable-Speed Wind Power Generation Using Doubly Fed Wound Rotor Induction Machine - A Comparison With Alternative Schemes|| IEEE Transactions On Energy Conversion, Vol. 17, No. 3, September 2002
- [12] H. Law, H. A. Doubt, B. J. Cooper, —Power Control Systems for the Orkney wind-turbine generators‘ Proc. of Intersociety energy conversion engineering conference; Vol./Issue: 4; 19 Aug 1984; San Francisco, CA, USA
- [13] H. Müller, M. Pöller, A. Basteck, M. Tilscher, J. Pfister, —Grid Compatibility of Variable Speed Wind Turbines with Directly Coupled Synchronous Generator and Hydro-Dynamically Controlled Gearbox‘ Proc. of Sixth Int‘l Workshop on Large-Scale Integration of Wind Power and Transmission Networks for Offshore Wind Farms, 26–28 October 2006, Delft, NL
- [14] Wikov-Wind W2000 —2MW Wind Turbine‘ data sheet from Wikov Wind a.s.; [www.wikov.com](http://www.wikov.com)

- [15] S. Heier, —Grid Integration of Wind Energy Conversion Systems||, 2nd Ed., Wiley, 2006.
- [16] T. Burton, D. Sharpe, N. Jenkins, E. Bossanyi, —Wind Energy Handbook||, Wiley, 2001
- [17] O. Wasynczuk, D. T. Man, and J. P. Sullivan, —Dynamic behaviour of a class of wind turbine generators during random wind fluctuations|| IEEE Trans. Power App. Syst., vol. 100, pp. 2837–2845, June 1981.
- [18] M. M. Hand and M. J. Balas, —Systematic Controller Design Methodology for Variable-Speed Wind Turbines,|| National Renewable Energy Laboratory, Tech. Rep. NREL/TP-500-29 415, Feb. 2002.
- [19] N.W. Miller, J. J. Sanchez-Gasca, W.W. Price, —Dynamic modelling of GE 1.5 and 3.6MW wind turbine generators for stability simulations|| in Proc. IEEE Power Engineering Society General Meeting, vol. 3, Jul. 2003, pp. 1977–1983.
- [20] A. D. Hansen, C. Jauch, and P. Sorensen, —Dynamic Wind Turbine Models in Power System Simulation Tool Digsilent|| Risø National Laboratory, Risø, Denmark, Tech. Rep. Risø-R-400(EN), Dec. 2003.
- [21] J. G. Slootweg, H. Polinder, S. W. H. de Haan, W. L. Kling, —General Model for Representing Variable Speed Wind Turbines in Power System Dynamics Simulations|| IEEE Transactions On Power Systems, Vol. 18, No. 1, Feb. 2003
- [22] Henrik Bindner, —Active Control: Wind Turbine Model||. Report number: R-920(EN) Risø National Laboratory, Denmark, 1999
- [23] Morimoto, S. Takeda, Y. Hirasu, T. Taniguchi, K. Expansion of operating limits for permanent magnet motor by optimum flux-weakening Proc. of Industry Applications Society Annual Meeting, 1989., Conference Record of the 1989 IEEE , 1-5 Oct. 1989 Page(s): 51 -56 vol.1
- [24] W. L. Soong, T.J.E. Miller: Field-weakening performance of brushless synchronous AC motor drives. Electric Power Applications, IEE Proceedings- , Volume: 141 , Issue: 6 , Nov. 1994 Pages:331 – 340
- [25] D. Casadei, G. Serra, A. Tani, Luca Zarri, “A Robust Method for Field Weakening Operation of Induction Motor Drives with Maximum Torque Capability”, IAS 2006, Tampa, Florida, 8 12 Oct. 2006, Paper N.IAS03P5, ISBN: 1-4244 0365-0.
- [26] Ned Mohan —Advanced Electric drives|| MNPERE Minneapolis MN – USA, 2001. ISBN 0-9715292-0-5.

---

# Chapter 5

## Experimental results

### 5.1 The experimental setup

The experimental setup built at the LEMAD (laboratory of electrical machine and drives), is composed by many devices, and has been conceived to test different kind of transmissions in the 60 kW, 2000 Nm range.

The experimental test setup is basically constituted by two main parts:

- The test bench (test drive, control system and instrumentation)
- The device under test, in this case a scaled model of E-CVT power split, and its supply, control and monitoring system.

#### 5.1.1 The test bench

The core of the test bench is a four quadrant regenerative AC/AC back to back converter supplying an induction machine, which constitutes the SIEMENS SINAMICS S120 drive system. This system is composed by the following elements:

- Induction machine SIEMENS (60 kW rated power at 400V).
- Back to back converter for IM/grid interface and its control unit (CU 320).
- PLC type SIMATIC S7-300, with auxiliaries.
- Touch screen control panel OPL77B and Analog I/O interface to the PLC unit.

Further components of the test bench are:

- A two speed gearbox placed at the IM shaft (1:1, 5:1)
- A torque/speed meter placed on the main shaft with a supply and evaluation instrument.

The scheme of the test bench is represented in *Fig. 5.1*, where it is possible to observe the signal exchange between the components of the system. In particular it is possible to send via analog I/O ports the torque/ speed setpoint signals. These signals are sent to the SIMATIC S7-300, which then communicates them by PROFIBUS interface at the control unit CU320 of the SIEMENS drive. In other words, it is possible to control the speed or the torque of the induction machine, realizing a perfect load emulator, or prime mover emulator, etc.

The PLC unit has been programmed by way of the STEP 7 software, and the desired torque characteristic at the main shaft has been obtained by simple math operations implemented on this unit.

The operator panel has also been programmed, in order to allow the operator to change easily and on-line the control parameters of the test drive, e.g. the choice on the speed/torque control. By using the panel it's possible to control the speed or the torque setpoint at the machine, and the gearbox ratio, allowing the test of different speed and torque range devices.

The torque meter/analyzer units have two settable ranges (200 or 2000 Nm) allowing the testing of very high torque traction drives

As shown in the next paragraphs the torque curves typical of a wind turbine have been implemented on the system, allowing to test the WT-CVT application by the use of a lab scale power split E-CVT device mounted on the test bench.

### 5.1.2 The lab scale E-CVT power split system

The power split system realized in LEMAD lab is composed by the following elements:

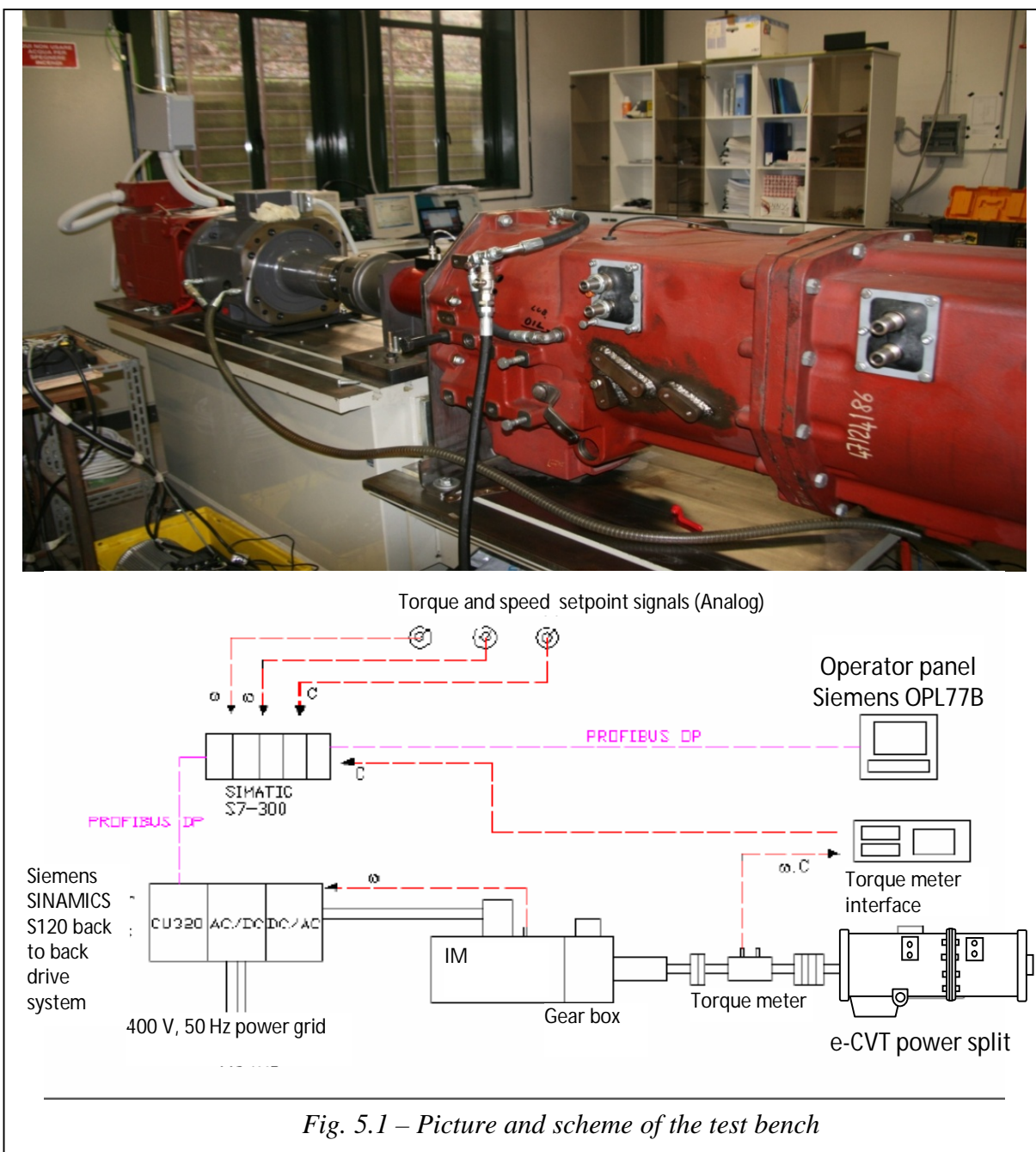


Fig. 5.1 – Picture and scheme of the test bench

- N°1 Power split E-CVT device;
- N°2 VSI power inverters for controlling the E-CVT machines;
- N°1 80 V Pb-Acid battery pack;
- N°1 NI C-RIO embedded programmable controller;
- N°1 Operator PC with CAN interface;
- N°2 CANBUS networks (1 Mbps);
- N°1 oil tank and hydraulic lubrication pump;
- N°1 automatic liquid cooling system.

#### A. Power split E-CVT device

The power split device used for the lab tests is made up by a planetary gear train coupled with two identical three phase induction machines:

- RING is coupled to one IM, rated power 50 kW;
- SUN is coupled to the other IM, rated power 50 kW;
- CARRIER is connected to the main shaft, connected to the test drive.

The more internal machine is connected to the SUN wheel, and it is not provided neither with a braking system, nor with a speed sensor. This problem has been overcome by inserting one incremental encoder on the carrier output shaft and one on the ring shaft on the back side of the chassis. By knowing two shaft speeds it is possible to apply the Willis equation (1.4) and find the third one. By knowing the SUN speed it's possible to make a speed control on this machine even at low speed, close to the null speed.

The device is equipped with two cooling chamber, where the cooling water circulates before passing in an external fan cooler.

It is also equipped with a circulating oil system, for lubrication of the gear train.

Two thermocouples outcome the motors phases, giving the possibility to read the windings temperature, and to start the cooling fan if the temperature rises above a certain threshold.

The electrical characteristics of the machines are reported in *Tab. 5.1*.

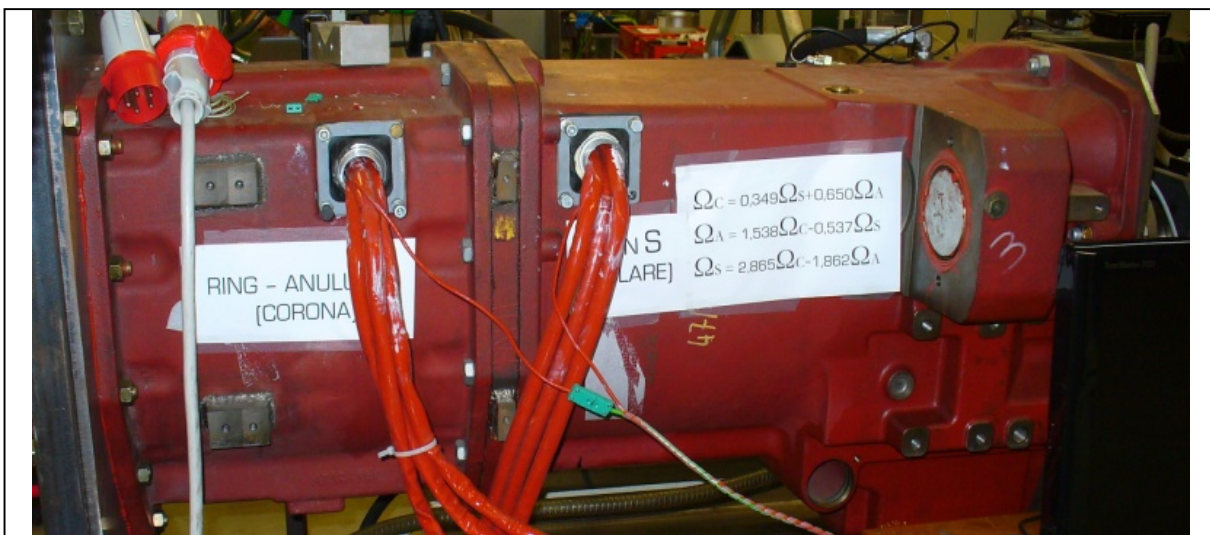


*Fig. 5.2 – Particular of the E-CVT power split chassis*

MOTORE ASINCRONO ANSALDO - A1H352C44M001				N° 1101
IP 56 IEC 34-5		HZ 0 - 410	I.CI. H	S = 1/2
KW	$\Delta V Y$	$\Delta A Y$	COS $\varphi$	RPM
50	145	275		1230
50	300	122		6000
80	175	350		1230
80	300	190		4500

Tab. 5.1 – Characteristics of the induction machine in the E-CVT device

The fundamental speed ratio of the planetary gear train is the following:

- R=103;
  - S=56;
  - $\tau_0=-1,84$ ;
- (5.1)

**B. VSI power inverters**

Low voltage VSI inverters for traction have been used (80Vdc), equipped with a DSP control board which intakes signals from one encoder and communicates by a 1Mbps CANBUS interface with the external world.

One more encoder signal is required at the SUN machine inverter, which has been equipped with an interface PCB, properly designed to acquire an encoder signal.

The inverters control boards communicate with the high level control system by CANBUS, from which they receive the control signals like speed setpoints and torque limitations, or control parameters, e.g. the speed regulator parameters.

The current control algorithm utilized in the control board is the rotor flux oriented

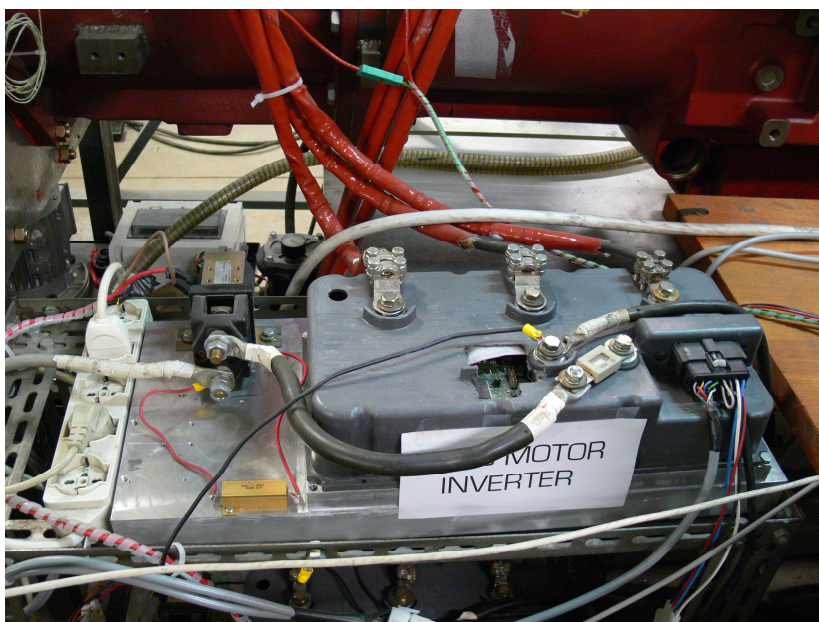


Fig. 5.3 – Particular of the VSI inverter

control for induction machines [25], in sensed or sensorless configuration, with a flux weakening algorithm for constant and decreasing power operation.

### C. *Battery pack*

The power split system is supplied by a lead acid battery pack with a 80 V rated voltage.

### D. *National Instruments Compact RIO*

A CompactRIO NI-RIO 9004 model has been used as the power split system control unit. This PAC (programmable automation controller) integrates a completely reconfigurable hardware, made up by an FPGA (field programmable gate array) device, a configurable set of I/O modules and a real time processor (*Fig. 5.4*). The FPGA should be used for the time-critical and easier operations (fixed point math), but not for the heaviest computational tasks, which should be left to the real-time processor supporting a floating point math.

The CRIO used for this application was equipped with the following I/O modules:

- AI  $\pm 60V$
- AI  $\pm 10V$
- AO  $\pm 10V$ : Used for outputting signals to the AI of the SIEMENS system, such as the “wind speed”, for the simulation of a wind generator.
- DI  $\pm 10V$ : Used for getting the pressure signal from the lubrication pump and signaling eventual anomalies.
- DO, switches, used for startup of the cooling system when the machine temperatures overcome a fixed value.
- Thermocouple, used to measure the temperature of the E-CVT machines.
- CAN, used to communicate with the operator PC and with the inverters control boards.

CRIO has been programmed for different application of the E-CVT, and to guarantee the correct operation of the experimental setup.

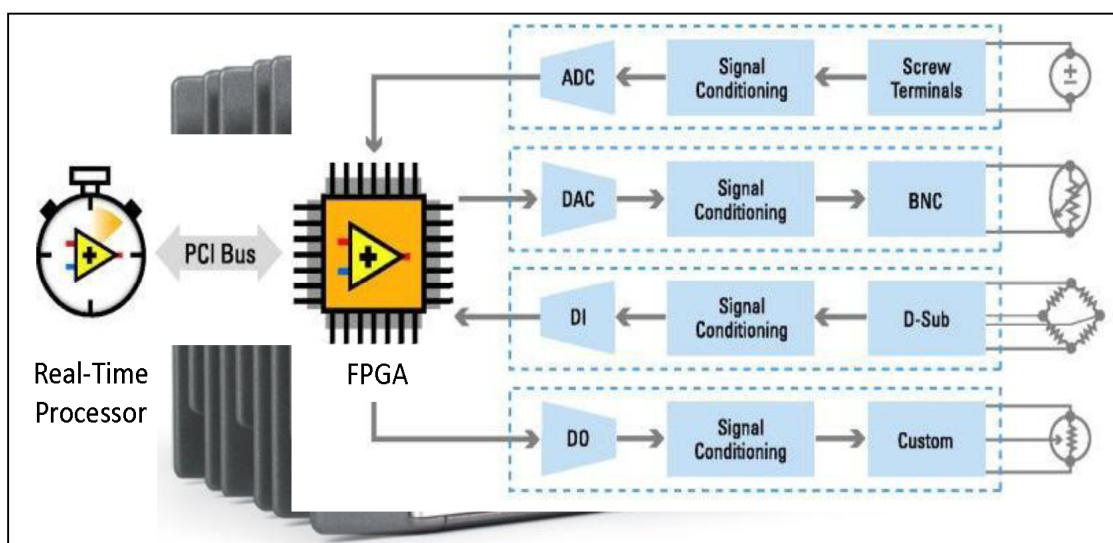


*Fig. 5.4 – The Compact RIO architecture*

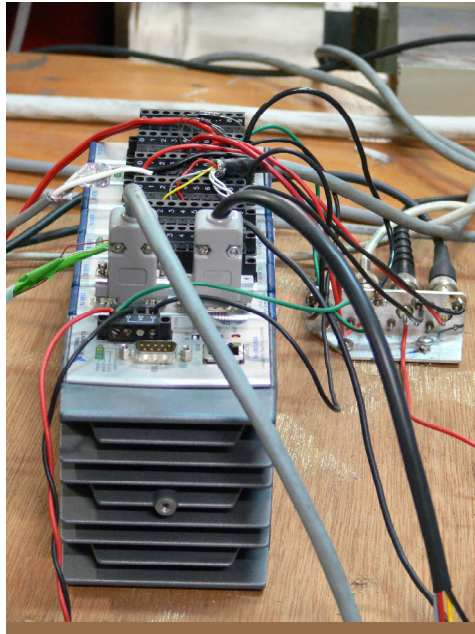


Fig. 5.5 – The CRIO used in lab

#### E. Operator PC with CAN interface

The PC of the operator runs all the LabVIEW interface software for the control of the system. Particularly two VIs (virtual instruments) have to be run for controlling the system:

- The “Console” VI, which communicates directly with the E-CVT inverters;
- The “HOST” VI, which communicates with the CRIO.

The overall communication system has been implemented on networks of the CAN type.

#### F. CANBUS

The Controller Area Network is a standard serial field-bus utilized preeminently in EMC disturbed environments, because of its robustness. The maximum transmission rate is 1Mbps, for lines shorter than 40 m.

In the lab application two CAN bus have been used:

- CAN bus 1: Communication between PC-Inverters-CRIO
- CAN bus 2: Communication between PC-RIO only

This differentiation has been adopted for one reason: the type of messages sent to the inverters by the PC are transmitted with a slower rate than the type from PC to CRIO. This aspect summed to the availability of two CAN ports on the CRIO and on the PCMCIA interface for PC carried to a two CAN bus configuration.

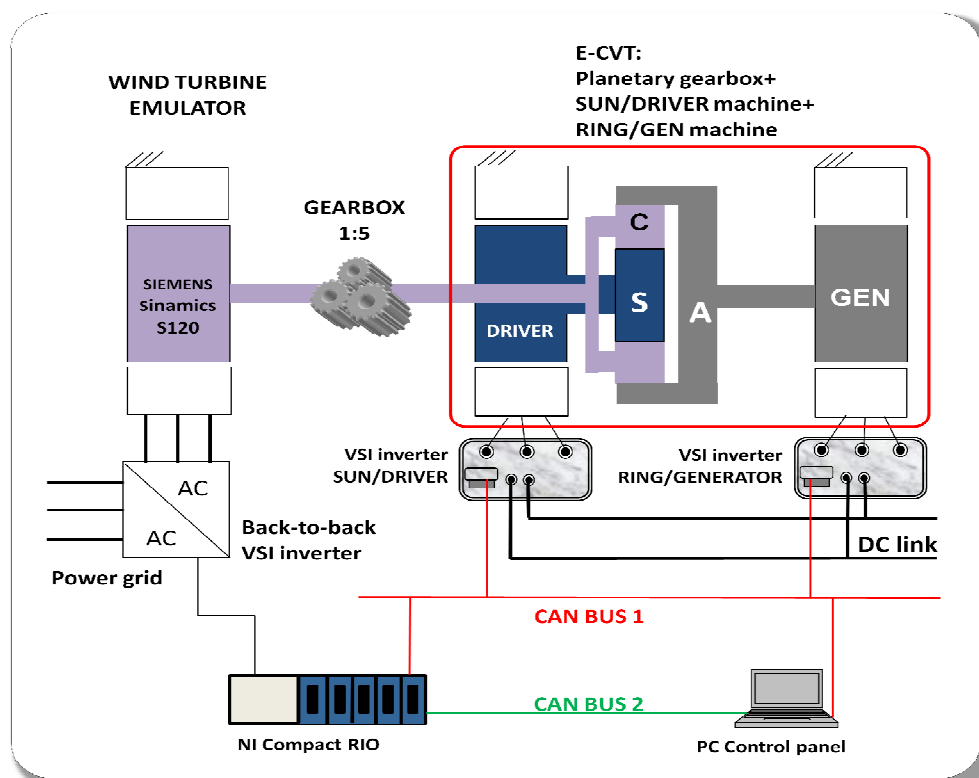


Fig. 5.6 – Overall experimental setup scheme

## 5.2 WT-CVT lab test: setting of the system

### 5.2.1 Scaling of the E-CVT system

The experiments on the WT-CVT have been conducted on a scaled system, which has been thought on the basis of the limitations present in the lab system.

The first limitation is the DC link voltage (80V). This low voltage makes impossible to reach high value of power, because the speed at constant torque is limited to a low value.

In particular the torque limit characteristic of both the induction machines, supplied by a 80 V voltage has the form represented in Fig. 5.7, with the following parameters:

- Rated torque:  $T_{r,IM}=260$  Nm
- Rated speed:  $n_{r,IM}=300$  rpm
- Maximum power @ 300 rpm:  $P_{r,IM}=9420$  W

For this reason the speed of the RING machine, which represents the GENERATOR of the turbine (and will be referred to as RING/GEN), has been set at  $n_{R/GEN}=300$  rpm.

Supposing to apply the unidirectional converter configuration  $\hat{\omega}_{C0} = 1$  (4.3), the rated CARRIER speed (which is the TURBINE) matches with the  $\omega_{C0} = -\omega_R \frac{\tau_0}{1-\tau_0}$  carrier speed at zero sun speed. In these conditions the rated carrier speed can be calculated as:

$$\omega_{C0} = \omega_{C,rated} = -\omega_R \frac{\tau_0}{1-\tau_0} = 195,2 \text{rpm} \quad (5.2)$$

### 5.2.2 Scaling of the turbine system

The torque developed by a wind turbine can be written as:

$$T_{WT} = \frac{1}{2} \rho \pi R_{WT}^3 c_T(\lambda) v_w^2 \quad (5.3)$$

where:

$$\lambda = \frac{\omega R}{v_w} \quad (5.4)$$

$$c_T(\lambda) = \frac{c_P(\lambda)}{\lambda} \quad (5.5)$$

The test drive is deputed to generate the turbine torque, in order to match the above calculated carrier rated speed (5.2). The torque curves based on (5.3) should be calculated on the basis of a  $c_p(\lambda)$  expression similar to that of (4.2). However it is impossible to implement this kind of operations on the utilized PLC: a sixth order polynomial approximation of the coefficient  $c_T(\lambda)$  has been introduced, as shown in [3]:

$$c_T(\lambda) = \sum_{i=1}^6 a_i \lambda^i \quad (5.6)$$

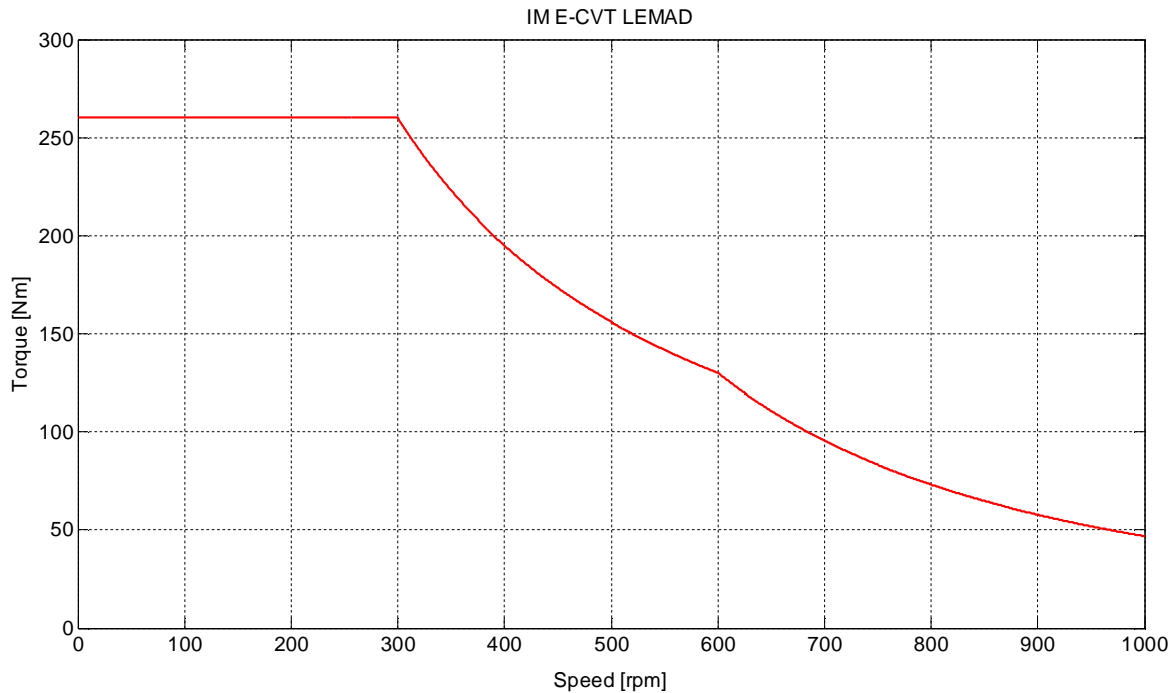
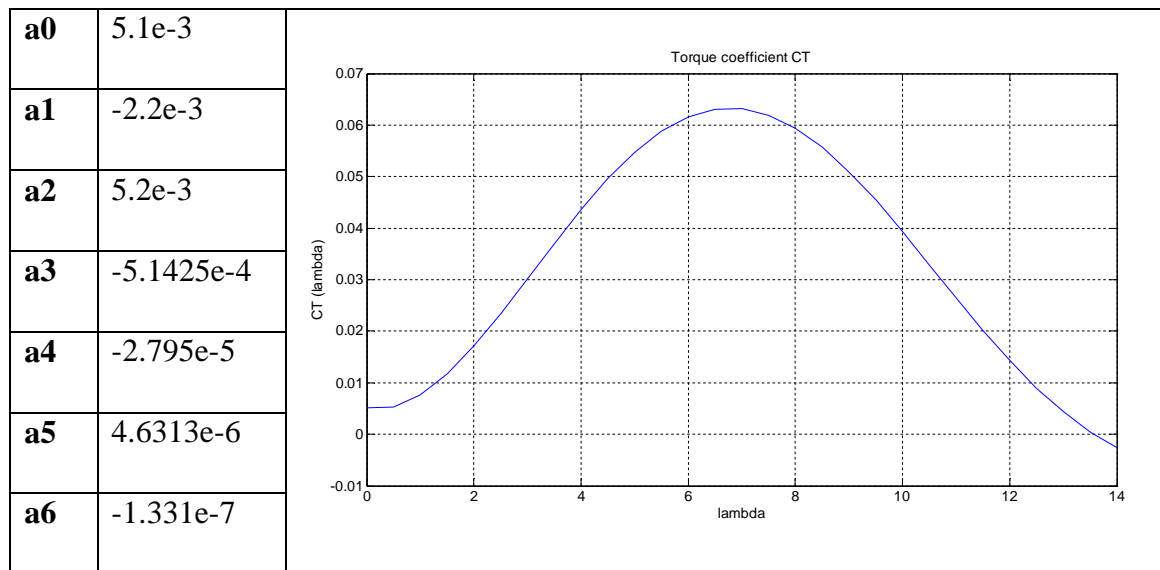


Fig. 5.7 – Induction machine torque limit characteristic



Tab. 5.2 – Polynomial definition of the coefficient  $c_T(\lambda)$

This operation is possible on the CPU used, because it's a linear combination of terms, and there are only sums and products. The coefficients  $a_i$  for  $c_T(\lambda)$  obtained in (5.3) are reported in Tab. 5.2.

This formulation of the WT produced torque allows to define the fictitious parameters of the wind turbine rotor that has been used in eq. (5.3) for the scaled lab system. The utilized parameters are reported in Tab. 5.3. It must be said that the radius indicated in Tab. 5.3 as the “rated” radius, is always used to get the parameter  $\lambda$ , and then it basically defines the speed range of the turbine. If a larger power is required is always possible to change the “real” radius, which is used for the torque expression (5.3), without affecting the speed range. In the present case a value of  $R_{real}=1,4$  m has been used to obtain the power characteristic of Tab. 5.3.

The power curves of the turbine are reported in Fig. 5.9. In order to obtain the MPPT curve, the SUN/DRIVER machine speed must be controlled dependently of the wind speed to take the turbine always on the maximum efficiency speed.

The transmission characteristics together with the over defined wind turbine power output yield to a particular configuration of the E-CVT system, requiring a determined torque

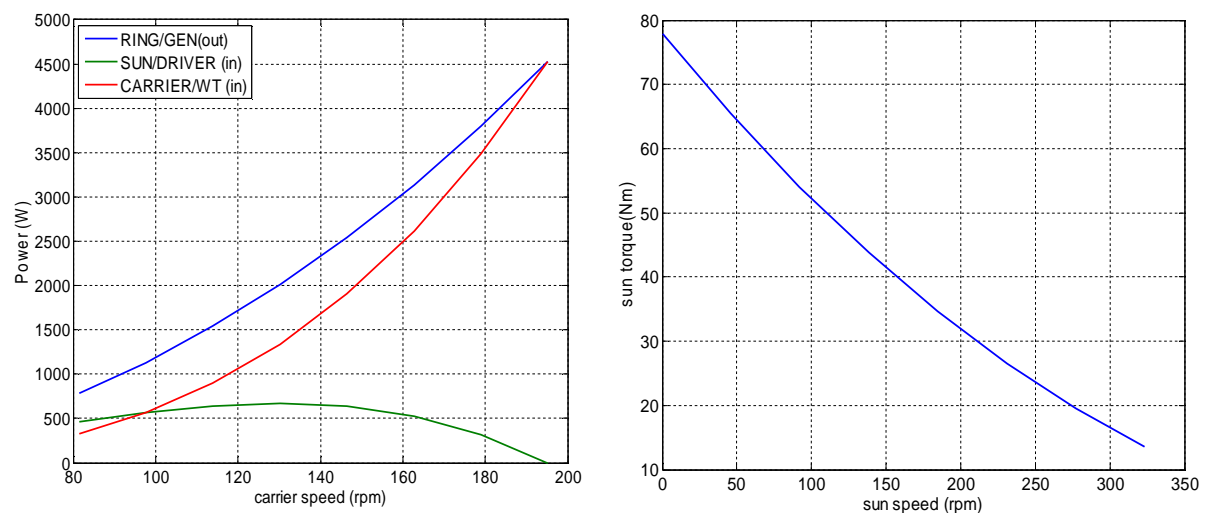


Fig. 5.8 – WT-CVT power curves (a) and driver required torque (b)

<i>Laboratory emulator – Wind turbine parameters</i>	
Rated radius $R_{rated}$ [m]	0,96
Real radius $R_{real}$ [m]	1,4
Rated wind speed [m/s]	12
Rated power [W]	4500
Rated speed [rpm]	195,2

Tab. 5.3 – Wind turbine emulator parameters

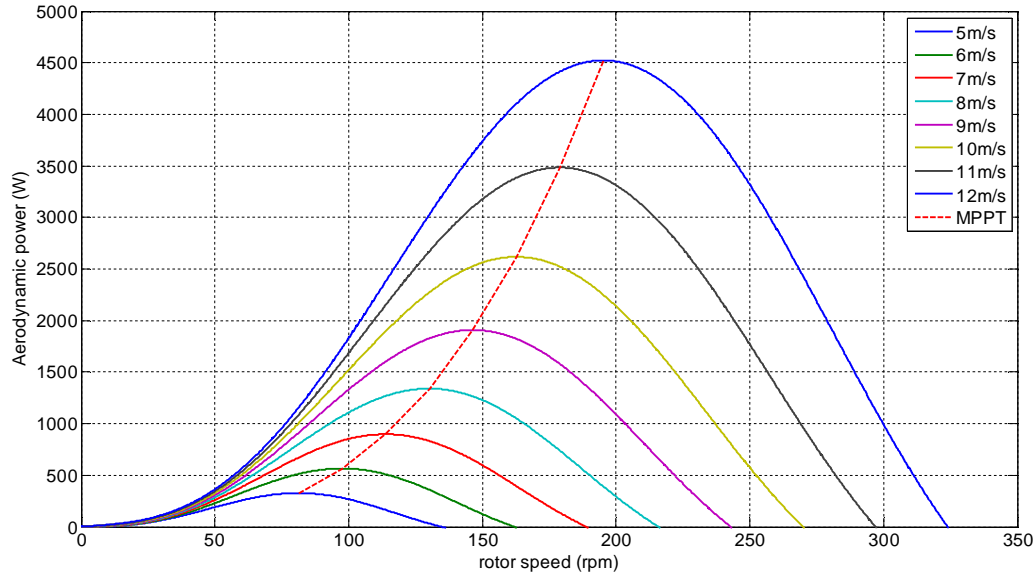


Fig. 5.9 – WT emulator power curves

characteristic at the SUN/DRIVER machine, as shown in Fig. 5.8. By the torque characteristic of the SUN/DRIVER machine, it is observed that a maximum 80 Nm torque is required to the machine, thus its maximum torque has been set to this value.

## 5.3 WT-CVT experimental results

Experiments have been carried out on the system configured as explained in the par. 5.2. Two kind of experiments have been executed, in order to validate the simulations made in Chapter 4:

- a. Wind speed below the rated;
- b. Wind gusts above the rated wind speed.

The settings of the control parameters for the RING/GEN machine, the SUN/DRIVER machine and the CARRIER/WT emulator have been resumed in the synoptic scheme of, where all the useful parameter settings of the system have been reported in Tab. 5.4.

### 5.3.2 Description of the tests

The experimental tests have been conducted by doing the following operations:

- Power request command to the inverters, to enable the speed setpoint.
- Start-up of the RING/GEN machine to the rated speed (300 rpm) at no load.
- Start-up of the wind speed signal, sent by the CRIO to the SIEMENS CPU.

<b>WT-CVT emulator control settings</b>			
<b>CARRIER/WT</b>		<b>PLANETARY GEAR SET</b>	
Rated power [W]	4500	Fundamental ratio $\tau_0$	-1,84
Rated speed [rpm]	195,2		
Rated torque [Nm]	220		
Rated wind speed [m/s]	12		
Max torque @ 162 rpm [Nm]	240		
<b>RING/GEN</b>		<b>SUN/DRIVER</b>	
Max RMS stator current [A]	200	Max RMS stator current [A]	75
RMS stator voltage [V]	54	RMS stator voltage [V]	Var
Frequency [Hz]	20	Frequency [Hz]	Var
Torque max limitation [Nm]	450	Torque max limitation [Nm]	80
Rated torque @ 12 m/s [Nm]	144	Rated torque @ 12 m/s [Nm]	78
Speed range [rpm]	≈300	Speed range [rpm]	0-323
Proportional speed loop gain [Nm*s/rad]	20	Proportional speed loop gain [Nm*s/rad]	20
Integral speed loop gain [Nm/rad]	0	Integral speed loop gain [Nm/rad]	4,4
Setpoint speed rate limiter [rpm/s]	200	Setpoint speed rate limiter [rpm/s]	200

*Tab. 5.4 – WT-CVT emulator settings*

- Operation of the SUN/DRIVER at variable speed according to the actual wind speed for MPPT operation.

Speed and torques of the shafts have been sampled and saved on the PC operator, thanks to the PCMCIA/CAN interface, which has a 10ms sample time on the CANbus 1 network. The results have been reported in normalized values, respect to the rated turbine torque and speed, as already done in par. 4.3.

### 5.3.3 Test of (a) typology

The first test demonstrates the capability of the system to control the turbine speed keeping (quasi) constant the generator speed at a step variable wind speed input (Fig. 5.10). It can be observed that while the generator speed remains close to 1,6 p.u., the turbine rotor speed varies from 1 p.u. to half the rated speed (Fig. 5.10.b). This is obtained varying the driver speed according to the wind speed variations (Fig. 5.10.e).

The oscillations on the speeds, particularly evident in the last part of the sampling

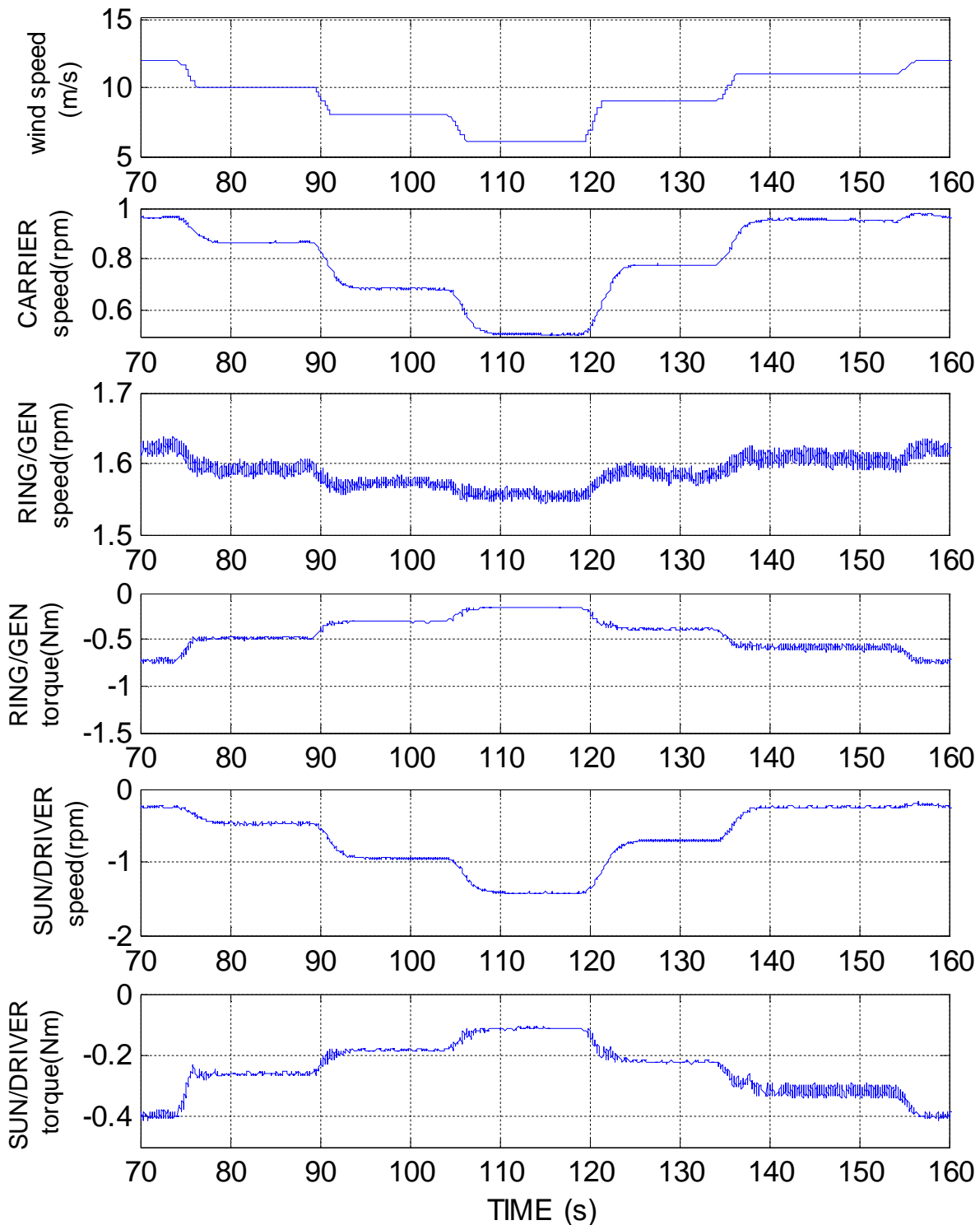
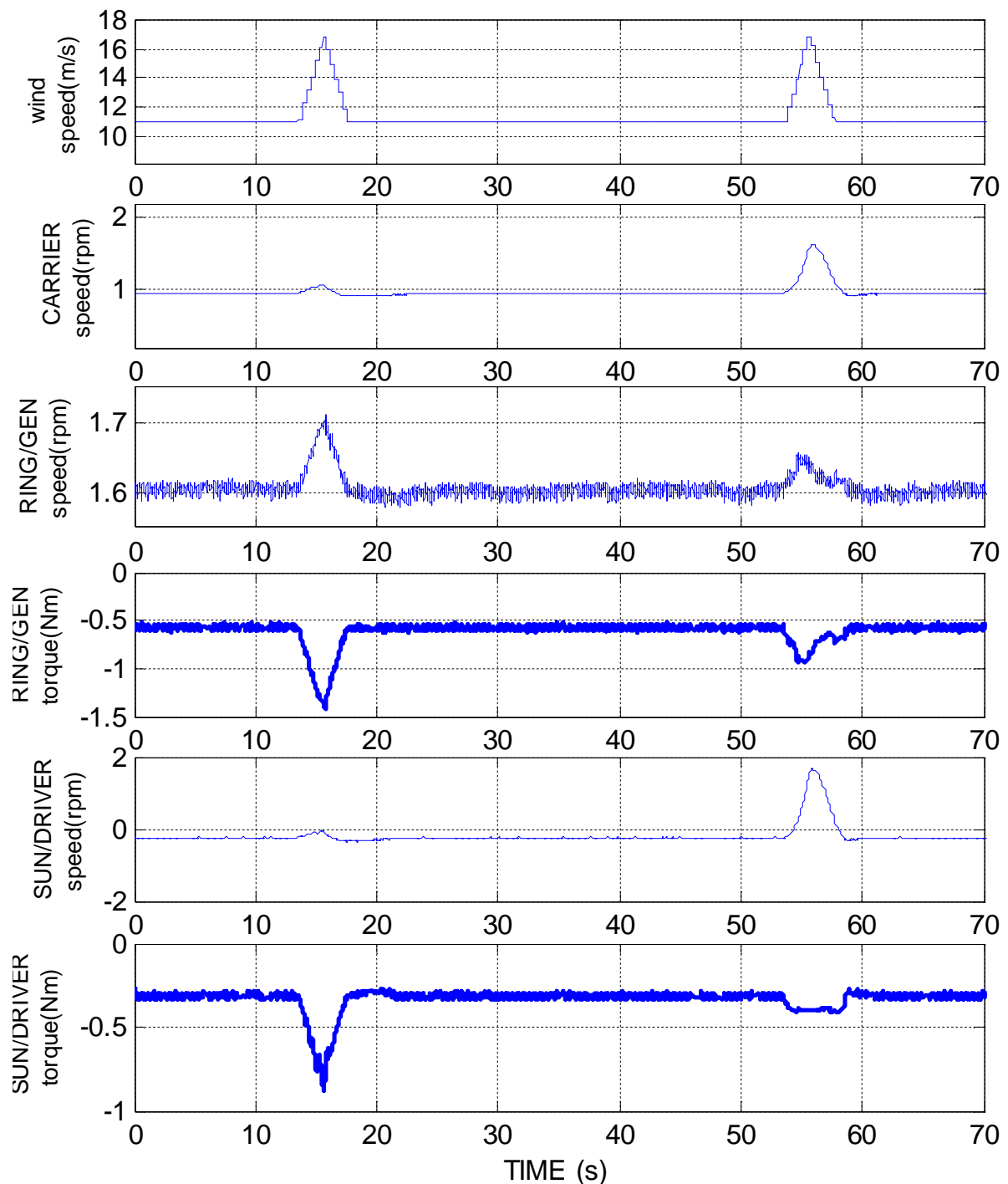


Fig. 5.10 – Experimental test (a) – Wind speed step variable

window part, are due to the not perfect acquisition of the SUN speed, which is obtained by elaboration over the other two measured speeds. The mechanical thread between the gear teeth creates some problems for the control system of the SUN machine, which introduces some torque oscillations.

Anyway, the regime speeds corresponds to the maximum power point for any wind speed, as it is possible to verify by the diagram of *Fig. 5.9*, and the system has an acceptable dynamic behavior.



*Fig. 5.11 – Experimental test (b) – Wind gusts at unlimited or limited driver torque*

### 5.3.4 Test of (b) typology

The second test examine the response of the system to a wind gust (*Fig. 5.11.a*, 11→17 m/s), in two different cases:

- The first gust (10-20s) simulates the behavior of a stiff transmission, where the SUN/DRIVER transmits all the torque from the CARRIER/ROTOR to the RING/GEN. In this case the over-torque at the generator shaft goes from 0,5 p.u. up to 1,5 p.u. (*Fig. 5.11.d*).
- In the second gust event (50-60s), the driver transmitted torque is limited to the rated value (as in the proposed case, *Fig. 5.11.f*), and it can be seen that the over-torque at the generator reduces of 0,5 p.u. respect to the previous case (*Fig. 5.11.d*). In this condition the turbine is free of accelerating, unlike the previous case (*Fig. 5.11.b*). This means that the gust power increase the kinetic energy of the rotor, instead of stressing the mechanical parts and the electrical generator.

## 5.4 Conclusions

An experimental test setup for testing of a E-CVT driveline built in the LEMAD lab has been described, and a strategy of scaling for the emulation of a wind turbine transmission of the power split type has been shown.

The experimental results obtained by the scaled lab system has confirmed the forecasts made by the simulations of par. 4.5, particularly on two peculiarity of the system capability:

- Controlling the wind turbine speed over a wide speed range by modifying the driver machine speed for MPPT purposes. The driver machine has a power rating of the 15÷16% of the generator rated power. The setpoint turbine speed is followed with good dynamical properties maximizing the power production below the rated wind speed.
- Moderate the torque transmitted by the driveline from the turbine to the generator, particularly during strong wind gusts, by keeping a limited driver torque or by limiting further the torque transmitted by the driver machine.

Further investigation can be made on the experimental system, even by the help of numerical simulations, regarding particularly the individuation of the best strategy of limitation of the driver machine torque.

## References

- [1] D. Casadei, G. Serra, A. Tani, Luca Zarri, “A Robust Method for Field Weakening Operation of Induction Motor Drives with Maximum Torque Capability”, IAS 2006, Tampa, Florida, 8-12 Oct. 2006, Paper N.IAS03P5, ISBN: 1-4244 0365-0.
- [2] <http://www.ni.com/compactrio/i/>
- [3] Weiwei Li; Dianguo Xu; Wei Zhang; Hongfei Ma; “Research on Wind Turbine Emulation based on DC Motor”, Industrial Electronics and Applications, 2007. ICIEA 2007. 2nd IEEE Conference on. Issue Date: 23-25 May 2007